The stressed right ventricle and its impact on the left ventricle

The Stressed Right Ventricle And Its Impact On The Left Ventricle

Mark K. Friedberg

Promotor
Prof. Dr. F.W. Prinzen

Copromotors
Dr. J. Lumens
Dr. F. Meijboom

Assessment Committee
Prof. Dr. T. Delhaas (chair)
Prof. Dr. H.-P. Brunner LaRocca
Dr. F. van Nieuwenhoven
Prof. Dr. R.M.F. Berger (UMCG)
Prof. Dr. J.-U. Voigt (KU Leuven)

The Stressed Right Ventricle And Its Impact On The Left Ventricle

Cover design by Mark K. Friedberg
Lay-out by Bianca Gorski-Feenstra
Printed by: Gilde Print

ISBN: 978-94-6419-169-1

The Stressed Right Ventricle And Its Impact On The Left Ventricle

PROEFSCHRIFT

Ter verkrijging van de graad van doctor aan de Universiteit Maastricht,
op gezag van de Rector Magnificus Prof. dr. Rianne M. Letschert,
volgens het besluit van het College van Decanen,
in het openbaar te verdedigen
op 21 april 2021 om 14:00 uur.

door

Mark K. Friedberg, MD

“To my loving and supportive family- My parents Jack and Janice, my spouse, Sharon and my sons, Daniel, Jonathan and Ethan.”

"...I found the task so truly arduous... that I was almost tempted to think... that the movement of the heart was only to be comprehended by God. For I could neither rightly perceive at first when the systole and when the diastole took place by reason of the rapidity of the movement..."

-William Harvey

Table of contents

Chapter 1

Introduction

1.1

Although in the absence of an intra-cardiac shunt, the right ventricle (RV) pumps exactly the same cardiac output as the left, it has received only a fraction of the attention paid to the left ventricle in research and clinical practice. This has led to some coining the RV 'the forgotten ventricle'. Yet, in many acquired and congenital conditions and heart diseases, the response of the RV is the key determinant of clinical outcomes including mortality. Therefore, how the RV adapts and responds to various stressors will determine how patients function and how long they live. Consequently, understanding RV physiology and its response to stress is critical towards the correct diagnosis, prognostication, management and treatment of these patients.

1.2. The Normal Right Ventricle

1.2.1 RV structure

In comparison to the symmetrical bullet shaped LV, the normal RV has a complex geometrical shape that has been likened to a pyramid. By echo or pathology, in the short axis (transverse plane), the RV appears crescent shaped-wrapping around the circular LV, with the septum bulging toward the RV throughout the cardiac cycle. This point becomes critical to adverse RV-LV interactions in RV pressure-loading and pulmonary hypertension (PH).

Most investigators divide the RV into 3 regions: (1) An inlet, (2) outlet, and (3) an apical body which is heavily trabeculated. The presence of a RV ventriculo-infundibular fold separates the tricuspid and pulmonary valves. This discontinuity influences echo evaluation of the RV inflow and outflow, which are in separate ultrasound planes; and also determines several surgical procedures such as the Ross operation and repair of tetralogy of Fallot.

When the RV is splayed open at pathology, 3 large muscular bands are apparent: (1) the parietal band, (2) the septo-marginal band, and (3) the moderator band. The parietal band together with the infundibular septum form the crista supraventricularis. The septo-marginal band runs inferiorly to join the moderator band. When hypertrophied, the septo-marginal and moderator bands can divide the RV into proximal and distal chambers which leads to different pressure-stresses in different RV regions.

The myofibers comprising the RV myocardium are arranged in 2 main layers: A superficial layer of predominantly circumferential or obliquely oriented myofibers and a deeper subendocardial layer of predominantly longitudinal fibers. As the normal post-natal RV pumps against the usually low-impedance pulmonary circulation, the dominant myofiber layer under normal circumstances

is the longitudinal layer.

1.2.2 Normal RV contraction and ejection

The low-impedance pulmonary circulation has pressures and resistance that are approximately 20% that of the systemic circulation. Consequently, in the post-natal circulation, RV volume exceeds LV volume, whereas RV mass is approximately one fifth to one sixth that of the LV. This leads to a higher RV surface-to- volume ratio versus the LV which in terms of ejection means that smaller amplitudes of wall motion are required to eject the same stroke volume as the LV. Due to the low-impedance pulmonary circulation, at end-systole, flow from the RV to pulmonary artery, continues despite a negative ventricular-arterial pressure gradient. This flow occurs due to inertial energy of blood in the outflow tract and is termed 'the hangout interval'.

The dominant RV longitudinal myofiber layer determines that under normal circumstances, RV pump function occurs predominantly via longitudinal shortening. This contrasts the dominant circumferential/ radial pumping action of the high-pressured LV. Consequently, most of the echocardiographic parameters used to assess RV function in clinical practice measure longitudinal RV motion.

RV pump function that ultimately lead to the ejection of blood into the pulmonary circulation is comprised of several mechanical events: (1) contraction of the longitudinal fibers, which draws the tricuspid annulus toward the RV apex; (2) inward movement of the RV free wall, which produces a bellows effect with the free wall coming towards the fixed septum (the septum being fixed by the higher LV pressures and synchronous timing of events) (3) infundibular contraction; and (iv) LV contraction, which substantially contributes to RV contraction and ejection through several mechanisms, but predominantly via the shared interventricular septum, and through the shared circumferentially oriented superficial myofibers that run across the RV and LV. Some authors have proposed that RV contraction occurs in a 'peristaltic' motion from the inlet to the outlet. However, as the apex is activated first, blood is first squeezed from the 'spongy' trabeculated apex. Regardless, it is apparent that regional contraction patterns differ in different parts of the RV. In contrast to the LV, rotational or twisting motion does not significantly contribute to RV ejection. Nonetheless, common circumferential fibers spiral together at the apex forming a common LV and RV apex.

1.3 Conditions that impose increased stress on the RV

Conditions that impose increased stress on the RV that ultimately lead to RV dysfunction can be broadly categorized in 4 groups: (1) Intrinsic myocardial disease (e.g. arrhythmogenic right ventricular cardiomyopathy; RV infarction), (2) Increased afterload (i.e. the load that the RV has to overcome during ejection), most commonly pressure-loading (e.g. pulmonary stenosis, pulmonary hypertension (3) Increased pre-load (i.e. the load before contraction), most commonly from volume-loading (e.g pulmonary regurgitation in repaired tetralogy of Fallot; atrial septal defect, (4) Electro-mechanical dyssynchrony (e.g. right bundle branch block in repaired tetralogy of Fallot). In this thesis, my work will relate to 2 prototypes of RV stressors: (1) RV pressure-loading from pulmonary stenosis or pulmonary hypertension and (2) Electro-mechanical dyssynchrony from right bundle branch block in repaired tetralogy of Fallot.

1.4 Pulmonary hypertension is a proto-type of severely increased RV afterload

PH, a prototype disease of increased RV afterload, is an often fatal condition defined by elevated pulmonary vascular resistance (secondary to pulmonary vascular disease or increased left sided pressures) and RV hypertension. The etiology of PH is multi-factorial, and PH can be primary or secondary to a multitude of other conditions and is beyond the scope of this introduction. PH is becoming more prevalent, especially in children as more survive prematurity, congenital heart disease and diaphragmatic hernia repair. Morbidity from PH can be severe including growth failure, cyanosis, syncope, arrhythmia and heart failure. Sudden death is common. While current therapies are based on pulmonary vasodilation, this is only partially successful and PH is progressive in most patients. In large registries, median survival was 2.8-years and only 10-months for children.

1.5 The RV response to increased pressure-loading and pulmonary hypertension

The RV (mal) response to increased pressure-loading can be characterized by 3 major events: (1) Dilatation, a compensatory event to maintain stroke volume (2) Decreased ejection (when the afterload is too high or the response inadequate) and, (3) Prolonged systole. This occurs due to increased isovolumic contraction time (not present or very short in the normal RV) and prolonged contraction. Of note, ejection time is shortened due to the high pulmonary vascular resistance in PH and isovolumic relaxation time is prolonged in relation to the increased resistance overall creating highly inefficient RV mechanics.

An increase in RV pressure results in increased wall stress. Although the RV hypertrophies to compensate for the increased wall stress (adaptive hypertrophy), this cannot adequately compensate and the increased wall stress leads to increased myocardial oxygen demand in relation to reduced supply, thereby reducing myocardial perfusion and creating relative ischemia, which worsens RV function and leads to further RV dilatation, and due to Laplace's law a further increase in wall stress. The stretch of the cardiomyocytes induces synthesis of pro-hypertrophic proteins through the integrin family of molecules as well as other molecular factors in cardiac myocytes, fibroblasts and endothelial cells. The integrins are a family of trans-mebrane proteins that have attachments to both the extracellular matrix and the cytoskeleton, and thereby act as molecular switches that transduce mechanical stress to intracellular chemical signals. This mechanical transduction is involved not only in pro-hypertrophic factors and contractile proteins but also in pathological processes such as fibrosis.

Eventually, if the afterload is sufficiently prolonged, severe or worsens, the RV cannot compensate and may not be able to maintain cardiac output. In a transition from 'adaptive hypertrophy' to 'mal-adaptive failure', RV contractility decreases and the RV further dilates. Because the increased wall tension that results from RV dilatation increases myocardial oxygen demand and decreases RV perfusion, a vicious circle of compromised contractility and dilatation ensues. Maladaptive neurohormonal signaling, abnormal RV myocyte energetics and metabolism that has been likened to processes that occur in malignancy, formation of reactive oxygen species and exaggerated inflammatory responses accelerate the development of right-heart failure. This process is most prominent in PH. However, the molecular mechanisms and events that underlie the transition from adaptive hypertrophy to RV failure remain poorly defined.

1.6 Repaired tetralogy of Fallot (rTOF) is a prototype of RV dysfunction related predominantly to increased volume loading, and, as shown by our work electro-mechanical dyssynchrony

TOF is the most common form of cyanotic CHD and is considered the archetype for the study of RV failure in congenital heart disease. TOF is comprised of four congenital abnormalities: pulmonary outflow tract narrowing, dextroposition of the aorta, presence of a malalignment ventricular septal defect and (eventual) RV hypertrophy. Anatomic repair for TOF is undertaken early in life to augment the pulmonary outflow tract through repair/removal of the pulmonary valve, excision of the sub-valvular muscle, and pulmonary artery enlargement. Surgery renders the pulmonary valve chronically regurgitant in the majority of adults, which increases the risk of late adverse events. Likewise, over 90% of patients develop a right bundle branch block (RBBB). Although survival after pediatric repair is excellent, with >95% of patients reaching adulthood,

morbidity and mortality accelerate in the third decade of life. Residual lesions are common, influence right ventricular (RV) and left ventricular (LV) function and impact symptoms, life quality, and long-term outcomes including HF, ventricular tachyarrhythmia and sudden cardiac death. Patients with rTOF are substantial contributors to the ever-escalating cost of congenital heart disease. Unfortunately, proven medical therapies for RV dysfunction, including in rTOF, are not available and current evidence-based guidelines are lacking. The cause of RV dysfunction in rToF is multifactorial, including pulmonary regurgitation and/or stenosis, surgical scars, fibrosis, outflow aneurysms, right bundle branch block (RBBB) induced electro- mechanical dyssynchrony, regional, and LV dysfunction. Among these, chronic pulmonary valve regurgitation, created predominantly by relief of RV outflow obstruction at the initial repair, is considered the main driver of RV remodeling (although our data detailed below cast doubt on this widely held premise). RV volume loading provokes RV dilatation and compensatory mechanisms to maintain wall stress and myocardial function, but eventual decompensation leads to RV dysfunction and exercise intolerance.

Aim of this thesis

The overall aim of this thesis is to describe the response of the RV to different stressors pertinent to patients with acquired and congenital heart disease. These stressors include pressure-loading in the forms of pulmonary stenosis and pulmonary hypertension, volume-loading in the form of pulmonary regurgitation and electro-mechanical dyssynchrony.

Using conventional and advanced echocardiography techniques, I aim to describe the functional response of the RV to these stressors and particularly regional and global myocardial function. I aim to bridge between basic and clinical research by using animal models to delineate the mechanisms underlying the observed RV response in patients. I further leverage these animal models to investigate the link between adverse geometry and temporal effects on the RV response and adverse RV-LV interactions. The aim is to describe novel mechanisms that can provide potentially new therapeutic targets.

Hypotheses:

- Pressure-loading causes adverse right ventricular remodeling and dysfunction that trigger RV myocardial fibrosis and left ventricular dysfunction.

- In repaired tetralogy of Fallot, RV electromechanical dyssynchrony has a stronger association with RV dysfunction and exercise intolerance than pulmonary regurgitation.

Outline of this thesis

I begin with an introduction followed by an invited peer reviewed review describing the unique RV physiology and characteristics, comparing the differences and similarities of the RV to the LV, focusing on the RV response to adverse loading and the current state of the art on RV-LV interactions.

Following the introduction (**Chapter 1**) and literature review (**Chapter 2**), I investigate the implications of pressure-loading and pulmonary hypertension on the RV. In **Chapter 3** I begin by comparing the pressure-loaded RV in children with pulmonary stenosis, which produces a more adaptive RV response, to the RV response in children with idiopathic pulmonary hypertension, which ultimately produces a maladaptive response. To demonstrate that RV pressure-loading and pulmonary hypertension do not exclusively affect the RV, but that they are conditions that affect both ventricles (which has important clinical implications), in **Chapter 4**, I investigate how the pressure-loaded RV impacts regional LV geometry and function. In **Chapter 5**, I expand on these differences in terms of the impact of RV pressure-loading and pulmonary hypertension on the LV (RV-LV interactions). In **Chapter 6**, I deepen the investigation of RV-LV interactions in RV pressure-loading/ pulmonary hypertension to study not only the effects of pressure alone, but also the temporal aspects of these interactions, which are intimately linked to the abnormal regional geometry induced by RV pressure-loading. In **Chapter 7**, I investigate how increased regional stress of RV pressure-loading translates into regional myocardial injury, specifically fibrosis, involving not only the RV, but also the LV. We demonstrate the central role of TGFβ1in mediating this injury. In **Chapter 8**, we further detail how these adverse RV-LV mechanical-molecular interactions are mediated by regional integrin molecular signaling, predominantly around the septal hinge-point regions.

In **Chapter 9**, I continue to investigate the impact of regional stress and regional differences in function, on global RV function, and its clinical impact on exercise capacity by performing a head-to head comparison on the effects of electro-mechanical dyssynchrony versus volume-loading, as highly pertinent to RV function in repaired tetralogy of Fallot (rTOF). This study uses statistical modeling of observed patient data, and computer modeling (CircAdapt) to test graded severity of one pathophysiology versus another. Electro-mechanical dyssynchrony produces regional disparities in RV wall stress through temporal delays secondary to right bundle block. By demonstrating its impact on RV remodeling, function and exercise capacity, we propose that electro-mechanical dyssynchrony is an important therapeutic target and compare its impact to the impact of RV volume-loading produced by pulmonary regurgitation, which is currently the major therapeutic target in the remodeled RV in rTOF. As the results of computer modeling cannot be definitively validated, I further aimed to test whether the hypotheses proposed by the computer model are observed in

clinical patients. Thus, we combine computer modeling with advanced statistical modeling of observed clinical data to delineate mechanism of RV remodeling and dysfunction.

I end the thesis by discussing the clinical implications of the findings (**Chapter 10**) and my interpretation of the implications, limitations and future directions (**Impact, Chapter 11**).

Chapter 2

Review of the literature

Right versus left ventricular failure: differences, similarities, and interactions

Authors
Mark K. Friedberg, Andrew N. Redington

(adapted from) Circulation. 2014;129(9):1033-1044.

Introduction

Ventricular 'failure' manifests in many forms, its underlying physiology ranging from overt left ventricular (LV) systolic dysfunction to isolated right ventricular (RV) diastolic disease, and the wide portfolio of resulting symptoms vary from chronic fluid retention to acute multi-organ dysfunction and death. In this review we will discuss the morphologic, functional and molecular similarities and differences in right (RV) and left (LV) ventricular response to adverse loading and failure. We will further discuss whether LV and RV function and failure can truly be discussed as separate entities and thereby examine interactions between the ventricles that on the one hand contribute to ventricular dysfunction, but on the other may also be harnessed for therapeutic benefit.

Are the LV and RV different?

Although they form the same organ, the RV and LV have quite different embryological origins.[1] While the LV originates from the primary heart field in the anterior plate mesoderm, the RV originates from the secondary heart field. Consequently, several genes have been identified that specifically control RV formation including, among others, Hand2 and Tbx20.[2] The normal RV functions as a systemic ventricle for the 9 months of human gestation. During fetal life, in addition to supplying the modest amount of pulmonary blood flow, the RV pumps blood to the systemic circulation of the lower body and placenta and contributes over half of the combined cardiac output.[3] With the transition from fetal to post-natal physiology; and with the reduction in pulmonary vascular resistance (PVR) over the first hours, days and months of life, the sub-pulmonary RV changes its morphology and geometry, becoming a thin-walled chamber; with changes in shape and septal position, and adopts its post-natal physiologic characteristics.[4] Because it faces a low impedance pulmonary circulation, the normal post-natal RV maintains a cardiac output equal to that of the LV at approximately a fifth of the energy cost. The trapezoidal RV pressure–volume loop reflects this difference, with little if any isovolumic periods. Consequently, RV output starts early during pressure generation, and is later maintained due to a 'hangout period', when antegrade flow continues into the pulmonary artery despite onset of RV relaxation[5]. In contrast, the typical rectangular LV pressure–volume loops reflect the LV's square-wave pump function; with distinct and well-developed isovolumic contraction and relaxation periods[6]. These differences also manifest at the myocyte level where RV myocytes display faster 'twitch' velocities than LV myocytes.[7]

Form follows function and the physiological differences in the pressure-volume loops are reflected in morphological differences between the ventricles (**Table 1**). The low-pressure RV is triangular in the sagittal plane and crescent shaped in cross-section due to the concave RV free wall and convex interventricular septum. The complex-shaped RV 'wraps' around the high-pressured, thick-

walled, bullet-shaped LV (**Figure 1**).

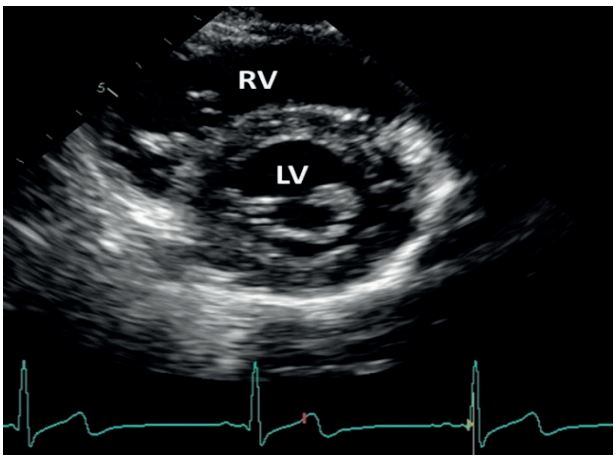

Figure 1. *Echocardiographic parasternal short-axis view in a normal child. In the short-axis the right-ventricle (RV) is crescent shaped, wrapping around the round left-ventricle (LV). Note that the RV wall thickness is much thinner than the LV.*

Consequently, while the normal RV has a lower volume-to-surface area ratio, and thinner wall than the LV[8], the low cavity pressure determines a lower wall stress and lower oxygen demands.

These anatomical differences are also apparent in myocardial architecture. In the LV, the outer and inner myocytes are predominantly longitudinal, whereas the mid-myocardial myocytes are oriented predominantly in the radial direction.[9] As a result, LV contraction is predominantly circumferential and radial with additional rotational and twisting motion. Conversely, RV myocytes are predominantly longitudinal creating a peristaltic contraction from inlet to outlet and a bellows-like motion of the free wall towards the septum.[10] That the two ventricles differ in their anatomy and physiology is irrefutable but, as we will discuss later, morphologically and functionally they are inextricably linked, not only in health, but as they react to disease.

Table 1. Differences between the right and right ventricles under normal conditions

	Left ventricle	Right ventricle
Evolutionary development	Early	Late
Embryological origin	Primary hand field	Secondary hand field
Morphological characteristics	Bullet shape, prolate ellipsoid	Complex, crescentic
Myocardial characteristics	Thick smooth walls, fine trabeculations	Thin, heavily trabeculated walls
Myocardial architecture	Predominant radial myocyte orientation in the mid-layers, Subendocardial myocytes follow right-handed helix configuration; subepicardial myocytes form left-handed helix	Predominant longitudinal myocyte orientation, angulated intrusion of superficial myocytes towards the endocardium
Physiological pump conditions	High resistance, high pressure pump, dominant radial thickening and contraction during ejection	Low resistance, low capacitance pump, peristaltic-like motion from inflow to outflow during ejection
Flow characteristics	Well defined isovolumic contraction and relaxation; no hang-out period	No or minimal isovolumic periods, hang-out period

Does the RV differ from the LV in its (mal) adaptation to adverse loading?

While the RV is not immune to the direct effects of coronary disease with resulting global or regional ischemia, in clinical practice, RV physiology and failure is most frequently impacted by the RV's response to increased preload or afterload. LV function is also affected by changes in load, but the RV is exquisitely dependent on, in particular, afterload. For example, Henning demonstrated that even small changes in total PVR, induced by modest increases in mean airway pressure during positive pressure ventilation, can lead to decreased RV contractile performance and lower cardiac output.[11] This occurred despite maintaining RV preload by volume infusions. MacNee demonstrated in an animal model how even modest increases in afterload lead to profound decreases in RV stroke volume.[12] In contrast, much larger changes in LV afterload induced only modest changes in LV stroke volume.[12] These experimental differences are reflected in clinical practice in LV versus RV handling of increased afterload. While patients with acute changes in systemic vascular resistance can compensate over a wide range, patients with acute pulmonary arterial hypertension (PAH), e.g. in the

setting of acute lung failure, frequently develop overt cardiac output and overt right heart failure .

Although when acute, even modest increases in RV afterload cause dramatic reductions in RV output, in most clinical scenarios, including PAH and RV outflow obstruction, changes in afterload are chronic and occur progressively. The germane question then becomes: Can the RV adapt to increased afterload and is this response 'adaptive' or 'maladaptive'. This in itself relates to the question-what is RV failure? If RV output is maintained, but the RV myocardium suffers detrimental remodeling and injury that ultimately affect its long-term function- the border between adaptation and failure becomes indistinct.

While we have emphasized the RV's vulnerability to increased afterload, it is clear from naturally occurring models (e.g. congenitally corrected transposition of the great arteries, Eisenmenger syndrome, systemic-pulmonary shunts) that the RV has the ability to maintain function and adequate output in the face of systemic pressure over prolonged periods. At the same time, it is also clear that the chronically pressure loaded RV is more prone to fail than the LV. Therefore, it is the ability of the RV to adapt to increased loading that is of interest.

Patients with Eisenmenger syndrome are an interesting example of RV adaptation. In Eisenmenger syndrome the RV faces continuous systemic level resistance from fetal life and throughout post-natal life. In contrast to the normal RV, the RV myocardium in Eisenmenger syndrome never thins. Consequently, these patients maintain similar RV and LV wall thickness from fetal to adult life (**Figure 2**).[13] Clinically, Eisenmenger patients have better RV function, higher cardiac index and lower risk of death than patients with other causes of PAH, despite having a higher pulmonary vascular resistance (**Figure 3**).[14] Therefore, it would seem that the RV has some capacity to retain fetal characteristics and maintain adequate function in the face of systemic resistance over many years.

Likewise, patients with a systemic RV following an atrial switch procedure for ventricular-arterial discordance (transposition of the great arteries) or congenitally corrected transposition of the great arteries can live for decades. At the same time, it is also apparent that these patients are prone to RV failure and increased mortality, albeit arrhythmias in the former and tricuspid regurgitation in the latter are important drivers of morbidity and mortality beyond RV myocardial failure per se (**Figure 4**).[15,16]

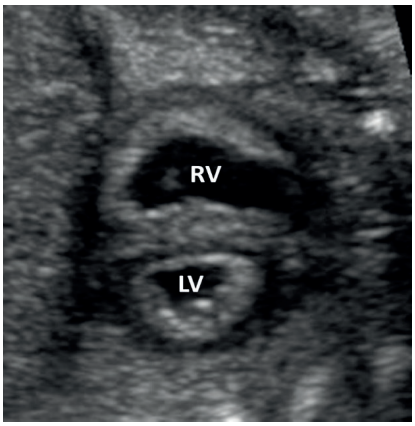

Figure 2
Fetal echocardiogram short axis view. Note the equal wall thickness of the right (RV) and left (LV) ventricles. The septum is in neutral position due to the equal pressures in the ventricles in normal fetal physiology

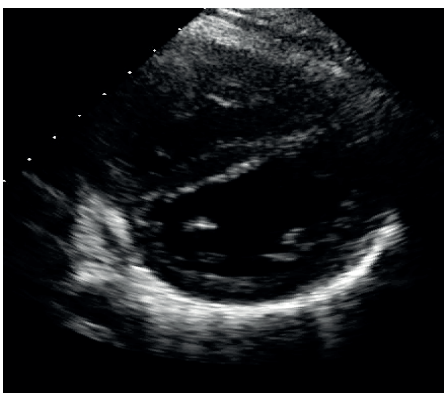

Figure 3
Parasternal short axis view in a patient with pre-tricuspid Eisenmenger syndrome. Note the similarities to the fetal echo with equally thick walls of the left and right ventricles and the neutral position of the interventricular septum.

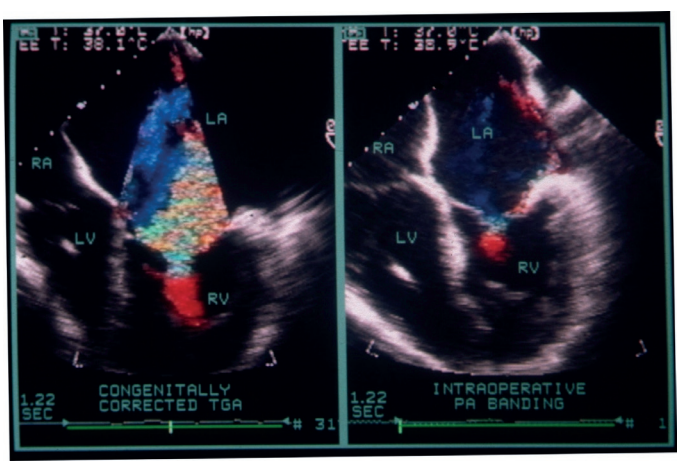

Figure 4
Color flow Doppler in a patient with congenitally corrected transposition of the great arteries. In this abnormality the left atrium connects to the right ventricle, which acts as the systemic pumping chamber to eject blood into the aorta. The right ventricle commonly fails over time. Structural tricuspid abnormalities and progressive RV dysfunction commonly lead to tricuspid regurgitation which is a major factor, perhaps more important than myocardial contractile dysfunction per se, driving morbidity and mortality in this condition.

How does the RV adapt to chronically increased afterload and does this differ from the LV?

In chronically increased afterload, the RV pressure volume relation shifts from a trapezoidal shape, reflecting its high-efficiency/low impedance (**Figure 5**) to a square or rectangular shape, indistinguishable from normal LV pressure volume loop (**Figure 5**).

We and others have demonstrated that this *compensated* RV adaptation to chronic afterload occurs through increased contractility, as seen by a steeper end-systolic pressure-volume relation (end-systolic elastance) (**Figure 5**).[17,18] This adaptation preserves cardiac output.[18] However, with disease progression, the RV ultimately fails leading to further RV dilatation and a rightward shift on the pressure–volume curve, and a resultant decrease in end-systolic elastance and compromised cardiac output (**Figure 5**).[17]

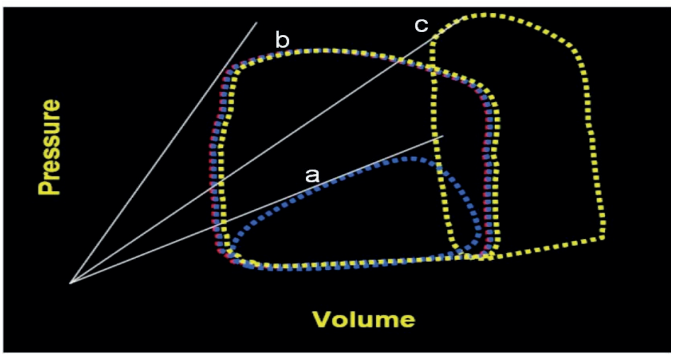

Figure 5
Right ventricular (RV) pressure volume loops obtained by conductance catheter. The diagram in the right panel demonstrates use of pressure volume loops. The white solid lines pass tangential to the end systolic pressure-volume points of a 'family' of loops produced by varying the loading conditions. The slope of this line gives the right ventricular end-systolic elastance. A steeper slope depicts higher end-systolic elastance. Loop 'a' depicts a normal RV P-V loop. Loop 'b' represents a 'compensated' chronically hypertensive RV. Loop 'c' is obtained from a decompensated hypertensive RV. Note the decrease in RV end-systolic elastance from the compensated RV depicted in loop 'b' to the decompensated RV depicted by loop 'c'.

The transformation in the pressure-volume curves to a LV pattern in the pressure-loaded RV are mirrored by changes in myocardial contraction patterns demonstrated by echocardiographic strain imaging. Petterson demonstrated that after the arterial switch operation, the systemic RV increases its circumferential contraction and decreases its longitudinal shortening, in a pattern indistinguishable from the normal LV.[19] This observation is somewhat surprising as diffusion tensor MRI imaging has demonstrated that the fiber orientation of the hypertrophied RV is not fundamentally different from the normal RV.[20] Likewise, some authors have suggested that the functionally single

systemic RV in hypoplastic left heart syndrome adapts a more circumferential versus longitudinal contraction pattern after stage 1 of surgical palliation (a particularly vulnerable period for these patients).[21] Yet, the RV in hypoplastic left heart syndrome continuously faces systemic resistance from fetal through post-natal life and it is difficult to attribute the change in RV contraction pattern to increased afterload alone.Nonetheless, at a molecular level, recent reviews and studies have highlighted differences between the RV and LV in terms of expression of genes involved in response to pressure loading and in LV and RV failure.[22] Likewise, there are differences in the RV response to certain effectors, including adrenergic hormones. While α1-adrenergic agonists increase LV contractility they may decrease RV contractility.[23] Chronic infusion of norepinephrine induces hypertrophy in the LV, but not in the RV.[24]

In response to increase afterload, the RV reverts to a fetal gene pattern with re-expression of genes normally expressed in the fetal but not the post-natal RV. This gene expression shift includes a shift from alpha to beta myosin heavy chain expression, an increase in adrenergic receptors, calcineurin activation[25-27] and increased phosphodiesterase type 5 (PDE5) expression.[28] While the fetal RV is undeniably a physiologic condition, and although these molecular changes allow stronger myocardial contraction to maintain cardiac output, they may also initiate myocardial remodeling that is a harbinger of long-term failure.

A detailed analysis of the accumulating experimental literature on progression from adaptive to maladaptive hypertrophy and from hypertrophy to failure is beyond the scope and objectives of this review. However, suffice it to say that not all studies of RV afterload however, show RV failure. One study in rodents study found that progressive pulmonary artery banding (PAB) induces RV hypertrophy, but not failure, as evidenced by increased contractility.[29] These findings may be explained by the RV pressure being only at ~60% of systemic levels in that study, a degree of severity that usually does not induce clinical symptoms in patients with pulmonary stenosis. While it is clear that it is not pressure overload alone that induces RV failure, and even if contractility increases as an 'adaptive' response to increased afterload, RV stroke volume and cardiac output may still fall, fulfilling the definition of failure for some.[30] Other rodent studies inducing systemic RV pressure levels have shown RV failure, RV dilation, decreased RV wall motion, elevated RV end-diastolic pressure, decreased cardiac output, clinical evidence of right heart failure, and decreased survival.[31]

Microarray gene chip studies of mice with LVH from aortic banding compared to mice with RVH from pulmonary banding have demonstrated both similar and different adaptive mechanisms between the LV and RV.[31] One pathway which is activated more in the pressure-loaded RV compared to the pressure loaded LV is the Wnt pathway. Wnt regulates glycogen synthase kinase-3b activity, a serine/threonine protein kinase that is active in multiple intracellular signaling pathways, including cell proliferation, migration, inflammation, glucose regulation, and apoptosis.[32] Therefore, there are potentially multiple differences

between the RV and LV in their adaptation to increased loading. GSK-3 was first discovered as a regulator of glycogen synthase[33] and there may be a difference between the RV and LV in metabolism and mitochondrial remodeling with different coupling of glycolysis to glucose oxidation. These metabolic changes would subsequently lead to hyperpolarization of the mitochondrial membrane potential in RV hypertrophy, inefficient energy metabolism and increased lactate production at an earlier stage of maladaption compared to the LV.[34] These molecular effects have potential therapeutic implications specific for the pressure loaded RV. For example, dichloroacetate, which improves glycolysis to glucose oxidation coupling and is clinically used in the treatment of inherited mitochondrial disorders, has been proposed to increase inotropy in the hypertrophied RV.[34] Likewise, PDE5 is not expressed in the normal RV, but is upregulated in the hypertrophied RV.[28] Accordingly, PDE5 inhibitors such as sildenafil have been found to increase RV contractility in experimental models of RV hypertrophy, but not in the normal RV.[28]

There may also be differences in the beneficial action of brain natiuretic peptide (BNP) in the 2 ventricles. BNP is expressed in both the RV and LV and serum levels correlate with the severity of both LV and RV failure in various conditions.[35] However, while there is evidence for improved cardiac output, symptoms, and ventricular performance in patients with LV failure treated with recombinant BNP (neseritide)[36], similar beneficial effects have not been shown in patients with PAH and RV failure.[37,38] In the setting of increased volume loading, the RV appears more prone than the LV to develop fibrosis as demonstrated in an experimental pig model with volume overload created by an aortocaval shunt.[39] Similarly, patients who have undergone surgical repair of tetralogy of Fallot and have long-standing RV volume-load secondary to pulmonary insufficiency develop RV fibrosis, even remote from surgical incision sites.[40] This is clinically important as a risk factor for increased propensity to arrhythmias, exercise intolerance and RV failure.[40,41] As has been shown for pressure loading, it has been suggested that these differences in response between the RV and LV to volume loading may stem from the different embryologic origin of the 2 ventricles.[39]

Over the past few years there has been increasing interest in the powerful role of microRNAs (miRNA) as regulators of a wide range of cardiovascular processes.[42] Their investigation has also raised the possibility for novel therapeutic targets.[43] Recent studies have highlighted both overlapping and varying expression between the failing RV and LV in various transcription factors, messenger RNA (mRNA) and miRNA expression. Some transcription factors, such as Iroquois homeobox 2 (Irx2), are expressed in the LV but not the RV. Others, including some nuclear receptors and insulin growth factor (IGF)-1 are expressed in both ventricles, but to different degrees.[44] The lack of Irx2 in the normal RV may explain why ANP is not expressed in the normal RV.[45] Failing RVs from rodents

with PAH induced by SU5416/hypoxia show a global increase in miRNA; although a specific decrease in miRNA 133a expression.[44] miRNA 133a is thought to play a role in suppression of cardiac fibrosis and its decreased expression has also been shown in the failing LV secondary to aortic constriction.[42,46] This result aligns with the observed marked upregulation of connective tissue growth factor/ CCN2 (CTGF) and other pro-fibrotic signaling molecules seen during RV and LV fibrosis in our and others models of RV afterload and RV failure.[44,47] In contrast, miRNA 21 and 34c* have been reported to increase during LV failure; but to decrease in experimental models of RV failure.[44] Reddy and colleagues investigated miRNAs during the transition from RV hypertrophy to RV failure and compared these with miRNA expression in LV hypertrophy or failure.[48] They demonstrated that during RV hypertrophy there was altered expression of miRNAs 199a-3p which is associated with cardiomyocyte survival and growth. With the progression to RV failure and reactivation of the fetal gene program there was increased expression of miR-208b; as well as miRs-34, 21 and 1 which are associated with apoptosis and fibrosis. These patterns of miRNA expression are largely similar to LV hypertrophy and failure. In contrast however, there were several notable differences between the RV and LV in miRNAs linked to cell survival, proliferation, metabolism, extracellular matrix turnover, and impaired proteosomal function (miRs 34a, 28, 148a, and 93) which were upregulated in RV hypertrophy or failure and downregulated or unchanged in LV hypertrophy or failure.[48] Similarly, the same group previously found that while molecular responses of the RV and the LV to increased afterload are mostly concordant, there are several key transcripts increased in the afterloaded RV but not in the afterloaded LV. These included clusterin, neuroblastoma suppression of tumorigenicity 1, Dkk3, Sfrp2, formin binding protein, annexin A7, and lysyl oxidase. From these molecular studies it would seem that while the LV and RV share many common response mechanisms to stress, there are several key differences that may warrant different management strategies in ventricular hypertrophy and their progression to failure. At a clinical level, a better understanding of these subcellular events may have implications for the development of novel, ventricle-specific, treatments. Inhibition of mir 208a has recently shown to markedly abrogate LV dysfunction in mouse and rat models of LV failure[49] and similar responses, albeit targeted towards a different miRNA signature, might be anticipated for RV failure.

Are the RV and LV really different?

As discussed in the preceding paragraph, while there are undoubtedly differences in the response of the RV and LV to adverse loading and differences in response of the more complex heart failure syndrome to various therapies, it is also evident that the 2 ventricles share many common features when they respond to adverse loading and when they fail. The 'fetal' gene pattern shift, and particularly the myosin heavy chain shift from the alpha to beta isoform, a hallmark of fetal gene re-activation, is also triggered in LV failure.[25] Likewise, the progression from compensated to decompensated hypertrophy occurs in both ventricles. A common finding in both RVH and LV hypertrophy (LVH) is collagen deposition, fibrosis and extracellular matrix remodeling.[50] Our own experimental data are consistent with this finding of common injury pathways in both ventricles.

In response to isolated RV afterload induced by PAB in a rabbit model we found RV as well as LV fibrosis in association with upregulation of transforming growth factor (TGF) b1 signaling in both ventricles (**Figure 6**). Just as RV fibrosis is commonly seen in the setting of both severe RV afterload as well as chronic pulmonary regurgitation, LV fibrosis is commonly seen in aortic stenosis as well as aortic regurgitation.[40,51,52]

Pharmacological agents that decrease either PVR or systemic vascular resistance may attenuate the progression of fibrosis in the RV and LV respectively. Likewise, mechanical unloading of the LV by left ventricular assist devices can attenuate fibrosis in both the RV and LV [53]. Microarray studies of thousands of genes have shown that while the response of the RV to pressure-induced hypertrophy was characterized by stronger transcriptional response compared to the LV; there was no evidence for qualitatively distinct regulatory pathways in the RV compared to the LV [54].

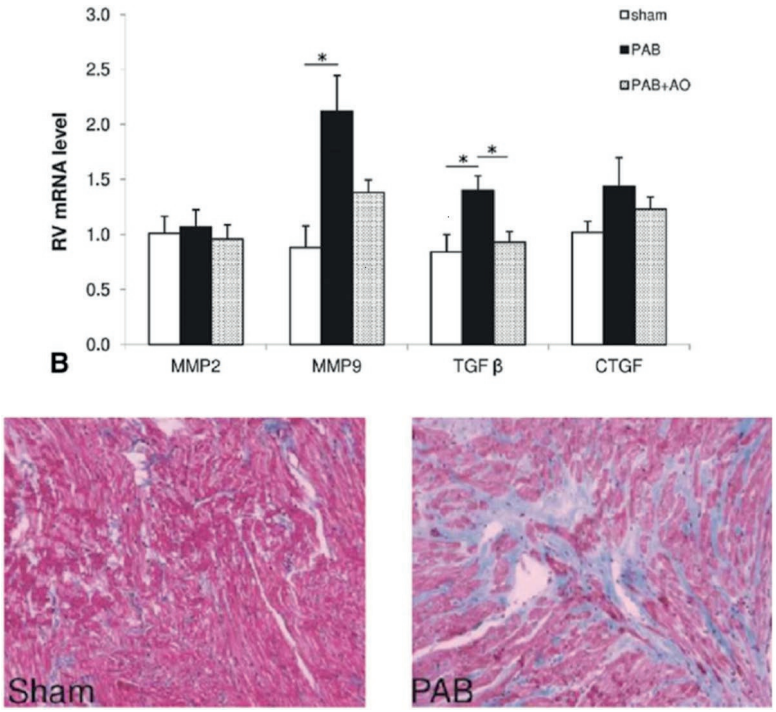

Figure 6

Representative sections showing Masson trichrome (MT) staining for collagen content. The bar graph of the quantitative analysis shows increased collagen in response to pulmonary arterial banding (PAB) in both the right ventricle (RV) and the left ventricle (LV). In association with increased fibrosis there is upregulation of pro-fibrotic signaling molecules including, transforming growth factor-β (TGFβ), connective tissue growth factor (CTGF) and matrix metalloproteinases (MMP) 2+9.[47]

Mechanical and functional interdependence between the RV and LV

While it has been customary to consider LV and RV function as separate entities, this approach is flawed. Not only do the ventricles share common injury mechanisms, but anatomically, they share fibers that encircle both ventricles, they are intimately attached through a common septum and they share a common pericardial space (**Figure 7**).[55] Consequently, the function of the two ventricles is inextricably linked, in both the structurally normal and abnormal heart.

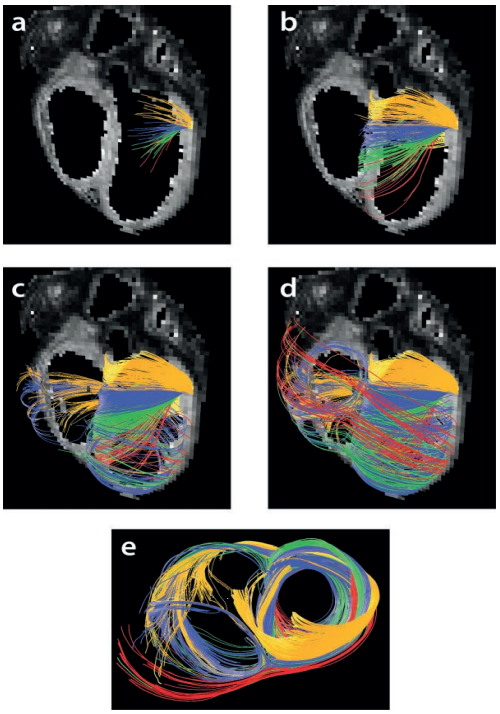

Figure 7
Diffusion tensor magnetic resonance imaging demonstrating orientation of myocytes. From the figure it is evident that fibers cross from the parietal walls of the left ventricle to the right ventricle. Note also how myocyte pathways intrude from epicardium to endocardium by means of a right hand helix movement about a transverse circular axis.86

The importance of LV to RV myocardial *"cross-talk"* was elegantly demonstrated in an experimental study of intact explanted hearts in which electrical, but not mechanical, continuity between the RV and LV was interrupted.[56] RV pacing led to little detectable mechanical activity (measured as developed pressure) in the LV. Conversely however, pacing-induced contraction of the electrically isolated LV was associated with development of an almost normal RV pressure trace as well as pulmonary blood flow.[56] Santamore further elucidated the individual effects of LV volume loading and dysfunction on RV developed pressure. Reducing LV volume from its optimal volume to zero caused a 5.7% decrease in RV developed pressure; while ligating the coronary supply to the LV free wall resulted in an additional 9.3% decrease in RV developed pressure. Cutting the LV free wall to prevent any developed LV free wall force caused a further 45% decrease in RV developed pressure.[57] Changes in RV developed pressure resulting from changes in LV volume and from coronary occlusion correlated with the degree of septal bulging into the RV cavity during systole, suggesting that the septum plays an important role in mediating ventricular-ventricular interactions. From these experiments, it was estimated that over 50% of the mechanical work of the normal RV may be

generated by LV contraction and that the LV free wall plays a pivotal role in RV function.[57] Similarly, Shertz showed that LV isovolumetric contraction results in simultaneous increases in RV stroke volume and RV developed pressure for a constant RV volume.[58] Hoffman expanded on these observations in '*in vivo*' experiments.[59] By replacing the RV myocardium with a non-contractile prosthesis, he was able to show virtually normal RV pressure generation, as a consequence of normal LV shortening. Just as interesting was the observation that intact RV geometry is crucial for normal LV mechanical performance. During gradual enlargement of the non-contractile RV free wall, there was a progressive reduction in both RV mechanical work, and LV mechanical work, i.e. as the RV dilated, LV pressure development and stroke work fell. These experimental phenomena have also been shown *in vivo* in the human heart during pre-excitation of one ventricle by pacing or during extra-systolic beats.[60] Normally, LV and RV electrical activation are temporally close enough that it is difficult to separate the peak dP/dT spike of each ventricle from each other. When LV electrical activation is sufficiently separated from RV electrical activation by a ventricular extra-systole or by left bundle branch block, the contribution of LV contraction to RV dP/dT becomes apparent.[60]

It is not only the LV which influences RV performance, but the RV profoundly impacts LV performance as well. With a change in RV volume, there are substantial changes in load-independent measures of LV function and indeed a shift in the LV pressure-volume relation.[61] These effects may be clinically relevant when the RV is volume unloaded by placement of a caval-pulmonary shunt. Danton showed in an experimental model that acute RV ischemia induced by coronary artery ligation induced LV dysfunction as measured by end-systolic elastance, a load-independent measure of LV contractility.[62] LV dysfunction secondary to RV ischemia was reversed by the addition of a caval-pulmonary shunt with restoration of LV end-systolic elastance. These 'load-independent' effects on LV contractility were likely mediated by the caval-pulmonary shunt relieving RV volume load, thereby limiting RV dilation and restoring LV cavity geometry.[62] One may envisage the impact of similar effects on LV function in the clinical setting of various congenital heart disease lesions; for example when a caval-pulmonary shunt is placed as part of a '1.5 ventricle repair' for RV hypoplasia or dysfunction.

In patients with PAH, in addition to decreased cardiac output that results directly from RV failure, RV dilatation displaces the interventricular septum leftward thereby impeding LV filling (**Figure 8**).[63-68] This secondary LV geometrical change is linearly related to cardiac output, whereas RV end-diastolic volume, in and of itself, is not related to cardiac output.[64] Similarly, in patients with tetralogy of Fallot and conduit stenosis, the prolonged septal shift induced by RV afterload and prolonged RV contraction leads to reduced LV filling as the septum bulges into the LV in diastole.[69] Relief of conduit stenosis reverses septal

curvature, shortens RV contraction, synchronizes LV and RV contraction and relaxation, improves LV filling and improves exercise capacity.[69] It is therefore not surprising that the LV eccentricity index, a simple echo index that quantifies the degree of anterior-posterior LV compression by the distended RV, correlates with survival in adults with PAH.[70] Similarly, we have recently found in children with iPAH, that both RV size and the LV eccentricity index were associated with death or need for lung transplantation.[71]

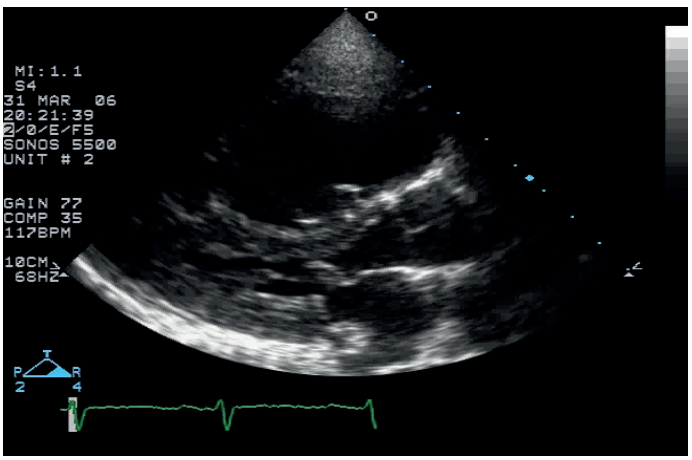

Figure 8
Echocardiographic long-axis view in a patient with severe pulmonary hypertension. Note the posterior bowing of the interventricular septum into the LV thereby impeding LV filling and function.

However, it is not the geometric consequences of septal shift alone that induces adverse ventricular interactions, but also the temporal relations of these events. Although in PAH the amount of time that blood is ejected into the lungs is significantly shortened[72], we have shown that the overall duration of RV contraction is actually markedly prolonged (**Figure 9**).[73] Consequently, in PAH there is a linear inverse relationship between heart rate and LV end-diastolic volume, suggesting that geometric and temporal events are linked in inducing adverse ventricular- ventricular interactions. These phenomenon have been demonstrated both by MRI and by echo, where septal shift, LV filling and the RV systolic/ diastolic duration ratio are linked to clinical outcome.[73,74] At the basis of these relations, lies a prolongation of RV systole, extending into LV systole, an adverse interaction worsened by increasing heart rate. Concomitantly, available RV filling time (i.e. diastolic duration) is severely shortened.[72] This leads to compromised RV and LV filling and filling rate.[61,74,75] This can be summarized as an increase in overall systolic time, but a truncated RV ejection time, and a significant decrease in the time available for filling. The shortened ejection time and volume reduced stroke volume secondary to increased afterload further contribute to decreased LV filling and cardiac output.[75]

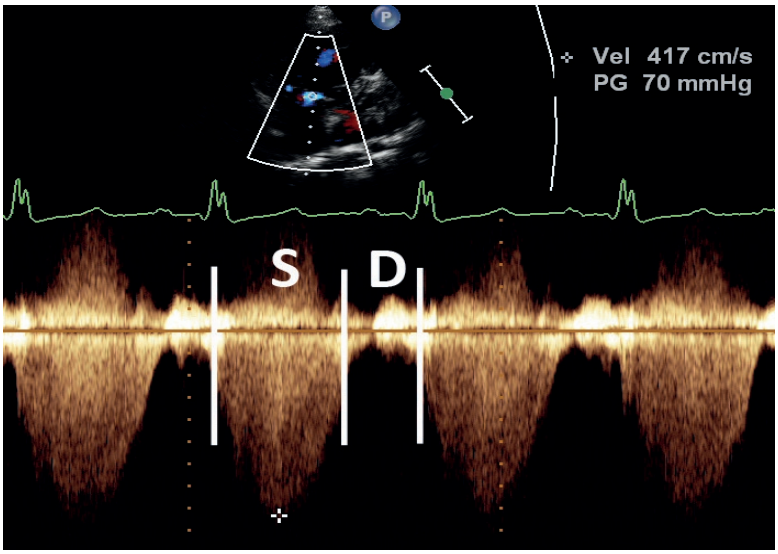

Figure 9

The systolic (S) to diastolic (D) duration ratio as measured from the Doppler signal of tricuspid valve regurgitation in a patient with pulmonary hypertension. In contrast to the normal situation where diastolic duration is equal to or longer than systolic duration, in this patient systolic duration is markedly longer than diastolic duration. This demonstrates the prolonged contraction time and shortened filling time of the right ventricle, which impairs right ventricular output and leads to adverse ventricular - ventricular interactions by limiting left ventricular pre-load.

In children with PAH there is a marked logarithmic decrease in diastolic duration and increase in the systolic/diastolic duration ratio when their heart rate increases as compared with controls.[73] We have shown that the ratio between systole and diastole measured from the duration of the tricuspid regurgitation Doppler signal and, which reflects both the overall prolonged systole and decreased ventricular filling, is linked to death or need for lung transplantation (**Figure 10**).[73] An increase of 0.1 in the S/D ratio was associated with a 13% increase in yearly risk for lung transplantation or death (HR 1.13, $p<0.001$). An S/D ratio < 1.00 was associated with low or no risk, an S/D ratio 1.00 - 1.40 was associated with a moderate risk and S/D ratio > 1.40 was associated with high risk of experiencing death or lung transplant.[73]

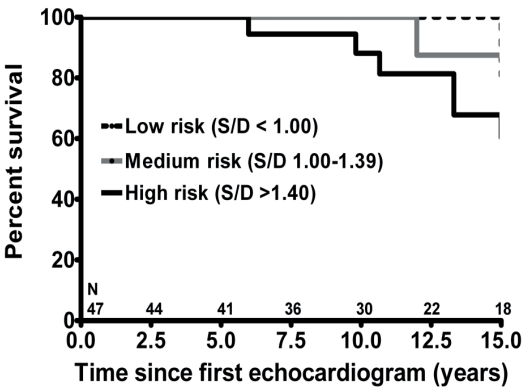

Figure 10

Adverse ventricular interactions translate into worse survival in children with PAH as shown by Kaplan-Meier survival analysis in 47 children with pulmonary arterial hypertension, stratified by the systolic: diastolic duration ratio. The percent of children free from clinical worsening, lung transplant or death, from time of the 1st echocardiogram is worse in children with a higher S:D ratio.73

RV hypertension, dilation and septal displacement also create RV dyssynchronous motion[76-78], as well as dyssynchronous contraction between the RV and LV.[60,78,79] This RV lateral wall and inter-ventricular dyssynchrony in PAH is not related to QRS duration or abnormal electrical activation such as occurs in left bundle branch block, but rather to RV wall stress, septal shift, LV end-diastolic volume and stroke volume.[60,79] These important ventricular-ventricular interactions almost certainly increase the S/D ratio, as interventricular dyssynchrony is related to lengthening of RV contraction.[79] Interventricular dyssynchrony as well as intraventricular delay, that may affect both myocardial mechanics and ventricular filling/ output has also been found to be important in other congenital heart disease (**Figure 11**). D'Andrea and colleagues showed that the interventricular mechanical delay, the difference between left and right isovolumic contraction time, is related to the risk of arrhythmia as well as exercise capacity in patients with tetralogy of Fallot.[80] Furthermore, other ventricular-ventricular interactions may also be at play in these patients. RV ejection fraction is linearly related to LV ejection fraction[81,82] and coexisting LV dysfunction is a key risk factor for functional decline and mortality.[83]

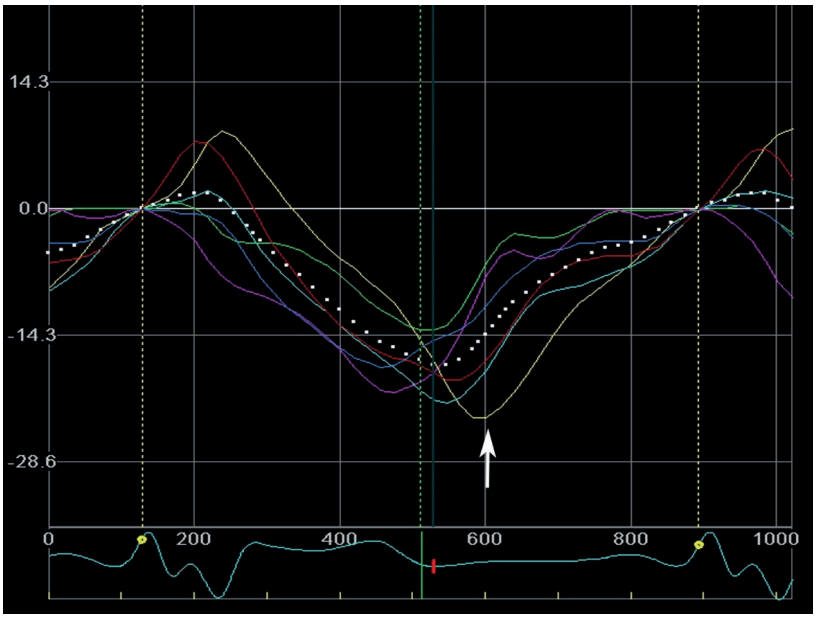

Figure 11

Right ventricular longitudinal strain curves representing myocardial shortening and lengthening in a child after surgical repair of tetralogy of Fallot. Each colored curve represents myocardial shortening and lengthening in a different RV segment. Note that the lateral basal segment (yellow curve) reaches its peak shortening considerably later than other segments. This mechanical disparity is likely driven by electromechanical abnormities in this condition and may contribute to right ventricular dysfunction.

Septal shift, LV geometry changes and temporal phenomena do not adequately explain all the effects of the ventricular-ventricular interactions discussed, however. We previously examined the effects of acute RV dilation, imposed by selective right coronary ischemia, on both RV and LV performance measured by conductance catheter.[84] With an intact pericardium, acute RV dilation led to a reduction, unsurprisingly, in LV size, but also to reduced load-independent indices of LV contractility. This change in LV volume was obviated by release of the pericardium, there being a similar degree of RV dilation but a non-significant fall in LV volume. However, acute RV dilation under these circumstances was still associated with a significant fall in load-independent measures of LV myocardial contractility. This could not be explained on the basis of changes in LV geometry, and almost certainly reflected abnormalities of myocardial cross talk under the circumstances of acute RV dilation.[63] Therefore, while septal shift in the setting of a relatively non-compliant pericardium is a crucial factor

in mediating ventricular interactions, myocardial cross-talk is another major component and likely occurs due to the presence of common myocardial tracts or fibers that are shared by both ventricles, especially in the superficial layers. As demonstrated elegantly in both pathological specimens and more recently by diffusion tensor imaging studies, these myofiber tracts originate predominantly in the superficial layer of the LV and cross to the RV (**Figure 7**).[85,86] As for the LV, the aggregated myocytes in the RV form helical angles and intrude in the oblique orientation from the epicardial to endocardial layers.[20,86] In response to afterload, the hypertrophied RV maintains this basic structure and does not form an extensive layer of circular myocytes that may explain the previously discussed shift from a longitudinal to circumferential strain pattern in the systemic RV.[20]

Although these shared myofibers likely play a role in mediating adverse ventricular-ventricular interactions they may also constitute a target for therapeutic intervention. We have developed a rabbit model of sustained increased RV afterload using adjustable pulmonary artery banding. This model allows study of isolated increased RV afterload on the LV, without potential confounding effects of altered genomics, pharmacological agents or hypoxia often used in animal models of PAH. We found that both acute and chronic isolated RV afterload induced by pulmonary artery banding leads to not only RV, but also LV global dysfunction. The functional compromise is accompanied in both ventricles by adverse remodeling as manifested by biventricular myocyte hypertrophy, reduced contractility and increased fibrosis.[47,87] While RV hypertrophy is an expected finding secondary to isolated RV afterload, the similar findings in the otherwise healthy LV is intriguing. We further demonstrated that under these circumstances of isolated RV afterload, the addition of mildly increasing LV afterload by systemic epinephrine or norepinephrine in acute RV failure (suggesting that systemic vasoconstriction, might be a viable strategy for the treatment of acute RV failure when LV function is well-preserved); or by the addition of mild aortic banding in both acute and chronic RV afterload, lead to an increase in load-independent indices of LV and RV contractility .[47,87] Perhaps more clinically relevant was our observation of maladaptive fibrotic responses in *both* ventricles following isolated RV afterload was associated with upregulation of genes classically involved in mediating fibrosis including TGFβ1, CTGF and endothelin (ET)-1 in the LV and RV. Likewise, in both ventricles, isolated RV afterload was associated with extra-cellular matrix degeneration expressed by upregulation of matrix metalloproteinases. Conversely, the observed improvement in LV and RV contractility induced by addition of mild LV afterload was associated with amelioration of biventricular myocyte hypertrophy and fibrosis as well as downregulation of fibrosis signaling.[47,87] Using a similar juvenile rabbit model of pulmonary artery banding, Kitahori found septal apoptosis, fibrosis, and reduced capillary density after 6 to 8 weeks of PAB which extended to the LV free-wall.[88] Visner demonstrated in dogs that impaired LV systolic function during acute RV hypertension induced

by pulmonary artery constriction was accounted for by rearrangements in LV dynamic geometry that primarily resulted from the anatomic contiguity of the 2 ventricles at the septal insertion points.[68] Septal shift is predominantly determined by the transeptal pressure gradient. Therefore, in the hypertensive RV, not only is septal function impaired, but the configuration of the displaced septum into the LV may increase local wall shear stress and regional injury.[66] Indeed, the RV septal insertion regions may be particularly prone to increased stress and subsequent fibrosis as they are exposed to high shear forces from LV circumferential and RV longitudinal shortening.[66,89,90] Recently, MRI delayed gadolinium enhancement, thought to represent fibrosis, at the RV septal insertion points has been found almost universally in adult patients with PAH and is in direct relation to the degree of RV afterload.[89,91,92] Fibrosis at the RV septal insertions was associated with reduced RV longitudinal contraction[92] and the extent RV fibrosis in PAH has been inversely related to RV ejection fraction, stroke volume and end-systolic volume; and also with increased mortality.[89] The improvement seen in RV and LV function with addition of a mild aortic band in our rabbit model may stem from amelioration of septal shift induced by the aortic band, improvement in ventricular geometry and also by inducing increased LV contractility through a modest increase in LV afterload. This in turn may lead to increased RV contractility through shared myofibers traversing both ventricles.

In clinical practice, increasing the sub-pulmonary left ventricle's afterload to improve cardiac function is used in patients who have congenitally corrected transposition of the great arteries and tricuspid regurgitation. In congenitally corrected transposition of the great arteries, the RV is the systemic ventricle and the systemically positioned tricuspid valve is often anatomically abnormal and regurgitant.[16] In this situation, the septum of the dilated systemic RV bulges towards the LV carrying with it the tensor apparatus of the tricuspid valve, leading to a viscious spiral of tricuspid regurgitation and RV dilation. By placement of a controlled pulmonary band to increase LV afterload on the one hand, while avoiding LV failure on the other, the septum shifts towards the LV and assumes a more neutral position thereby changing TV annular configuration and reducing TR. It is also interesting to postulate whether pulmonary artery banding in this situation increases LV contractility, thereby leading to an increase in systemic RV contractility through shared myocardial fibers; as we hypothesized for the addition of aortic banding in our aforementioned rabbit model. Recently this mechanism has been harnessed in the setting of dilated left ventricular cardiomyopathy. Schranz and colleagues have performed pulmonary artery banding in 12 infants and toddlers with left heart failure, showing remarkable improvements in LVEF, reduction in LV size, and improved mitral regurgitation.[93] While clearly preliminary, this may be another method of harnessing potential beneficial ventricular-ventricular interactions that deserves further investigation.

While it is intuitive to discuss ventricular-ventricular interactions when there

are 2 functioning ventricles, ventricular cross-talk may be just as important to ventricular mechanics when there is predominantly only one functioning ventricle, as occurs when either the RV or LV is severely under-developed. Using magnetic resonance imaging, Fogel demonstrated in children with a functionally single ventricle that regional myocardial strain, twist, and radial motion are markedly different to that seen in biventricular hearts.[94] In hypoplastic left heart syndrome for example, the absence of a developed LV may alter TV annular configuration and worsen TR, an important risk factor for adverse outcomes in this high-risk population.[95] Likewise, a larger interventricular septum may be a risk factor for death or transplant in this population.[96] This may be yet another manifestation of the effects of ventricular-ventricular interactions on RV function. While further discussion of these phenomena in the functionally single ventricle is beyond the purview of this review, we strongly believe that an improved understanding of regional and global responses of the myocardium in these patients will likely lead to novel therapeutic strategies, such are evolving from studies of the 'biventricular' heart discussed above.

In conclusion, while the RV and LV demonstrate important differences in embryology, form and function, they also share many common characteristics when they adapt to adverse loading or when they fail. Whether a number of key differences in their molecular response to failure will provide a potential platform for RV specific intervention remains to be seen. Furthermore, ventricular-ventricular interactions are important to cardiac function in both physiology and in disease. Through shared myocardial fibers, the interventricular septum and the common pericardium, LV contraction contributes to RV pressure development and RV loading impacts LV function. Targeting pathways specific to the stressed or failing RV, pathways that are common to both ventricles and targeting the interactions between the ventricles may ultimately lead to novel therapies to treat RV and LV failure.

References

1. Zaffran S, Kelly RG, Meilhac SM, Buckingham ME, Brown NA. Right ventricular myocardium derives from the anterior heart field. Circ Res. 2004; 95:261-268.
2. Thomas T, Yamagishi H, Overbeek PA, Olson EN, Srivastava D. The bHLH factors, dHAND and eHAND, specify pulmonary and systemic cardiac ventricles independent of left-right sidedness. Dev Biol. 1998; 196:228-236.
3. Rudolph AM. Congenital cardiovascular malformations and the fetal circulation. Arch Dis Child Fetal Neonatal Ed. 2010; 95:F132-136.
4. Mertens LL, Friedberg MK. Imaging the right ventricle--current state of the art. Nat Rev Cardiol. 2010; 7:551-563.
5. Dell'Italia LJ, Walsh RA. Acute determinants of the hangout interval in the pulmonary circulation. Am Heart J. 1988; 116:1289-1297.
6. Redington AN. Right ventricular function. Cardiol Clin. 2002; 20:341-349, v.
7. Rouleau JL, Paradis P, Shenasa H, Juneau C. Faster time to peak tension and velocity of shortening in right versus left ventricular trabeculae and papillary muscles of dogs. Circ Res. 1986; 59:556-561.
8. Chin KM, Kim NH, Rubin LJ. The right ventricle in pulmonary hypertension. Coron Artery Dis. 2005; 16:13-18.
9. Sengupta PP, Korinek J, Belohlavek M, Narula J, Vannan MA, Jahangir A, Khandheria BK. Left ventricular structure and function: basic science for cardiac imaging. J Am Coll Cardiol. 2006; 48:1988-2001.
10. Geva T, Powell AJ, Crawford EC, Chung T, Colan SD. Evaluation of regional differences in right ventricular systolic function by acoustic quantification echocardiography and cine magnetic resonance imaging. Circulation. 1998; 98:339-345.
11. Henning RJ. Effects of positive end-expiratory pressure on the right ventricle. J Appl Physiol. 1986; 61:819-826.
12. MacNee W. Pathophysiology of cor pulmonale in chronic obstructive pulmonary disease. Part One. Am J Respir Crit Care Med. 1994; 150:833-852.
13. Hopkins WE. The remarkable right ventricle of patients with Eisenmenger syndrome. Coron Artery Dis. 2005; 16:19-25.
14. Hopkins WE, Ochoa LL, Richardson GW, Trulock EP. Comparison of the hemodynamics and survival of adults with severe primary pulmonary hypertension or Eisenmenger syndrome. J Heart Lung Transplant. 1996; 15:100-105.
15. Dos L, Teruel L, Ferreira IJ, Rodriguez-Larrea J, Miro L, Girona J, Albert DC, Goncalves A, Murta M, Casaldaliga J. Late outcome of Senning and Mustard procedures for correction of transposition of the great arteries. Heart. 2005; 91:652-656.
16. Prieto LR, Hordof AJ, Secic M, Rosenbaum MS, Gersony WM. Progressive tricuspid valve disease in patients with congenitally corrected transposition of the great arteries. Circulation. 1998; 98:997-1005.
17. Redington AN, Gray HH, Hodson ME, Rigby ML, Oldershaw PJ. Characterisation of the normal right ventricular pressure-volume relation by biplane angiography and simultaneous micromanometer pressure measurements. Br Heart J. 1988; 59:23-30.
18. Gaynor SL, Maniar HS, Bloch JB, Steendijk P, Moon MR. Right atrial and ventricular

adaptation to chronic right ventricular pressure overload. Circulation. 2005; 112:I212-218.
19. Pettersen E, Helle-Valle T, Edvardsen T, Lindberg H, Smith HJ. Contraction pattern of the systemic right ventricle shift from longitudinal to circumferential shortening and absent global ventricular torsion. J Am Coll Cardiol. 2007; 49:2450-2456.
20. Nielsen E, Smerup M, Agger P, Frandsen J, Ringgard S, Pedersen M, Vestergaard P, Nyengaard JR, Andersen JB, Lunkenheimer PP, Anderson RH, Hjortdal V. Normal right ventricular three-dimensional architecture, as assessed with diffusion tensor magnetic resonance imaging, is preserved during experimentally induced right ventricular hypertrophy. Anat Rec (Hoboken). 2009; 292:640-651.
21. Khoo NS, Smallhorn JF, Kaneko S, Myers K, Kutty S, Tham EB. Novel insights into RV adaptation and function in hypoplastic left heart syndrome between the first 2 stages of surgical palliation. JACC Cardiovasc Imaging. 2011; 4:128-137.
22. Bogaard HJ, Abe K, Vonk Noordegraaf A, Voelkel NF. The right ventricle under pressure: cellular and molecular mechanisms of right-heart failure in pulmonary hypertension. Chest. 2009; 135:794-804.
23. Wang GY, McCloskey DT, Turcato S, Swigart PM, Simpson PC, Baker AJ. Contrasting inotropic responses to alpha1-adrenergic receptor stimulation in left versus right ventricular myocardium. Am J Physiol Heart Circ Physiol. 2006; 291:H2013-2017.
24. Irlbeck M, Muhling O, Iwai T, Zimmer HG. Different response of the rat left and right heart to norepinephrine. Cardiovasc Res. 1996; 31:157-162.
25. Lowes BD, Minobe W, Abraham WT, Rizeq MN, Bohlmeyer TJ, Quaife RA, Roden RL, Dutcher DL, Robertson AD, Voelkel NF, Badesch DB, Groves BM, Gilbert EM, Bristow MR. Changes in gene expression in the intact human heart. Downregulation of alpha-myosin heavy chain in hypertrophied, failing ventricular myocardium. J Clin Invest. 1997; 100:2315-2324.
26. Bakerman PR, Stenmark KR, Fisher JH. Alpha-skeletal actin messenger RNA increases in acute right ventricular hypertrophy. Am J Physiol. 1990; 258:L173-178.
27. Bartelds B, Borgdorff MA, Smit-van Oosten A, Takens J, Boersma B, Nederhoff MG, Elzenga NJ, van Gilst WH, De Windt LJ, Berger RM. Differential responses of the right ventricle to abnormal loading conditions in mice: pressure vs. volume load. Eur J Heart Fail. 2011; 13:1275-1282.
28. Nagendran J, Archer SL, Soliman D, Gurtu V, Moudgil R, Haromy A, St. Aubin C, Webster L, Rebeyka IM, Ross DB, Light PE, Dyck JR, Michelakis ED. Phosphodiesterase type 5 is highly expressed in the hypertrophied human right ventricle, and acute inhibition of phosphodiesterase type 5 improves contractility. Circulation. 2007; 116:238-248.
29. Faber MJ, Dalinghaus M, Lankhuizen IM, Steendijk P, Hop WC, Schoemaker RG, Duncker DJ, Lamers JM, Helbing WA. Right and left ventricular function after chronic pulmonary artery banding in rats assessed with biventricular pressure-volume loops. Am J Physiol Heart Circ Physiol. 2006; 291:H1580-1586.
30. Leeuwenburgh BP, Helbing WA, Steendijk P, Schoof PH, Baan J. Biventricular systolic function in young lambs subject to chronic systemic right ventricular pressure overload. Am J Physiol Heart Circ Physiol. 2001; 281:H2697-2704.
31. Urashima T, Zhao M, Wagner R, Fajardo G, Farahani S, Quertermous T, Bernstein D. Molecular and physiological characterization of RV remodeling in a murine model of pulmonary stenosis. Am J Physiol Heart Circ Physiol. 2008; 295:H1351-H1368.

32. Woodgett JR. Regulation and functions of the glycogen synthase kinase-3 subfamily. Semin Cancer Biol. 1994; 5:269-275.
33. Embi N, Rylatt DB, Cohen P. Glycogen synthase kinase-3 from rabbit skeletal muscle. Separation from cyclic-AMP-dependent protein kinase and phosphorylase kinase. Eur J Biochem. 1980; 107:519-527.
34. Nagendran J, Gurtu V, Fu DZ, Dyck JR, Haromy A, ross DB, Rebeyka IM, Mcihelakis ED. A dynamic and chamber-specific mitochondrial remodeling in right ventricular hypertrophy can be therapeutically targeted. J Thorac Cardiovasc Surg. 2008; 136:168-178, 178 e161-163.
35. Wei CM, Heublein DM, Perrella MA, Lerman A, Rodeheffer RJ, McGregor CG, Edwards WD, Schaff HV, Burnett JC Jr. Natriuretic peptide system in human heart failure. Circulation. 1993; 88:1004-1009.
36. Colucci WS, Elkayam U, Horton DP, Abraham WT, Bourge RC, Johnson AD, Wagoner LE, Givertz MM, Liang CS, Neibaur M, Haught WH, LeJemtel TH. Intravenous nesiritide, a natriuretic peptide, in the treatment of decompensated congestive heart failure. Nesiritide Study Group. N Engl J Med. 2000; 343:246-253.
37. Michaels AD, Chatterjee K, De Marco T. Effects of intravenous nesiritide on pulmonary vascular hemodynamics in pulmonary hypertension. J Card Fail. 2005; 11:425-431.
38. Klinger JR, Thaker S, Houtchens J, Preston IR, Hill NS, Farber HW. Pulmonary hemodynamic responses to brain natriuretic peptide and sildenafil in patients with pulmonary arterial hypertension. Chest. 2006; 129:417-425.
39. Modesti PA, Vanni S, Bertolozzi I, Cecioni I, Lumachi C, Perna AM, Boddi M, Gesini GF. Different growth factor activation in the right and left ventricles in experimental volume overload. Hypertension. 2004; 43:101-108.
40. Babu-Narayan SV, Kilner PJ, Li W, et al. Ventricular fibrosis suggested by cardiovascular magnetic resonance in adults with repaired tetralogy of fallot and its relationship to adverse markers of clinical outcome. Circulation. 2006; 113:405-413.
41. Wald RM, Haber I, Wald R, et al. Effects of regional dysfunction and late gadolinium enhancement on global right ventricular function and exercise capacity in patients with repaired tetralogy of Fallot. Circulation. 2009; 119:1370-1377.
42. van Rooij E, Sutherland LB, Qi X, et al. Control of stress-dependent cardiac growth and gene expression by a microRNA. Science. 2007; 316:575-579.
43. van Rooij E, Marshall WS, Olson EN. Toward microRNA-based therapeutics for heart disease: the sense in antisense. Circ Res. 2008; 103:919-928.
44. Drake JI, Bogaard HJ, Mizuno S, et al. Molecular signature of a right heart failure program in chronic severe pulmonary hypertension. Am J Respir Cell Mol Biol. 2011; 45:1239-1247.
45. Raizada V, Thakore K, Luo W, et al. Cardiac chamber-specific alterations of ANP and BNP expression with advancing age and with systemic hypertension. Mol Cell Biochem. 2001; 216:137-140.
46. Liu N, Bezprozvannaya S, Williams AH, et al. microRNA-133a regulates cardiomyocyte proliferation and suppresses smooth muscle gene expression in the heart. Genes Dev. 2008; 22:3242-3254.
47. Apitz C, Honjo O, Humpl T, et al. Biventricular structural and functional responses to aortic constriction in a rabbit model of chronic right ventricular pressure overload. J Thorac Cardiovasc Surg. 2012; 144:1494-1501.

48. Reddy S, Zhao M, Hu DQ, et al. Dynamic microRNA expression during the transition from right ventricular hypertrophy to failure. Physiol Genomics. 2012; 44:562-575.
49. Montgomery RL, Hullinger TG, Semus HM, et al. Therapeutic inhibition of miR-208a improves cardiac function and survival during heart failure. Circulation. 2011; 124:1537-1547.
50. Unverferth DV, Fetters JK, Unverferth BJ, et al. Human myocardial histologic characteristics in congestive heart failure. Circulation. 1983; 68:1194-1200.
51. Weidemann F, Herrmann S, Stork S, et al. Impact of myocardial fibrosis in patients with symptomatic severe aortic stenosis. Circulation. 2009; 120:577-584.
52. Hein S, Arnon E, Kostin S, et al. Progression from compensated hypertrophy to failure in the pressure-overloaded human heart: structural deterioration and compensatory mechanisms. Circulation. 2003; 107:984-991.
53. Kucuker SA, Stetson SJ, Becker KA, et al. Evidence of improved right ventricular structure after LVAD support in patients with end-stage cardiomyopathy. J Heart Lung Transplant. 2004; 23:28-35.
54. Kreymborg K, Uchida S, Gellert P, et al. Identification of right heart-enriched genes in a murine model of chronic outflow tract obstruction. J Mol Cell Cardiol. 2010; 49:598-605.
55. Sanchez-Quintana D, Anderson RH, Ho SY. Ventricular myoarchitecture in tetralogy of Fallot. Heart. 1996; 76:280-286.
56. Damiano RJ, Jr., La Follette P, Jr., Cox JL,et al. Significant left ventricular contribution to right ventricular systolic function. Am J Physiol. 1991; 261:H1514-1524.
57. Santamore WP, Lynch PR, Heckman JL, et al. Left ventricular effects on right ventricular developed pressure. J Appl Physiol. 1976; 41:925-930.
58. Schertz C, Pinsky MR. Effect of the pericardium on systolic ventricular interdependence in the dog. J Crit Care. 1993; 8:17-23.
59. Hoffman D, Sisto D, Frater RW, et al. Left-to-right ventricular interaction with a noncontracting right ventricle. J Thorac Cardiovasc Surg. 1994; 107:1496-1502.
60. Feneley MP, Gavaghan TP, Baron DW, et al. Contribution of left ventricular contraction to the generation of right ventricular systolic pressure in the human heart. Circulation. 1985; 71:473-480.
61. Taylor RR, Covell JW, Sonnenblick EH, Ross J, Jr. Dependence of ventricular distensibility on filling of the opposite ventricle. Am J Physiol. 1967; 213:711-718.
62. Danton MH, Byrne JG, Flores KQ, et al. Modified Glenn connection for acutely ischemic right ventricular failure reverses secondary left ventricular dysfunction. J Thorac Cardiovasc Surg. 2001; 122:80-91.
63. Moulopoulos SD, Sarcas A, Stamatelopoulos S, et al. Left ventricular performance during by-pass or distension of the right ventricle. Circ Res. 1965; 17:484-491.
64. Gan CT, Lankhaar JW, Marcus JT, et al. Impaired left ventricular filling due to right-to-left ventricular interaction in patients with pulmonary arterial hypertension. Am J Physiol Heart Circ Physiol. 2006; 290:H1528-1533.
65. Marcus JT, Vonk Noordegraaf A, Roeleveld RJ, et al. Impaired left ventricular filling due to right ventricular pressure overload in primary pulmonary hypertension: noninvasive monitoring using MRI. Chest. 2001; 119:1761-1765.
66. Nelson GS, Sayed-Ahmed EY, Kroeker CA, et al. Compression of interventricular septum during right ventricular pressure loading. Am J Physiol Heart Circ Physiol. 2001; 280:H2639-2648.

67. Roeleveld RJ, Marcus JT, Faes TJ, et al. Interventricular septal configuration at mr imaging and pulmonary arterial pressure in pulmonary hypertension. Radiology. 2005; 234:710-717.
68. Visner MC, Arentzen CE, O'Connor MJ, et al. Alterations in left ventricular three-dimensional dynamic geometry and systolic function during acute right ventricular hypertension in the conscious dog. Circulation. 1983; 67:353-365.
69. Lurz P, Puranik R, Nordmeyer J, et al. Improvement in left ventricular filling properties after relief of right ventricle to pulmonary artery conduit obstruction: contribution of septal motion and interventricular mechanical delay. Eur Heart J. 2009; 30:2266-2274.
70. Raymond RJ, Hinderliter AL, Willis PW, et al. Echocardiographic predictors of adverse outcomes in primary pulmonary hypertension. J Am Coll Cardiol. 2002; 39:1214-1219.
71. Kassem E, Humpl T, Friedberg M. Prognostic significance of 2-dimensional, M-mode, and Doppler echo indices of right ventricular function in children with pulmonary arterial hypertension. Am Heart J. 2013; 165:1024-1031.
72. Duffels MG, Hardziyenka M, Surie S, et al. Duration of right ventricular contraction predicts the efficacy of bosentan treatment in patients with pulmonary hypertension. Eur J Echocardiogr. 2009; 10:433-438.
73. Alkon J, Humpl T, Manlhiot C, et al. Usefulness of the right ventricular systolic to diastolic duration ratio to predict functional capacity and survival in children with pulmonary arterial hypertension. Am J Cardiol. 2010; 106:430-436.
74. Mahmud E, Raisinghani A, Hassankhani A, et al. Correlation of left ventricular diastolic filling characteristics with right ventricular overload and pulmonary artery pressure in chronic thromboembolic pulmonary hypertension. J Am Coll Cardiol. 2002; 40:318-324.
75. Gurudevan SV, Malouf PJ, Auger WR, et al. Abnormal left ventricular diastolic filling in chronic thromboembolic pulmonary hypertension: true diastolic dysfunction or left ventricular underfilling? J Am Coll Cardiol. 2007; 49:1334-1339.
76. Kalogeropoulos AP, Georgiopoulou VV, Howell S, et al. Evaluation of right intraventricular dyssynchrony by two-dimensional strain echocardiography in patients with pulmonary arterial hypertension. J Am Soc Echocardiogr. 2008; 21:1028-1034.
77. Lopez-Candales A, Dohi K, Rajagopalan N, et al. Right ventricular dyssynchrony in patients with pulmonary hypertension is associated with disease severity and functional class. Cardiovasc Ultrasound. 2005;3:23.
78. Vonk-Noordegraaf A, Marcus JT, Gan CT, et al. Interventricular mechanical asynchrony due to right ventricular pressure overload in pulmonary hypertension plays an important role in impaired left ventricular filling. Chest. 2005;128:628S-630S.
79. Marcus JT, Gan CT, Zwanenburg JJ, et al. Interventricular mechanical asynchrony in pulmonary arterial hypertension: left-to-right delay in peak shortening is related to right ventricular overload and left ventricular underfilling. J Am Coll Cardiol. 2008;51:750-757.
80. D'Andrea A, Caso P, Sarubbi B, et al. Right ventricular myocardial activation delay in adult patients with right bundle branch block late after repair of Tetralogy of Fallot. Eur J Echocardiogr. 2004;5:123-131.
81. Davlouros PA, Kilner PJ, Hornung TS, et al. Right ventricular function in adults with repaired tetralogy of Fallot assessed with cardiovascular magnetic resonance imaging: detrimental role of right ventricular outflow aneurysms or akinesia and adverse right-to-left ventricular interaction. J Am Coll Cardiol. 2002;40:2044-2052.

82. Kempny A, Diller GP, Orwat S, et al. Right ventricular-left ventricular interaction in adults with Tetralogy of Fallot: A combined cardiac magnetic resonance and echocardiographic speckle tracking study. Int J Cardiol. 2012;154:259-64.
83. Ghai A, Silversides C, Harris L, et al. Left ventricular dysfunction is a risk factor for sudden cardiac death in adults late after repair of tetralogy of Fallot. J Am Coll Cardiol. 2002;40:1675-1680.
84. Brookes C, Ravn H, White P, et al. Acute right ventricular dilatation in response to ischemia significantly impairs left ventricular systolic performance. Circulation. 1999;100:761-767.
85. Sanchez-Quintana D, Climent V, Ho SY, et al. Myoarchitecture and connective tissue in hearts with tricuspid atresia. Heart. 1999;81:182-191.
86. Smerup M, Nielsen E, Agger P, et al. The three-dimensional arrangement of the myocytes aggregated together within the mammalian ventricular myocardium. Anat Rec (Hoboken). 2009;292:1-11.
87. Apitz C, Honjo O, Friedberg MK, et al. Beneficial effects of vasopressors on right ventricular function in experimental acute right ventricular failure in a rabbit model. Thorac Cardiovasc Surg. 2012;60:17-23.
88. Kitahori K, He H, Kawata M, et al. Development of left ventricular diastolic dysfunction with preservation of ejection fraction during progression of infant right ventricular hypertrophy. Circ Heart Fail. 2009;2:599-607.
89. McCann GP, Gan CT, Beek AM, et al. Extent of MRI delayed enhancement of myocardial mass is related to right ventricular dysfunction in pulmonary artery hypertension. AJR Am J Roentgenol. 2007;188:349-355.
90. Beyar R, Dong SJ, Smith ER, et al. Ventricular interaction and septal deformation: a model compared with experimental data. Am J Physiol. 1993;265:H2044-2056.
91. Sanz J, Dellegrottaglie S, Kariisa M, et al. Prevalence and correlates of septal delayed contrast enhancement in patients with pulmonary hypertension. Am J Cardiol. 2007;100:731-735.
92. Shehata ML, Lossnitzer D, Skrok J, et al. Myocardial delayed enhancement in pulmonary hypertension: pulmonary hemodynamics, right ventricular function, and remodeling. AJR Am J Roentgenol. 2011;196:87-94.
93. Schranz D, Rupp S, Muller M, et al. Pulmonary artery banding in infants and young children with left ventricular dilated cardiomyopathy: A novel therapeutic strategy before heart transplantation. J Heart Lung Transplant. 2013;32:475-481.
94. Fogel MA, Weinberg PM, Fellows KE, et al. A study in ventricular-ventricular interaction. Single right ventricles compared with systemic right ventricles in a dual-chamber circulation. Circulation. 1995;92:219-230.
95. Takahashi K, Inage A, Rebeyka IM, et al. Real-time 3-dimensional echocardiography provides new insight into mechanisms of tricuspid valve regurgitation in patients with hypoplastic left heart syndrome. Circulation. 2009;120:1091-1098.
96. Walsh MA, McCrindle BW, Dipchand A, et al. Left ventricular morphology influences mortality after the Norwood operation. Heart. 2009;95:1238-1244.

Chapter 3

The stressed RV in pulmonary hypertension and pressure loading: Insights in pediatric patients

Regional right ventricular remodeling and function in children with idiopathic pulmonary arterial hypertension versus those with pulmonary valve stenosis: Insights into mechanics of RV dysfunction

Authors
Mieke M.P. Driessen, Folkert J. Meijboom, Wei Hui, Andreea Dragulescu, Luc Mertens, Mark K. Friedberg

(adapted from) Echocardiography. 2017; 34(6):888-897

Abstract

Background: RV pressure overload in the context of pulmonary stenosis (PS) has a much better prognosis than in the context of idiopathic pulmonary arterial hypertension (iPAH), which may be related to differences in global and regional RV remodeling and systolic function. We compared RV mechanics in children with PS to those with iPAH, aiming to identify mechanisms and markers of RV dysfunction.

Methods: Eighteen controls, 18 iPAH and 16 PS patients were retrospectively studied. Age, BSA and sex distribution were comparable. Two-dimensional echocardiography, blood flow and tissue Doppler and longitudinal RV deformation were analyzed. ANCOVA - including RV systolic pressure (RVSP) and length as covariates – was used to compare patient groups.

Results: RVSP was higher in iPAH versus PS (96.8±25.4 vs. 75.4±18.9 mmHg, p=0.011). Compared to controls, PS patients showed mild dilation (p<0.01) and decreased longitudinal deformation (p<0.001) at the RV apex. Compared to both PS and controls, iPAH patients showed marked spherical RV dilation (p<0.001), reduced global RV free wall and septal longitudinal deformation (iPAH -22.07±4.35% vs. controls -28.18±1.69%; -9.98±4.30% vs. -17.45±2.52%; p<0.001) and RV post-systolic shortening (p<0.001). RV transverse shortening (radial performance) was increased in PS (31.75±10.35%; p<0.001) but reduced in iPAH (-1.62±11.11% vs. controls 12.00±7.74%; p<0.001).

Conclusion: Children with iPAH demonstrate adverse global and regional RV remodeling and mechanics compared to those with PS. Mechanisms of RV systolic dysfunction in iPAH include decreased longitudinal deformation, decreased or absent transverse shortening and post-systolic shortening. These markers may be useful to identify children at risk of RV failure.

Introduction

Right ventricular (RV) dysfunction is an important determinant of morbidity and mortality in various cardiovascular pathologies, especially those related to RV pressure- or volume overload.[1-3] However, early identification and characterization of a poorly adapting RV and consequently RV failure continues to be difficult.

Patients with pulmonary valvular stenosis (PS) and idiopathic pulmonary arterial hypertension (iPAH) both experience chronically increased RV systolic pressure, but the clinical course and natural history of these conditions differ vastly.[4,5] While a large proportion of iPAH patients present with, or rapidly develop, symptomatic heart failure[5,6], PS patients are often asymptomatic or present with only mild exercise intolerance.[4] Moreover, mortality vastly differs between the groups - high in iPAH and very low in PS.[4,5] Although the duration and possibly character of increased RV pressure differs between the 2 conditions, the RV response also seems very different. A study by Jurcut et al. demonstrated this difference in adult iPAH and PS patients, showing global RV dilation and decreased global RV free wall (RVFW) longitudinal deformation in iPAH versus PS patients.[7] Although contraction is predominantly longitudinal in the normal RV; septal contraction, regional RVFW deformation, RVFW radial function and septal-RVFW synchrony all contribute to RV performance.[8,9] Thus, differences in RVFW radial function, septal deformation and regional RV remodeling and deformation may all contribute to differences in RV function, and consequently clinical outcome, of pediatric PS vs. iPAH patients. However, these are incompletely characterized in children. Furthermore, comparing RV mechanics in these two clinically distinct patient groups may provide useful insights into the mechanisms of RV failure in pediatric patients with increased RV pressure, as well as imaging markers of RV dysfunction.[7] Accordingly, the aim of this study was to characterize regional and global RV remodeling and mechanics in children with PS compared to iPAH – to provide insights into mechanisms of RV maladaptation and potential imaging markers for identification of RV dysfunction.

Methods

Study population

We retrospectively studied children with iPAH and PS, comparing them to healthy controls with similar age and BSA. The study population has previously been described in a paper on interventricular interaction and LV diastolic function.[10] Echocardiographic studies performed between 2006 and 2013 were included. The diagnosis of iPAH was established by right-heart catheterization with a mean pulmonary artery pressure ≥ 25 mmHg, pulmonary capillary wedge pressure ≤15 mmHg and pulmonary vascular resistance of >3 Wood units.[11] All iPAH patients were on pulmonary vasodilator therapies. Valvular PS patients were included if they had a peak pulmonary valve gradient of ≥36 mmHg and did not have previous interventions or additional intra-cardiac abnormalities - with the exception of a small, hemodynamically insignificant atrial or ventricular septal defect. Healthy controls served as a reference group for RV geometry and function. Controls were healthy volunteers or children evaluated for an innocent murmur with normal medical history, physical examination and echocardiography. The study was approved by the institutional research ethics board.

Echocardiography

Two-dimensional echocardiographic measurements were made offline using commercially available software (SyngoDynamics, Siemens, Erlangen, Germany). Measurements were performed in accordance with pediatric guidelines.[12] Images were acquired at our institution with either Philips or GE ultrasound platforms. In PS patients, the echocardiogram closest to potential balloon valvuloplasty was analyzed (all but one patient subsequently underwent balloon angioplasty) to include the echocardiogram with the highest pulmonary valve gradient. As many iPAH patients were diagnosed prior to implementation of a functional echo protocol – we chose to include the first echocardiogram with full functional evaluation rather than the echocardiogram at time of right heart catheterization. Systemic blood pressure was measured manually at the time of echocardiography, placing the cuff on the right upper arm.

Two-dimensional measurements

M-mode measurements of the RV and LV end-diastolic diameters were made at the level of the mitral valve leaflet tips. Z-scores were calculated using institutional reference values. Using the same M-mode registration, RVFW inward transverse displacement was measured and transverse shortening calculated (**Figure 1**). RV fractional area change (FAC), tricuspid annular plane systolic excursion (TAPSE) and RV dimensions were measured from a focused apical 4-chamber view.[12] To assess RV geometry, RV dimensions were

measured at the apical, mid and basal levels (**Figure 2**). Right atrial (RA) area was measured at end RV systole and end RA systole.

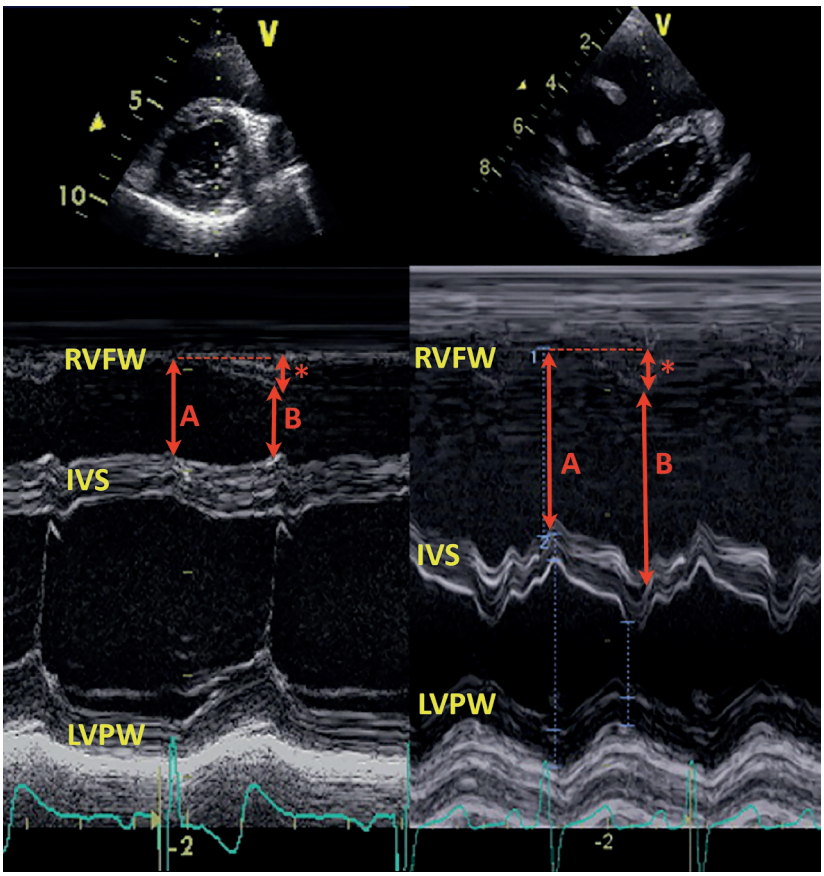

Figure 1: Short-axis M-mode echocardiography depicting transverse RV shortening
The left hand panel depicts an example of a healthy control and on the right an example of an iPAH patient. Transverse shortening is calculated as [a – b] / a. The asterisks (*) indicate the absolute RVFW displacement. RVFW= right ventricular free wall; IVS= interventricular septum; LVPW= left ventricular posterior wall.

Blood flow and Tissue Doppler imaging

Continuous wave (CW) Doppler was used to measure maximal pulmonary valve flow velocities in systole and end-diastole. RVSP was estimated using the modified Bernoulli equation from tricuspid regurgitation CW Doppler. We did not add an assumed right atrial pressure to the RVSP. Many PS patients did not have tricuspid regurgitation. The resistance the ventricle has to overcome during systole determines RVSP, we therefore used the maximal pulmonary valve gradient in these patients to estimate RVSP. Pulsed wave tissue Doppler imaging (TDI) at the basal RV free wall (RVFW), interventricular septum (IVS) and LV free wall (LVFW) were used to measure peak systolic (S') and early diastolic (E') tissue velocities and TDI-derived RV myocardial performance index.

Speckle tracking analysis

A focused RV apical 4-chamber view was used for speckle tracking strain analysis (Tomtec4.6, UnterSchleissheim, Germany). The RVFW and IVS endocardial borders were traced and adequate tracking visually confirmed (**Figure S1**). If more than one segment did not track adequately the patient was excluded from analysis. The following parameters were measured for both regional and global IVS and RVFW strain: peak systolic longitudinal strain (peak deformation during ejection time, i.e. before or at pulmonic valve closure), time to peak (TTP) and post-systolic shortening (PSS). Post-systolic shortening is defined as deformation continuing after pulmonic valve closure, calculated as (%) = ((peak strain – peak systolic strain))/peak strain) *100.[13] Time to pulmonic valve closure was determined using pulsed wave Doppler measurement in the RV outflow tract – using a cardiac cycle with an equivalent RR interval.

Reproducibility

Ten representative datasets were randomly selected for reproducibility measurements. The second analysis by the first observer was performed at least 1-month after the first measurement. Both observers were blinded to the prior results. The same cardiac cycle was used to perform reproducibility measurements.

Statistical analysis

Distribution of the continuous variables was assessed using a combination of boxplot, normal probability plot and Shapiro-Wilk test. Normally distributed variables are represented as mean [± standard deviation] and non-normally distributed variables as median [range]. Categorical variables are presented as a frequency (%) and were compared using Chi-square test. Normally distributed continuous data of PS and PAH patients were compared to healthy controls using

ANOVA with posthoc Dunnet's. Non-normally distributed data was compared using Mann-Whitney U test. To compare the imaging parameters between patient groups ANCOVA analysis was used, to adjust for covariates (RVSP and RV length) that possibly confound the association of patient group to the dependent variable. In other words, if the differences in outcome variables between patient groups are completely determined by differences in RVSP or RV length (for strain) – between group analysis with ANCOVA will yield a non-significant result.[13] As a rule of thumb at least 10 subjects are needed for each factor in a multivariable model. Using 3 factors: RVSP, iPAH as a dummy variable and RV length, 30 subjects are needed for analysis. Correlation between continuous parameters was assessed using squared correlation coefficient. Reproducibility was assessed by determining the mean difference with limits of agreement, intra-class correlation coefficient (for absolute agreement) and paired Student T-test. A two-sided alpha level of 0.05 was considered statistically significant. All data analyses were performed using IBM SPSS statistics version 22.0.

Results

Patient characteristics are listed in **Table 1**. There were no significant differences in age, BSA or sex distribution between groups. iPAH patients had higher RVSP and RV:LV pressure ratio compared with PS. Therefore, we corrected all analyses for RVSP as described above. Right bundle branch block was present in none of the PS patients and in 2/18 (11%) of the iPAH patients.

General echocardiographic measurements

Children with iPAH had significantly more dilated RVs compared with healthy controls and PS (**Table 2**). Compared to controls, the RV apex in PS trended to be mildly dilated, but the normal triangular geometry was maintained (**Figure 2**). In contrast, iPAH patients demonstrated spherical RV geometry with significantly higher mid:basal and apical:basal diameter ratio (**Figure 2**). TAPSE and S' were decreased in both patient groups compared to controls (**Table 2**) but did not differ significantly between iPAH and PS (**Table 2**).

Table 1: Patient characteristics

	Controls (n=18)	PS (n=16)	PAH (n=18)	P-value PS vs. iPAH
Age (years)	11.2±5.0	10.3±4.7	11.5±5.6	0.736
BSA (m^2)	1.31±0.44	1.23±0.48	1.16±0.41	0.547
Male sex (%)	10 (56%)	9 (56%)	9 (50%)	0.716
Medication: **- PDE-5 Inhibitor** **- ETR-antagonist** **- Prostaglandins**	None	None	 7 (39%) 13 (72%) 9 (50%)	-
RVSP (mmHg)[1]	-	75.4±18.9	96.8±25.4	0.011
RV : LV pressure ratio1	-	0.71 [0.41 – 1.57]	1.10 [0.46-1.50]	0.007
Heart rate (bpm)	70±12.5	81±17.5	89.2±22.3**	0.261
TR severity n(%) **- None/Trace** **- Mild** **- Moderate** **- Severe**	 18 (100%) - - -	 15 (94%) 1 (6%) - -	 6 (33%) 3 (17%) 5 (28%) 4 (22%)	

*Normally distributed continuous data is presented as mean ± standard deviation and non-normal as median [range]. Normally distributed data of PS and PAH were compared to controls using ANOVA with Dunnet's, Non-normally distributed data using Mann-Whitney U test. Categorical data were compared using Chi-square test. [1] Student T-test was used. *p≤0.05; **p≤0.01; *p≤0.001. PS = pulmonary valve stenosis; iPAH = idiopathic pulmonary hypertension; BSA= body surface area; PDE-5 = prostaglandin diesterase-5; ETR = endothelin receptor; RV = right ventricular; SP = systolic pressure; LV = left ventricular*

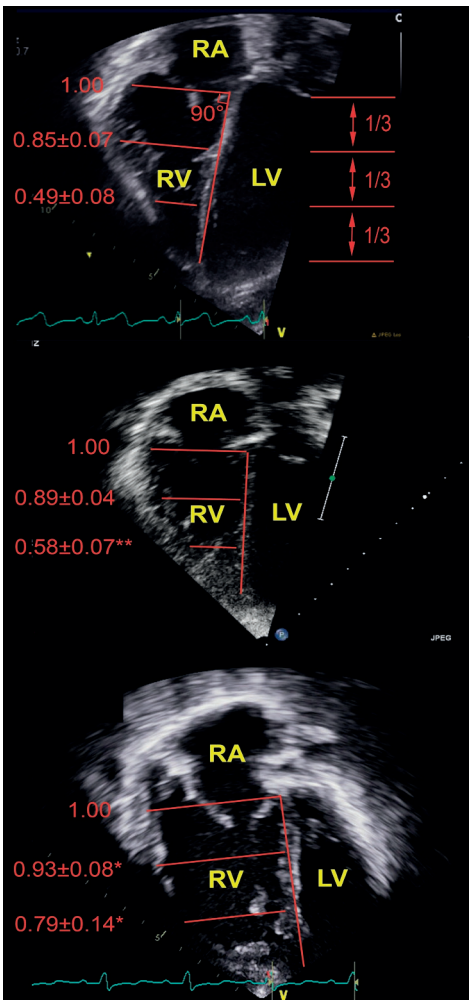

Figure 2: RV geometry

*Mid and apical to basal ratios measured in the modified-RV apical 4-chamber view. Continuous data were normally distributed and represented as mean ± standard deviation. Patient groups are compared to controls using ANOVA with posthoc Dunnet's and to each other using ANCOVA with covariate RVSP; #p≤0.05; **p≤0.01; *p≤0.001. A= controls; B= pulmonary valve stenosis; C= idiopathic pulmonary arterial hypertension. RA= right atrium; RV= right ventricle; LV= left ventricle.*

Measurements of diastolic function were worse in iPAH compared to controls and PS including larger end-diastolic and end-systolic RA area, lower TV E/A ratio and lower TDI E'. TV E and A waves were fused in 1 PS and 3 iPAH patients (**Table 2**). RV E/E' ratio was mildly higher in PS compared to controls and PH patients.

Table 2: Basic echocardiographic measurements

	Healthy (n=18)	PS (n=16)	iPAH (n=18)	P-value PS vs. iPAH
RVDd (mm) **z-score**	18.5 ± 4.4 0.24 ± 1.02	20.3 ± 5.2 1.2 ± 1.56	34.3 ± 9.9* 4.80 ± 2.00*	<0.001 <0.001
LVEDD (mm) **z-score**	42.6±6.6 0.16±0.92	39.2±7.3 -0.53±1.12	31.4±8.1* -3.86±3.26*	0.106 0.011
FAC (%)	47.2 [39.2-53.7]	42.5 [36.7-68.1]	18.5 [8.1-34.3]*	<0.001
RVd basal (mm)	33.5 ± 5.0	34.4 ± 7.4	48.3 ± 10.0*	<0.001
RVd major (mm)	60.4 ± 10.9	56.4 ± 11.2	66.6 ± 12.3	0.007
TDI s' (cm/sec)	12.9 ± 1.9	10.7 ± 1.7**	11.7 ± 2.5	0.233
TAPSE (mm)	21.4 ± 3.2	18.5 ± 2.9#	16.8 ± 4.7**	0.303
RVFS MM (%)	12.00 ± 7.74	31.75 ± 10.35*	-1.62 ± 11.11**	<0.001
RVFW disp (mm)	4.41 ± 0.86	8.50 ± 2.77*	6.27 ± 2.00	0.046
RV TEI index	0.29 ± 0.05	0.25 ± 0.04	0.50 ± 0.13*	<0.001
RA ED area (mm^2)	12.1 ± 3.73	13.8 ± 4.7	20.12 ± 8.7*	0.013
TV E/A ratio[1]	2.37 [1.24-5.44]	1.81 [0.92-2.60]	1.51[0.71-1.69]**	0.022
RA ES area (mm^2)	6.6 ± 2.7	8.1 ± 3.2	13.2 ± 6.8*	0.043
RV TDI e' (cm/sec)	14.2 ± 2.5	13.1 ± 3.6	10.5 ± 3.5**	0.009
RV E/e'	4.1 ± 0.8	6.2 ± 1.0*	4.8 ± 1.5	0.029

*Normally distributed continuous data is presented as mean ± standard deviation and non-normal as median [range]. Normally distributed data of PS and PAH were compared to controls using ANOVA with Dunnet's and to each other using ANCOVA including the covariate RVSP. Non-normally distributed data were compared with Mann-Whitney U test. #p≤0.05; **p≤0.01; *p≤0.001. [1] E/A fusion in 1 PS and 3 iPAH patients; TV inflow was available in 15 controls, 11 PS patients and 13 iPAH patients. RVd = right ventricular dimension; TDI S'= Tissue Doppler imaging Systolic velocity; TAPSE = tricuspid annular systolic excursion; RVFS= Right ventricular fractional shortening; RVFW= right ventricular free wall; RVtr = right ventricular transverse movement slope; RA ES = right atrial end-systolic; RA ED= right atrial end-diastolic*

RVFW transverse shortening

Absolute RVFW transverse displacement was increased in both PS and iPAH patients compared with healthy controls (PS p<0.001&PAH p=0.07) and highest in PS patients (p=0.046). However, the transverse shortening fraction was increased only in PS patients compared with controls (p<0.001; **Table 2 & Figure 1**). In contrast, despite maintained transverse RVFW displacement, transverse shortening fraction was decreased or even reversed in iPAH (-1.62±11.11%; p<0.001) compared with controls and PS patients due to paradoxical leftward septal motion in RV systole.

Longitudinal strain

Strain analysis was feasible in 44 out of 52 subjects (85%). RVFW and IVS longitudinal strain were significantly reduced in iPAH patients compared with PS and controls, independent of RV length and RVSP (**Figure 3a**). That RVSP alone does not adequately explain the differences in longitudinal deformation is also evident in **Figure 4** where at similar RVSP, longitudinal strain in iPAH is lower than PS. Moreover, the correlation between RVSP and RVFW, IVS and RV total strain is opposite in iPAH and PS (**Figure 4**). Longitudinal deformation in PS *increases* with increasing RVSP whereas in iPAH patients it *decreases* with increasing RVSP. RV total and RVFW longitudinal strain in PS patients were comparable to controls while IVS longitudinal strain trended to being mildly reduced vs. controls (p=0.062).

Regional RVFW strain is shown in **Figure 3b**. In healthy controls strain values were comparable in all segments. In both PS and iPAH patients apical RVFW strain was reduced compared with mid (iPAH & PS both p<0.05) and basal segments (PS p<0.01, iPAH not significant p=0.06).

Post-systolic shortening was more frequent and of greater magnitude in iPAH patients compared to PS and controls (**Table 3**). Furthermore, in controls and in PS, post-systolic shortening occurred almost exclusively at the basal segment; whereas in iPAH both the mid and basal segments were affected. In addition, there was significantly more RV intra-ventricular delay – indicated by a larger IVS to RVFW TTP delay in iPAH patients (iPAH 35 [8-169] vs. PS 12[1-69] vs. controls 12 [0-45] ms; p<0.001).

As the mean RVSP was higher in the iPAH group, a sub-analysis was performed in 11 iPAH patients and 15 PS patients with comparable RVSP between 50-110 mmHg, to further control for RVSP. The mean RVSP of these subgroups was iPAH vs. PS 83.8 ± 18.6 mmHg vs. 77.4 ± 17.6 mmHg (p=0.387). Despite similar RVSP, RVFW, IVS and RVtot longitudinal strain were decreased in iPAH compared with PS (15.1±4.8% vs 30.7±1.7% (p<0.001), 10.3±4.6% vs. 17.7±2.5% (p=0.001) and 12.6±4.8% vs. 23.0±1.9% (p<0.001), respectively)

and post-systolic shortening was more frequent in iPAH vs. PS (6 (55%) vs. 0 (0%)). Similarly, RVFS and RV displacement were decreased in iPAH vs. PS (-4.64±11.28% vs. 31.75±10.35% (p<0.001) and 6.00±2.25 mm vs. 8.50±2.77 mm (p=0.034), respectively).

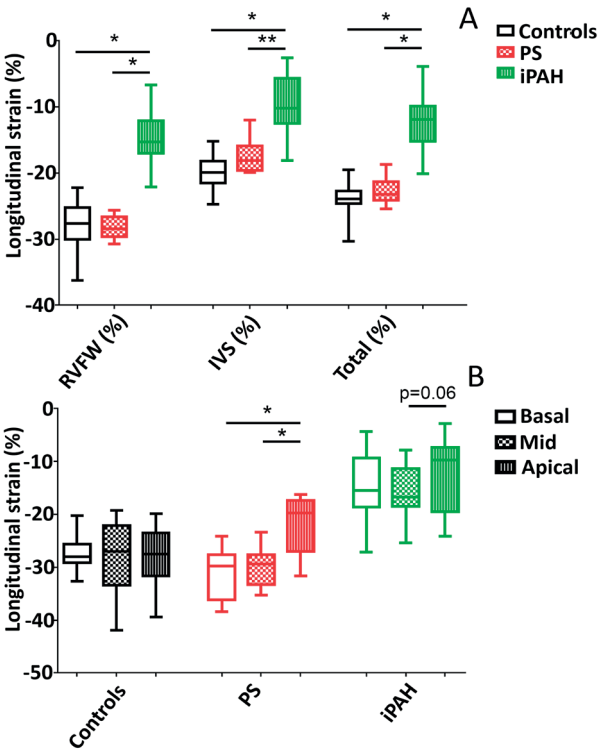

Figure 3a: Differences in global strain between patient groups.
*Patient groups and controls were compared using ANCOVA with RVSP and RV length as covariates.*p<0.001 and **p<0.01.*

Figure 3b: Regional strain differences within patient groups.
*Differences in regional longitudinal strain within each group were assessed using a paired t-test; *p<0.001.*

RVFW= right ventricular free wall; IVS=interventricular septum; PS= pulmonary valve stenosis; iPAH= idiopathic pulmonary arterial hypertension

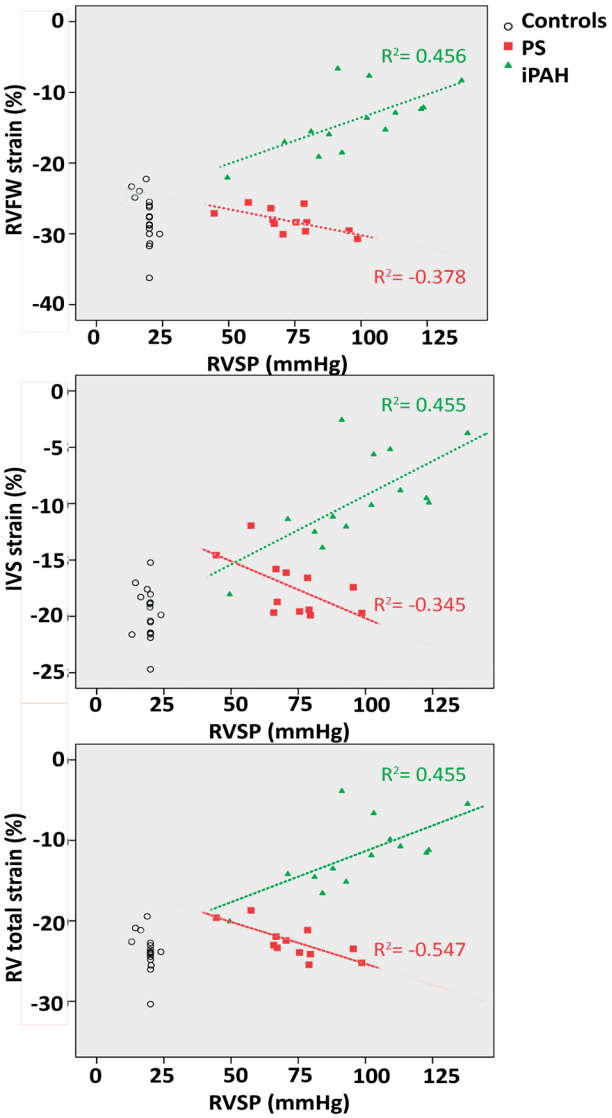

Figure 4: Longitudinal strain vs RVSP

Longitudinal strain of each individual patient plotted against RVSP, healthy controls in black, PS patients in red and iPAH in green. The squared correlation coefficient (R^2) for RVFW, IVS and total RV strain versus RVSP was calculated in PS and iPAH patients. Top: RVFW strain, middle: IVS strain and bottom: RV total.

Table 3: Longitudinal strain analysis

	Healthy (n=17)	PS (N=12)	iPAH (n=15)	
Number of pts				
with PSS (%)	5 (29.4%)	3 (25.0%)	10 (66.7%)#	0.031
- basal	1 (5.8%)	-	10 (66.7%)*	<0.001
- mid	2 (11.8%)	-	2 (13.3%)	0.704
- apical				
Severity of PSS				
(%)	0.9 [0.1-	5.4 [0.6-5.7]	15.4 [0.5-	-
- basal	10.0]	-	45.9]	-
- mid	0.4	-		-
- apical	0.5 & 1.4		4.2 [0.4-18.8]	
			2.9 & 50.2	
RVFW TTP (msec)	444 ± 60	494 ± 59	553 ± 92*	0.063
IVS TTP (msec)	437 ± 64	493 ± 77	562 ± 137**	0.109
RV-IVS diff (msec)	12 [0-45]	12 [1-69]	35 [8-169]**	0.009

*Post-systolic shortening and time to peak longitudinal strain (TTP) compared between all groups. Categorical data were compared using Chi-square test, only apical PSS was assessed using Fisher's exact test. Normally distributed continuous data is presented as mean ± standard deviation and non-normal as median [range]. Normally distributed data of PS and PAH were compared to controls using ANOVA with Dunnet's and to each other using ANCOVA including the covariate RVSP. Non-normally distributed data were compared with Mann-Whitney U test. #p≤0.05; **p≤0.01; *p≤0.001. RVFW= right ventricular free wall; IVS= interventricular septum*

Reproducibility (Table 4)

Intra- and interobserver reproducibility were good for strain measurements and RVFW transverse displacement and fractional shortening. RV apical:basal and mid:basal diameter ratio had good intra-observer, but poor inter-observer agreement.

Table 4: Inter- and Intraobserver reproducibility

	Intra-observer			Inter-observer		
	Mean Δ [Limits]	**p-value**	**ICC**	**Mean Δ [Limits]**	**p-value**	**ICC**
RVFW strain (%)	1.01 [-4.00; 6.11]	p=0.252	0.94*	-0.66 [-6.46; 5.14]	p=0.501	0.93*
IVS strain (%)	-2.10 [-7.59; 3.39]	p=0.042	0.79*	-1.21 [-7.87; 5.45]	p= 0.289	0.83*
RVtot strain (%)	-1.42 [-6.03; 3.19]	p=0.089	0.91*	-1.05 [-6.46; 4.46]	p= 0.268	0.91*
RVFW disp (mm)	0.12 [-1.82; 2.06]	p=0.710	0.96*	-6.7 [-12.2; -1.14]	p<0.001	0.91*
RVFS MM (%)	-1.47 [-10,27; 7.33]	p=0.327	0.93*	2.81 [-12.47; 18.09]	p= 0.285	0.85*
Mid:bas ratio	-0.025 [-0.107; 0.057]	p= 0.09	0.66**	-0.11 [-0.39; 0.07]	p=0.003	NS
Ap:bas ratio	0.033 [-0.109; 0.043]	p= 0.03	0.87*	-0.12 [-0.32; 0.08]	p=0.004	NS

*Mean difference and limits of agreement; significance tested using paired T-test and interclass correlation coefficient (ICC), * p<0.001 and **p<0.01. RV= right ventricular; RVFW= RV free wall; IVS= interventricular septum; RVFS MM= RV fractional shortening on m-mode; mid:bas = mid to basal; ap:bas = apical to basal; NS= not significant*

Discussion

The current study assessed the effect of RV pressure overload on global and regional right ventricular remodeling and function, comparing two distinct patient groups. Our results show that 1) global RV dilation and RV systolic dysfunction in iPAH patients is characterized by: spherical geometry, apical remodeling and dysfunction, decreased longitudinal deformation of both IVS and RVFW and highly inefficient RV kinetics – as evidenced by increased post-systolic shortening and increased IVS-RVFW discoordination – compared to PS and controls. 2) In contrast, PS patients maintain near-normal RV geometry, normal RV cavity size and global systolic function. Nevertheless, they also exhibit mild apical remodeling with a corresponding decrease in regional apical deformation. 3) Transverse shortening is augmented in pediatric PS while effective RV transverse shortening is reduced in pediatric iPAH – suggesting that the iPAH-RV inadequately compensates for the loss in longitudinal function. 4) iPAH patients demonstrate diastolic dysfunction while PS patients have comparable diastolic function to controls. These differences are not entirely explained by differences in RVSP alone and suggest either different RV adaptation or different progression rate of RV disease in iPAH vs. PS – possibly explaining the differences in clinical outcomes.

RV regional remodeling and function

In both PS and iPAH, the RV has to generate a higher RV systolic pressure to eject blood. Higher RV systolic pressure increases RV systolic wall stress – which leads to RV hypertrophy in an attempt to reduce wall stress. If the reduction of wall stress is insufficient – RV dysfunction and dilation will eventually ensue. The RV in iPAH is markedly dilated, and moreover, remodels to a spherical shape, with the most pronounced dilation at the apex. Conversely, although PS patients have mild apical remodeling, they do not exhibit global RV dilation or increased sphericity. This suggests that the RV in PS is adapted better to increased pressure-loading and possibly has reduced wall stress compared to iPAH.

The differences in RV remodeling in iPAH vs. PS are paralleled by worse ventricular performance. Longitudinal RVFW function is the most frequently used vector to assess RV function in clinical practice.[7,14,15] TAPSE and TDI S' are used most frequently and were equally decreased in both pressure overloaded groups compared to controls. In contrast, there are clear differences in overall RV function of PS vs iPAH patients, although TAPSE and TDI S' may still be useful in follow-up of each individual patient group. This finding may relate to more severe tricuspid regurgitation and apical rotation in iPAH, as reported by Motoji et al. to overestimate TAPSE in iPAH.[16,17] In our study, global longitudinal RVFW deformation was worse in iPAH compared to PS and marked post-systolic

shortening – not accounted for by TAPSE and TDI S' – was present exclusively in iPAH. Post-systolic shortening has also been reported in adult iPAH and relates to intra-ventricular dyssynchrony and inefficient RV contraction leading to decreased RV output.[7,18] We further demonstrate that the correlation of RVSP to global longitudinal deformation is divergent in iPAH versus PS: in iPAH higher RVSP corresponds with decreased deformation, while in PS it corresponds with increased deformation. Several possible explanations may account for these differences: RV remodeling and maladaptation is present in iPAH, but not in PS, with progressive dilation.[19] Secondly, more TR in iPAH may contribute to RV dilatation and decreased deformation.[20] Lastly, higher end-systolic wall stress may occur in iPAH vs. PS, akin to higher LV end-systolic wall stress reported in aortic coarctation vs. valvar aortic stenosis.[21]

Analysis of regional RVFW longitudinal deformation shows that apical RVFW longitudinal deformation is decreased in both conditions. This can be explained by apical remodeling in both groups, which – following Laplace's law - will lead to higher regional wall stress and in turn decreased regional deformation. As the volume of the RV apex is proportionally increased, apical remodeling and dysfunction may be an important determinant of RV function and reduced cardiac output. Both our group and Dambrauskaite et al. have previously shown that apical strain is related to disease severity in iPAH.[21-23] Furthermore, Fernandez-Friera et al. demonstrated reduced apical RV ejection fraction – by magnetic resonance imaging – in adult iPAH patients.[24] As apical remodeling and decreased longitudinal deformation were also found in PS – with normal global systolic RV function – it might be a sensitive echocardiographic marker of RV dysfunction.

Transverse RV free wall motion and septal deformation

Reduced longitudinal deformation should ideally be compensated by a commensurate increase in circumferential deformation or transverse function to maintain adequate cardiac output.[9] We assessed this by M-mode, using the RV transverse fractional shortening fraction. In PS patients this measurement was increased, but in iPAH severely decreased, and even paradoxical compared to controls. Therefore, it seems this compensatory mechanism fails in iPAH patients, possibly contributing to RV dysfunction and failure. Transverse RV function was previously related to survival in iPAH by Kind et al.[23] It is important to note that the transverse inward RVFW movement itself trended towards being *increased* in iPAH patients vs. controls and decreased transverse shortening is related to the paradoxical leftward IVS displacement, caused by an adverse septal gradient during prolonged RV free wall shortening.[14] This displacement interferes with efficiency of RV ejection and LV function.[25] Transverse RV fractional shortening could be a simple and easily quantifiable imaging marker for evaluation of RV performance, in addition to conventional

measures. Its relation to parameters of global RV systolic function, such as RV ejection fraction, and inter-test variability need to be further investigated before implementing this measure in clinical practice.

Besides RVFW longitudinal and transverse function, septal deformation and LV contraction contribute to RV ejection.[8,14,26] Longitudinal deformation of the IVS is decreased in pediatric iPAH patients compared to controls and PS, whereas it is maintained in PS patients. Furthermore, iPAH patients show a greater dispersion between IVS and RVFW time to peak systolic deformation, resulting in discoordinated RV contraction (i.e. dyssynchrony).[27] Intraventricular dyssynchrony may be an effect of electromechanical delay – as demonstrated in tetralogy patients – mechanical delay or both. While QRS duration was higher in iPAH patients vs. PS patients, as right bundle branch block was infrequent in our iPAH patients, intraventricular dyssynchrony seems mainly related to mechanical delay in our iPAH cohort. Together with post-systolic shortening and regional dysfunction, this leads to highly inefficient RV contraction.

Pathophysiology

Adverse RV mechanics in iPAH versus PS reflects either faster progression to RV failure in pediatric iPAH patients, a different RV response to pressure load or a combination of both. Our study design cannot determine these pathophysiological mechanisms and further research is clearly needed. However, there are theoretical considerations that might explain the observed differences. Firstly, as discussed above, characteristics of the RV afterload might differ between iPAH and PS. Total RV work is a composite of multiple factors and depends on the properties of the proximal and distal pulmonary vasculature. These properties include pulmonary vascular resistance, compliance and pressure wave reflection. These are worse in iPAH leading to increased RV load.[1,28]

Secondly, the RV response to its given afterload might differ. In PS the RV faces increased pressure load from fetal or early post-natal life. In contrast, in pediatric iPAH postnatal adaptation to low pulmonary resistance has likely already occurred, as many of our results are similar to the results of Jurcut et al in adult patients. The RV encounters increased workload after the neonatal period, requiring adaptation to higher afterload over a much shorter time span.[29] Related molecular differences may determine RV adaption to increased pressure load, which is supported by the usually better RV function seen in Eisenmenger syndrome.[30] Moreover, factors such as RV myocardial ischemia and deranged RV metabolism are likely more prominent in iPAH versus PS.[31] These factors contribute to RV dilation, wall stress, and fibrosis and ultimately worsen oxygen demand/supply mismatch.[31] Fibrosis in itself may differ between the 2 conditions, as it relates to ventricular compliance and diastolic function,

which in our study was largely maintained in PS but impaired in iPAH.[32]

Clinical Implications

Although pulmonary vasodilators have improved survival in iPAH, in many patients the disease progresses and survival depends on RV (dys)function.[33] Thus far, drug treatment in iPAH has been mainly aimed at lowering pulmonary vascular resistance, thereby improving RV function. Moreover, independently of pulmonary vascular resistance, early identification of RV maladaptation and failure remains a challenge. Therefore, early detection and evaluation of RV (apical) dilation, systolic and diastolic dysfunction, increased post-systolic shortening and decreased transverse shortening may identify patients with poorly adapted RVs who are at higher risk of RV failure and death. These parameters should therefore be further assessed in future studies.

Limitations

This was a retrospective study in a relatively small sample with inherent limitations, as some measurements could not be reliably performed (i.e. degree of hypertrophy). Nonetheless, all measurements of systolic RV function were available and differences were highly significant between groups. We used echocardiographic estimates of RVSP and not invasive measurements, as the latter were not routinely available within 6-months of the echocardiogram. Echocardiographic estimates might lead to both over- and underestimation of invasive measurements. TR estimates of RVSP may be overestimated when severe tricuspid regurgitation is present. Likewise, using PV Doppler gradients to estimate RVSP may be inaccurate, but adequate TR to estimate RVSP was not present in most of the PS patients.[34] Furthermore, RVSP was significantly lower in PS vs. iPAH patients, due to interventional thresholds in PS. We accounted for this important difference in 2-ways: 1) We performed linear regression to account for RVSP and 2) we performed additional subgroup analysis in PS and iPAH patients with similar RVSP – all showing consistent results. This was a mechanistic, descriptive study and while the differences in natural history and clinical presentation between PS and iPAH are well recognized[4,11] – and form the very basis for this study – we could not evaluate functional capacity.

Conclusion

In conclusion, children with iPAH demonstrate adverse RV remodeling and mechanics compared to children with PS. This may explain the markedly different natural history and clinical presentation and reflects either a faster progression of RV disease and/or a difference in RV adaptation. In this study, we highlight several mechanisms of RV maladaptation in pediatric iPAH patients that, although potentially applicable in clinical practice, are not routinely used or largely overlooked. These include – post-systolic shortening, apical remodeling, regional strain differences, decreased transverse shortening and diastolic dysfunction. Our results form the basis for further investigation of these parameters as markers of RV failure to identify children at risk of adverse outcome in congenital heart disease and iPAH.

References

1. Di Maria MV, Younoszai AK, Mertens L, et al: RV stroke work in children with pulmonary arterial hypertension: estimation based on invasive haemodynamic assessment and correlation with outcomes. Heart 2014; 100:1342-1347.
2. Valente AM, Gauvreau K, Assenza GE, et al: Contemporary predictors of death and sustained ventricular tachycardia in patients with repaired tetralogy of Fallot enrolled in the INDICATOR cohort. Heart 2014; 100:247-253.
3. van Wolferen SA, Marcus JT, Boonstra A, et al: Prognostic value of right ventricular mass, volume, and function in idiopathic pulmonary arterial hypertension. Eur Heart J 2007; 28:1250-1257.
4. Tinker J, Howitt G, Markman P, et al: The Natural History of Isolated Pulmonary Stenosis. Br Heart J 1965; 27:151-160
5. Haworth SG, Hislop AA: Treatment and survival in children with pulmonary arterial hypertension: the UK Pulmonary Hypertension Service for Children 2001-2006. Heart 2009; 95:312-317.
6. Berger RM, Beghetti M, Humpl T, et al: Clinical features of paediatric pulmonary hypertension: a registry study. Lancet 2012; 379:537-546.
7. Jurcut R, Giusca S, Ticulescu R, et al: Different patterns of adaptation of the right ventricle to pressure overload: a comparison between pulmonary hypertension and pulmonary stenosis. J Am Soc Echocardiogr 2011; 24:1109-1117.
8. Klima U, Guerrero JL, Vlahakes GJ: Contribution of the interventricular septum to maximal right ventricular function. Eur J Cardiothorac Surg 1998; 14:250-255.
9. Pettersen E, Helle-Valle T, Edvardsen T, et al: Contraction pattern of the systemic right ventricle shift from longitudinal to circumferential shortening and absent global ventricular torsion. J Am Coll Cardiol 2007; 49:2450-2456.
10. Driessen MM, Hui W, Bijnens BH, et al: Adverse ventricular-ventricular interactions in right ventricular pressure load: Insights from pediatric pulmonary hypertension versus pulmonary stenosis. Physiol Rep 2016; 4:10.
11. Barst RJ, Ertel SI, Beghetti M, et al: Pulmonary arterial hypertension: a comparison between children and adults. Eur Respir J 2011; 37:665-677.
12. Lopez L, Colan SD, Frommelt PC, et al: Recommendations for quantification methods during the performance of a pediatric echocardiogram: a report from the Pediatric Measurements Writing Group of the American Society of Echocardiography Pediatric and Congenital Heart Disease Council. J Am Soc Echocardiogr 2010; 23:465-95.
13. D'hooge J, Heimdal A, Jamal F, et al: Regional strain and strain rate measurements by cardiac ultrasound: principles, implementation and limitations. Eur J Echocardiogr 2000; 1:154-170.
14. Haddad F, Hunt SA, Rosenthal DN, et al: Right ventricular function in cardiovascular disease, part I: Anatomy, physiology, aging, and functional assessment of the right ventricle. Circulation 2008; 117:1436-1448.
15. Forfia PR, Fisher MR, Mathai SC, et al: Tricuspid annular displacement predicts survival in pulmonary hypertension. Am J Respir Crit Care Med 2006; 174:1034-1041.
16. Weidemann F, Eyskens B, Sutherland GR: New ultrasound methods to quantify regional myocardial function in children with heart disease. Pediatr Cardiol 2002; 23:292-306.

17. Motoji Y, Tanaka H, Fukuda Y, et al: Association of Apical Longitudinal Rotation with Right Ventricular Performance in Patients with Pulmonary Hypertension: Insights into Overestimation of Tricuspid Annular Plane Systolic Excursion. Echocardiography 2016; 33:207-215.
18. Marcus JT, Gan CT, Zwanenburg JJ, et al: Interventricular mechanical asynchrony in pulmonary arterial hypertension: left-to-right delay in peak shortening is related to right ventricular overload and left ventricular underfilling. J Am Coll Cardiol 2008; 51:750-757.
19. Dragulescu A, Grosse-Wortmann L, Redington A, et al: Differential effect of right ventricular dilatation on myocardial deformation in patients with atrial septal defects and patients after tetralogy of Fallot repair. Int J Cardiol 2013; 168:803-810.
20. Kamperidis V, Marsan NA, Delgado V, et al: Left ventricular systolic function assessment in secondary mitral regurgitation: left ventricular ejection fraction vs. speckle tracking global longitudinal strain. Eur Heart J 2016; 37:811-816.
21. Borow KM, Colan SD, Neumann A: Altered left ventricular mechanics in patients with valvular aortic stenosis and coarction of the aorta: effects on systolic performance and late outcome. Circulation 1985; 72:515-522.
22. Dambrauskaite V, Delcroix M, Claus P, et al: Regional right ventricular dysfunction in chronic pulmonary hypertension. J Am Soc Echocardiogr 2007; 20:1172-1180.
23. Okumura K, Humpl T, Dragulescu A, et al: Longitudinal assessment of right ventricular myocardial strain in relation to transplant-free survival in children with idiopathic pulmonary hypertension. J Am Soc Echocardiogr 2014; 27:1344-1351.
24. Fernandez-Friera L, Garcia-Alvarez A, Guzman G, et al: Apical right ventricular dysfunction in patients with pulmonary hypertension demonstrated with magnetic resonance. Heart 2011; 97:1250-1256.
25. Dohi K, Onishi K, Gorcsan J,3rd, et al: Role of radial strain and displacement imaging to quantify wall motion dyssynchrony in patients with left ventricular mechanical dyssynchrony and chronic right ventricular pressure overload. Am J Cardiol 2008; 101:1206-1212.
26. Kind T, Mauritz GJ, Marcus JT, et al: Right ventricular ejection fraction is better reflected by transverse rather than longitudinal wall motion in pulmonary hypertension. J Cardiovasc Magn Reson 2010; 12:35-429X-12-35.
27. Lopez-Candales A, Dohi K, Bazaz R, et al: Relation of right ventricular free wall mechanical delay to right ventricular dysfunction as determined by tissue Doppler imaging. Am J Cardiol 2005; 96:602-606.
28. Mahapatra S, Nishimura RA, Sorajja P, et al: Relationship of pulmonary arterial capacitance and mortality in idiopathic pulmonary arterial hypertension. J Am Coll Cardiol 2006; 47:799-803.
29. Zhang L, Allen J, Hu L, et al: Cardiomyocyte architectural plasticity in fetal, neonatal, and adult pig hearts delineated with diffusion tensor MRI. Am J Physiol Heart Circ Physiol 2013; 304:H246-H252.
30. Hopkins WE, Waggoner AD: Severe pulmonary hypertension without right ventricular failure: the unique hearts of patients with Eisenmenger syndrome. Am J Cardiol 2002; 89:34-38.
31. Bogaard HJ, Natarajan R, Henderson SC, et al: Chronic pulmonary artery pressure elevation is insufficient to explain right heart failure. Circulation 2009; 120:1951-1960.
32. Okumura K, Slorach C, Mroczek D, et al: Right ventricular diastolic performance in children with pulmonary arterial hypertension associated with congenital heart disease: correlation of echocardiographic parameters with invasive reference standards by high-fidelity micromanometer

catheter. Circ Cardiovasc Imaging 2014; 7:491-501.
33. Peacock AJ, Crawley S, McLure L, et al: Changes in right ventricular function measured by cardiac magnetic resonance imaging in patients receiving pulmonary arterial hypertension-targeted therapy: the EURO-MR study. Circ Cardiovasc Imaging 2014; 7:107-114.
34. Ozpel it E, Akdeniz B, Ozpelit EM, et al: Impact of Severe Tricuspid Regurgitation on Accuracy of Echocardiographic Pulmonary Artery Systolic Pressure Estimation. Echocardiography 2015; 32:1483-1490.

Supplementary figure: example of post-systolic shortening

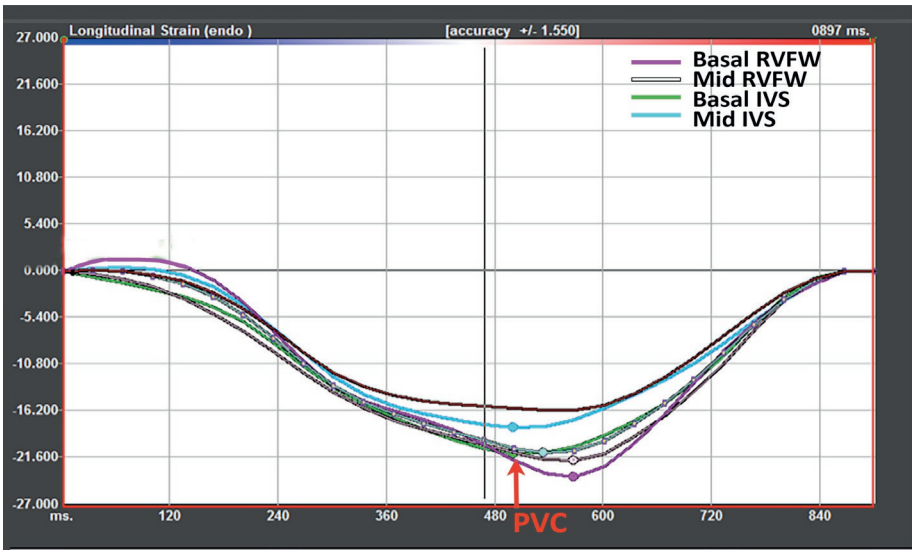

This figure shows the mid and basal strain of the right ventricular free wall (RVFW) and interventricular septum (IVS). The pulmonary valve closure (PVC) is marked by the arrow, shortening occurring after PVC is known as post-systolic shortening (PSS).

Chapter 4

Impact of the pulmonary hypertensive RV on the LV

Left Ventricular Myocardial Function in Children with Pulmonary Hypertension: Relation to Right Ventricular Performance and Hemodynamics

Authors
Dale A. Burkett, Cameron Slorach, Sonali S. Patel, Andrew N. Redington, D. Dunbar Ivy, Luc Mertens, Adel K. Younoszai, Mark K. Friedberg

(adapted from) Circ. Cardiovasc Imaging. 2015; 8(8): pii: e003260

Abstract

Background: Through ventricular interdependence, pulmonary hypertension (PH) induces left ventricular (LV) dysfunction. We hypothesized that LV strain/strain rate, surrogate measures of myocardial contractility, are reduced in pediatric PH and relate to invasive hemodynamics, right ventricular (RV) strain, and functional measures of PH.

Methods and Results: At two institutions, echocardiography was prospectively performed in 54 pediatric PH patients during cardiac catheterization, and in 54 matched controls. PH patients had reduced LV global longitudinal strain (LS) (-18.8 [-17.3 - -20.4]% vs. -20.2 [-19.0 - -20.9]%, P=0.0046) predominantly due to reduced basal (-12.9 [-10.8 - -16.3]% vs. -17.9 [-14.5 - -20.7]%, P<0.0001) and mid (-17.5 [-15.5 - -19.0]% vs. -21.1 [-19.1 - -23.0]%, P<0.0001) septal strain. Basal global circumferential strain (CS) was reduced (-18.7 [-15.7 - -22.1]% vs. -20.6 [-19.0 - -22.5]%, P=0.0098), as were septal and free-wall segments. Mid CS was reduced within the free-wall. Strain rates were reduced in similar patterns. "Basal septum" LS, the combined average LS of basal and mid interventricular septal segments, correlated strongly with degree of PH (r=0.66, P<0.0001), pulmonary vascular resistance (r=0.60, P<0.0001), and RV free-wall LS (r=0.64, P<0.0001). Brain natriuretic peptide levels correlated moderately with septal LS (r=0.48, P=0.0038). PH functional class correlated moderately with LV free-wall LS (r=-0.48, P=0.0051). The septum, shared between ventricles and affected by septal shift, was the most affected LV region in PH.

Conclusions: Pediatric PH patients demonstrate reduced LV strain/strain rate, predominantly within the septum, with relationships to invasive hemodynamics, RV strain, and functional PH measures.

Introduction

While RV failure is an important determinant of morbidity and mortality in PH[1-3], the RV shares muscle fibers, the interventricular septum (IVS), and the pericardial sac with the left ventricle (LV). Consequently, changes in one ventricle affect the other – a concept termed ventricular interdependence.[4-6] Through ventricular interdependence – mediated in part by leftward septal shift – RV dysfunction in PH induces LV dysfunction.[7-13] Though LV dysfunction, particularly altered LV myocardial performance, is emerging as a determinant of outcomes in PH[9], few studies characterize LV function simultaneously with invasive hemodynamics or evaluate the mechanisms of such changes. Likewise, little is known about LV myocardial function and its association with RV function and pulmonary hemodynamics in pediatric PH, including those with congenital heart disease (CHD).

Accordingly, we aimed to define LV segmental myocardial (dys)function in pediatric PH by speckle-tracking echocardiography (STE) performed during cardiac catheterization, and the relationships with RV myocardial function and invasively-determined PH severity. We hypothesized that (1) children and young adults with PH have reduced LV longitudinal and circumferential strain/strain rate, and (2) that such alterations relate to invasive hemodynamics, RV mechanics, and functional PH measures.

Methods

Study Population

Children and adolescents were prospectively enrolled at Children's Hospital Colorado (CHCO) and the Hospital for Sick Children (SickKids) in Toronto. Between November 1, 2008 and October 1, 2013, patients underwent simultaneous transthoracic echocardiography and clinically-indicated right-heart catheterization for initial evaluation of suspected PH or routine follow-up of previously documented pre-capillary PH (mean pulmonary artery pressure ≥25 mmHg, pulmonary capillary wedge pressure [PCWP] ≤15 mmHg at catheterization)[14] under general anesthesia. The study was approved by the Institutional Review Board at both institutions. Informed consent was obtained for all patients.

Sixty-four patients underwent simultaneous catheterization and echocardiography – 44 at CHCO, 20 at SickKids. To avoid confounding LV changes in PH, we excluded single ventricle physiology, actively paced patients, cardiomyopathies, heart transplant, (branch) pulmonary artery stenosis, uncontrolled systemic hypertension, left-sided obstructive lesions or PCWP >15 mmHg.[14] Ten patients were excluded (Supplemental Material), leaving 54 patients – 37 from CHCO, 17 from SickKids.

Right-Heart Catheterization

Right-heart catheterization was performed under general anesthesia, by individuals blinded to echocardiographic measurements. Cardiac index was either measured (thermodilution) or calculated (modified Fick equation); pulmonary (Qp) and systemic (Qs) blood flow were documented. We measured right atrial, RV, pulmonary artery, PCWP and/or left atrial, and systemic arterial pressures (Supplemental Material). Pulmonary vascular resistance was indexed to body surface area (PVRi).

Echocardiography

During the baseline condition of cardiac catheterization with the catheter in the main pulmonary artery, we performed echocardiography optimized for STE strain imaging,[15] using a General Electric (GE) Vivid 7 or E9 (GE Healthcare, USA). Images included apical four- and two-chamber views, and LV parasternal short-axis views at the "base" (mitral valve), "mid" (papillary muscles) and "apex" (apical to papillary muscles). We calculated Simpson's biplane LV ejection fraction (EF) and volumes,[16] and eccentricity index (mid parasternal short-axis).[17] All measurements were performed on 3-5 cardiac cycles and results averaged.

Speckle-Tracking Echocardiography

For STE analysis (EchoPAC version 113, GE Healthcare), endomyocardial borders were traced on two-dimensional images with the region of interest adjusted to myocardial wall thickness. RV free-wall (RVFW) and LV (IVS included as part of the LV analysis) longitudinal strain (LS) and strain rate (LSR) were assessed from the apical four-chamber view, dividing each wall into 3 segments: basal, mid, and apical. LV circumferential strain (CS) and strain rate (CSR) were assessed at the parasternal short-axis base, mid and apex, each divided into 6 segments: anteroseptal (1), anterior (2), lateral (3), posterior (4), inferior (5), septal (6). Wall tracking was visually assessed throughout the cardiac cycle and the region of interest adjusted as needed to ensure accurate tracking.[18] If ≥4 segments tracked well (visually and by EchoPAC assessment), the curve was accepted and segments that tracked poorly were not analyzed.

Ensuring similar heart rates to images used for strain, aortic valve closure (from pulsed-wave Doppler) defined end-systole. We documented peak systolic strain (before/at aortic valve closure) for (1) individual segmental strain curves and (2) global strain (average of peak systolic strain from segments tracking well). In 70.0% of strain analyses, 2-4 consecutive heartbeats were analyzed and averaged to account for beat-to-beat variability; in 20.4%, one beat was available for analysis; 9.6% were inadequate for analysis; RV and LV image quality were similar. In total, 595 strain analyses were completed for the 54 study patients. Apical minus basal rotation at aortic valve closure provided twist, indexed to LV length to provide torsion. Peak apical minus basal systolic rotation rates provided peak twist rate, indexed to LV length to provide torsion rate.

Demographics & Functional Classification

We documented PH etiology, CHD (and repair), intra-/extra-cardiac shunting, medications, and plasma brain natriuretic peptide (BNP; CHCO patients) at the time of catheterization. World Health Organization (WHO) functional classifications documented <6 months from catheterization were recorded. Transplant and death status were collected at study completion. Predicted 1-, 3-, and 5-year survival for PH patients was estimated using the Pulmonary Hypertension Connection equation.[19,20]

Control Population

Echocardiograms were obtained on 54 (37 at CHCO, 17 at SickKids) age-, gender- and institution-matched healthy children who were volunteers or underwent evaluation for murmur, chest pain, palpitations, syncope, or family history of CHD, with a normal medical history (Supplemental Material) and echocardiogram.[16] Analyses followed the same protocol as study patients. No controls underwent catheterization.

Reproducibility

A single observer (D.B.) analyzed echocardiograms for all PH patients and CHCO controls; a separate observer (C.S.) analyzed echocardiograms for SickKids controls. Both observers were blinded to clinical and catheterization data. To assess interobserver variability, SickKids PH echocardiograms (31.5% of PH patients) were re-analyzed by a second observer (C.S.). To assess intraobserver variability, 10% of all echocardiograms were re-analyzed at least 8 weeks apart.

Statistical Analysis

Data were not normally distributed when assessed by the Shapiro-Wilk test. Continuous data are presented as median with interquartile range (unless otherwise noted); categorical data are presented as frequencies (%). Comparative analysis was performed using Wilcoxon Mann-Whitney and Chi-square testing as appropriate. Exact methods were utilized as necessary. Spearman correlation coefficients were used to assess relationships between LV mechanics, invasive hemodynamics, RV mechanics, and functional PH measures. Some significant relationships identified through correlation analyses were re-evaluated using regression analysis to control for potential confounders. Inter-rater and intra-rater reliability were calculated using intraclass correlation coefficients with 95% confidence interval (CI). Given multiple comparisons between PH and controls, a *P*-value of <0.01 was considered significant. Statistical analyses used SAS software, version 9.3 (SAS Corporation, Cary, NC).

Results

Patient Characteristics

Patient characteristics are presented in **Table 1**. In total, 108 subjects were analyzed: 54 PH patients and 54 controls. The only study patient <1 year-old (7 months) did not have PH on initial evaluation so he and his matched control were not used in comparisons between PH versus controls. Most patients were female (34/53, 64.2%) and born with CHD (33/53, 62.3%) (Supplemental Material). Some (21/53, 39.6%) had a potentially active shunt at catheterization; these patients had a median Qp:Qs of 1.16 (1.00 – 1.55). One quarter (14/53, 26.4%) of patients had idiopathic PH. “Other” etiologies included CHD, lung disease/hypoxia, hematologic disorders, chronic thromboembolism, or combination of etiologies.

Table 1. Patient Characteristics

	PH Patients (n = 53)	Control Subjects (n = 53)	*P*-Value
Age, yr (range)	8 (0 - 23)	8 (0 - 23)	0.99
Female, n (%)	34 (64.2%)	34 (64.2%)	1.00
Weight, kg	32.5 (14.7 - 51.4)	30.6 (16.3 - 54.8)	0.67
Height, cm	133.0 (98.0 - 161.0)	136.0 (104.5 - 162.0)	0.60
Body Surface Area, m^2	1.12 (0.63 - 1.52)	1.10 (0.69 - 1.57)	0.68
Heart Rate, bpm	81 (70 - 100)	79 (65 - 93)	0.33
Congenital Heart Disease, n (%)	33 (62.3%)	...	...
Shunt Present at Catheterization	21 (39.6%)	...	...
Idiopathic PH, n(%)	14 (26.4%)		
World Health Organization Class, n (%)			
Not Available	15 (28.3%)	...	...
I / II	15 (28.3%) / 16 (30.2%)	...	...
III / IV	6 (11.3%) / 1 (1.9%)	...	...
Cardiac Catheterization			
MPAP, mm Hg	33.0 (25.0 - 43.0)	...	...
MAP, mm Hg	58.0 (55.0 - 63.0)	...	...
MPAP/MAP	0.59 (0.42 - 0.72)	...	...
SPAP, mm Hg	52.0 (38.0 - 63.0)	...	...
DPAP, mm Hg	23.0 (15.0 - 32.0)	...	...
Transpulmonary Gradient, mmHg	23.0 (16.0 - 35.0)	...	...
Diastolic Transpulmonary Gradient, mm Hg	13.0 (6.0 - 26.0)	...	...
Mean RAP, mm Hg	7.0 (5.0 - 8.0)	...	...
Cardiac Index, L/min/m^2	3.38 (2.98 - 3.82)	...	...
Qp/Qs	1.00 (1.00 - 1.00)	...	...
PVRi, WU·m^2	6.79 (4.10 - 10.89)	...	...
PVR/SVR	0.37 (0.25 - 0.60)	...	...
Echocardiography			
LV End-Diastolic Volume, ml	52.0 (26.0 - 90.0)	49.0 (29.0 - 79.5)	0.86
Indexed LV End-Diastolic Volume, ml/m^2	44.3 (37.2 - 59.8)	37.9 (32.8 - 48.4)	0.07
LV End-Systolic Volume, ml	19.0 (12.0 - 46.0)	16.5 (9.5 - 27.5)	0.27
Indexed LV End-Systolic Volume, ml/m^2	20.3 (14.2 - 28.1)	12.9 (9.8 - 16.5)	0.0006*
LV Ejection Fraction, %	56.0 (50.0 - 63.0)	66.0 (62.0 - 69.0)	<0.0001*
LV End-Diastolic Eccentricity Index	1.18 (1.09 - 1.28)	1.02 (0.96 - 1.06)	<0.0001*
LV End-Systolic Eccentricity Index	1.27 (1.11 - 1.50)	0.99 (0.96 - 1.03)	<0.0001*

Caption on next page

Presented as n (%) or median (interquartile range), unless otherwise noted. PH indicates pulmonary hypertension; MPAP, mean pulmonary artery pressure; MAP, mean arterial (systemic) pressure; SPAP, systolic pulmonary artery pressure; DPAP, diastolic pulmonary artery pressure; RAP, right atrial pressure; Qp/Qs, pulmonary-to-systemic blood flow ratio; PVRi, indexed pulmonary vascular resistance; PVR/SVR, pulmonary-to-systemic vascular resistance ratio; LV, left ventricle.

Most PH patients (47/53, 88.7%) were on single (15/53, 28.5%), dual (12/53, 22.6%), triple (9/53, 17.0%), or quadruple (20.7%, 11/53) medical therapy. Medications included: phosphodiesterase type 5 inhibitors (35/53, 66.0%), endothelin receptor antagonists (26/53, 49.1%), prostacyclin analogues (18/53, 34.0%), anticoagulants (15/53, 28.3%), calcium channel blockers (12/53, 22.6%), supplemental oxygen (10/53, 18.9%), and digoxin (1/53, 1.9%). There was 1 lung transplant and 1 death during the study period. Estimated 1-, 3-, and 5-year survival rates were 94.7 (92.7-96.8)%, 85.0 (79.5-90.6)%, and 76.3 (68.3-84.9)% (respectively).

Cardiac index was preserved in PH patients and did not correlate with mean pulmonary artery pressure (r=0.06, P=0.67) or PVRi (r=-0.27, P=0.07). LV eccentricity index was increased in PH patients, consistent with leftward septal shift. Indexed LV end-systolic volume was larger in PH patients, despite controlling for shunts. LV EF was decreased in PH patients compared to controls, though within normal limits. Comparison of CHCO and SickKids controls demonstrated no differences in global strain measures (P>0.05 for all).

1) Ventricular Mechanics

Longitudinal Strain/Strain Rate

Representative strain curves are shown in **Figure 1**. LS data are shown in **Table 2**, LSR data in **Supplemental Table 1**. LV global and IVS LS were decreased, as were basal and mid IVS segments. Mid IVS segment LSR was reduced. LS was decreased in the RVFW and its 3 segments. Basal and mid RVFW segments' LSR were reduced.

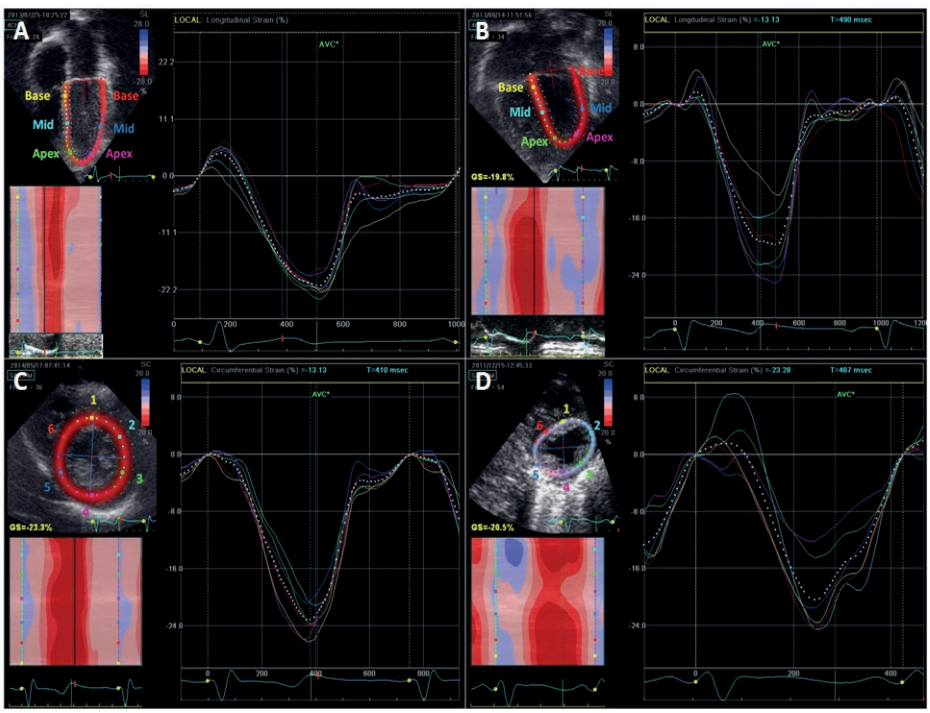

Figure 1

Representative left ventricular strain curves. (A-B), Longitudinal strain, of control (A) and pulmonary hypertension (B) patients. (C-D), Mid circumferential strain, of control (C) and pulmonary hypertension (D) patients.

Table 2. Left and Right Ventricular Longitudinal Strain

Longitudinal Strain, %	PH Patients (n=53)	Control Subjects (n=53)	P-Value
LV Global	-18.8 (-17.3 - -20.4)	-20.2 (-19.0 - -20.9)	0.0046*
LV Free-Wall	-20.5 (-17.9 - -22.2)	-19.9 (-17.9 - -21.0)	0.30
Basal	-20.6 (-17.5 - -23.5)	-18.9 (-16.3 - -22.5)	0.24
Mid	-18.0 (-14.9 - -20.8)	-18.0 (-16.0 - -21.2)	0.61
Apical	-22.2 (-18.4 - -26.1)	-22.0 (-18.6 - -24.5)	0.31
IVS	-17.0 (-15.3 - -19.5)	-20.8 (-19.4 - -22.2)	<0.0001*
Basal	-12.9 (-10.8 - -16.3)	-17.9 (-14.5 - -20.7)	<0.0001*
Mid	-17.5 (-15.5 - -19.0)	-21.1 (-19.1 - -23.0)	<0.0001*
Apical	-23.4 (-19.1 - -26.2)	-23.0 (-20.7 - -26.0)	0.84
RVFW	-21.5 (-18.5 - -25.4)	-29.1 (-26.6 - -33.8)	<0.0001*
Basal	-23.6 (-18.4 - -28.3)	-30.4 (-24.1 - -36.0)	0.0002*
Mid	-22.7 (-20.1 - -26.8)	-30.5 (-27.1 - -35.8)	<0.0001*
Apical	-19.1 (-13.0 - -22.8)	-28.2 (-23.6 - -32.0)	<0.0001*

Presented as median (interquartile range). PH indicates pulmonary hypertension; LV, left ventricle; IVS, interventricular septum; RVFW, right ventricular free-wall.

Circumferential Strain/Strain Rate

LV CS data are shown in **Table 3**, CSR data in **Supplemental Table 2**. Basal CS was decreased globally, and within septal (6) and lateral (3) segments, with trends towards reduction within the septum – comprised of both septal (6) and anteroseptal (1) segments. Basal CSR was reduced within the septum and the septal (6) segment, with a trend towards reduced lateral (3) CSR.

Mid CS was reduced in the lateral (3) segment, with trends towards reduction in the posterior (4) segment and the free-wall – comprised of anterior (2), lateral (3), posterior (4) and inferior (5) segments. There were no significant changes in mid CSR.

Apical CS and CSR were unchanged in PH patients.

Table 3. Left Ventricular Circumferential Strain

Circumferential Strain, %	PH Patients (n=53)	Control Subjects (n=53)	*P*-Value
Basal			
Global	-18.7 (-15.7 - -22.1)	-20.6 (-19.0 - -22.5)	0.0098*
Septum (6, 1)	-22.0 (-16.6 - -24.7)	-24.1 (-21.0 - -28.1)	0.0140
Septal (6)	-19.7 (-14.5 - -24.7)	-23.2 (-20.9 - -27.7)	0.0009*
Anteroseptal (1)	-23.8 (-18.8 - -26.7)	-24.4 (-21.2 - -30.5)	0.14
Free-Wall (2, 3, 4, 5)	-17.1 (-14.8 - -21.3)	-19.3 (-16.6 - -21.2)	0.057
Anterior (2)	-21.5 (-14.6 - -26.7)	-20.9 (-16.6 - -24.0)	0.68
Lateral (3)	-12.9 (-9.0 - -18.1)	-19.5 (-16.0 - -21.0)	0.0002*
Posterior (4)	-13.6 (-8.5 - -19.1)	-18.0 (-12.4 - -20.4)	0.057
Inferior (5)	-17.7 (-13.1 - -23.1)	-18.8 (-14.7 - -24.0)	0.38
Mid			
Global	-19.4 (-16.8 - -20.8)	-19.7 (-17.8 - -21.3)	0.20
Septum (6, 1)	-23.1 (-19.6 - -26.0)	-23.4 (-19.5 - -25.8)	0.87
Septal (6)	-22.0 (-18.3 - -24.7)	-23.0 (-20.6 - -25.4)	0.21
Anteroseptal (1)	-23.4 (-19.9 - -26.6)	-23.0 (-20.0 - -26.0)	0.70
Free-Wall (2, 3, 4, 5)	-17.2 (-14.4 - -19.6)	-18.8 (-16.6 - -19.8)	0.0493
Anterior (2)	-23.1 (-18.5 - -25.8)	-21.2 (-19.0 - -24.2)	0.32
Lateral (3)	-15.2 (-12.7 - -17.4)	-17.6 (-14.3 - -20.8)	0.0033*
Posterior (4)	-12.6 (-10.1 - -16.3)	-16.0 (-12.3 - -18.3)	0.0237
Inferior (5)	-18.9 (-13.8 - -21.6)	-19.0 (-15.7 - -21.0)	0.66
Apical			
Global	-22.5 (-19.7 - -25.8)	-22.0 (-19.5 - -24.2)	0.35
Septum (6, 1)	-23.0 (-20.1 - -26.7)	-23.4 (-18.7 - -26.2)	0.72
Septal (6)	-22.4 (-18.6 - -26.7)	-23.5 (-18.3 - -25.9)	0.95
Anteroseptal (1)	-24.3 (-20.5 - -26.3)	-23.0 (-19.0 - -26.0)	0.33
Free-Wall (2, 3, 4, 5)	-23.0 (-19.1 - -26.3)	-20.5 (-18.3 - -24.5)	0.26
Anterior (2)	-26.3 (-20.6 - -30.5)	-23.9 (-20.0 - -28.0)	0.0475
Lateral (3)	-22.8 (-16.4 - -26.7)	-21.0 (-16.4 - -26.0)	0.58
Posterior (4)	-20.2 (-15.8- -25.0)	-20.5 (-16.0 - -24.7)	0.99
Inferior (5)	-22.1 (-18.2 - -26.3)	-22.7 (-18.2 - -25.0)	0.59

Presented as median (interquartile range). PH indicates pulmonary hypertension.

Rotational Mechanics

There were non-significant trends towards increased torsion (1.47 [1.03-2.08] vs. 1.27 [0.69-1.59]^0/cm, *P*=0.08) and torsion rate (15.09 [11.76-22.13] vs. 11.60 [9.82-20.08]^0/cm/s, *P*=0.06) in PH.

Sub-group Analysis

Separating PH patients by presence of CHD or an active shunt revealed no differences in LV mechanics between groups (*P*>0.05 for all). Separating PH patients with shunts (n=21) by those with pre- versus post-tricuspid valve shunts revealed no differences in LV mechanics (P>0.05 for all); those with right-to-left shunts had pre-tricuspid valve shunts.

To quantify ventricular dysfunction with increasingly severe PH, patients were separated into quartiles by the ratio of pulmonary-to-systemic mean arterial pressures (MPAP/MAP) - a more meaningful representation of PH in children than pulmonary pressures alone. Median MPAP/MAP (1.00 [0.81-1.04]) and PVRi (15.8 [11.7-19.1]WU·m^2) for the most severe quartile (Quartile 4) were significantly higher than each of the other three quartiles (*P*<0.0001 for both). Cardiac index was similar across quartiles (*P*>0.05). Quartile 4, compared to each of the other quartiles (**Figure 2**) and to controls (**Supplemental Table 3**), demonstrated reduced IVS (including basal and mid segments) and RVFW LS; LV free-wall trended towards increased LS compared to controls (*P*=0.0354). CS measures did not vary significantly between quartiles, but the basal lateral (3) segment was decreased compared to matched controls.

As PVRi often guides clinical decisions, patients were separated into mild (<5), moderate (5-8), and significant (>8) PVRi elevation tertiles to identify potential strain differences. Basal IVS and RVFW LS were reduced with at least moderately elevated PVRi (≥5), compared to PVRi <5 (**Figure 3**). The highest PVRi tertile also demonstrated significantly reduced mid IVS and IVS LS compared to those with PVRi <5.

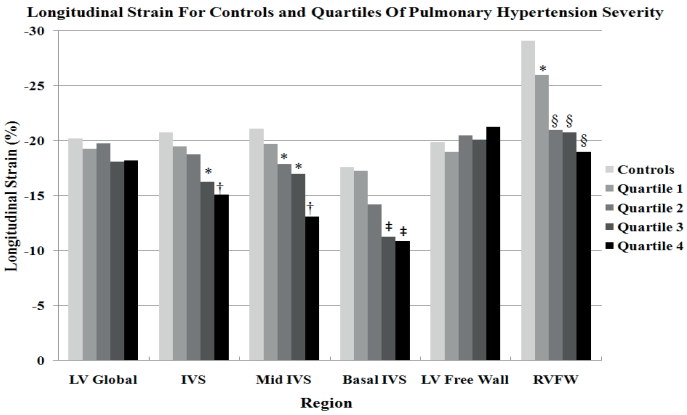

Figure 2.

*Bar graph demonstrating regional median longitudinal strain for controls and pulmonary hypertension quartiles (based on mean pulmonary-to-systemic arterial pressure ratio). Comparisons are between quartiles and all controls, as matched controls for each quartile were not different from the entire control cohort (P>0.05 for all). * indicates quartile is significantly different from controls (P<0.007); † indicates quartile 4 significantly different than all other quartiles and controls (P<0.009); ‡ indicates quartiles 3 and 4 significantly different than 1, 2 and controls (P<0.0004); § indicates quartiles 2, 3, and 4 significantly different than 1 and controls. LV indicates left ventricle; IVS, interventricular septum; RVFW, right ventricular free-wall.*

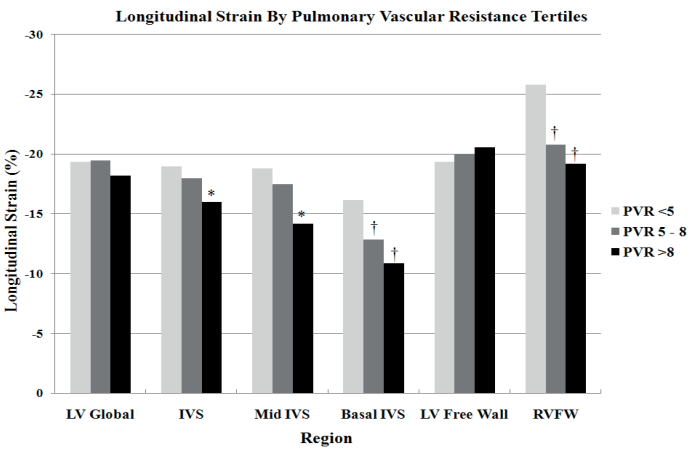

Figure 3.

*Bar graph demonstrating regional median longitudinal strain in pulmonary hypertension patients divided by pulmonary vascular resistance tertiles. * indicates tertile 3 is significantly different from 1 and 2 (P<0.005); † indicates tertile is significantly different from tertile 1 (P<0.006).*

2) LV Free-Wall and Septal Strain Relationships

Invasive Hemodynamics, RV Mechanics, and LV Strain

Correlations between MPAP/MAP or PVRi, RVFW LS, and LV strain are presented in **Figure 4** and **Table 4**; for **Table 4**, Bonferoni's correction was used to lower significance to $P<0.001$. Strong correlations were seen between invasive measures and basal septum LS – an average of the longitudinal strains of basal and mid IVS segments; moderate correlations were seen with IVS and RVFW LS.

Basal septum LS correlated strongly with MPAP/MAP ($r=0.68$, $P<0.0001$) and moderately with PVRi ($r=0.57$, $P=0.0001$) after adjusting for RVFW LS, and strongly with MPAP/MAP ($r=0.62$, $P<0.0001$) after adjusting for both RVFW LS and eccentricity index. RVFW LS correlated strongly with septal and basal septum LS, and moderately with LV global LS. RVFW LS correlated weakly with the following CS measures: basal global and septum, and the septal (6) and lateral (3) segments. Trends were seen with mid CS measures; there were no correlations with apical CS ($P>0.05$ for all).

Systolic eccentricity index correlated moderately with mid IVS segment ($r=0.57$, $P=<0.0001$) and basal septum ($r=0.46$, $P<0.0001$) LS, and weakly with basal IVS segment LS ($r=0.35$, $P=0.0011$) and CS of the basal septum ($r=0.34$, $P=0.0017$), basal septal (6) segment ($r=0.30$, $P=0.0074$) and anteroseptal (1) segment ($r=0.32$, $P=0.0032$).

Functional Measures and Ventricular Strain

BNP levels correlated moderately with IVS LS ($r=0.48$, $P=0.0038$), but neither free-wall. WHO functional classification correlated moderately with RVFW LS ($r=0.44$, $P=0.0089$) and (inversely) with LV free-wall LS ($r=-0.48$, $P=0.0051$). LV free-wall LS correlated strongly with expected 5-year survival in those with the most severe PH (Quartile 4) ($r=-0.85$, $P=0.0008$).

Reproducibility

Intraobserver intraclass correlation coefficients (95% CI) were: RV global LS = 0.99 (0.99-0.99); LV global LS = 0.87 (0.71-0.95); basal global CS = 0.93 (0.83-0.98); mid global CS = 0.94 (0.85-0.97); apical global CS = 0.91 (0.81-0.97). Interobserver intraclass correlation coefficients (95% CI) were: RVFW = 0.72 (0.50-0.86); LV global LS = 0.70 (0.41-0.86); basal global CS = 0.75 (0.52-0.88); mid global CS = 0.60 (0.32-0.79); apical global CS = 0.90 (0.80-0.96).

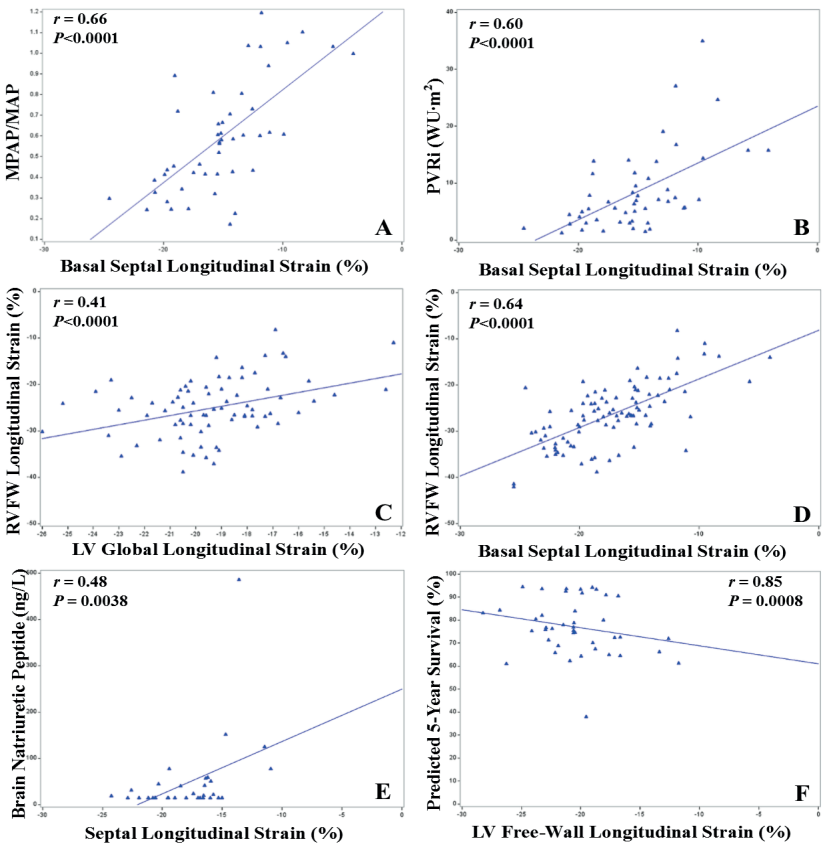

Figure 4.

Relations between LV strain, invasive hemodynamics and RVFW strain. A, MPAP/MAP vs. basal septal LS. B, PVRi vs. basal septal LS. C, RVFW LS vs. LV global LS. D, RVFW LS vs. basal septal LS. E, Brain natriuretic peptide vs. septal LS. F, Predicted 5-year survival for Quartile 4 vs. LV free-wall LS. LV indicates left ventricle; RVFW, right ventricular free-wall; MPAP/MAP, mean pulmonary-to-systemic arterial pressure; LS, longitudinal strain; PVRi, indexed pulmonary vascular resistance.

Table 4. Correlations between LV Strain, Invasive Hemodynamics and RVFW Strain

Strain Variable	MPAP/MAP		PVRi, WU·m2		RVFW Strain, %	
	r	*P*-Value	*r*	*P*-Value	*r*	*P*-Value
Longitudinal Strain, %						
LV Global	0.16	0.28	0.19	0.18	0.41	<0.0001*
LV Free-Wall	-0.30	0.0391	-0.21	0.15	-0.02	0.82
IVS	0.50	0.0003*	0.48	0.0003*	0.62	<0.0001*
Basal Septal	0.66	<0.0001*	0.60	<0.0001*	0.64	<0.0001*
RVFW	0.55	<0.0001*	0.50	0.0002*	...	...
Circumferential Strain, %						
BASAL - Global	0.06	0.71	0.13	0.40	0.37	0.0004*
Septum (6, 1)	-0.07	0.67	0.002	0.99	0.37	0.0004*
Septal (6)	-0.16	0.30	-0.06	0.68	0.35	0.0009*
Anteroseptal (1)	0.04	0.82	0.05	0.75	0.33	0.0014
Free-Wall (2, 3, 4, 5)	0.17	0.28	0.25	0.09	0.23	0.0305
Lateral (3)	0.31	0.06	0.15	0.38	0.38	0.0005*
MID - Global	0.15	0.30	0.30	0.0349	0.26	0.0127
Septum (6, 1)	0.16	0.30	0.31	0.0304	0.27	0.0077
Septal (6)	0.08	0.30	0.28	0.0501	0.24	0.0215
Anteroseptal (1)	0.25	0.82	0.33	0.0201	0.26	0.0128
Free-Wall (2, 3, 4, 5)	0.09	0.54	0.15	0.29	0.14	0.18
Lateral (3)	0.37	0.0105	0.27	0.056	0.25	0.0147
Posterior (4)	0.15	0.32	0.12	0.40	0.29	0.0066

*P<0.001 considered significant. Basal septal indicates an average longitudinal strain of basal and mid IVS segments. IVS indicates interventricular septum; LV, left ventricle; MPAP/MAP, mean pulmonary-to-systemic arterial pressure ratio; PVRi, indexed pulmonary vascular resistamce; and RVFW, right ventricular free-wall. *P<0.001*

Discussion

Using simultaneous STE and cardiac catheterization, we evaluated segmental LV strain/strain rate in pediatric PH, and relations to invasive hemodynamics, RV mechanics, and functional PH measures. Our main findings are the following: (1) LV myocardial mechanics, primarily within the septum, are altered in pediatric PH; (2) altered LV myocardial mechanics are associated with invasive hemodynamics, RV myocardial function, and functional PH measures.

Altered LV Mechanics

Though decreased compared to controls, EF was within normal limits in PH, as was cardiac index, and yet LV strain/strain rate were reduced, primarily at the basal septum. Though this requires further study, LV strain could be an earlier marker of LV dysfunction in this setting, consistent with literature in PH and other conditions.[8,9,21,22]

Reduced LV global LS was predominantly due to decreased basal and mid IVS segment LS, as the apex and free-wall were preserved. Septal strain progressively decreased with worsening PH. Nonetheless, reduced CS in free-wall segments suggests LV involvement beyond the septum, consistent with observations in adult PH.[8] CS generally demonstrated smaller reductions than LS, and minimal differences in severe PH. Leftward septal shift or other interventricular interactions may affect longitudinal fibers more than circumferential and predominate in severe PH. These changes occurred independent of an active shunt, CHD, or a post-tricuspid valve shunt, though all patients with right-to-left shunts had pre-tricuspid valve shunts.

A smaller apical cavity radius imparting less wall-stress, or that the apex shares less septum with the dysfunctional RV apex[23,24], might explain preserved LV apical mechanics. Rotational mechanics were also preserved, in contrast to findings in adult PH .[8] Although our pediatric population generally had less severe PH than published adult populations[8,9], which could explain preserved mechanics, we still observed reduced LV septal (more so than free-wall) mechanics.

Possible etiologies for the observed changes include reduced LV filling, geometric changes, and altered myocardial contractility. Smaller LV volumes in adult PH suggest reduced filling.[8-10] We unexpectedly found larger indexed end-systolic volumes despite age- and gender-matching. A lower EF in PH patients may result in larger end-systolic volumes. Still, LV filling is likely altered by leftward septal shift and/or reduced RV output[7,10-13], which might account for strain (which is load-dependent) being more altered than strain rate (less load-dependent).

Myocardial injury could also impair mechanics. LV fibrosis develops in experimental RV pressure-loading[25], while LV free-wall atrophy, decreased myosin-based cross-bridges, and fibrosis/edema are seen in chronic adult PH.[26] The distribution of such changes and presence in pediatric PH require further study.

LV Free-Wall and Septal Strain Relationships

The strongest correlations with RVFW strain, and only LV correlations with invasive hemodynamics, occurred with LS of the basal septum, which shifts leftward in PH. Eccentricity index, which quantifies this septal shift, also correlated with basal septum strain, supporting an association between LV geometry and myocardial mechanics. Basal septum LS correlated with invasive hemodynamics even after adjusting for both RV strain and septal shift, suggesting direct pressure-loading effects on septal function. CS demonstrated weaker relationships than LS, and correlated with RVFW strain, perhaps reflecting that superficial, circumferentially-oriented fibers are shared with the RV.

Although basal septal strain was substantially reduced in severe PH, increased free-wall LS maintained global LS within normal limits. Increasing LV free-wall LS correlated with worsening WHO functional class and predicted survival in severe PH, suggesting LV free-wall longitudinal function may impact outcomes in severe PH by compensating for septal dysfunction to maintain LV pump function. Additionally, although BNP levels are not associated with basic LV echocardiographic parameters in PH[27], they correlated with septal strain here, possibly suggesting increased wall stress in the flattened septum.

To separately evaluate the RV and LV, some have excluded the IVS.[9] However, this region was one of the most affected in PH and correlated better with invasive hemodynamics and functional measures than other regions, including the RVFW.

Study liminations

Although pediatric studies commonly have low patient numbers, this study is larger than many regarding PH. Few deaths/transplants limited our ability to evaluate relationships with these outcomes. We attempted to predict survival using available estimates, recognizing these have not been validated in children. Though heterogeneous, our patients reflect the pediatric PH population. Patients presented to tertiary care centers for clinically indicated catheterization, potentially introducing selection bias. However, the hemodynamic range suggests a mixture of well-, and poorly-controlled PH.

Though we attempted to have a consistent catheterization protocol between sites, differences were present. SickKids utilized Millar catheters for RV pressure measurements; otherwise, fluid-filled catheters were used at both locations. Oxygen consumption was measured by mass spectrometry at SickKids and estimated by the LaFarge table at CHCO. Both methods are compliant with respective institutional practice, accepted standards of care, and used to guide PH management. Over-/under-wedged PCWP affects estimations of left atrial pressure. However, wedge pressures are accepted estimations of mean left atrial pressure during right heart catheterization, and mean left atrial pressure was preferentially used when obtained.

Though all PH patients were under general anesthesia, we did not dictate the induction, maintenance, or duration. Subtle differences in anesthetics and ventilation strategies could potentially affect hemodynamics, and thus strain/strain rate and comparisons with unsedated controls. Results could be confounded if anesthesia altered strain/strain rate independent of hemodynamics, though we are unaware of data documenting that maintenance anesthetics alone alter strain/strain rate. Altitude differences between Denver and Toronto can affect PVRi and MPAP; thus we used matched controls from respective institutions.

Conclusion

Pediatric PH patients demonstrate reduced LV longitudinal and circumferential strain and strain rate, primarily within the septum, with relationships to invasive hemodynamics, altered RV strain, septal shift, and functional PH measures.

References

1. D'Alonzo GE, Barst RJ, Ayres SM, et al. Survival in patients with primary pulmonary hypertension. Results from a national prospective registry. Ann Intern Med. 1991; 115:343-349.
2. Voelkel NF, Quaife RA, Leinwand LA, et al. Right ventricular function and failure: report of a National Heart, Lung, and Blood Institute working group on cellular and molecular mechanisms of right heart failure. Circulation. 2006; 114:1883-1891.
3. Bogaard HJ, Abe K, Vonk Noordegraaf A, Voelkel NF. The right ventricle under pressure: cellular and molecular mechanisms of right-heart failure in pulmonary hypertension. Chest. 2009; 135:794-804.
4. Santamore WP, Dell'Italia LJ. Ventricular interdependence: significant left ventricular contributions to right ventricular systolic function. Prog Cardiovasc Dis. 1998; 40:289-308.
5. Damiano RJ, Jr., La Follette P, Jr., Cox JL, et al. Significant left ventricular contribution to right ventricular systolic function. Am J Physiol. 1991; 261:H1514-1524.
6. Baker AE, Dani R, Smith ER, et al. Quantitative assessment of independent contributions of pericardium and septum to direct ventricular interaction. Am J Physiol. 1998; 275:H476-483.
7. Dittrich HC, Chow LC, Nicod PH. Early improvement in left ventricular diastolic function after relief of chronic right ventricular pressure overload. Circulation. 1989; 80:823-830.
8. Puwanant S, Park M, Popovic ZB, et al. Ventricular geometry, strain, and rotational mechanics in pulmonary hypertension. Circulation. 2010; 121:259-266.
9. Hardegree EL, Sachdev A, Fenstad ER, et al. Impaired left ventricular mechanics in pulmonary arterial hypertension: identification of a cohort at high risk. Circ Heart Fail. 2013; 6:748-755.
10. Gan C, Lankhaar JW, Marcus JT, et al. Impaired left ventricular filling due to right-to-left ventricular interaction in patients with pulmonary arterial hypertension. Am J Physiol Heart Circ Physiol. 2006; 290:H1528-1533.
11. Tonelli AR, Plana JC, Heresi GA, Dweik RA. Prevalence and prognostic value of left ventricular diastolic dysfunction in idiopathic and heritable pulmonary arterial hypertension. Chest. 2012; 141:1457-1465.
12. Marcus JT, Gan CT, Zwanenburg JJ, et al. Interventricular mechanical asynchrony in pulmonary arterial hypertension: left-to-right delay in peak shortening is related to right ventricular overload and left ventricular underfilling. J Am Coll Cardiol. 2008; 51:750-757.
13. Stojnic BB, Brecker SJ, Xiao HB, et al. Left ventricular filling characteristics in pulmonary hypertension: a new mode of ventricular interaction. Br Heart J. 1992; 68:16-20.
14. Galie N, Hoeper MM, Humbert M, et al. Guidelines for the diagnosis and treatment of pulmonary hypertension: the Task Force for the Diagnosis and Treatment of Pulmonary Hypertension of the European Society of Cardiology (ESC) and the European Respiratory Society (ERS), endorsed by the International Society of Heart and Lung Transplantation (ISHLT). Eur Heart J. 2009; 30:2493-2537.
15. Mor-Avi V, Lang RM, Badano LP, et al. Current and evolving echocardiographic techniques for the quantitative evaluation of cardiac mechanics: ASE/EAE consensus statement on methodology and indications endorsed by the Japanese Society of Echocardiography. J Am Soc Echocardiogr. 2011; 24:277-313.
16. Lai WW, Geva T, Shirali GS, et al. Guidelines and standards for performance of a pediatric echocardiogram: a report from the Task Force of the Pediatric Council of the American Society of

Echocardiography. J Am Soc Echocardiogr. 2006; 19:1413-1430.
17. Ryan T, Petrovic O, Dillon JC, et al. An echocardiographic index for separation of right ventricular volume and pressure overload. J Am Coll Cardiol. 1985; 5:918-927.
18. Voigt JU, Pedrizzetti G, Lysyansky P, et al. Definitions for a common standard for 2D speckle tracking echocardiography: consensus document of the EACVI/ASE/Industry Task Force to standardize deformation imaging. Eur Heart J Cardiovasc Imaging. 2015; 16:1-11.
19. Thenappan T, Shah SJ, Rich S, et al. Survival in pulmonary arterial hypertension: a reappraisal of the NIH risk stratification equation. Eur Respir J. 2010; 35:1079-1087.
20. Thenappan T, Glassner C, Gomberg-Maitland M. Validation of the pulmonary hypertension connection equation for survival prediction in pulmonary arterial hypertension. Chest. 2012; 141:642-650.
21. Thavendiranathan P, Poulin F, Lim KD, et al. Use of myocardial strain imaging by echocardiography for the early detection of cardiotoxicity in patients during and after cancer chemotherapy: a systematic review. J Am Coll Cardiol. 2014; 63:2751-2768.
22. Fernandes FP, Manlhiot C, Roche SL, et al. Impaired left ventricular myocardial mechanics and their relation to pulmonary regurgitation, right ventricular enlargement and exercise capacity in asymptomatic children after repair of tetralogy of Fallot. J Am Soc Echocardiogr. 2012; 25:494-503.
23. Dambrauskaite V, Delcroix M, Claus P, et al. Regional right ventricular dysfunction in chronic pulmonary hypertension. J Am Soc Echocardiogr. 2007; 20:1172-1180.
24. Rajagopal S, Forsha DE, Risum N, et al. Comprehensive assessment of right ventricular function in patients with pulmonary hypertension with global longitudinal peak systolic strain derived from multiple right ventricular views. J Am Soc Echocardiogr. 2014; 27:657-665 e653.
25. Friedberg MK, Cho MY, Li J, et al. Adverse biventricular remodeling in isolated right ventricular hypertension is mediated by increased transforming growth factor-beta1 signaling and is abrogated by angiotensin receptor blockade. Am J Respir Cell Mol Biol. 2013; 49:1019-1028.
26. Manders E, Bogaard HJ, Handoko ML, et al. Contractile dysfunction of left ventricular cardiomyocytes in patients with pulmonary arterial hypertension. J Am Coll Cardiol. 2014; 64:28-37.
27. Nagaya N, Nishikimi T, Okano Y, et al. Plasma brain natriuretic peptide levels increase in proportion to the extent of right ventricular dysfunction in pulmonary hypertension. J Am Coll Cardiol. 1998; 31:202-208.

Supplemental material

Supplemental/Expanded Methods

Study Population

Of the 64 patients that underwent simultaneous catheterization and echocardiography, ten patients were excluded: aortic coarctation +/- mitral stenosis (3), pulmonary vein stenosis (2), elevated left ventricular (LV) end-diastolic pressure (2), branch pulmonary artery stenosis (1), multiple ventricular septal defect occlusion devices felt to possibly confound ventricular mechanics (1), lack of raw echocardiography data preventing off-line analysis (1). This left 54 patients – 37 from Children's Hospital Colorado, 17 from SickKids.

Right-Heart Catheterization

Cardiac index was either measured (thermodilution) or calculated (modified Fick equation); pulmonary (Qp) and systemic (Qs) blood flow were documented (Qs not documented in 5 patients). The following pressures were measured: right atrial, RV, pulmonary artery (mean measured in all, diastolic/systolic not documented in 2 patients), pulmonary capillary wedge and/or left atrial, and systemic arterial (not documented in 4 patients). Transpulmonary gradients were calculated as the difference between mean or diastolic pulmonary artery pressure and left atrial pressure (pulmonary capillary wedge pressure served as a surrogate when left atrial pressure not obtained). Pulmonary vascular resistance was calculated and indexed to body surface area (PVRi).

Speckle-Tracking Echocardiography

In the majority (70.0%) of strain analyses, 2-4 consecutive heartbeats were each analyzed and averaged to account for beat-to-beat variability; if only one beat was available for analysis (20.4%), this was used; in a minority (9.6%), inadequate echocardiographic windows prevented analysis; right ventricular (RV) and LV image quality were similar. In total, 595 strain analyses were completed for the 54 study patients.

Demographics & Functional Classification

Six-minute walk distance (6MWD) was recorded if documented <6 months from catheterization. PHrelated hospitalization data was collected at study completion.

Control Population

Our control population consisted of age-, gender-, and institution-matched healthy children who were healthy volunteers or underwent evaluation for murmur, chest pain, palpitations, syncope, or family history of congenital heart disease (CHD) with a normal full echocardiogram.[1] We excluded those with a family history of bicuspid aortic valve,[2] documented arrhythmias, chemotherapy exposure, family history of cardiomyopathy, systemic illness, or documented/suspected genetic abnormality.

Supplemental/Expanded Results

Patient Characteristics

Most pulmonary hypertension (PH) patients were born with CHD (33/53, 62.3%), defined as any structural defect, including a patent foramen ovale; some of these patients had multiple defects (7/33, 21.2%). Common abnormalities were atrial (24/53, 45.3%) and ventricular (5/53, 9.4%) septation defects and patent ductus arteriosus (11/53, 20.8%). Other CHD (5/53, 9.4%) included atrioventricular septal defect, transposition of the great arteries, and anomalous pulmonary venous drainage due to a posterior/leftward deviated atrial septum, repaired without pulmonary vein manipulation/obstruction. Of those with CHD, 36.4% (12/33) underwent repair, leaving 63.6% (21/33) unrepaired. Therefore, 39.6% (21/53) of all PH patients had an active shunt at catheterization; these patients had a median Qp:Qs (pulmonary-to-systemic blood flow ratio) of 1.16 (1.00 – 1.55). Twenty-two (40.7%) PH patients underwent 6MWD. Sixteen patients had ≥1 PH-related hospital admission (24 admissions total).

Ventricular Mechanics

Sub-group Analysis

Patients were separated into quartiles by the ratio of pulmonary-to-systemic mean arterial pressures (MPAP/MAP), and also into tertiles by PVRi, as described in the Results section. To determine if age cofounded severity of PH, we evaluated the age of the most severe population and the remaining cohort. There was no significant difference between the median age for Quartile 4 of MPAP/MAP (12.0 [8.016.0] years) versus the rest of the cohort (8.0 [2.5-15.5] years) (P=0.23). Similarly, there was no significant difference between the median age for Tertile 3 of PVRi (12.0 [8.0-16.0] years) versus the rest of the cohort (8.0 [3.0-15.0] years) (P=0.18).

Rotational Mechanics

Despite no significant differences between apical and basal rotation/rotation rates, there were trends towards increased torsion (1.47 [1.03-2.08] vs. 1.27 [0.69-1.59]^0/cm, *P*=0.08) and torsion rate (15.09 [11.76-22.13] vs. 11.60 [9.82-20.08]^0/cm/s, *P*=0.06) in PH.

Supplemental Tables

Supplemental Table 1. Left and Right Ventricular Longitudinal Strain Rate

Longitudinal Strain Rate, 1/s	PH Patients (n=53)	Control Subjects (n=53)	*P*-Value
LV Global	-1.46 (-1.23 - -1.60)	-1.41 (-1.24 - -1.62)	0.99
LV Free-Wall	-1.65 (-1.42 - -1.81)	-1.56 (-1.33 - -1.72)	0.19
Basal	-1.94 (-1.58 - -2.31)	-1.70 (-1.45 - -2.04)	0.21
Mid	-1.29 (-1.06 - -1.53)	-1.31 (-1.15 - -2.04)	1.00
Apical	-1.54 (-1.37 - -1.92)	-1.53 (-1.33 - -1.80)	0.40
IVS	-1.17 (-1.05 - -1.39)	-1.33 (-1.17 - -1.46)	0.055
Basal	-1.03 (-0.84 - -1.24)	-1.07 (-0.93 - -1.21)	0.50
Mid	-1.03 (-0.85 - -1.16)	-1.22 (-1.04 - -1.40)	0.0010*
Apical	-1.56 (-1.31 - -1.79)	-1.62 (-1.37 - -1.85)	0.72
RVFW	-1.61 (-1.31 - -1.97)	-2.10 (-1.63 - -2.44)	0.0003*
Basal	-1.77 (-1.35 - -2.23)	-2.18 (-1.87 - -3.19)	0.0004*
Mid	-1.52 (-1.21 - -1.81)	-1.94 (-1.67 - -2.70)	<0.0001*
Apical	-1.48 (-1.06 - -1.85)	-1.65 (-1.29 - -1.98)	0.09

Presented as median (interquartile range). PH indicates pulmonary hypertension; LV, left ventricle;

IVS, interventricular septum; RVFW, right ventricular free-wall.

Supplemental Table 2. Left Ventricular Circumferential Strain Rate

Circumferential Strain Rate, 1/s	PH patients (n=53)	Control Subjects (n=53)	*P*-Value
Basal			
Global	-1.70 (-1.39 - -2.01)	-1.85 (-1.63 - -2.37)	0.0157
Septum (6, 1)	-1.67 (-1.34 - -1.97)	-1.99 (-1.56 - -2.71)	0.0037*
Septal (6)	-1.56 (-1.17 - -1.85)	-2.05 (-1.45 - -2.58)	0.0014*
Anteroseptal (1)	-1.77 (-1.38 - -2.10)	-1.96 (-1.55 - -2.77)	0.0232
Free-Wall (2, 3, 4, 5)	-1.69 (-1.35 - -1.93)	-1.78 (-1.67 - -2.11)	0.09
Anterior (2)	-1.84 (-1.42 - -2.21)	-2.04 (-1.48 - -2.38)	0.20
Lateral (3)	-1.40 (-1.05 - -1.86)	-1.72 (-1.39 - -2.16)	0.0122
Posterior (4)	-1.61 (-1.11 - -1.94)	-1.81 (-1.49 - -2.20)	0.10
Inferior (5)	-1.81 (-1.46 - -2.32)	-1.92 (-1.53 - -2.15)	0.46
Mid			
Global	-1.51 (-1.27 - -1.81)	-1.64 (-1.39 - -1.86)	0.26
Septum (6, 1)	-1.51 (-1.22 - -1.84)	-1.57 (-1.32 - -1.98)	0.30
Septal (6)	-1.46 (-1.27 - -1.79)	-1.57 (-1.31 - -1.92)	0.24
Anteroseptal (1)	-1.52 (-1.22 - -1.91)	-1.61 (-1.29 - -2.01)	0.41
Free-Wall (2, 3, 4, 5)	-1.48 (-1.25 - -1.82)	-1.63 (-1.39 - -1.79)	0.28
Anterior (2)	-1.81 (-1.42 - -2.08)	-1.85 (-1.52 - -2.16)	0.67
Lateral (3)	-1.33 (-1.08 - -1.64)	-1.61 (-1.28 - -1.84)	0.058
Posterior (4)	-1.38 (-1.06 - -1.87)	-1.46 (-1.23 - -1.74)	0.33
Inferior (5)	-1.48 (-1.17 - -1.84)	-1.53 (-1.30 - -1.89)	0.50
Apical			
Global	-1.80 (-1.48 - -2.13)	-1.77 (-1.49 - -2.06)	0.69
Septum (6, 1)	-1.71 (-1.43 - -2.08)	-1.62 (-1.36 - -1.94)	0.41
Septal (6)	-1.59 (-1.29 - -2.09)	-1.54 (-1.36 - -1.97)	0.77
Anteroseptal (1)	-1.77 (-1.43 - -2.03)	-1.62 (-1.32 - -2.06)	0.25
Free-Wall (2, 3, 4, 5)	-1.88 (-1.52 - -2.20)	-1.86 (-1.51 - -2.24)	0.99
Anterior (2)	-2.19 (-1.88 - -2.55)	-2.04 (-1.47 - -2.67)	0.20
Lateral (3)	-1.67 (-1.52 - -2.25)	-1.86 (-1.50 - -2.19)	0.70
Posterior (4)	-1.67 (-1.29 - -2.16)	-1.87 (-1.46 - -2.14)	0.19
Inferior (5)	-1.62 (-1.25 - -2.28)	-1.64 (-1.51 - -2.01)	0.70

Presented as median (interquartile range). PH indicates pulmonary hypertension.

Supplemental Table 3. Characteristics & LV Strain of the Most Severe Pulmonary Hypertension

	PH Quartile 4 (n=13)	Control Subjects (n=53)	*P*-Value
Cardiac Catheterization			
MPAP, mm Hg	60.0 (46.0 - 61.0)	...	...
MPAP/MAP	1.00 (0.81 - 1.04)	...	...
SPAP, mm Hg	84.0 (63.0 - 90.0)	...	...
DPAP, mm Hg	42.0 (33.0 - 46.0)	...	...
Transpulmonary Gradient, mm Hg	51.0 (38.0 - 54.0)	...	...
Diastolic Transpulmonary Gradient, mm Hg	35.0 (26.0 - 39.0)	...	...
Mean RAP, mm Hg	7.0 (5.0 - 9.0)	...	...
Cardiac Index, L/min/m2	3.52 (3.23 - 3.98)	...	...
PVRi, WU·m2	15.80 (11.71 - 19.10)	...	...
PVR/SVR	0.85 (0.77 - 1.12)	...	...
Echocardiography			
LV End-Diastolic Volume, ml	77.0 (39.0 - 105.0)	65.0 (46.0 - 89.0)	0.75
Indexed LV End-Diastolic Volume, ml/m2	61.5 (45.6 - 82.4)	49.4 (35.1 - 54.1)	0.27
LV End-Systolic Volume, ml	33.0 (16.0 - 47.0)	21.0 (14.0 - 31.0)	0.46
Indexed LV End-Systolic Volume, ml/m2	23.5 (21.4 - 33.1)	16.5 (12.0 - 18.9)	0.0502
LV Ejection Fraction, %	58.0 (50.0 - 66.0)	64.0 (62.0 - 69.0)	0.07
LV End-Diastolic Eccentricity Index	1.43 (1.15 - 1.76)	1.04 (0.96 - 1.07)	0.0006*
LV End-Systolic Eccentricity Index	1.82 (1.30 - 2.17)	0.97 (0.96 - 1.03)	0.0001*
Longitudinal Strain, %			
LV Global	-18.2 (-16.2 - -19.8)	-19.5 (-19.1 - -20.7)	0.08
LV Free-Wall	-21.3 (-20.0 - -23.3)	-18.9 (-18.1 - -20.0)	0.0354
Basal	-20.7 (-15.2 - -26.9)	-18.4 (-14.2 - -22.2)	0.43
Mid	-20.0 (-16.7 - -22.2)	-18.0 (-15.0 - -21.7)	0.46
Apical	-23.8 (-21.9 - -27.1)	-22.7 (-19.1 - -25.1)	0.20
IVS	-15.1 (-13.6 - -17.0)	-21.0 (-20.1 - -21.7)	0.0015*
Basal	-10.9 (-6.1 - -12.7)	-18.0 (-14.5 - -20.4)	0.0025*
Mid	-13.1 (-12.1 - -16.7)	-23.0 (-19.8 - -23.0)	0.0002*
Apical	-23.4 (-22.5 - -26.4)	-22.9 (-21.0 - -26.6)	0.98
RVFW	-19.0 (-13.9 - -22.2)	-30.3 (-27.5 - -33.5)	<0.0001*
Basal	-18.7 (-15.2 - -22.9)	-31.8 (-25.6 - -35.8)	0.0048*
Mid	-18.9 (-11.2 - -25.2)	-34.0 (-30.2 - -35.0)	<0.0001*
Apical	-16.7 (-11.2 - -21.2)	-28.9 (-22.0 - -30.9)	0.0012*
Circumferential Strain, %			
Basal Lateral (3)	-8.3 (-5.1 - -14.0)	-18.9 (-15.5 - -21.4)	0.0050*
Mid Lateral (3)	-12.5 (-9.2 - -15.5)	-16.0 (-14.0 - -20.5)	0.0316

Caption on next page

Presented as median (interquartile range). LV indicates left ventricle; PH, pulmonary hypertension; MPAP, mean pulmonary artery pressure; MAP, mean arterial (systemic) pressure; SPAP, systolic pulmonary artery pressure; DPAP, diastolic pulmonary artery pressure; RAP, right atrial pressure; PVRi, indexed pulmonary vascular resistance; PVR/SVR, pulmonary-to-systemic vascular resistance ratio; IVS, interventricular septum; RVFW, right ventricular free-wall.

Supplemental References

1. Lai WW, Geva T, Shirali GS, Frommelt PC, Humes RA, Brook MM, Pignatelli RH, Rychik J. Task Force of the Pediatric Council of the American Society of E, Pediatric Council of the American Society of E. Guidelines and standards for performance of a pediatric echocardiogram: a report from the Task Force of the Pediatric Council of the American Society of Echocardiography. J Am Soc Echocardiogr. 2006;19:1413-1430.
2. Biner S, Rafique AM, Ray I, Cuk O, Siegel RJ, Tolstrup K. Aortopathy is prevalent in relatives of bicuspid aortic valve patients. J Am Coll Cardiol. 2009;53:2288-2295.

Chapter 5

Adverse ventricular-ventricular interactions in right ventricular pressure-load: Insights from pediatric pulmonary hypertension versus pulmonary stenosis

Authors
Mieke MP Driessen, Wei Hui, Bart H Bijnens, Andreea Dragulescu, Luc Mertens, Folkert J Meijboom, Mark K. Friedberg, MD

(adapted from) Physiol Rep. 2016 Jun;4(11). pii: e12833.

Abstract

Background: Right ventricular (RV) pressure overload has a vastly different clinical course in children with idiopathic pulmonary arterial hypertension (iPAH) than in children with pulmonary stenosis (PS). While RV function is well recognized as a key prognostic factor in iPAH, adverse ventricular-ventricular interactions and LV dysfunction are less well characterized and the pathophysiology is incompletely understood. We compared ventricular-ventricular interactions as hypothesized drivers of biventricular dysfunction in pediatric iPAH vs. PS.

Methods and Results: Eighteen iPAH, 16 PS patients and 18 age- and size-matched controls were retrospectively studied. Cardiac cycle events were measured by M-mode and Doppler echocardiography. Measurements were compared between groups using ANOVA with posthoc Dunnet's or ANCOVA including RV systolic pressure (RVSP; iPAH 96.8±25.4 vs. PS 75.4±18.9 mmHg; p=0.011) as a covariate. RV free-wall thickening was prolonged in iPAH vs. PS, extending beyond pulmonary valve closure (638±76 vs. 562±76 vs. 473±59 ms controls). LV and RV isovolumetric relaxation were prolonged in iPAH (p<0.001; LV 102.8±24.1 vs. 63.1±13.7 ms; RV 95 [61-165] vs. 28 [0-43]), associated with adverse septal kinetics; characterized by rightward displacement in early systole and leftward displacement in late RV systole (i.e. early LV diastole). Early LV diastolic filling was decreased in iPAH (73±15.9 vs. PS 87.4±14.4 vs. controls 95.8±12.5 cm/sec; p=0.004).

Conclusions: Prolonged RVFW thickening, prolonged RVFW isovolumetric times and profound septal dyskinesia are associated with interventricular mechanical discoordination and decreased early LV filling in pediatric iPAH much more than PS. These adverse mechanics affect systolic and diastolic biventricular efficiency in iPAH and may form the basis for worse clinical outcomes.

New & noteworthy: We used clinically derived data to study the pathophysiology of ventricular-ventricular interactions in right ventricular pressure overload, demonstrating distinct differences between pediatric pulmonary arterial hypertension (iPAH) and pulmonary stenosis (PS). Altered timing of right ventricular free wall contraction and profound septal dyskinesia are associated with interventricular mechanical discoordination and decreased early LV filling in iPAH much more than PS. These adverse mechanics affect systolic and diastolic biventricular efficiency, independent of right ventricular systolic pressure.

Introduction

In both idiopathic pulmonary arterial hypertension (iPAH) and pulmonary valvular stenosis (PS) the right ventricle (RV) increases its systolic pressure in order to overcome the increased impedance. However, pediatric iPAH is associated with worse exercise capacity, morbidity and mortality compared to PS.[1,2] While RV morphology and dysfunction are well-established drivers of morbidity and mortality in iPAH, and are different from PS[3,4], adverse ventricular-ventricular interactions and left ventricular (LV) dysfunction are emerging as important determinants of iPAH outcomes.[5]

The RV and left ventricle (LV) are interdependent through common myocardial fibers, the interventricular septum (IVS) and the pericardial space.[6,7] Of these, the IVS plays a crucial role in mediating ventricular-ventricular interactions as it shares fibers with both ventricles, is subject to interventricular pressure gradients and directly impacts biventricular geometry.[8,9] Septal and LV contraction contribute substantially to RV systolic function and ultimately cardiac output.[10,11] Likewise, RV loading, geometry and function impact LV function.[5,9,12,13] In RV pressure overload, these adverse ventricular-ventricular interactions negatively impact LV filling, geometry and systolic function.[5,12,13] The mechanisms and pathophysiology of these adverse interactions is incompletely characterized, but may partly explain the different clinical course of these groups.[7] Comparing ventricular-ventricular interactions pediatric iPAH vs PS can further our understanding of RV adaptation to increased pressure-load.

Accordingly, the aim of this study was to characterize the pathophysiology and mechanisms of ventricular-ventricular interactions and their impact on biventricular function in the pressure-loaded RV in iPAH vs. PS, using detailed analysis of septal kinetics and cardiac cycle-timing events. We hypothesized that adverse septal kinetics and temporal mechanics are associated with worse ventricular-ventricular interactions in children with iPAH vs. PS.

Methods

Patients with echocardiography performed between 2004 and 2013 were retrospectively studied. iPAH patients were diagnosed according to the Dana Point guidelines – i.e. a mean pulmonary arterial pressure of ≥25 mmHg at rest with a pulmonary vascular resistance of ≥3 Wood units and a pulmonary capillary wedge pressure of ≤15 mmHg.[14] Patients with valvular PS were included if they had no associated intra-cardiac abnormalities with the exception of a small, hemodynamically insignificant, atrial or ventricular septal defect. Healthy controls matched for age and BSA, were selected from a database consisting of volunteers or children evaluated for an innocent cardiac murmur with normal medical history, physical examination and echocardiography. The Institutional Research Ethics Board approved the study.

Echocardiography

Analysis was performed on digitally stored echocardiograms (SyngoDynamics, Siemens, Erlangen, Germany) by *a single* observer. In iPAH patients the first full functional echocardiogram at our institution was analyzed. Measurements were performed as suggested in the 2010 guidelines for the pediatric echocardiogram by Lopez et al.[15] A full functional study includes the following 2-D echocardiography views: parasternal short axis at mid-papillary level (M-mode & 2-D echocardiography), standard apical 4-chamber, separate RV focused 4-chamber view and apical 2-chamber. Pulsed and continuous wave Doppler interrogation was performed for all valves and Tissue Doppler Imaging (TDI) of RV free wall (RVFW), LV lateral wall and interventricular septum (IVS).

Echocardiographic dimensions

M-mode RV and LV end-diastolic (EDD) and end-systolic dimensions (ESD) and LV ejection fraction[16] were measured from parasternal short-axis views; and Z-scores calculated using institutional values. The LV eccentricity index (lateral divided by anterior-posterior LV diameter) was measured using a mid-LV short-axis view at end-systole, early-diastole and end-diastole.[17] RV end-diastolic and end-systolic areas were measured in the apical 4-chamber view to calculate the RV fractional area change.[15] Tricuspid annular planar systolic excursion (TAPSE) and TDI systolic velocity (s') were measured as measurements of RV systolic performance.

Biventricular and Septal kinetics

Detailed qualitative and quantitative analysis of IVS, RVFW and LV posterior wall (LVPW) motion throughout the cardiac cycle used parasternal mid-ventricular M-mode tracings to define septal motion in relation to the RVFW and LVPW.

Pulsed wave Doppler echocardiography was used to measure valve events (i.e. valve opening and closure - detailed below) in relation to the mechanical events. Quantitative measurements included: time to onset and peak septal, RVFW and LVPW contraction and time to peak leftward septal displacement (when present; # **Figure 1**). The electrocardiogram (ECG) QRS onset was used as a reference for timing and event measurements.

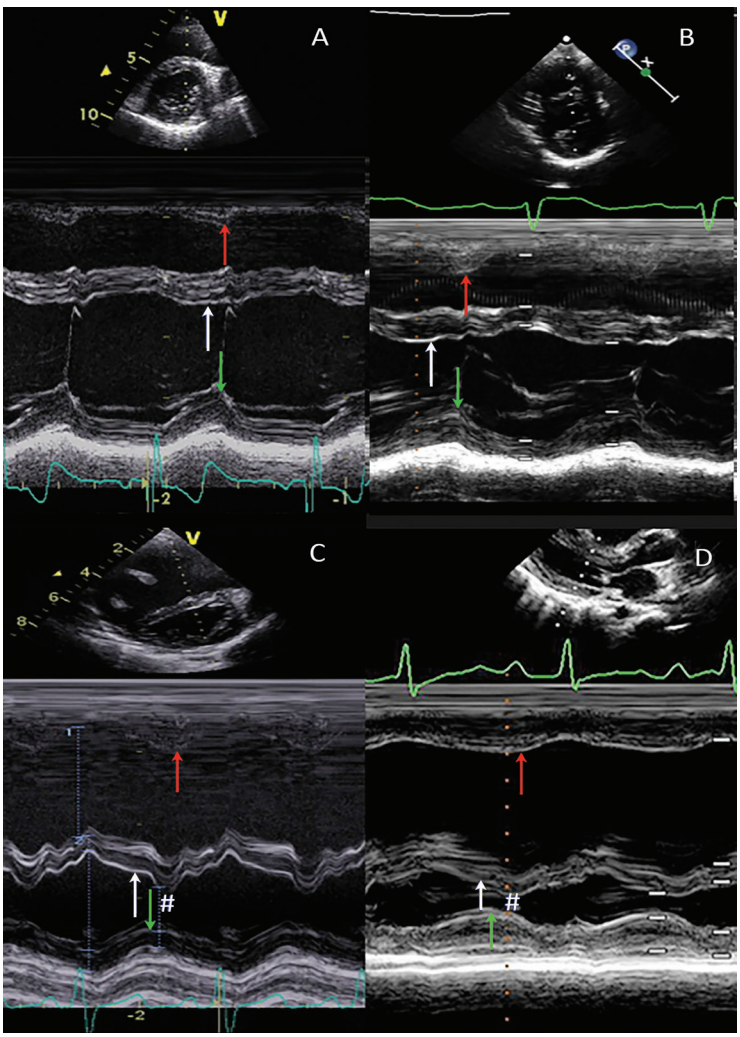

Figure 1: M-mode cross-sections

Four representative examples of m-mode cross-section parasternal short or long axis at the level of MV annulus are shown. The time to peak radial motion of right ventricular free wall, septum and left ventricular posterior wall are depicted with arrows. Figure 1a: control, figure 1b: pulmonary stenosis and figure 1c+1d: idiopathic pulmonary arterial hypertension. Abnormal

Doppler echocardiography

RV systolic pressure (RVSP) was estimated from the TR jet using the modified Bernoulli equation. In PS patients the PV systolic gradient was used to estimate RVSP if the TR spectral Doppler tracing was incomplete. As inferior vena cava collapsibility is not validated or measured routinely in children, right atrial pressure was not added to the RVSP.

Pulsed Doppler tracings were sampled in the RV and LV inflow and outflow tracts. Atrio-ventricular and ventriculo-arterial valve opening and closure times and mitral and tricuspid valve early (E) and late (A) filling velocities were measured. LV isovolumetric relaxation time was derived from a pulsed wave Doppler tracing straddling the LV inflow and outflow. Pulsed wave Tissue Doppler imaging (TDI) at the basal RV free wall, IVS and LV free wall was acquired and the peak systolic (TDI s') and early diastolic (TDI e') tissue velocities measured. The isovolumetric contraction and relaxation times were also measured on TDI.

An average of three measurements was used for all TDI and Doppler velocity measurements.[15] Timing measurements were taken from cardiac cycles with <10% variation in RR interval. To allow comparison between different heart rates, *all* timing measurements were normalized for the RR interval.

Reproducibility

In 15 randomly selected patients all M-mode and blood flow Doppler measurements including IVS, RVFW and LVPW timing and valve events were re-measured by the first observer (with a 1 month interval) and by a second observer, blinded to the first measurement.

Statistical analysis

Continuous variables are represented as mean ± standard deviation or median [range] as appropriate. Categorical variables are presented as a frequency (%). PS and iPAH were compared to controls using the ANOVA with posthoc Dunnet's or Mann-Whitney U test, as appropriate. To assess the effect of patient group on the dependent variable (outcome measurements) we used ANCOVA – as it enables analysis of a covariate that possibly confounds the analysis (in our case RVSP). In other words, if the relationship between patient group and the outcome variable is completely determined by RVSP – statistical analysis would yield a non-significant result for between group analysis.

Intra- and interobserver reproducibility was assessed by determining the mean difference with limits of agreement, intra-class correlation coefficient (absolute agreement) and comparing measurements with a paired Student T-test. An

alpha level of 0.05 was considered statistically significant.

Results

A total of 52 subjects, including 18 iPAH, 16 PS patients and 18 age and BSA-matched controls were studied. Baseline and demographic data are listed in Table 1. Age, BSA and sex were similar between the 3-groups. All iPAH patients were on pulmonary vasodilator treatments at time of echocardiography: 7 (39%) on phosphodiesterase inhibitors, 13 (72%) on endothelin-receptor antagonists and 9 (50%) on prostacyclins. iPAH patients had significantly higher resting heart rates compared with controls. ECG QRS duration was significantly longer in iPAH vs. PS patients and controls, although none met criteria for complete RBBB. RVSP and RV:LV pressure ratio were higher in iPAH patients compared with PS. iPAH patients had significantly more RV dilatation compared with controls and with PS patients; and measures of regional longitudinal and global RV function were worse (all p<0.001;**Table 1**).

LV dimensions and functional parameters

Measures of LV dimensions and function are listed in Table 2. In PS patients these were comparable to controls. Using linear regression to account for differences in RVSP, iPAH patients had smaller LV EDD and LV ESD compared with PS patients and controls. LVEF was higher in iPAH. Both PS and iPAH patients had lower MV E/A ratio and similar E/E' ratio than controls. The early diastolic LV filling velocity was lower in iPAH compared with controls and PS patients (p<0.001 and p=0.004, respectively).

Event timing and septal movement

Figure 1 shows representative M-mode examples of each group. In **Figure 2** the average timing of peak contraction and valve timing are represented schematically, including only patients with a complete dataset.

Table 1: Baseline Characteristics

	Controls (n=18)	PS (n=16)	iPAH (n=18)	p-value PS vs iPAH
Age (yrs.)*	11.2 ± 5.0	10.3 ± 4.7	11.5 ± 5.6	0.736
BSA (m^2)*	1.31 ± 0.44	1.23 ± 0.48	1.16 ± 0.41	0.547
Male sex (%)	10 (56%)	9 (56%)	9 (50%)	0.716
Heart rate (bpm)	70 ± 13	81 ± 18	89 ± 22#	0.261
QRS ECG (ms)	-	84 ± 11	99 ± 18	0.005
RVSP (mmHg)	-	75.4 ± 18.9	96.8 ± 25.4	0.011
RV : LV pressure	-	0.71 [0.41-1.57]	1.10 [0.46-1.50]	0.007
RVDd (mm)	18.5 ± 4.4	20.3 ± 5.2	34.4 ± 9.9*	<0.001
z-score	0.24 ± 1.02	1.2 ± 1.56	4.82 ± 1.99*	<0.001
RVDbas (mm)	33.5 ± 5.0	34.4 ± 7.4	48.3 ± 10.0*	<0.001
RVDmaj (mm)	60.4 ± 10.9	56.4 ± 11.2	66.6 ± 12.3	0.010
FAC (%)	47.2 [39.2-53.7]	42.5 [36.7-68.1]	18.5 [8.1-34.3]*	<0.001

*Patients were compared to controls using ANOVA with posthoc Dunnet's test # p=0.002 and *p<0.001. PS and iPAH were compared using independent Student T-test. PS=pulmonary stenosis; iPAH=idiopathic pulmonary arterial hypertension; Yrs.= years; BSA= body surface area; bpm= beats per minute; RVSP=right ventricular systolic pressure; LV=left ventricular; RVDd=right ventricular diastolic dimension parasternal long-axis; RVDbas = basal AP4CH-dimension; RVmajor= long AP4CH-dimension; FAC= fractional area change.*

Healthy controls

Normal IVS motion is characterized by 3 major components (**Figures 1a+2a**): 1) the IVS starts to contract on average 58±3 ms after QRS onset, maintaining a stable position throughout systole. 2) Peak IVS systolic excursion occurs ~30 ms before

peak RVFW and LVPW thickening, which peak near-simultaneously (Table 3). 3) During early RVFW and LVPW relaxation there is subtle bidirectional post-systolic IVS motion (# in **Figure 1a**). The pulmonary valve (PV) opens slightly before, and closes simultaneously with, the aortic valve (AV). The mitral (MV) and tricuspid valves (TV) open and close near-simultaneously (**Figures 1a+2a**).

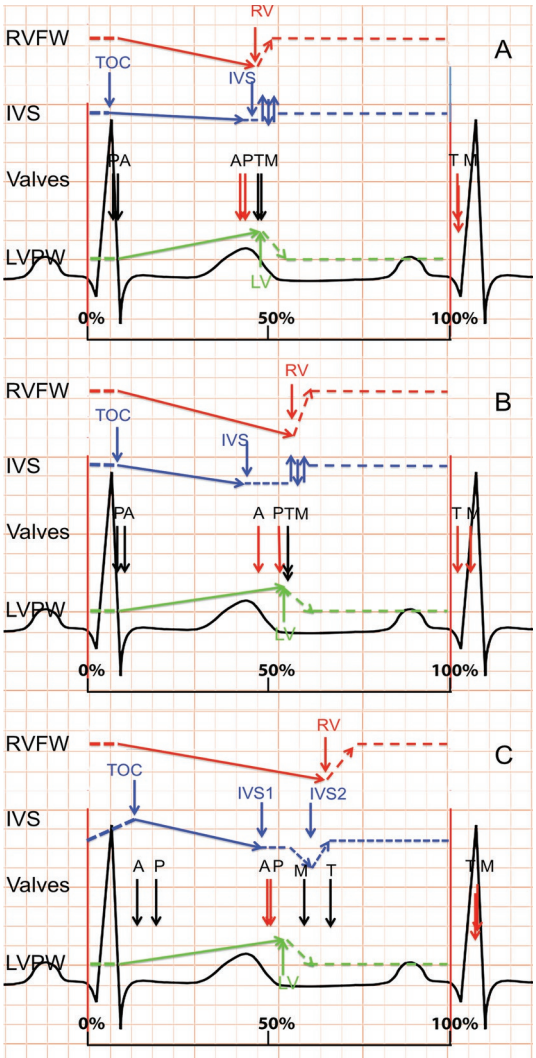

Figure 2

Schematic representation of peak contraction and valve timing (opening in black and closure in red), relative to RR interval, for each group. A=controls; B=pulmonary stenosis; C= idiopathic pulmonary arterial hypertension. Abbreviations: TOC=time of onset contraction; IVS=interventricular septum; LV=left ventricular free wall; RV=right ventricular free wall; A=aortic valve; P=pulmonic valve; M=mitral valve; T=tricuspid valve

PS

In PS, qualitative IVS motion is similar to controls with some differences in the timing and position of the IVS: Onset of IVS contraction is delayed compared to controls (90±23 vs. 58±3 ms; p<0.01), with a corresponding mild delay in AoV opening (95±15 vs. 83±14 ms; p<0.05) which coincides with PV opening. Peak IVS systolic excursion and the early-diastolic bidirectional IVS motion (**Figure 1a+b**) are similar to controls. Peak RVFW and LVPW thickening are delayed compared with controls but remain near simultaneous (peak RVFW 562±76 and LVPW 538±70 ms **Table 3, Figure 1b+2b**). This results in prolonged mechanical discoordination between the IVS and both free walls (IVS to LVPW delay 121 ms) compared to controls. The septum is mildly leftward displaced during systole. Peak RVFW thickening is slightly later than peak LVPW thickening; correspondingly the PV closes later than the AoV with a prolonged RV ejection time (514±68 vs. 461±57 ms in controls). As systole lasts longer in PS compared to controls, MV and TV opening are delayed in PS despite normal isovolumetric relaxation times. The opening of the MV and TV valves is simultaneous.

iPAH

Qualitatively and quantitatively septal motion and timing of biventricular contraction and relaxation in iPAH patients differ substantially from PS patients and controls (figure 1a-d). Onset of IVS contraction is delayed to 122±36 ms after QRS-onset (PS 90±23; controls 58±3 ms; p<0.01). The IVS is displaced towards the RVFW during this delay and RVFW isovolumetric contraction is prolonged (iPAH 90 [58-139] vs. PS 61 [48-85] & controls 70 [61-102] ms; p<0.01). The delayed onset of effective IVS and RVFW contraction corresponds with a delay in both PV and AoV opening compared to PS and controls (**Table 3**). In contrast to controls and PS, the PV opens after the AoV. In contrast to PS and controls the IVS thickens only mildly and is displaced markedly towards LVPW throughout systole (**figure 1&2**), reflected by the high LV eccentricity index (**Table 2**). Similar to PS, both RVFW and LVPW peak thickening are prolonged compared to controls. Peak RVFW thickening is more prolonged in iPAH vs. PS (iPAH 638±76 vs. PS 562±76 and controls 473±59 ms; p<0.05), extending well beyond peak LVPW thickening and PV closure (564±80 & 500±73 ms, respectively). Resulting in LV-RV systolic discoordination and post-systolic RVFW thickening. Despite prolonged RVFW thickening, effective RV ejection time is short (364±62 vs. 374±48 ms in controls). During post-systolic RVFW thickening, the IVS displaces even further leftward (#**Figures 1c, 1d & 2c**), persisting throughout diastole. LV and RV isovolumetric relaxation times are prolonged in iPAH compared with PS and controls. Both MV and TV opening are delayed and discoordinated compared to controls and PS – the TV opening much later than the MV. The MV opens whilst the septum is still displaced

towards the LVPW (MV opening 592±90 vs. peak IVS displacement 613±63 ms). This is associated with decreased early mitral diastolic filling velocity (E) compared to PS and controls (73.9±15.9 vs. 87.4±14.4 and 95.8±12.5 cm/sec; p=0.004) and both LV and RV inflow durations are significantly shortened compared with controls (but not PS).

Subgroup analysis similar RVSP

A sub-analysis was performed in patients with comparable RVSP (50-110 mmHg); 11 iPAH patients and 15 PS patients could be included, with mean RVSP of 83.8±18.6 mmHg vs. 77.4±17.6 mmHg (p=0.387). Differences in timing between iPAH and PS patients were similar to those observed in the entire cohort; time to peak RVFW thickening was delayed in iPAH (630±82 vs 562±76 msec; p=0.042), ending well after PVC (477±82 vs 514±70 msec in PS) and peak LVPW thickening (566±81 vs. 538±69 msec; p=0.369). The time to onset of IVS contraction was prolonged in iPAH vs PS patients (123±38 vs. 90±24 msec; p=0.015), moving rightward during this interval. All iPAH patients showed IVS displacement (#) after peak LVPW thickening (611±67 vs. peak LVPW 566±81 msec). In PS patients IVS displacement was only seen during end-systole, preceding or coinciding with peak LVPW thickening.

Discussion

Our results show that adverse ventricular-ventricular interactions and septal displacement are markedly worse in RV pressure-load associated with pediatric iPAH compared to PS. Pediatric iPAH was associated with profound RV early and end systolic (i.e. early LV diastolic) septal displacement and biventricular mechanical discoordination in both systole and diastole – reducing contractile efficiency and early LV filling. In contrast, in PS LV-RV coordination was preserved in both in systole and diastole and only mild septal displacement was seen at end-systole. These adverse v-v interactions seem primarily related to altered timing of RVFW systolic events seen in iPAH more than PS, and attest to both RV inefficiency and LV diastolic compromise.

Systolic interaction

Septal position depends on the trans-septal pressure-gradient combined with the tendency of the septum to straighten when contracting.[18] Changes of RV load therefore influence septal configuration and end-systolic septal curvature was one of the first sensitive, non-invasive markers of RV pressure overload.[9,17,18] Furthermore, adult iPAH studies have related septal kinetics to disease severity.[19,20] However, studies detailing IVS kinetics throughout the cardiac

cycle remain very limited. Our results extend those of previous studies and demonstrate abnormal septal kinetics in pediatric iPAH patients throughout the entire cardiac cycle, while those in PS were limited to end-systole. In iPAH pronounced septal displacement was not only seen in late RV systole (prolonged RVFW thickening) – towards the LVPW – but also during early systole - towards the RVFW (# **Figure 1c&d & Figure 2c**).

Abnormal iPAH septal motion coincided with differences in timing of RVFW systolic events in iPAH vs. PS patients. Firstly, iPAH patients have prolonged RV isovolumetric contraction (median 90 ms vs. 61 ms in PS) – and hence prolonged pressure generation – coinciding with the early systolic rightward septal displacement. This delays not only effective RV, but also LV ejection in iPAH. Secondly, prolonged peak RVFW systolic excursion is delayed in iPAH much more than PS (mean of 638 vs. 562 ms) and results in end-systolic LVPW-RVFW-IVS mechanical discoordination and post-systolic thickening *only* in the iPAH group. Previous studies in adults described the negative impact of end-systolic RV-LV dyssynchrony on RV systolic function.[13,21] During end-systolic discoordination – RV work is inefficiently spent on displacing the septum leftward rather than ejecting blood – thereby decreasing RV pump efficiency (**Figure 2**). Moreover, despite the delayed peak RVFW thickening also observed in PS patients, their isovolumetric times remain short and RVFW and LVPW remain coordinated, without impediment of RV systolic function.

Diastolic interactions

Early LV filling was decreased in our pediatric iPAH population but was normal in PS when compared to controls (**Table 2**). Additionally, isovolumetric relaxation times were prolonged in iPAH resulting in pronounced delay of MV and TV opening and also diastolic discoordination. Previous studies attributed abnormal LV filling in adult iPAH, to either direct ventricular-ventricular interaction, i.e. septal displacement, or in-series interaction, i.e. LV underfilling due to decreased RV cardiac output.[6,9,13,22-24] Contrary to our findings, Lurz et al. demonstrated similar results in patients with RV pressure overload in the context of congenital heart disease.[25] We observed marked septal displacement – i.e. direct interaction – in iPAH but not PS during early LV diastole (**Figure 2**), occurring at time of mitral valve opens – impeding filling. Likewise, pediatric iPAH patients exhibited both post-systolic RVFW thickening and leftward septal displacement, both previously associated with RV systolic dysfunction and lower RV stroke volume.[13,21,23] In addition, our pediatric iPAH cohort had markedly remodeled RVs. Santamore et al. showed that increased RV end-diastolic volume independently alters LV diastolic pressure-volume relations, decreasing LV filling.[9] Lastly, in contrast to PS and controls – there was a marked delay between MV and TV opening (592 vs. 667 ms after QRS onset) – which is a novel finding. In light of literature and our current results, it would seem that

both in-series and direct interactions are present.[26]

Table 2: LV dimensions and global function

	Controls (n=18)	PS (n=16)	iPAH (n=18)	P-value iPAH to PS
LVEDd (mm)	42.6 ± 6.6	39.2 ± 7.3	31.4 ± 8.1*	0.101
z-score	-0.01 ± 1.05	-0.53 ± 1.12	-3.86 ± 3.27*	0.011
LVEDs (mm)	26.2 ± 4.6	23.6 ± 4.9	16.9 ± 6.9*	0.052
z-score	-0.24 ± 0.85	-0.82 ± 1.14	-3.70 ± 3.27*	0.029
LVEF-teich (%)	76.1 ± 6.0	77.2 ± 7.3	83.7 ± 8.7**	0.032
E vel (cm/sec)[1]	95.8 ± 12.5	87.4 ± 14.4	73.9 ± 15.9*	0.004
MV E/A ratio[1]	2.66 ± 0.90	1.70 ± 0.56*	1.44 ± 0.40*	0.594
MV E/E' ratio[2]	5.0 [4.3-9.1]	5.1 [4.1-7.1]	6.1 [4.3-9.9]	0.238
Sys ecc index	1.07 ± 0.03	1.23 ± 0.15#	2.49 ± 0.96*	<0.001
BDia ecc index[3]	1.17 ± 0.05	1.38 ± 0.16**	3.23 ± 1.22*	<0.001

*Controls compared with pulmonary stenosis (PS) and idiopathic pulmonary arterial hypertension (iPAH) patients using ANOVA with posthoc Dunnet's; *p≤0.001, **p≤0.01 and # P<0.05. Patient groups are compared using ANCOVA including right ventricular systolic pressure as a covariate. 1total fusion in 1 iPAH, missing in 4 iPAH and 1 PS patient; 2missing in 6 iPAH and 2 PS patients. LV= left ventricular; EDd=end-diastolic dimension; EF=ejection fraction; E=early diastolic filling velocity; A=late diastolic filling velocity; ecc=eccentricity index; Sys=systolic; Bdia= begin diastolic.*

Table 3: Timing of contraction and valve opening and closure

	Controls (*N* = 18)	PS (*N* = 16)	iPAH (*N* = 18)	*P*-value iPAH to PS
RVFW peak (msec)[1]	473 ± 59	562 ± 76**	638 ± 76*	0.031
LVPW peak (msec)[1]	478 ± 48	538 ± 70#	564 ± 80*	0.547
Septal peak (msec)[1]	442 ± 74	435 ± 70	478 ± 51	0.212
Septal-D peak*[1]	-	-	613 ± 63	-
TOC (msec)[1]	58 ± 31	91 ± 24**	122 ± 36*	0.003
PV opening (msec)[2]	66 ± 12	81 ± 29	178 ± 76*	0.001
PV closure (msec)[2]	445 ± 52	514 ± 68*	500 ± 73	0.079
ET RVOT (msec)	374 ± 48	451 ± 60*	364 ± 62	0.001
AV opening (msec)[2]	83 ± 14	95 ± 15#	130 ± 40*	0.15
AV closure (msec)[2]	433 ± 52	461 ± 57	490 ± 63#	0.923
ET LVOT (msec)	354 ± 44	362 ± 46	375 ± 45	0.538
MV opening (msec)[3]	492 ± 52	537 ± 69#	592 ± 90*	0.520
TV opening (msec)[3]	478 ± 55	541 ± 88#	667 ± 98*	0.04
IVRT LV (msec)	63 ± 14	73 ± 16	103 ± 24*	0.015
TDI IVCT RV (msec)	70 [61-102]	61 [48-85]	90 [58-139]**	<0.001
TDI IVRT RV (ms)	28 [0-43]	33 [24-123]	95 [61-165]*	<0.001
MV inflow (msec)[3]	545 ± 49	531 ± 63	482 ± 82#	0.827
TV inflow (msec)[3]	557 ± 62	484 ± 87	399 ± 88*	0.251

*Timing measurements normalized for the RR interval, patients compared with controls using ANOVA with Dunnet's; #P < 0.05, *P < 0.01, **P < 0.001. Pulmonary stenosis (PS) are compared to idiophatic pulmonary arterial hypertension (iPAH) patients using ANCOVA using right ventricular systolic pressure as a covariate.*

RVFW, Right ventricular free wall; LVPW, Left ventricular posterior wall; D, diastolic peak; TOC, time to onset of contraction; PV, pulmonary valve; AV, aortic valve; MV, mitral valve; TV, tricuspid valve; IVRT, isovolumetric relaxation time.

[1]RVFW peak missing in 4 controls, 2 PS and 1 iPAH patients, these were excluded for all M-mode measurements.

[2]VA valve opening missing in 6 iPAH and 1 PS patient.

[3]AV opening was missing in 5 iPAH and 1 PS patient.

Differences between iPAH and PS

Septal kinetics and ventricular-ventricular interactions differed substantially between PS and iPAH. Peak systolic RV pressures were higher in pediatric iPAH vs. PS. Although this contributes to the differences between the patient populations, RVSP was included as a covariate in our analysis and the results were consistent across the entire range of RVSP – rendering this an insufficient explanation in and of itself.[27] As outlined above – altered timing of RVFW systolic events seems to be the main driver of adverse ventricular-ventricular interactions and septal displacement. The prolonged RV isovolumetric contraction time might partly relate to the longer QRS duration (mean 99.4 vs. 83.9 ms in PS), but seems insufficient to explain the large dispersion in peak RVFW thickening (638 ms in iPAH vs. 562 ms in PS). Irrespective of peak RV systolic pressures, afterload as defined by end-systolic wall stress, may be higher in iPAH vs. PS – in analogy with LV data, thereby resulting in a higher RV load in iPAH.[28] RV load in iPAH patients might be even further augmented by factors such decreased capacitance and reflected waves. The marked RV dilation in iPAH also contributes to septal displacement and decreased early LV filling – both directly and as a result of confinement within the common pericardial space.[9,29] Evidence of different RV adaptation to congenital lesions – such as PS, versus - later onset – iPAH is growing and the subject of separate studies investigating myocardial remodeling.[27] Furthermore, changes in RV afterload also alter IVS stress, possibly triggering adverse myocardial remodeling – with increased myocardial fibrosis.[30] In combination, with the adverse hemodynamics detailed above, this would be expected to worsen the biventricular inefficiency observed in the current study.

Clinical implication

Pulmonary vasodilators are the cornerstone of iPAH treatment and – by lowering pulmonary vascular resistance – decrease wall stress, improve trans-septal gradient and thus ventricular-ventricular interactions. However, despite combination therapy, RV pressure often remains elevated as observed in our iPAH cohort. Our data suggest that improvement of the timing of contraction, to decrease mechanical LVPW and RVFW discoordination, may be a worthwhile therapeutic target in iPAH. This may be achieved electro-mechanically – via pacing – or medically – by reversing myocardial remodeling that causes mechanical delays. Both approaches have been explored. Lumens et al. investigated RV pacing in a computer model of iPAH-RV failure and demonstrated improved RV end-diastolic volumes, RVFW myofiber work and pump function through improved distribution of workload.[31] Likewise, RV pacing improved LV diastolic filling in experimental isolated hearts and in an observational human study of chronic thrombo-embolic PAH.[32,33] We previously showed that pharmacological

intervention can also modulate adverse ventricular-ventricular interactions. In a rat model of iPAH, carvedilol improved biventricular remodeling, myocardial fibrosis and improved LV and RV Tau – shortening biventricular isovolumetric periods.[34]

Study limitations

This was a retrospective study with inherent limitations. Doppler data was missing in a small number of patients. Likewise, invasive hemodynamic data were not consistently available at time of echocardiography. iPAH is uncommon in children and the sample size is relatively small. However, the observations were consistent between patients. We were unable to provide clinical outcomes or exercise data. Although this is a drawback of the retrospective nature of our study – differences in natural history between iPAH and PS have been well described and we emphasized the mechanics and pathophysiology underlying these known differences.

Conclusion

Prolonged RVFW thickening, prolonged isovolumetric times and profound early and late systolic septal displacement are related to RV mechanical inefficiency, interventricular mechanical discoordination and decreased early LV filling in pediatric iPAH patients. These were absent in PS – suggesting that increased RVSP in itself is insufficient to explain the differences. Our findings show that iPAH affects systolic and diastolic mechanics in the right and left ventricles, and that the interaction between them is a prominent component of abnormal mechanics.

References

1. Haddad F, Doyle R, Murphy DJ, Hunt SA. Right ventricular function in cardiovascular disease, part II: pathophysiology, clinical importance, and management of right ventricular failure. Circulation 2008; 117:1717-1731,.
2. Haworth SG, Hislop AA. Treatment and survival in children with pulmonary arterial hypertension: the UK Pulmonary Hypertension Service for Children 2001-2006. Heart 2009; 95:312-317.
3. Peacock AJ, Crawley S, McLure L, et al. Changes in right ventricular function measured by cardiac magnetic resonance imaging in patients receiving pulmonary arterial hypertension-targeted therapy: the EURO-MR study. Circ Cardiovasc Imaging 2014;7: 107-114.
4. van Wolferen SA, Marcus JT, Boonstra A, et al. Prognostic value of right ventricular mass, volume, and function in idiopathic pulmonary arterial hypertension. Eur Heart J 2007; 28:1250-1257.
5. Hardegree EL, Sachdev A, Fenstad ER, et al. Impaired left ventricular mechanics in pulmonary arterial hypertension: identification of a cohort at high risk. Circ Heart Fail 2013; 6:748-755.
6. Belenkie I, Sas R, Mitchell J, Smith ER, Tyberg JV. Opening the pericardium during pulmonary artery constriction improves cardiac function. J Appl Physiol (1985) 2004;96: 917-922.
7. Friedberg MK, Redington AN. Right versus left ventricular failure: differences, similarities, and interactions. Circulation 2014; 129:1033-1044,.
8. Buckberg GD, RESTORE Group. The ventricular septum: the lion of right ventricular function, and its impact on right ventricular restoration. Eur J Cardiothorac Surg 2006; 29 Suppl 1:S272-S278,.
9. Santamore WP, Lynch PR, Meier G, et al. Myocardial interaction between the ventricles. J Appl Physiol 1976; 41:362-368.
10. Klima U, Guerrero JL, Vlahakes GJ. Contribution of the interventricular septum to maximal right ventricular function. Eur J Cardiothorac Surg 1998; 14:250-255
11. Santamore WP, Lynch PR, Heckman JL, et al. Left ventricular effects on right ventricular developed pressure. J Appl Physiol 1976; 41:925-930.
12. Dohi K, Onishi K, Gorcsan J 3rd, et al. Role of radial strain and displacement imaging to quantify wall motion dyssynchrony in patients with left ventricular mechanical dyssynchrony and chronic right ventricular pressure overload. Am J Cardiol 2008; 101: 1206-1212
13. Marcus JT, Gan CT, Zwanenburg JJ, et al. Interventricular mechanical asynchrony in pulmonary arterial hypertension: left-to-right delay in peak shortening is related to right ventricular overload and left ventricular underfilling. J Am Coll Cardiol 2008; 51:750-757
14. Barst RJ, Ertel SI, Beghetti M, Ivy DD. Pulmonary arterial hypertension: a comparison between children and adults. Eur Respir J 2011; 37:665-677
15. Lopez L, Colan SD, Frommelt PC, et al. Recommendations for quantification methods during the performance of a pediatric echocardiogram: a report from the Pediatric Measurements Writing Group of the American Society of Echocardiography Pediatric and Congenital Heart Disease Council. J Am Soc Echocardiogr 2010; 23:465-95
16. Teichholz LE, Kreulen T, Herman MV et al. Problems in echocardiographic volume determinations: echocardiographic-angiographic correlations in the presence of absence of asynergy. Am J Cardiol 1976; 37:7-11

17. Ryan T, Petrovic O, Dillon JC, et al. An echocardiographic index for separation of right ventricular volume and pressure overload. J Am Coll Cardiol 1985; 5:918-927
18. Kingma I, Tyberg JV, Smith ER. Effects of diastolic transseptal pressure gradient on ventricular septal position and motion. Circulation 1983; 68:1304-1314
19. Mori S, Nakatani S, Kanzaki H, et al. Patterns of the interventricular septal motion can predict conditions of patients with pulmonary hypertension. J Am Soc Echocardiogr 2008; 21: 386-393
20. Sciancalepore MA, Maffessanti F, Patel AR, et al. Three-dimensional analysis of interventricular septal curvature from cardiac magnetic resonance images for the evaluation of patients with pulmonary hypertension. Int J Cardiovasc Imaging 2012; 28:1073-1085
21. Lopez-Candales A, Dohi K, Rajagopalan N, et al. Right ventricular dyssynchrony in patients with pulmonary hypertension is associated with disease severity and functional class. Cardiovasc Ultrasound 2005; 3:23
22. Gan C, Lankhaar JW, Marcus JT, et al. Impaired left ventricular filling due to right-to-left ventricular interaction in patients with pulmonary arterial hypertension. Am J Physiol Heart Circ Physiol 2006; 290:H1528-H1533
23. Lumens J, Blanchard DG, Arts T, et al. Left ventricular underfilling and not septal bulging dominates abnormal left ventricular filling hemodynamics in chronic thromboembolic pulmonary hypertension. Am J Physiol Heart Circ Physiol 2010; 299:H1083-H1091
24. Marcus JT, Vonk Noordegraaf A, Roeleveld RJ, et al. Impaired left ventricular filling due to right ventricular pressure overload in primary pulmonary hypertension: noninvasive monitoring using MRI. Chest 2001; 119: 1761-1765
25. Lurz P, Puranik R, Nordmeyer J, et al. Improvement in left ventricular filling properties after relief of right ventricle to pulmonary artery conduit obstruction: contribution of septal motion and interventricular mechanical delay. Eur Heart J 2009; 30:2266-2274
26. Baker AE, Dani R, Smith ER, et al. Quantitative assessment of independent contributions of pericardium and septum to direct ventricular interaction. Am J Physiol 1998; 275:H476-H483
27. Bogaard HJ, Natarajan R, Henderson SC, et al. Chronic pulmonary artery pressure elevation is insufficient to explain right heart failure. Circulation 2009; 120:1951-1960
28. Borow KM, Colan SD, Neumann A. Altered left ventricular mechanics in patients with valvular aortic stenosis and coarction of the aorta: effects on systolic performance and late outcome. Circulation 1985; 72: 515-522
29. Belenkie I, Horne SG, Dani R, et al. Effects of aortic constriction during experimental acute right ventricular pressure loading. Further insights into diastolic and systolic ventricular interaction. Circulation 1995; 92: 546-554
30. Sanz J, Dellegrottaglie S, Kariisa M, et al. Prevalence and correlates of septal delayed contrast enhancement in patients with pulmonary hypertension. Am J Cardiol 2007; 100:731-735
31. Lumens J, Arts T, Broers B, et al. Right ventricular free wall pacing improves cardiac pump function in severe pulmonary arterial hypertension: a computer simulation analysis. Am J Physiol Heart Circ Physiol 2009; 297:H2196-H2205
32. Handoko ML, Lamberts RR, Redout EM, et al. Right ventricular pacing improves right heart function in experimental pulmonary arterial hypertension: a study in the isolated heart. Am J Physiol Heart Circ Physiol 2009; 297:H1752-H1759
33. Hardziyenka M, Surie S, de Groot JR, et al. Right ventricular pacing improves haemodynamics in right ventricular failure from pressure overload: an open observational proof-of-principle study

in patients with chronic thromboembolic pulmonary hypertension. Europace 2011; 13: 1753-1759
34. Okumura K, Kato H, Honjo O, et al. Carvedilol improves biventricular fibrosis and function in experimental pulmonary hypertension. J Mol Med (Berl) 2015; 93:663-674.

Chapter 6

Temporal RV-LV interactions and the effect of heart rate modulation on biventricular function in RV pressure-loading

Heart rate reduction improves biventricular function and interactions in experimental pulmonary hypertension

Authors
Olga Gomez, Kenichi Okumura, Osami Honjo, Mei Sun, Ryo Ishii, Bart Bijnens*, Mark K. Friedberg

* Co-senior authors.

(adapted from) Am J Physiol Heart Circ Physiol. 2018;314(3):H542-H551.

Abstract

Objectives: To investigate mechanisms of heart rate (HR) reduction on biventricular function and interactions in experimental pulmonary arterial hypertension (PAH).

Methods: We compared cardiac-cycle mechanics and interventricular interactions in 15 sham, 8 monocrotaline-PAH, 9 PAH+carvedilol and 8 PAH+ivabradine rats. We used echocardiography to assess biventricular function, timing of cardiac- cycle events and septal position in PAH rats; and related HR reduction effect on biventricular function measured by echocardiography and conductance catheter.

Results: HR was 302 in PAH+carvedilol, 303 in PAH+ivabradine vs. 359 bpm in PAH ($p<0.01$, respectively). Shams showed temporal alignment between right (RV) and left ventricular (LV) events; while PAH-rats showed increased biventricular isovolumic contraction times (ICT), delayed RV peak-radial motion and impaired early relaxation. Temporal malalignment was associated with decreased tricuspid and mitral diastolic annular peak velocities ($E´$) (3.7 vs. 6.4 and 3.4 vs. 5.3, $p<0.001$ respectively), delayed and shortened biventricular filling and reduced early-diastolic LV- filling (E) velocity (0.56 vs. 0.81, $p<0.01$). LV eccentricity index was increased in systole (2.0 vs. 1.2, $p<0.001$), early-diastole (2.1 vs. 1.1, $p < 0.001$) and end-diastole (1.6 vs. 1.1, $p<0.001$) in PAH vs. shams. HR reduction with carvedilol and ivabradine shortened biventricular ICT, time-to biventricular peak-radial motion, improved RV relaxation and increased early-diastolic LV filling through reduced inter-ventricular interaction and improved timing. These improvements corresponded with enhanced hemodynamics (increased cardiac-output, RV contractility and diastolic relaxation).

Conclusions: HR reduction by carvedilol and ivabradine improve biventricular filling and hemodynamics in experimental PAH through re-alignment of RV-LV cardiac-cycle events and improved interventricular interactions.

New and Noteworthy
Carvedilol improves biventricular function in experimental-PAH but the mechanisms of HR reduction vs. beta-blocker effect are inadequately defined. We demonstrate that reducing HR using either carvedilol or ivabradine (I_f inhibitor without beta-blocker effect), improves RV filling and biventricular hemodynamics through the re-alignment of RV-LV cardiac-cycle events and improved interventricular interactions.

Introduction

Right ventricular (RV) as well as left ventricular (LV) dysfunction drive mortality in pulmonary hypertension (PAH).[8,9,15] We previously showed that the ratio of RV systolic to diastolic duration (S:D ratio) is increased in PAH children in association with worse exercise tolerance and survival.[1] A high S:D ratio in PAH reflects prolonged leftward septal shift by the hypertensive RV and associated reduced LV filling, already compromised by the short diastolic duration; thereby reflecting adverse interventricular interactions.[7] With increasing heart rate (HR), diastole shortens and the S:D ratio increases exponentially; markedly so in PAH patients versus a much smaller change in controls.[1,21] Based on these clinical observations and on prior findings that carvedilol improves RV function in experimental PAH[2,3] we hypothesized that reducing HR in PAH would prolong diastole and decrease the S:D ratio, and might improve interventricular interactions leading to increased filling. This formed the rationale for studying carvedilol's effects in experimental PAH.[15] In that study, we found that carvedilol improved biventricular contractility and relaxation, measured by pressure-volume loops, reduced biventricular fibrosis, increased cardiac output, exercise capacity and a trend towards improved survival.[15]

However, the impact of HR reduction on biventricular function, interventricular interactions and timing of events in the cardiac cycle in PAH is incompletely defined; and whether carvedilol improves biventricular function in experimental PAH through HR reduction or through adrenergic receptor blockade remains unknown. Ivabradine is a selective inhibitor of the sinoatrial inward hyperpolarization-activated current (I_f) that reduces HR, without beta-blocker effects and without direct effects on global LV systolic function, coronary flow or pulmonary vascular resistance.[22-24] Therefore, ivabradine constitutes a very good tool to assess the effects of HR reduction on biventricular function in PAH, and to differentiate whether carvedilol´s beneficial effects are due to HR reduction or due to its anti-adrenergic properties. Delineating these effects is important as morbidity and mortality in PAH remain high, therapeutic options limited and beta-adrenergic receptor blockers are relatively contraindicated in this condition.[6,19] We hypothesized that reducing HR improves interventricular interactions in PAH independent of beta-adrenergic blockade. Accordingly, we aimed to investigate the effects of carvedilol and ivabradine on cardiac-intervals and interventricular interactions in a rat model of PAH.

GLOSSARY

RV= right ventricle

PAH= pulmonary arterial hypertension

LV= left ventricle

S:D ratio= systolic to diastolic ratio

HR= heart rate

ECG=electrocardiogram

ICT= isovolumic contraction time

ET= ejection time

IRT= isovolumic relaxation time

TAPSE= tricuspid annular systolic excursion

MAPSE= mitral annular systolic excursion

IVS= interventricular septum

EC= eccentricity index

ICC= intraclass correlation coefficient for absolute agreement

SERCA2a=sarco-endoplasmic-reticulum-Ca^{2+}-ATPase2a

Methods

We analyzed echocardiograms from male Sprague-Dawley monocrotaline-induced PAH rats (Charles River Laboratories, Senneville, Canada) from overlapping groups from previously reported experiment.[15] For the purposes of this investigation we excluded 2 PAH rats from the original experiment that had profound terminal bradycardia at echocardiography and studied 3 new animals not included in that experiment. For the current study we additionally studied a group of PAH rats treated with ivabradine. Animal care and experiments were conducted according to institutional Animal Ethic Committee and National Institutes of Health guidelines.

Experimental Protocol

The experimental protocol has been described previously.[15] Rats were 6-weeks old at protocol onset and randomly assigned to the following groups: (a) Shams: received a single subcutaneous injection of 0.9% saline (1 ml) (b) PAH: received a single subcutaneous injection of monocrotaline (60 mg/kg) to induce PAH, (c) PAH+carvedilol: rats were orally treated with carvedilol (15 mg/kg/day, for 3-weeks) and (d) PAH+ivabradine: rats were orally treated with ivabradine (10 mg/kg/d, for 3-weeks), the last two groups starting therapy 2-weeks after monocrotaline injection. Rats were euthanized by cardiac extraction under deep isoflurane 3% anesthesia at the terminal experiment, 5-weeks after the start of the protocol.

Echocardiography

Using a Vivid-E9 with 12-MHz phased-array transducer (General Electric, Wauwatosa, WI) under light isoflurane 3% sedation, 2D, M-mode, color and pulsed-Doppler were obtained with simultaneous electrocardiogram (ECG) display from rats surviving to the terminal experiment (5-weeks after the monocrotaline injection). Digital data were analyzed offline (EchoPac, version 8.0, GE). 3-cardiac cycles were analyzed using the ECG R-wave as a reference. Cardiac-cycle duration (RR-interval) and HR were recorded.

Tissue Doppler Imaging and Pulsed Doppler measurements

Tricuspid and mitral inflows were recorded from an apical 4-chamber view. Tricuspid and mitral inflow early (E) and late (A) velocities were measured from 3 cardiac-cycles and the mean value calculated. As illustrated in **Figure 1A**, time to tricuspid valve and mitral valve opening were measured from the onset of the ECG R-wave to the onset of tricuspid and mitral Doppler flow, respectively. Right ventricular (RV) and left ventricular (LV) inflow duration were measured from the Doppler early diastolic (E)-wave onset to late diastolic

(A)-wave termination. Pulmonary artery outflow was measured from a short-axis view. Pulmonary and aortic outflow were measured from short-axis and apical 5-chamber views, respectively. We used the conventional definition of the RV and LV isovolumic contraction times, as incorporating the electro-mechanical delay and isovolumic contraction time as measured from the onset of the ECG Q-wave to onset of pulmonary or aortic Doppler flow, respectively (**Figure 1B**).

Ejection time was measured from pulmonary and aortic Doppler flows. LV isovolumic relaxation time was measured from termination of aortic flow to onset of the following mitral E-wave using a Doppler sample straddling the LV inflow and outflow. RV isovolumic relaxation time was calculated as the time from pulmonary valve closure to tricuspid valve opening (ensuring images had the same HR). For all timing measurements, 3-cardiac cycles were analyzed. We also recorded total cardiac-cycle duration (measured as the ECG, RR-interval) and HR. Tricuspid and mitral lateral annulus pulsed tissue Doppler velocities (systolic velocity (S´), early (E´) and late (A´) diastolic velocities) were obtained from 3-cardiac cycles and the results averaged.

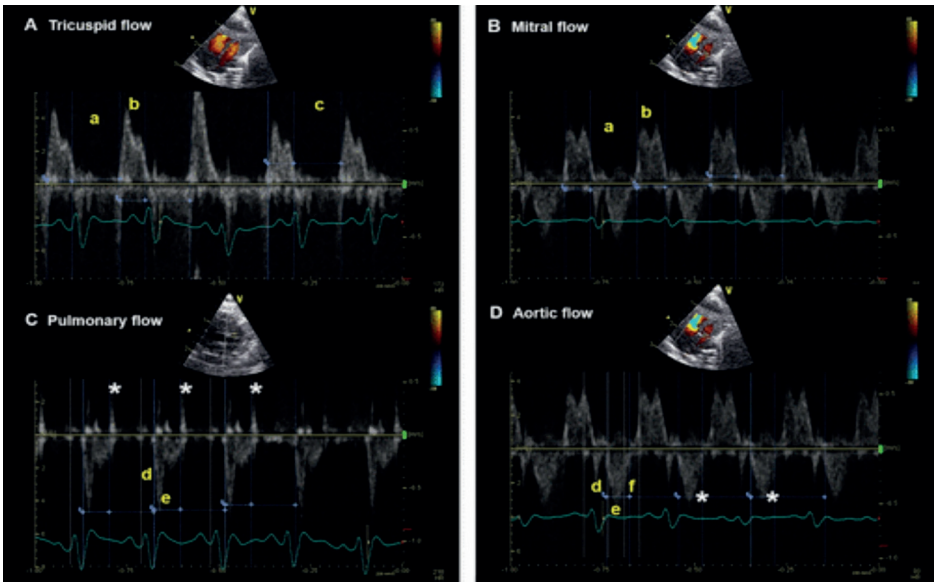

Figure 1

*A: timing measurements of tricuspid valve inflow. The time to tricuspid valve opening (measurement a) was measured from the onset of the ECG R wave to the onset of tricuspid flow. Right ventricular inflow duration (measurement b) was measured from the early diastolic (E) wave onset to late diastolic (A) wave termination. The time from closure to opening of the tricuspid valve (measurement c) was calculated from late diastolic (A) wave termination to the next early diastolic (E) wave onset. B: timing measurements of mitral valve inflow. The time to mitral valve opening (measurement a) was measured from the onset of the ECG R wave to the onset of mitral flow. Left ventricular inflow duration (measurement b) was measured from the early diastolic (E) wave onset to late diastolic (A) wave termination. C: pulmonary outflow from a short-axis right ventricular outflow view. Right ventricular isovolumic contraction time (measurement d) was measured from the onset of ECG R wave to the onset of the pulmonary flow. Ejection time (measurement e) was measured from pulmonary flow (*pulmonary valve closure). Right ventricular isovolumic relaxation time was calculated from closure to opening of the tricuspid valve (measurement c from A, including the isovolumic contraction the ejection the isovolumic relaxation times) and then subtracting the isovolumic contraction (measurement d) the ejection time (measurement e) from that interval. D: simultaneous sampling of aortic outflow and mitral inflow from an apical five-chamber view. Left ventricular isovolumic contraction time (measurement d) was measured from the onset of ECG R wave to the onset of the aortic flow. Ejection time (measurement e) was measured from aortic flow (*aortic valve closure). Left ventricular isovolumic relaxation time (measurement f) was measured from termination of the aortic flow to the onset of mitral early diastolic flow (E wave). The total cardiac cycle was defined as the ECG R-R interval.*

M-mode measurements

Time to maximum tricuspid and mitral annular systolic excursion (TAPSE, MAPSE) were measured in an apical 4-chamber view from the ECG-R wave onset (**Figure 2**). Time to peak RV and LV free-wall radial thickening were measured from the short-axis (**Figure 3A**). The pattern and sequence of interventricular septal (IVS) motion and time to maximal early-diastolic LV septal bowing were evaluated by M-mode.

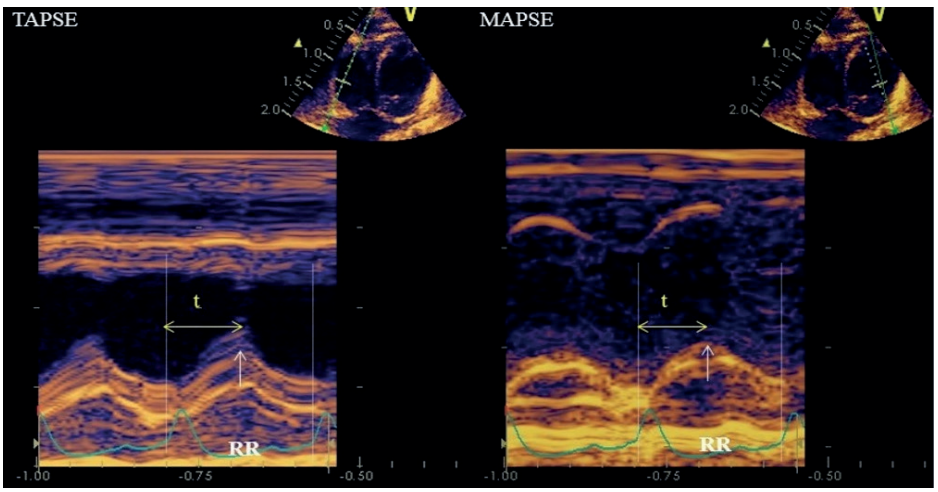

Figure 2

Time (t) from the onset of the ECG R wave (dotted line) to the maximum tricuspid annular systolic excursion (TAPSE) and mitral annular systolic excur- sion (MAPSE) by M-mode ECG in an apical four- chamber view from a rat with pulmonary arterial hyper- tension. The total cardiac cycle was defined as the ECG R-R interval (RR).

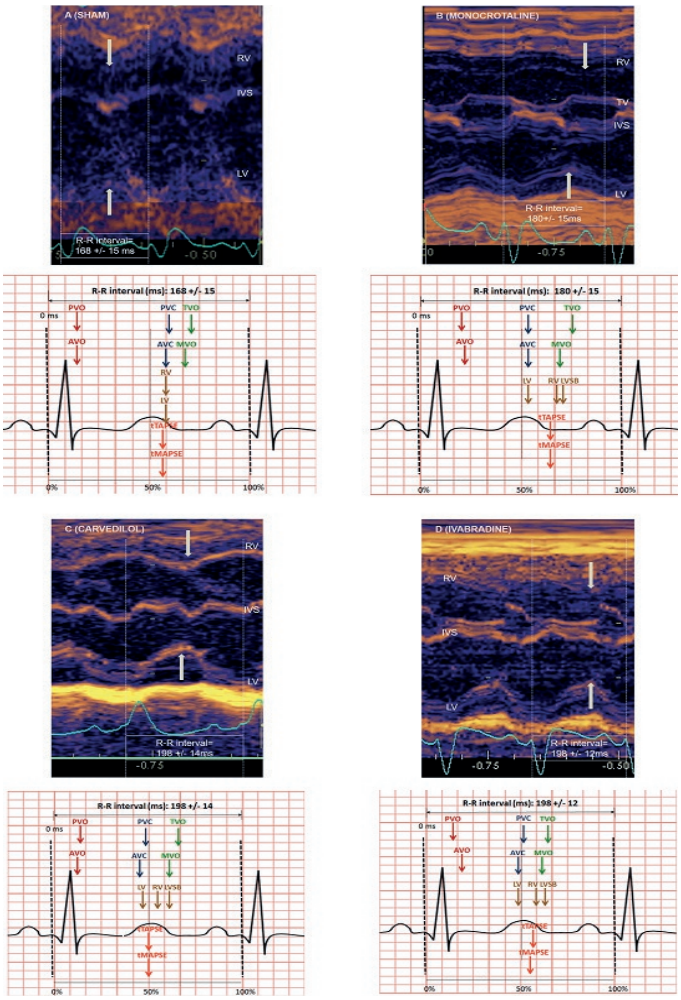

Figure 3

M-mode echocardiography depicting left ventricular (LV) and right ventricular (RV) free wall radial motion (arrows) in sham (A), pulmonary arterial hypertension (PAH; B), PAH carvedilol (C), and PAH ivabradine (D) groups. Note bowing of the interventricular septum (IVS) toward the left in LV early diastole [early diastolic LV septal bowing (LVSB)]. Mean R-R interval by group is shown. TV, tricuspid valve. A–D, bottom: schematic representation of the summary of timing measurements in sham (A), PAH (B), PAH carvedilol (C), and PAH ivabradine (D) groups. Doppler timing: PVO, pulmonary valve opening; AVO, aortic valve opening; PVC, pulmonary valve closure; AVC, aortic valve closure; TVO, tricuspid valve opening; MVO, mitral valve opening. M-mode timing: RV, RV peak radial motion; LV, LV peak radial motion; tTAPSE, maximum tricuspid systolic annular excursion; tMAPSE, maximum mitral systolic annular excursion.

2D assessment and interventricular interactions

The fractional area change (FAC) was calculated as end-diastolic-end-systolic/ end-diastolic RV areas from a 4-chamber view. The LV eccentricity index (EC) was obtained from a short-axis view at the LV papillary muscle level at end-systole, early-diastole and end-diastole (**Figure 4**). Images were analyzed frame-by-frame, simultaneously with the ECG, to describe the IVS configuration and position through the cardiac-cycle.

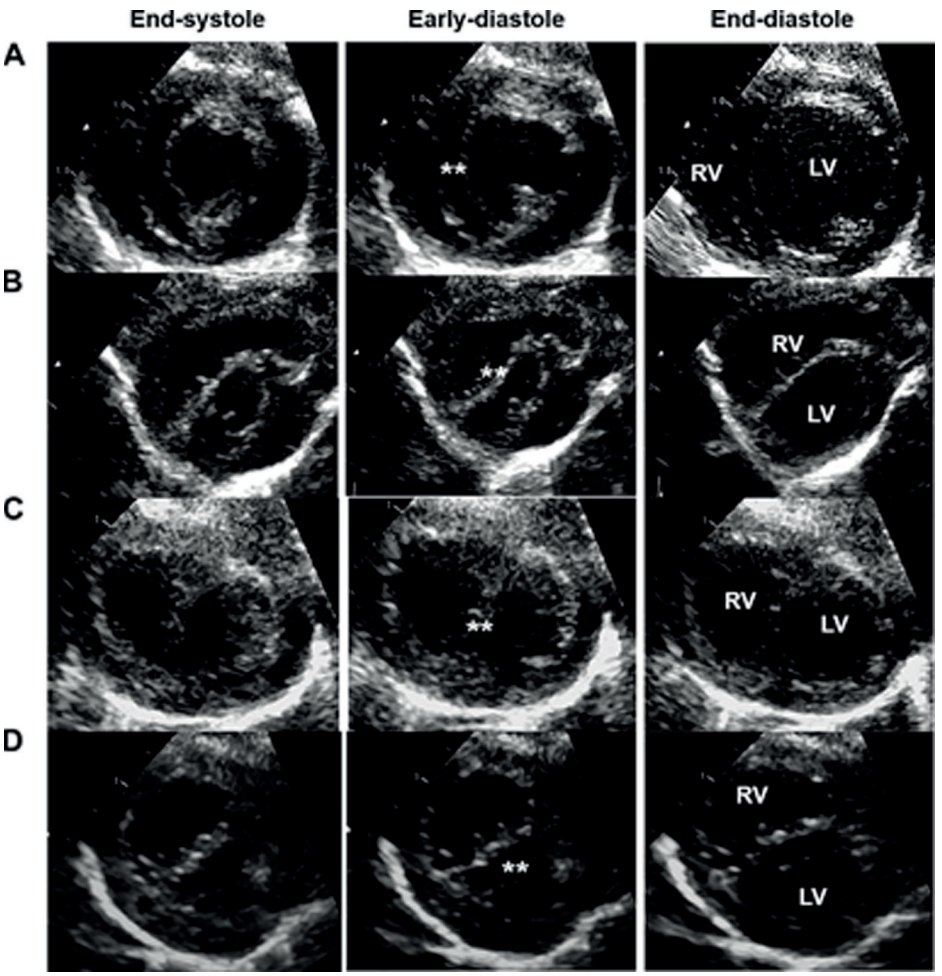

Figure 4

Short-axis view at left ventricular (LV) papillary muscle level in sham (A), pulmonary arterial hypertension (PAH; B), PAH carvedilol (C), and PAH ivabra- dine (D) groups. RV, right ventricle. The position of the interventricular septum (**) throughout the cardiac cycle is shown.

Invasively measured hemodynamics

At the terminal experiment, hemodynamics were measured immediately after echocardiography using a high-fidelity 2F conductance catheter (Millar Instruments, Houston, Tx) under 3% isoflurane anesthesia. Cardiac output (CO), end-systolic and diastolic volumes and pressures were determined from pressure-volume loops. The maximal rate of ventricular pressure rise and decay (dp/dt max, dp/dt min) were calculated. Tau was assessed as the time constant of mono-exponential decay of ventricular pressure during isovolumic relaxation. Myocardial contractility (elastance, Ees) was determined from a family of pressure-volume loops recorded during transient occlusion of the inferior vena cava. After measuring RV hemodynamics, the catheter was inserted through the LV apex to measure LV hemodynamics.

Statistical analysis

All timing measurements were normalized to the RR-interval and expressed as percentage of the cardiac-cycle. Data are presented as mean±standard deviation. Differences between groups were analyzed with one-way analysis of variance and *post- hoc* least significant difference test (SPSS, IBM). Intra- and inter-observer reliability were evaluated in 20-rats (n=5/ group). A two-way mixed-model (targets conceived as random samples) intraclass correlation coefficient (ICC) for absolute agreement was calculated.[5] A p-value < 0.05 was considered significant.

Results

Forty rats were studied (15 shams, 8 PAH, 9 PAH+carvedilol, 8 PAH+ivabradine). Their body weight (significantly reduced in all PAH groups as compared to Sham) and echocardiographic timing measurements are summarized in **Table 1** and **Figures 3A-D**. Invasive hemodynamic and functional parameters were obtained from 8 shams, 5 PAH, 9 PAH +carvedilol rats and 7 PAH+ivabradine rats (**Table 2)**.

Heart Rate

HR was reduced by 16% in the PAH+carvedilol and PAH+ivabradine groups vs. shams (302 and 304 beats per minute vs. 359 beats per minute, p<0.001 respectively). PAH rats had statistically similar HR as compared to shams (334 vs 359 beats per minute, *p=0.295*) (**Table 1**). The results of the LV+S/RV (Fulton) ratio were: Control: 0.28±0.03; PAH: 0.68±0.1; PAH+carvedilol: 0.55±0.12; PAH+ivabradine: 0.76±0.1 (all p<0.001 versus control).

Table 1. Summary of echo measurements

	Sham (n=15)	PAH (n=8)	PAH +carve-dilol (n=9)	PAH+ ivabradine (n=8)
Body weight (gr)	472.6±48.6	397.1±53.3*	403.6±73.8*	349.2±22.1**
HR (bpm)	359± 31.2§§§,µµµ	334± 27.6	302.5 ± 21.8***	303.6± 17.1***
RR- interval (ms)	167.6 ± 14.9§§§,µµµ	180.1± 15.2	198.5± 14.5***	198.5± 12.2***
Functional parameters				
TV E (cm/s)	0.50 ± 0.1	0.69 ± 0.1	0.57 ± 0.3	0.54 ± 0.1
TV A (cm/s)	0.70 ± 0.1	0.55 ± 0.1	0.69 ± 0.3	0.54 ± 0.2
RV E´(cm/s)	6.4 ± 2.1ŧŧ,µ	3.7 ± 1.3**,§	6.0 ± 1.2 ŧ	4.25± 0.7*
RV A´(cm/s)	6.1 ± 1.8ŧ	4.0 ± 1.5*	5.0 ± 1.4	4.1 ± 1.5
RV S´(cm/s)	6.3 ± 1.3ŧŧŧ	3.5 ± 0.6***,§§,µµ	6.1 ± 1.5ŧŧ	5.9 ± 1.1ŧŧ
RV FAC (%)	43.0± 5.0ŧŧŧ,§	24.5 ± 7.1***,µµ	33.8 ± 7.6*	36.1 ± 7.3 ŧŧ
MV E (cm/s)	0.81 ± 0.1 ŧŧ	0.56 ± 0.1**	0.71 ± 0.2	0.67± 0.1
MV A (cm/s)	0.74 ± 0.1	0.65 ± 0.1	0.64 ± 0.2	0.58± 0.1
LV E´(cm/s)	5.3 ± 1.1ŧŧ	3.4 ± 1.1**,§§,µ	5.3 ± 1.1 ŧ	4.9± 0.1 ŧ
LV A´(cm/s)	6.2 ± 0.4ŧ,µ	4.5 ± 2.0*	4.7 ± 1.8	4.4 ± 0.9*
LV S´(cm/s)	6.8 ± 1.3 ŧ	4.6 ± 2.0*	5.9 ± 1.7	6.25± 1.5
Left ventricle eccentricity index				
End-systolic EC	1.2 ± 0.1ŧŧŧ,µµ	2.0 ± 0.4***,§§	1.4 ± 0.3ŧŧ	1.70 ± 0.3**
Early-diastolic EC	1.1 ± 0.1ŧŧŧ,µµµ	2.1 ± 0.5***,§§	1.5 ± 0.4ŧŧ	1.9 ± 0.4***
End-diastolic EC	1.1± 0.1ŧŧŧ,§,µµµ	1.6 ± 0.3***	1.4 ± 0.3*	1.6 ± 0.3***
Pulsed Doppler timing parameters				
RV ICT	15.2 ± 3.7ŧŧ	21.8 ± 3.3**,§,µ	15.6 ± 6.4ŧ	15.9 ± 1.7ŧ
RV ET	44.0 ± 4.0ŧŧ,§§,µµ	35.7 ± 3.6**	35.4 ± 9.2**	35.9 ± 2.0**
Time-to-PVC	59.2 ± 6.5§	57.3 ± 3.6	48.4± 13.4*	51.75± 3.21
Time-to-TVO	70.3 ± 6.4	77.7 ± 8.9§,µµ	66.5 ± 8.6ŧ	64.5± 4.0ŧŧ
RV inflow duration	41.2 ± 5.5ŧŧŧ,§§,µ	26.8 ± 3.4***	30.1 ± 7.2**	32.1 ± 7.3**
RV IRT	10.6 ± 4.5	23.1 ± 15.5	18.9 ± 17.5	14.1± 2.7
LV ICT	15.8± 4.2ŧŧŧ	23.6 ± 4.9***,§§§,µ	14.0 ± 3.0ŧŧŧ	17.5 ± 2.6ŧŧ
LV ET	42.1 ± 4.1ŧŧŧ,§§§,µµµ	30.7 ± 3.7***	31.0 ± 3.4***	31.0 ± 3.0***
Time-to-AVC	57.9 ± 6.9§§§,µµ	54.4 ± 4.3§§	45.0 ± 4.2***,ŧŧ	48.4± 1.9**
Time-to-MVO	68.6 ± 6.2§§	70.7 ± 3.9§§,µ	60.5 ± 6.1**,ŧŧ	63.0 ± 4.2 ŧ
LV inflow duration	39.3 ± 2.9ŧ	33.3 ± 4.8*,§	39.3 ± 5.6ŧ	37.7 ± 5.0
LV IRT	12.9 ± 2.4	15.5 ± 3.1	14.9 ± 2.4	13.8 ± 2.3
M-mode timing parameters				
Time-to-RV peak-radial motion	58.0 ± 5.1ŧŧŧ	71.3 ± 10.0***,§§§,µµ	54.6 ± 6.8ŧŧŧ	58.6 ± 8.6ŧŧ
Time- to- LV peak- radial motion	58.5 ± 5.8§§,µµ	54.9 ± 5.5	46.3 ± 11.2**	48.6 ± 7.5**
Time-to- maximum LVSB	----	75.5 ± 9.6§,µ	59.7 ± 9.5ŧ	63.2 ± 9.2ŧ
Time-to-maximum TAPSE	57.3 ± 6.8ŧŧ	69.2 ± 6.6**,§§§,µµ	50.3 ± 8.8ŧŧŧ	57.0 ± 5.7ŧŧŧ
Time-to-maximum MAPSE	56.0 ± 8.1ŧ	66.9 ± 3.6**,§§	51.3 ± 10.5ŧŧ	56.3± 8.1

Caption on next page

Data shown as mean ± SD. Timing measurements are normalized to their RR-interval and are expressed as percentages. PAH= pulmonary hypertension, HR= heart rate, bpm= beats per minute, ms= milliseconds. **Functional echocardiographic parameters**: TV=tricuspid valve, MV= mitral valve, LV= left ventricle, RV= right ventricle, FAC= Fractional area change. **Doppler timing:** ICT= isovolumic contraction time, ET=ejection time, PVC= pulmonary valve closure, TVO= tricuspid valve opening, AVC= aortic valve closure, MVO= mitral valve opening, IRT= isovolumic relaxation time. **M-mode timing**: IVS= interventricular septum, LVSB= early-diastolic LV septal bowing, TAPSE= tricuspid systolic annular excursion, MAPSE= mitral systolic annular excursion.
*p<0.05, **p<0.01, ***p<0.001 vs sham rats.
^{t}p<0.05, ^{tt}p<0.01, ^{ttt}p<0.001 vs PAH rats.
§p<0.05, §§p<0.01, §§§p<0.001 vs PAH-carvedilol rats.
^{µ}p<0.05, ^{µµ}p<0.01, ^{µµµ}p<0.001 vs PAH-ivabradine rats.

Cardiac-cycle events

In shams, the pulmonary and aortic valves open and close near-simultaneously (**Figure 3A**), while the tricuspid valve opens slightly after the mitral valve. Compared with shams, PAH-rats had significantly increased RV ICT, delayed tricuspid valve opening and reduced RV ET as well as filling time. PAH-rats also showed increased LV ICT and reduced LV ET as well as filling time (**Figure 3B**). With HR reduction, RV ET and filling time remained short in PAH+carvedilol and PAH+ivabradine (**Figures 3C-D**) (due to high pulmonary vascular resistance, **Table 1**), but timings changed: RV as well as LV ICT shortened significantly, thus shifting timing of valve opening towards normality. Filling time (although only significantly for the LV with carvedilol) had a tendency to normalize. The delay in RV cardiac-cycle events detailed above in PAH-rats correlated with a significant left-to-right radial motion misalignment between the RV and LV seen on M-mode. RV peak-radial motion occurred significantly later and for a longer duration (**Figure 3B**). Consequently, LV relaxation started while the RV was still contracting. RV and LV longitudinal shortening was largely simultaneous, but significantly delayed in PAH-rats (**Table 1, Figure 3B**) as compared to shams, in which RV and LV peak-radial motion and early-relaxation occurred simultaneously, coinciding with peak-longitudinal TAPSE and MAPSE (**Figure 3A**). Due to prolonged RV systole, reduced RV ejection time in PAH-rats, RV filling time was significantly shortened (**Table 1**) and delayed to late-diastole, coinciding with atrial contraction (**Figure 3B**). As shown in **Table 1**, these findings were also associated with reduced tricuspid and mitral lateral annulus tissue Doppler systolic (S´), early (E´) and late (A´) diastolic velocities. The addition of carvedilol and ivabradine significantly improved LV-RV radial contractile alignment (**Figures 3C-D**), with RV free-wall peak-radial contraction occurring earlier; and as observed on M-mode, faster early RV relaxation (**Figures 3B-D**). Carvedilol also reduced times to peak TAPSE and MAPSE compared with the PAH-group (**Table 1, Figure 3C**)

and normalized both tricuspid and mitral lateral annulus systolic and diastolic velocities (**Table 1**). Ivabradine reduced time to peak TAPSE compared with PAH-group (**Table 1, Figure 3D**) but its effects on tricuspid and mitral annulus systolic and diastolic velocities were more modest (**Table 1**).

Interventricular interactions

Visual analysis of M-mode in shams showed simultaneous IVS, RV and LV lateral free-wall motion, without early-diastolic LV septal bowing (**Figure 3A**). Conversely, 90% of PAH-rats showed early-diastolic leftward septal bowing as a consequence of LV-RV disparate radial motion and delayed RV relaxation described above (**Figure 3B**). Frame-by-frame 2D assessment of IVS configuration in the short-axis view confirmed M-mode findings: shams had a circular LV with normal round IVS curvature and position throughout the cardiac-cycle (**Figure 4A**), while in PAH-rats the RV was markedly enlarged, the LV flattened and 'D-shaped' throughout the cardiac-cycle (**Figure 4B**); with the IVS displaced leftward in systole and early-diastole and flattened into late-diastole. These findings were associated with significantly higher LV EC throughout the cardiac-cycle in PAH-rats vs. controls (**Table 1**). Based on visual M-mode assessment (**Figures 3C-D**) carvedilol and ivabradine led to faster early RV relaxation and significantly reduced time to maximal LV septal bowing compared with untreated PAH-rats (**Table 1, Figures 3B+D**). This corresponded with the shorter tau found in these animals (**Table 2**). Moreover, carvedilol significantly reduced LV EC index in systole and early-diastole (**Table 1**). Although the RV remained enlarged and TV inflow duration short in both treated groups, the improvement in interventricular coupling in early-diastole translated into an increased early diastolic LV filling (E) velocities and normalized lateral mitral annular peak diastolic tissue velocities (**Table 1**). Biventricular early-systolic function was also improved with carvedilol as reflected by reduced time to maximal TAPSE and MAPSE and increased tricuspid and mitral lateral annular peak-systolic tissue velocities (**Table 1**).

Hemodynamics and function

Hemodynamics and function variables are summarized in **Table 2**. RV peak systolic pressure and RV/LV systolic pressure ratio were increased in all PAH groups vs. shams and not different between PAH groups. The improved RV and LV mechanics, timing and interventricular interactions detailed above with HR reduction corresponded with improved hemodynamics as seen by increased CO, RV contractility (dP/dTmax, Ees) and diastolic relaxation (dP/dTmin, Tau).

Table 2. Summary of invasive hemodynamic and functional parameters

	Sham (n=8)	PAH (n=5)	PAH +carvedilol (n=9)	PAH + ivabradine (n=7)
CO (mL/min)	103.6 ± 60.5	34.9 ± 22.3	57.9 ± 33.8	79.8 ± 27.4
Right ventricle parameters				
Peak Systolic pressure (mmHg)	23.4 ± 1.9ŧ,§§,µµµ	58.1 ± 21.6*	55.4 ± 24.5**	68.1 ± 14.9***
End-diastolic pressure (mmHg)	1.7 ± 1.2	1739.7 ± 457	1.43± 1.3	2.5 ± 1.6
dP/dt max (mmHg /sec)	1011.7 ± 397.6§§,µµµ	-1720.5± 671	1980.2 ± 696.7**	2313.8± 430.9***
dP/dt min (mmHg /sec)	-740.0 ± 166.1§,µ	26.9 ± 11.2	-1827.9 ± 1006.9*	-2063.3 ± 840.8*
Ees (mmHg/mL)	121.4 ± 90.2	13.2± 2.4*,µ	114.7 ± 69.8	191.4 ± 70.3
Tau (ms)	7.00 ± 1.4ŧŧ		10.11 ± 2.9	8.6 ± 2.2ŧ
Left ventricle parameters				
Peak Systolic pressure (mmHg)	78.1 ± 14.1	65.4 ± 17.9	66.1 ± 22.7	76.0 ± 26.7
End-diastolic pressure (mmHg)	3.9± 0.7	3.4± 3.0	2.5± 1.5	4.0± 1.2
dP/dt max (mmHg /sec)	3195.2 ± 618.2	2768.3 ± 1212	3048.9 ± 1389.0	3236.4 ± 1133.1
dP/dt min (mmHg /sec)	-2650.4 ± 649.6	-1537.2 ± 822	-1989.3± 1035.9	-1804.8± 706.0
Ees (mmHg/mL)	289.7 ± 344.0	53.8 ± 11.0	330.7 ± 284.6	157.3 ± 93.2
Tau (ms)	8.6 ± 1.5	9.3 ± 4.9	9.3 ± 3.9	8.0± 2.4
RVp/LVp	0.3± 0.1ŧ,§§,µµ	0.9 ± 0.3*	0.9± 0.3**	0.9 ± 0.2**

Data shown as mean ± SD. PAH= pulmonary hypertension, CO= cardiac output, Ees= end-systolic elastance.

**p<0.05, **p<0.01, ***p<0.001 vs sham rats.*

ᵗ p<0.05, ᵗᵗ p<0.01, ᵗᵗᵗ p<0.001 vs PAH rats.

§ p<0.05, §§ p<0.01, §§§ p<0.001 vs PAH-carvedilol rats.

µ p<0.05, µµ p<0.01, µµµ p<0.001 vs PAH-ivabradine rats.

Intra-observer and inter-observer reliability:
Intra-observer and inter-observer reproducibility for echo measurements was good (**Table 3**).

Table 3. Intra-observer and inter-observer variability

Echocardiographic parameter	Intra-observer ICC	95%-CI	*p**	Inter-observer ICC	95%-CI	*p**
t-MVO	0.95	(0.81-0.98)	0.000	0.92	(0.57-0.98)	0.000
RV ICT	0.78	(0.24-0.94)	0.011	0.96	(0.88-0.99)	0.000
t-LV peak-radial motion	0.86	(0.54-0.96)	0.001	0.82	(0.44-0.94)	0.002
t-maximum TAPSE	0.76	(0.14-0.93)	0.016	0.92	(0.76-0.97)	0.000
LV End-systolic EC	0.78	(0.34-0.93)	0.003	0.63	(-0.03-0.87)	0.024

ICC= intraclass correlation coefficient; 95%-CI= 95% confidence interval; RV= right ventricle, LV= left ventricle, t-MVO=time-to-mitral valve opening; ICT= isovolumic contraction time; t-LV=time-to-LV peak-radial motion; t-TAPSE=time-to-maximum tricuspid systolic annular excursion; EC=eccentricity index. p < 0.05 considered significant.*

Discussion

We evaluated the mechanical effects of HR reduction on cardiac-cycle events and function in experimental PAH. We demonstrate that despite persistent PAH, carvedilol and ivabradine improve early RV relaxation and realign RV-LV radial motion by reducing biventricular ICT and normalizing longitudinal biventricular motion. In particular, these effects improve early LV filling and therefore biventricular systolic and diastolic function and hemodynamics. This detailed analysis provides a mechanistic basis for carvedilol's beneficial effects on biventricular function in PAH and strengthens the basis for investigating its use in clinical PAH.[2,3,15]

Heart-rate effects

Improved interventricular interactions were at least partially, attributable to HR. However, although carvedilol and ivabradine significantly decreased HR in PAH-rats, RV diastolic duration did not lengthen significantly, nor did ejection time shorten. Nonetheless, we observed improvements in biventricular diastolic function and ventricular filling. Of note, the mean HR was not different in the PAH-group compared to shams, which differs from the PAH-rats presented in our previous experiment.[15] This difference may be explained by 3 rats not being the same individuals.

Systolic radial alignment

Carvedilol led to re-alignment of RV-LV peak-radial motion. Earlier RV peak-radial motion in the PAH+HR reduction was associated with significant biventricular ICT shortening (**Table 1**). Left-right delay in peak myocardial shortening in PAH patients is caused by prolonged rather than delayed RV contraction[12] including increased ICT. This causes early-diastolic LV septal bowing, decreased LV filling and decreased stroke volume, all important features in the PAH-group. Computer modeling suggests that electrically pre-exciting the RV leads to simultaneous RV-LV contraction thereby improving biventricular function and filling.[11] We now show similar beneficial effects on these critical events with carvedilol and ivabradine, despite persistent PAH. Moreover, we demonstrate inefficient RV contraction in PAH as RV peak-radial contraction occurs after pulmonary valve closure, and close to tricuspid valve opening (**Figure 3B**), consistent with RV post-systolic contraction present in PAH patients.[12,13] Overall, HR reduction improved interventricular radial mechanical synchrony due to earlier and shorter ICT and better aligned RV radial mechanics.

Improvements in systolic and diastolic function

RV contractility and relaxation were improved with HR reduction using pressure-volume loop derived end-systolic elastance, time-constant of RV relaxation (tau) and dP/dT minimum (**Table 2**). These are consistent with the improved RV relaxation seen by M-mode and tissue Doppler velocities in the current study and associated with improved LV filling. Early RV relaxation, as measured by *tau* and decreased diastolic tissue Doppler velocities, is abnormal in clinical PAH even when contractility is still preserved early in the disease course.[4,14] Both impaired relaxation and post-systolic contraction compromise diastolic function.[12,13] In the present study we demonstrate that carvedilol and ivabradine not only improve RV relaxation and diastolic performance as seen by tissue Doppler imaging, M-mode and Doppler flow, but also enhance biventricular function in early systole. Thus, improved RV relaxation seems important in explaining not only improved RV diastolic, but also systolic function, S:D ratio and early-diastolic interventricular interactions. Together, the re-alignment of radial mechanics and earlier longitudinal motion towards normal induced by HR reduction, lead to improved early-diastolic LV geometry and improved LV filling in early diastole. Peak systolic pressure and cardiac output in the ivabradine-treated group tended to be higher than the carvedilol-treated group. The carvedilol treated group may have somewhat lower peak systolic pressures and cardiac output due to a negative inotropic effect versus ivabradine. However, the RV/LV pressure ratio was the same in all groups allowing comparison between them in terms of the pulmonary hypertension.

Postulated mechanisms of action

We did not study the molecular mechanisms underlying the biventricular mechanics investigated in the current study, but these are worthy of a short hypothesis-generating discussion. As ivabradine induced similar effects to carvedilol, the effects could be attributable to a lower HR. However, rather than lengthening RV and LV filling time per se, the effect is based on a change in the timing of events, where ICT shortens and leads to a normalization of the timings in the cardiac cycle that were importantly changed due to the PAH. Related to this, the interventricular interaction changes with HR reduction, thereby attenuating the important septal shift in early diastole. From M-mode images, a restoration of the early outwards motion of the RV wall can be seen, thus also improving early LV filling. While it is difficult to completely distinguish between heart rate reducing effects versus other components of beta-blocker effects of carvedilol, the similar improvement in ventricular function and contractility seen in both the carvedilol and ivabradine treated groups suggests that it is heart rate reduction, rather than beta-blockade per se, that leads to improved function. We postulate that this occurs through re-alignment of RV and LV events and improved diastolic relaxation.

The exact mechanisms remain to be elucidated. One postulated mechanism may relate to the timing of actin-myosin cross-bridging. Increased afterload reduces myocyte shortening velocity and prolongs shortening.[25] Thus, RV pressure remains higher for a longer duration than the LV. Consequently, RV actin-myosin cross-bridge cycling may lengthen (hyper-bridging) resulting in stiffer myocardium at end-ejection, prolonging IRT and hampering early-relaxation. Although not proven in this study, HR reduction and associated changes in ICT may improve RV early-relaxation by reducing actin-myosin crossbridging, resulting in more compliant myocardium at end-systole.[10,25] This could explain the observed improvements in RV relaxation, contractility, LV-RV interactions and LV early-diastolic filling, as well as the trend to reduced RV and LV end-diastolic pressures.

We previously showed that carvedilol upregulates RV sarco-endoplasmic-reticulum-Ca^{2+}-ATPase2a (SERCA2a) expression in experimental PAH with a similar trend in the LV.[15] Downregulated SERCA2a in failing myocardium impairs intracellular calcium cycling, affecting troponin-C binding and actin-myosin crossbridging, worsening contractile and diastolic function.[17] Conversely, restoration of SERCA2a improves calcium cycling and cardiac function.[17] Based on our current results and prior findings, we hypothesize that HR reduction may improve calcium handling and myocardial relaxation by restoring SERCA2a. This requires confirmation in further studies. Likewise, we previously found biventricular fibrosis in PAH-rats and its amelioration with carvedilol through downregulated transforming-growth-factor-beta signaling.[15] Decreased fibrosis may further explain the observed improvement in systolic and diastolic

performance, reduced leftward septal bowing and improved interventricular interactions. Likewise, in our prior study, RV and LV cardiomyocyte diameter were increased with PAH and decreased with carvedilol (reaching statistical significance for the RV), albeit not to baseline size .[15] Whether there is a differential effect of pure HR reduction (ivabradine) or additional contractility modulation (carvedilol) remains to be studied.

Clinical implications

Many PAH patients expire from RV failure[9], but cardiac-specific treatments are lacking.[6] Beta-adrenergic receptor blockers, and HR reduction in general, improve heart function and survival in left heart failure[16], but are currently contraindicated in PAH because of potential detrimental effects on cardiac output.[19] However, we and others have demonstrated in experimental PAH, that beta-adrenergic receptor blockers, and selective inhibition of the sinoatrial inward hyperpolarization-activated current, improve biventricular function, stroke volume, cardiac output and exercise capacity, despite persistent PAH.[3,15,18] These changes were accompanied by a lower RV S:D ratio[15], a clinically relevant finding as increased S:D ratio is associated with mortality in pediatric PAH.[1] Moreover, in early PAH, the RV maintains contractility, but there may be coexisting abnormal early relaxation.[14] The results of the current study suggest the need for carefully controlled human trials to test the safety and efficacy of HR reduction in PAH recognizing that the density and distribution of cardiac adrenergic receptors (in the case of beta-blockers) can differ between rodents and humans, which can impact the clinical implications of our findings.

Study limitations

The aim of the present study was to investigate carvedilol's and ivabradine's effects on cardiac-cycle events and mechanics in PAH and we did not evaluate molecular mechanisms. Likewise, we did not directly assess RV compliance or crossbridging. The limitations of experimental PAH models are well known. Relevant to the current study, we previously demonstrated in a monocrotaline-PAH that carvedilol did not act through alleviation of myocarditis or lung inflammation, both absent in these animals.[15] Importantly, PAH was persistent, allowing study of carvedilol's and ivabradine's biventricular effects without the confounding effect of decreased pulmonary vascular resistance. The 12-mHz probe used in this study is of relatively low frequency. However, we have found that in rats the 12-Mhz transducer often produces better quality images than very high frequency transducers designed predominantly for use in mice and

have recently reported good feasibility and reproducibility using a 10 Mhz probe in a rabbit model.[20] In the current study, we also performed inter and intra-observer reliability which was found to be good (**Table 3**) Moreover, the same probe was used across all groups and thus the comparison is subject to the same conditions and is valid.

Conclusion

In conclusion, we demonstrate that in experimental PAH, HR reduction improves RV early-relaxation and diastolic function, leading to re-alignment of systolic RV-LV peak-radial mechanics and interventricular interactions. These improved mechanics and biventricular function were associated with improved cardiac output and hemodynamics.

References

1. Alkon J, Humpl T, Manlhiot C et al. Usefulness of right ventricular systolic to diastolic duration ratio to predict functional capacity and survival in children with pulmonary arterial hypertension. Am J Cardiol. 2010; 3:430-436
2. Bogaard HJ, Abe K, Vonk-Noordegraaf A et al. The right ventricle under pressure: Cellular and molecular mechanisms of right heart failure in pulmonary hypertension. Chest. 2009; 135:794–804.
3. Bogaard HJ, Natarajan R, Mizuno S at al. Adrenergic receptor blockade right heart remodeling and dysfunction in pulmonary hypertensive rats. Am J Res Crit Car Med. 2010; 182:652-660.
4. Faludi R, Komócsi A, Bozó J et al. Isolated diastolic dysfunction of right ventricle: stress-induced pulmonary hypertension. Eur Respir J. 2008; 31(2):475–476.
5. Fleiss J. Statistical Methods for Rates and Proportions. In John Wiley and Sons: New York (2nd edition). 1981
6. Galie N, Hoeper MM, Humbert M et al. The Task Force for the Diagnosis and Treatment of Pulmonary Hypertension of the European Society of Cardiology (ESC) and the European Respiratory Society (ERS) endorsed by the International Society of Heart and Lung Transplantation (ISHLT). Guidelines for the diagnosis and treatment of pulmonary hypertension. Eur Respir J. 2009; 34:1219–1263
7. Gan CT, Lankhaar JW, Marcus JT et al. Impaired left ventricular filling due to right-to-left ventricular interactions in patients with pulmonary arterial hypertension. Am J Physiol Heart Circ Physiol. 2006; 290:1528-1533.
8. Hardegree EL, Schadev A, Fentad ER et al. Impaired left ventricular mechanics in pulmonary arterial hypertension. Cir Heart Fail. 2013; 6: 748-755.
9. Humbert M, Sitbon O, Simonneau G. Treatment of pulmonary arterial hypertension. N Engl J Med 2004; 351:1425–1436.
10. Lee JA, Allen DG. Calcium sensitizers: mechanisms of action and potential usefulness as inotropes. Cardiovasc Res. 1997; 36:10-20.
11. Lumens J, Arts T, Broers B et al. Right ventricular free wall pacing improves cardiac pump function in severe pulmonary arterial hypertension: a computer simulation analysis. Am J Physiol Heart Circ Physiol. 2009; 297: H2196-H2205
12. Marcus JT, Gan TJ Zwanenburg J et al. Interventricular mechanical asynchrony in pulmonary arterial hypertension. Left-to-right delay in peak shortening related to right ventricular overload and left ventricular underfilling. J Am Coll Cardiol. 2008; 51:750-757.
13. Mauritz G-J, Marcus JT, Westerhof N et al. Prolonged right ventricular post-systolic isovolumic period in pulmonary arterial hypertension is not a reflection of diastolic dysfunction. Heart. 2011; 97:473–478.
14. Murch SD, La Gerche A, Roberts T et al. Abnormal right ventricular relaxation in pulmonary hypertension. Pulm Circ. 2015; 5:370-375.
15. Okumura K, Kato H, Honjo O et al. Carvedilol improves biventricular fibrosis and function in experimental pulmonary hypertension. J Mol Med. 2015; 93:663-74.
16. Packer M, Coats AJS, Fowler MB et al. Effect of carvedilol on survival in severe chronic heart failure. N Engl J Med 2001; 344:1651–1658.
17. Periasamy M, Bhupathy P, Baby GJ. Regulation of sarcoplasmic reticulum ca2+ ATPase pump

expression and its relevance to cardiac muscle physiology and pathology. Cardiovasc Res 2008; 77:265-273
18. Perros F, Ranchoux B, Izikki M et al. Nebivolol for Improving Endothelial Dysfunction, Pulmonary Vascular Remodeling, and Right Heart Function in Pulmonary Hypertension. J Am Coll Cardiol. 2015; 65:668–680
19. Provencher S, Herve P, Jais X et al. Deleterious effects of Beta-adrenergic receptor blockers on exercise capacity and hemodynamics in patients with portopulmonary hypertension. Gastroenterology. 2006; 130:120–126
20. Ramos SR, Pieles G, Hui W, et al. Comprehensive echocardiographic assessment of biventricular function in the rabbit, animal model in cardiovascular research: feasibility and normal values. Int J Cardiovasc Imaging. 2018; 34(3): 367-375.
21. Sarnari R, Kamal RY, Friedberg MK et al. (2009) Doppler assessment of the systolic to diastolic duration in normal children: relation to heart rate, age and body surface area. J Am Soc Echocardiography; 22:928-932.
22. Simon L, Ghaleb B, Puybasset L, et al. Coronary and hemodynamic effects of s 16257, a new bradycardic agent, in resting and exercising conscious dogs. J Pharmacol Exp Ther. 1995; 275:659-666
23. Thollon C, Bidouard JP, Cambarrat C, et al. Stereospecific in vitro and in vivo effects of the new sinus node inhibitor (+)-s 16257. Eur J Pharmacol. 1997; 339:43-51.
24. Thollon C, Cambarrat C, Vian J, et al. Electrophysiological effects of s 16257, a novel sino-atrial node modulator, on rabbit and guinea-pig cardiac preparations: Comparison with ul-fs 49 . Br J Pharmacol. 1994;112:37-42
25. de Tombe PP, ter Keurs HE. The velocity of cardiac sarcomere shortening: mechanisms and implications. Muscle Res Cell Motil. 2012; 33:431–437.

Chapter 7

The effects of RV pressure-loading on activation of biventricular fibrosis

Adverse Biventricular Remodeling in Isolated Right Ventricular Hypertension is Mediated by Increased TGFβ1 Signaling and is Abrogated by Angiotensin Receptor Blockade Using Losartan.

Authors
Mark K. Friedberg, Mi-Young Cho, Jing Li, Renato S. Assad, Mei Sun, Sagar Rohailla, Osami Honjo, Christian Apitz, Andrew N. Redington

(adapted from) Am J Respir Cell Mol Biol. 2013 Dec;49(6):1019-28

Abstract

Objectives: The pressure-loaded right ventricle (RV) adversely impacts left ventricular (LV) function. We recently found that these ventricular-ventricular interactions lead to LV myocardial fibrosis through TGFβ signaling. The main objective is to investigate the mechanisms mediating biventricular fibrosis in RV afterload and their potential modification by angiotensin receptor blockade.

Methods: An adjustable pulmonary artery band (PAB) was placed in rabbits. In sham operated controls, the band was left un-inflated (n=6). In the RV afterload group the PAB was sequentially inflated to generate systemic RV pressure at 28 days (n=8). In a 3rd group the PAB was inflated to systemic levels and the angiotensin receptor blocker losartan was added (n=6). Five weeks after surgery the animals were sacrificed for assessment of biventricular hypertrophy, fibrosis, apoptosis and components of their signaling pathways.

Results: PAB animals developed biventricular hypertrophy, fibrosis and apoptosis versus shams, which were decreased with losartan. RV and LV TGFβ, CTGF; ET1, ENDRB and MMP2/9 mRNA levels were increased in PAB animals vs. shams and decreased with losartan. Given marked biventricular CTGF upregulation in PAB and downregulation with losartan, we investigated CTGF signaling. RV and LV Smad 2/3/4 protein levels, and LV RhoA mRNA levels were increased with PAB and reduced with losartan.

Conclusions: Isolated RV afterload induces biventricular fibrosis and apoptosis which are reduced by angiotensin receptor blockade. Adverse ventricular-ventricular interactions induced by isolated RV afterload appear to be mediated through TGFβ1-CTGF and ET-1 pathways.

Abbreviations

RV = right ventricle
LV = left ventricle
PAB = pulmonary artery banding
TGFβ = transforming growth factor β
OCT = Optimal Cutting Temperature
HE= haematoxylin-eosin
PSR = picrosirius red F3BA
RNA = Ribonucleic acid
CTGF =connective tissue growth factor
TUNEL= terminal deoxynucleotidyl transferase-mediated dUTP nick-end labeling
MMP = matrix metalloproteinase
ENDRA = endothelin receptor type A

ENDRB = endothelin receptor type B
ET1 =endothelin 1

Introduction

Pulmonary hypertension continues to carry high morbidity and mortality. While most research has focused on reducing pulmonary vascular resistance; treatment is ultimately limited by disease progression and ventricular failure. Although prognosis is linked to right ventricular (RV) performance, the hypertensive RV significantly impacts left ventricular (LV) filling, output and function. We have developed a rabbit model of systemic RV afterload induced by pulmonary artery banding (PAB) and found that RV- afterload induced ventricular-ventricular interactions extend far beyond hemodynamic interactions, to profoundly affect LV myocardial health.[1] A particularly striking finding was that isolated RV afterload lead not only to marked RV fibrosis, but to LV fibrosis as well. Interestingly, the addition of mild aortic afterload by aortic banding modified the RV hypertrophic response and decreased not only the RV fibrosis (in keeping with a demonstrable improvement in RV contractility), but also LV fibrosis.[1] The improvement in both RV and LV fibrosis was associated with reversal of PAB-induced increases in pro-fibrotic signaling, particularly transforming growth factor β1 (TGFβ1).[1] However, the clinical utility of aortic banding in PAH patients is limited. Given the observed increase in biventricular TGFβ1 with PAB and its reduction with aortic banding; and given the well-documented potential to modulate TGFβ1 through inhibition of angiotensin II, there is potential to pharmacologically modify ventricular-ventricular interactions for reduction of myocardial fibrosis. However, despite important therapeutic potential this has not been studied in modulating RV-afterload induced biventricular injury. Accordingly, the objectives of this study were to investigate the effects of angiotensin receptor blockade on biventricular fibrosis in response to isolated RV afterload.

Methods

Animal Model

Preparation: Sham operation and PAB were performed in 3 kg adult New Zealand white male rabbits (Charles River, Canada). Anesthesia was initiated with isoflurane 3%, and acepromazine 1.1 mg/kg and maintained with isoflurane 1.5-2%. Ventilation was controlled to maintain normal blood gases. Heart rate and oxygen saturation were continuously monitored.

Banding Devices: Incremental PAB was achieved using a an adjustable banding device (ABS, Silimed, Brazil)[13] implanted beyond the pulmonary valve via left thoracotomy as detailed previously.[1] Animals were then allocated to either the sham operated control group, PAB group or to the PAB with losartan group. After a 7-day recovery period the PAB and PAB with losartan groups received stepwise percutaneous inflation of the pulmonary cuff to induce RV pressure overload by 21 days. RV pressure was monitored by Doppler-echocardiography using tricuspid regurgitation, PAB gradient and septal position.

PAB groups were further randomized to receive oral losartan treatment or inactive vehicle placebo thus creating 3 groups: sham (n=6), PAB-Vehicle control (n=8) and PAB-Losartan groups (n=6). Losartan at 10 mg/kg/day or placebo were administered orally starting after the 7-day recovery period. Drug treatment continued until 5-weeks following PAB at which time animals were sacrificed.

Tissue collection

Animals were euthanized and the heart dissected for measurement of RV weight, LV + septal weight and their ratio (RV/LV+IVS). LV and RV tissue were immediately snap-frozen in liquid nitrogen and stored at -80^{o}C for RNA and protein analysis. A second sample was fixed in 10% neutral-buffered formaldehyde and embedded in paraffin. A 3rd sample was snap-frozen in Optimal Cutting Temperature (OCT) compound for cryosection to detect apoptosis. 5µm cross-sections of RV and LV were cut and stained with haematoxylin-eosin (HE) and picrosirius red F3BA (PSR) to determine myocyte morphology and collagen content.

Cardiac Collagen Volume Fraction

The cardiac collagen volume fraction was calculated as the ratio of the sum of total interstitial collagen area to the sum of total collagen and non-collagen area in the entire visual field of PSR stained sections using automated planimetry (Adobe Photoshop CS2, San Jose, CA, USA).

Cardiac Morphometry

Myocyte diameter was measured in HE stained sections. To reduce the error of measuring myocytes that were not precisely cut perpendicular to their long axis a point-to-point perpendicular line was placed across all longitudinally cut myocytes at the nucleus level and the average diameter of all longitudinally directed myocytes with a distinct cell border within the sampling field calculated (NIH ImageJ analysis). Transverse or obliquely cut myocytes were excluded. Relative ventricular wall thickness was determined.[2]

Real-time RT-PCR analysis

Total RNA was extracted from RV and LV tissue using TRIzol Reagent (Invitrogen Corp., Grand Island, NY, USA). Reverse transcription was performed with 1 μg of total RNA using SuperScript® III First-Strand Synthesis System (Invitrogen). Real-time PCR reaction was carried out with SYBR Green Master Mix (Applied Biosystems). GAPDH was used as the endogenous reference. Primers are listed in the appendix.

Western Blot Analysis

Protein was extracted from the freshly prepared or snap-frozen myocardium using standard methodology as previously reported.[3] An equal amount of protein (30 μg) from each sample was separated by 10% SDS–polyacrylamide gels and transferred onto nitrocellulose membranes (Bio-Rad). Membranes were incubated with Smad 2/3, Smad 4 (Cell Signalling Technology Inc), CTGF (Abcam), EDNRB (Fitzgerald Industries) overnight at 4°C. The membranes were then washed and subsequently incubated with peroxidase-conjugated secondary antibody (Santa Cruz, CA) and detected with the ECL plus Detection Kit (Amersham, Piscataway, NJ). Immunoblots were scanned using a Storm 840 analyzer (Molecular Dynamics) and quantified using ImageQuant 5.0 software (Molecular Dynamics).

Apoptosis Index Determination

The terminal deoxynucleotidyl transferase-mediated dUTP nick-end labeling (TUNEL) assay was used to monitor apoptic cells in cryostat sections. The assay was performed according to the recommendations of the manufacturer (Boehringer Mannheim). Fluorescein-conjugated dUTP incorporated in nucleotide polymers was detected and quantified by fluorescence microscopy. TUNEL-positive nuclei were distinguished from the TUNEL-negative nuclei by counterstaining with Hoechst 33258 and were counted after being photographed. The count was done blindly. The percentage of nuclei labeled by TUNEL per unit of cells stained with Hoechst nuclear dye reflected the apoptotic index.

Statistical analysis

Grouped data are expressed as means ± SD. Comparisons were made by one-way ANOVA with intergroup comparisons analyzed using Bonferroni post-hoc testing (GraphPad Prism 4.0, San Diego, CA). Statistical significance was accepted at $p < 0.05$. Analyses were performed in a blinded fashion. Experiments were approved by the institutional Animal Ethics Committee and performed in accordance with the "Guiding Principles in the Care and Use of Animals" of the American Physiologic Society.

Results

PAB Animal Model

After surgery all animals gained weight and showed no clinical signs of heart failure. Water and food were available ad libitum and intake was normal. The groups were similar in terms of age and body weight at the initiation and end of the experimental protocol. One animal in the sham control group died suddenly in the last week of the protocol.

Ventricular Morphology

At 5 weeks post-PAB, there were significant differences in gross morphology between the groups. The PAB group developed RV hypertrophy and dilatation versus sham operated controls, which was decreased with losartan. In PAB, RV weight (PAB 2.9±0.4 vs. sham 1.87±0.5 grams, $p<0.01$) and the RV/(RV+LV) weight ratio (PAB 0.36±0.03 vs. sham 0.27±0.04, $p<0.01$) were increased compared with sham-operated controls. Losartan reduced RV hypertrophy with a trend towards reduced RV weight (2.42±0.43 grams, $p= 0.056$ vs. PAB) and reduced RV/(RV+LV) weight ratio (0.30±0.03 $p<0.05$ vs.PAB) (**Figure 1A**). RV myocyte diameter was significantly enlarged in the PAB group (22.3±2.3 vs. sham 16±1.04μ, $p< 0.001$) and returned to normal with losartan (14.8± 2.2μ, $p<0.001$ vs. PAB) (**Figure 1B**). RV wall thickness was significantly increased in the PAB group (27±6 vs. sham 16±5.7 pixels, $p<0.001$) and decreased with losartan (23±4.5 pixels vs PAB $p< 0.05$) (**Figure 1C**). LV and septal thickness were similar between the groups.

A

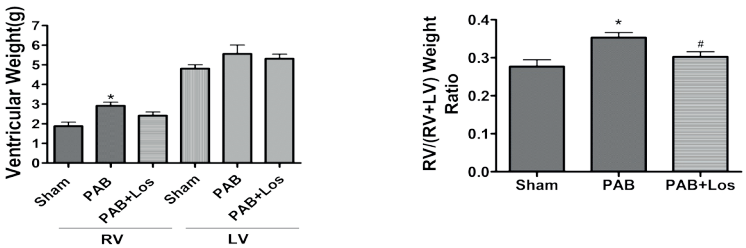

B

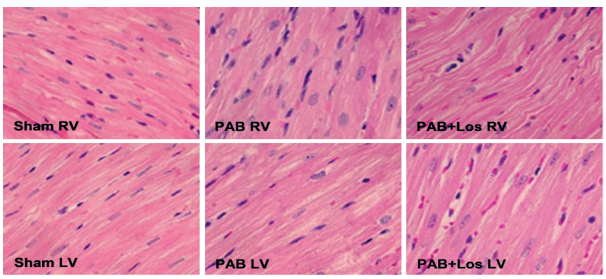

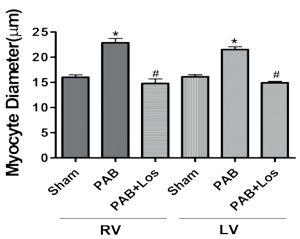

C

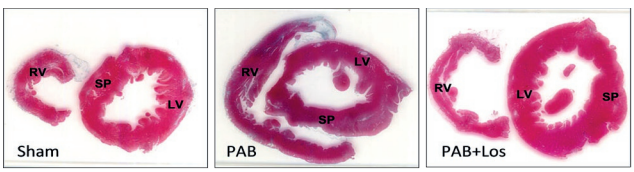

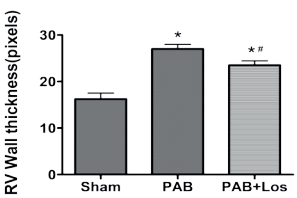

Caption on next page

Figure 1

*Losartan treatment blunts cardiac hypertrophy in response to PAB. A, Bar graphs showing ventricular weight and RV/(RV+LV) weight ratio (n = 6) at 5 weeks after PAB. B, H&E staining showing myocyte morphology in sham, PAB and PAB with losartan groups of RV, LV and quantification analysis of longitudinally directed myocyte diameters (n =6, 200 cells per section) at 5 weeks after PAB surgery. C, Heart cross-section and morphometric quantification of ventricular wall thickness (n=6 for sham, n=8 for PAB, and n=6 for PAB + losartan). *p < 0.05 vs. sham; #p < 0.05 vs. PAB groups.*

Cardiac Fibrosis

A small amount of collagen is normally present in the LV and RV interstitial and perivascular space (**Figure 2A-a,d,g,j**). Cardiac collagen volume was markedly increased at week 5 post PAB (RV: PAB 10.78±3.7% vs. sham 3.7±0.67% p<0.001; LV: 5.28±1.3% vs. sham 2.86±0.6% vs. sham p<0.001) with a patchy and non-uniform pattern, mainly at the RV free wall, RV junction with the interventricular septum and LV endocardium (**Figure 2A-b,e,h,k**). Losartan significantly attenuated collagen volume in the RV (2.69±0.69%, p< 0.001 vs. PAB) and LV (1.77±0.7%, p<0.001 vs. PAB) (**Figure 2A-c,f,i,l, 2B)**.

Cardiac Fibrosis

A small amount of collagen is normally present in the LV and RV interstitial and perivascular space (**Figure 2A-a,d,g,j**). Cardiac collagen volume was markedly increased at week 5 post PAB (RV: PAB 10.78±3.7% vs. sham 3.7±0.67% p<0.001; LV: 5.28±1.3% vs. sham 2.86±0.6% vs. sham p<0.001) with a patchy and non-uniform pattern, mainly at the RV free wall, RV junction with the interventricular septum and LV endocardium (**Figure 2A-b,e,h,k**). Losartan significantly attenuated collagen volume in the RV (2.69±0.69%, p< 0.001 vs. PAB) and LV (1.77±0.7%, p<0.001 vs. PAB) (**Figure 2A-c,f,i,l, 2B)**.

Expression of cardiac pro-fibrotic mediators

We explored well know pro-fibrotic cardiac mediators. **Figure 3** shows RV mRNA expression of TGFβ (PAB 1.66±0.16 vs sham 1±0.14 vs. losartan 0.87±0.12, p=0.003), CTGF (1.41±0.27 vs. 1±0.14 vs. 0.42±0.12, p=0.01); ET1 (2.08±0.4 vs. 1±0.18 vs. 0.41±0.12, p=0.005), ENDRB (1.90±0.3 vs. 1±0.13 vs. 1.1±0.18, p=0.04) and MMP9 (2.39±0.37 vs. 1±0.33 vs. 0.64±0.32, p=0.006). mRNA levels of these molecules were significantly increased in PAB animals compared with shams and significantly decreased with losartan treatment. EDRA (1.13± 0.11 vs. 1± 0.11 vs. 1.29±0.25, p=0.5) and MMP2 (1.06±0.15 vs. 1±0.08 vs. 0.75±0.14, p=0.28) were not significantly changed with PAB or with losartan compared with shams.

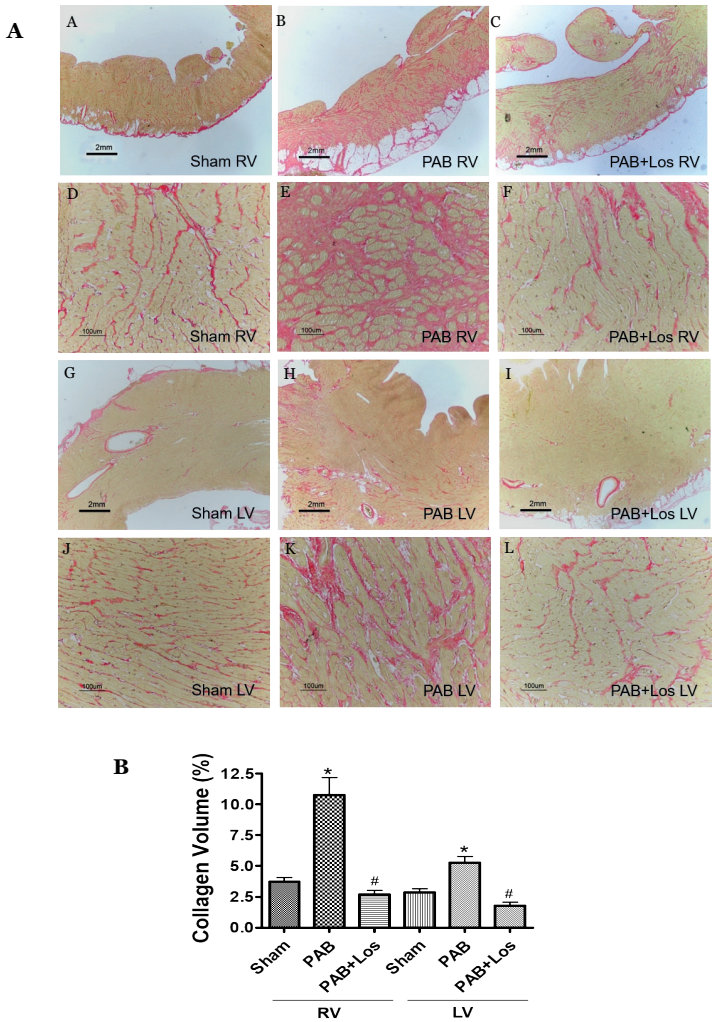

Figure 2

*Losartan treatment inhibits fibrosis induced by PAB. Cardiac collagen volume was examined with PSR-staining. A, Cardiac collagen volume in the RV (a-f), LV (g-j) of sham-operated controls (a, d, g, j), PAB (b, e, h, k) and PAB with losartan (c, f, i, l) animals. Scale bars: 2mm and 100 μm. B, Quantitative collagen volume fractions in various groups were analyzed by an image-analyzing system (n=6 for sham, n=8 for PAB, and n=6 for PAB +Losartan). *p < 0.05 vs. sham; #p < 0.05 vs. PAB groups.*

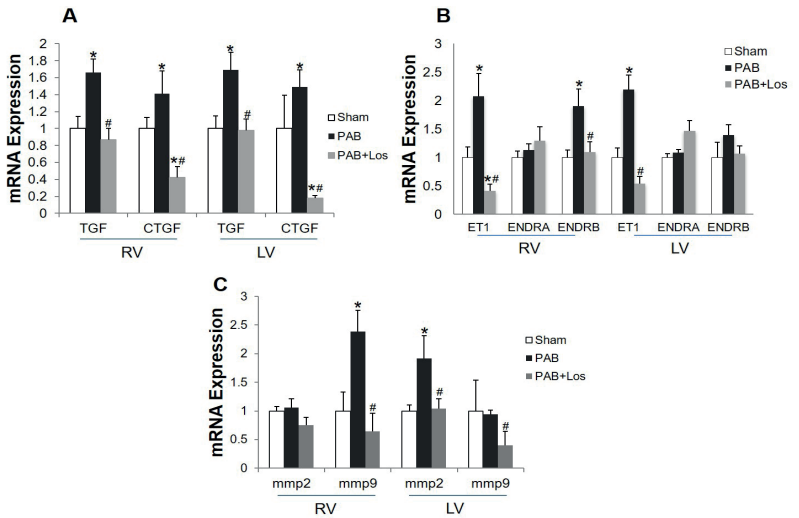

Figure 3

*Real-time RT-PCR data showing levels of gene expression in response to losartan treatment at 5 weeks post PAB. A-B. Genes related to pro-fibrotic mediators TGF-β, CTGF, ET1, ENDRA and ERDRB; C. MMP2 and MMP9 gene expression. *p < 0.05 vs. sham; #p < 0.05 vs. PAB group (n=6).*

LV mRNA levels of TGFβ, CTGF, ET1 and MMP2 were dramatically changed with PAB and with losartan (**Figure 3**). TGFβ mRNA levels were markedly elevated in PAB animals compared with shams (1.69±0.59 vs. 1.0±0.37, p=0.01) and reduced with losartan to sham levels (0.98±0.32, p<0.05 vs PAB). CTGF mRNA levels were significantly elevated with PAB (1.49±0.56 vs. 1±0.9 p=0.005) and almost entirely suppressed with losartan (0.18±0.07, p<0.01 vs. PAB) (**Figure 3A**). ET1 was significantly elevated in PAB compared with shams (2.19±0.7 vs. 1±0.41, p<0.01) and dramatically decreased with the addition of losartan compare to PAB (0.54±0.31 vs. 2.19±0.7, p<0.001). LV ENDRA levels were unchanged in PAB compared with shams (1.08±0.17 vs. 1.0±0.17), but trended towards being increased with losartan (1.47±0.18, p=0.058 vs. shams; ANOVA p=0.01). There was a non-statistically significant trend towards increased LV ENDRB mRNA levels in PAB vs. shams (1.39±0.53 vs. 1±0.66, p=0.06) and decreased to sham levels with losartan (1.07±0.3, p=0.58 vs. shams) (**Figure 3B**). MMP2 was significantly elevated with PAB (1.92±0.17 vs. 1±0.1, p=0.005) and trended to being reduced with losartan (1.04±0.17, p=0.06) (**Figure 3C**).

RV protein levels of the pro-fibrotic signaling molecules Smad 2/3 (PAB 1±0.2 vs. sham 0.6±0.2 p<0.05), Smad 4 (PAB 1.1±0.12 vs. sham 0.66±0.2 p< 0.05) and CTGF (1.77±0.24 vs. sham 0.97± 0.5 P<0.001) were significantly increased with PAB, and reduced to control levels with losartan (**Figure 4**). RV ENDRB was also increased in the PAB group and decreased with losartan treatment (PAB 0.93±0.4 vs sham 0.63±0.26 p>0.05). LV protein levels of Smad 2/3, Smad 4, CTGF and ENDRNB showed similar patterns to the RV, being increased with PAB compared to shams and reduced with losartan treatment (**Figure 4**).
Other up/downstream molecular signaling pathways of TGFβ /CTGF are presented in the supplemental results.

Cardiac Apoptosis

The number of apoptotic cardiomyocytes was very low (0.18%) in sham-operated controls. PAB induced apoptosis in 0.53% of RV myocytes. Losartan reduced myocyte apoptosis to 0.23% (p<0.001) (**Figure 6A, B**). LV cardiomyocyte apoptosis although increased with PAB compared with sham, did not reach statistical significance (**Figure 5A, B**).

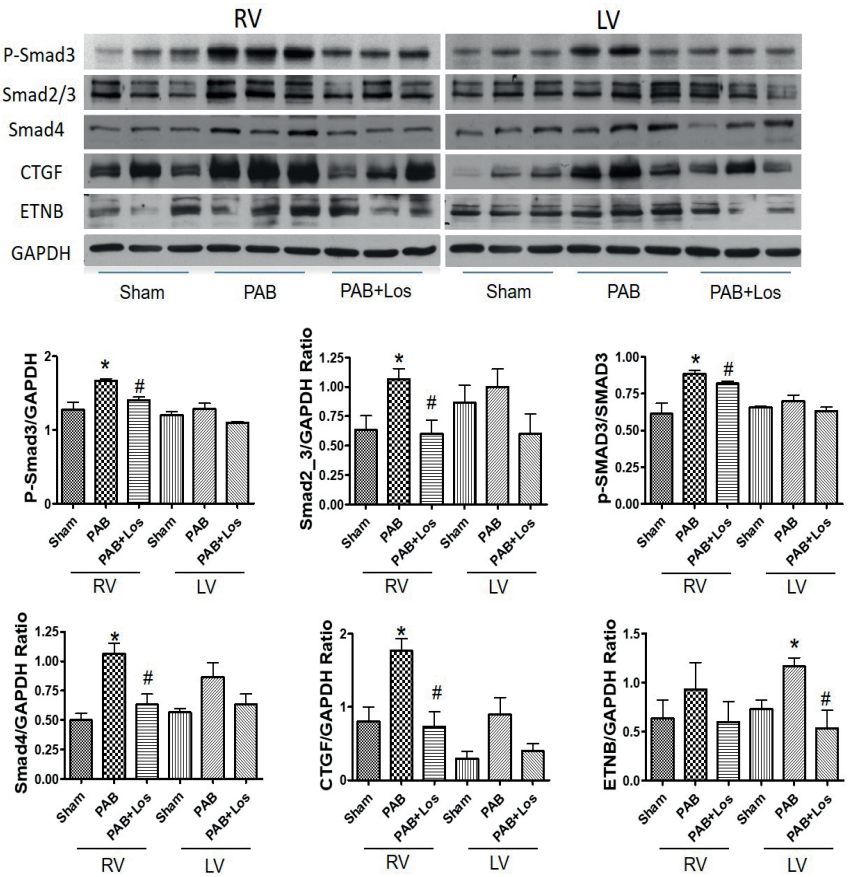

Figure 4

*A. Western blot analysis for smad 2/3, smad 4, CTGF and ENDRB proteins level at 5 weeks post PAB. B, Quantification data of Smad 2/3, Smad 4, CTGF and ETNB. GAPDH was used as the sample loading control. *p < 0.05 vs. sham; #p < 0.05 vs. PAB group.*

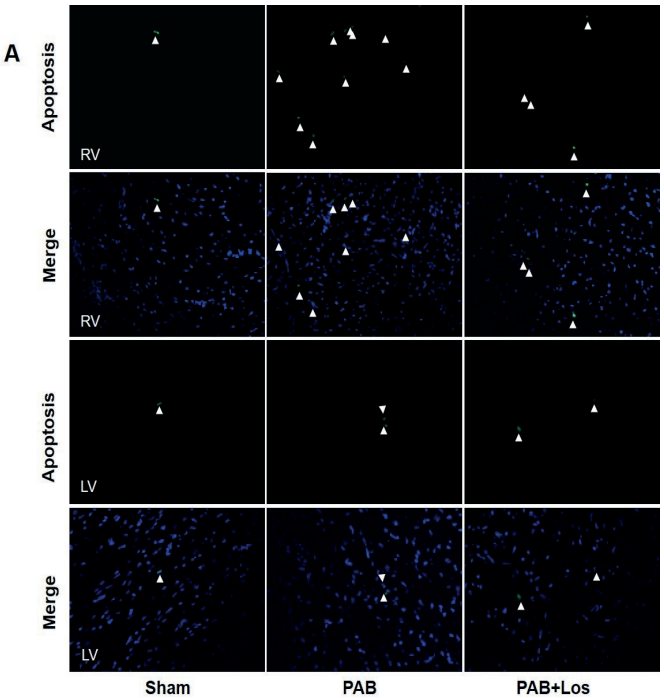

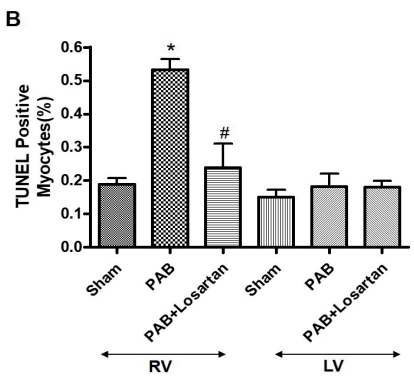

Figure 5

*Myocyte apoptosis in response to PAB and losartan treatment at 5 weeks post PAB. Myocyte apoptosis in sham, PAB and PAB with losartan. Arrows show apoptotic nuclei of cardiomyocytes indicated by green (a-c, g-i). Blue spots represent nuclei stained by DAPI and merged images are shown in d- f and j-l. Magnification: x200. B, Percentage of apoptotic myocytes in sham (n=6), PAB (n=8) and PAB with losartan (n=6). *p < 0.05 vs. sham; #p < 0.05 vs. PAB group.*

Discussion

The results of this study extend the understanding of our previous observation of LV myocardial fibrosis induced by ventricular-ventricular interactions secondary to isolated RV afterload and demonstrate a potential novel therapeutic approach to adverse biventricular remodeling. Our results suggest that ventricular-ventricular interactions leading to biventricular hypertrophy, fibrosis and apoptosis are mediated by TGFβ1, CTGF and ET1 signaling; and that this biochemical crosstalk can be ameliorated by angiotensin receptor blockade. This powerful therapeutic effect occurs despite the persistence of severe RV afterload.

Although it is well recognized that RV function is a key determinant of outcomes in PAH, the substantial impact of RV afterload on LV myocardial damage through adverse ventricular-ventricular interactions has received little attention and is not currently a therapeutic target. At a physiologic level, ventricular-ventricular interactions occur in the setting of a dilated and/or hypertensive RV via shared myocardial fibers, septal interactions and pericardial constraint, and have been shown to profoundly affect LV systolic function, increased systolic to diastolic duration ratio and impaired LV filling.[1,4,5]

While these physiologic interactions have been well described, relatively little is known about their biochemical and histologic consequences. Of importance to the current study is the recent recognition that the burden of myocardial fibrosis (measured by late gadolinium enhancement by MRI) is strongly associated with the presence of biventricular dysfunction[6], and is a risk factor for clinical deterioration in patients with pulmonary hypertension.[7] Our data potentially provide mechanistic insights into these clinical observations, and provide evidence for a novel pharmacologic intervention that might modify their manifestations. We have shown that isolated RV afterload leads to a largely similar pattern of pro-fibrotic molecular signaling in the left and right ventricle, with consequent biventricular myocardial fibrosis and apoptosis that is largely abrogated by angiotensin receptor blockade. Although losartan has been shown to improve fibrosis in other settings, it has not been previously studied in abrogating adverse ventricular-ventricular interactions secondary to RV afterload.

Our data are consistent with prior LV studies showing interstitial fibrosis to be associated with activation of myocardial signaling pathways that upregulate TGFβ, CTGF, ET1 and matrix metalloproteinases.[8] Our previous study examining physiologic manipulation of these responses[9], as well as the results of the current study in a rabbit model of RV mechanical afterload, suggests that these profibrotic molecules mediate biochemical crosstalk that causes biventricular fibrosis in RV afterload. Although not confirmatory of a causative

role, particularly notable was the increase in LV CTGF mRNA with PAB and decrease in CTGF mRNA following losartan.

Role of TGFβ1 and CTGF in cardiac fibrosis in response to RV afterload

TGFβ1 is a known key mediator of cardiac fibrosis interacting with other signaling factors such as angiotensin-II and CTGF (CCN2) to promote cardiac remodeling and fibrosis.[8,10] Although not previously studied in PAH, CTGF has been shown to mediate chronic fibrotic effects of TGFβ1.[11] Platelets, and perhaps other cell types, have been shown to release CTGF predominantly at sites of tissue injury. Our data suggest that isolated RV afterload, leads to biventricular injury via these pathways, presumably as the result of mechanical interactions that increases regional wall stress in both ventricles. This hypothesis invoking local CTGF production would be in keeping with prior data suggesting that CTGF's action is largely autocrine, acting synergistically with TGFβ1 to promote extra-cellular matrix protein deposition and sustained fibrosis.[12]

Angiotensin-II, TGFβ and CTGF signaling

The anti-fibrotic effect of losartan and its association with decreased CTGF signaling in our animal model is consistent with existing literature in pressure and volume loaded failing ventricles where angiotensin-II production is associated with fibrosis.[8] Angiotensin-II acts with TGFβ1 to cause ventricular hypertrophy and fibrosis.[8] Angiotensin-II upregulates TGFβ1 through the angiotensin type-1 receptor, and TGFβ1 is necessary for induction of myocyte hypertrophy and fibrosis caused by angiotensin-II.[13] CTGF acts downstream of TGFβ1 and is required for TGFβ1 effect on fibrosis in many conditions.[11] LV and RV CTGF mRNA levels were strongly up regulated in our RV afterload model; and downregulated after losartan. CTGF family proteins have previously been shown to play a role in several cardiovascular diseases.[14] We now demonstrate a possible role for CTGF in mediating ventricular-ventricular interactions in RV afterload. Particularly interesting in regards to our results is the increase in CTGF in the hypertrophic LV of the murine 2-kidney, 1-clip model (a model studying angiotensin-II).[15] Those data may explain the observed reduction in LV CTGF levels following inhibition of angiotensin-II by losartan. CTGF is over-expressed in many human fibrotic conditions although its role in biventricular fibrosis in PAH has not previously been studied.[16] Conversely, inhibition or downregulation of CTGF ameliorates fibrosis.[17] Our results suggest that further study is warranted regarding CTGF's role in mediating biventricular fibrosis in clinical RV afterload.

Given the strong increase in CTGF with PAB and its decrease with losartan, we explored its up and downstream regulation.[11,18,19] In our study, Smad 2, 3 and

4 were upregulated by PAB and downregulated with the addition of losartan. Therefore, it is plausible that CTGF mediated biventricular fibrosis occurs, at least in part, through Smad signaling. Smad signaling is well recognized in mediating TGFβ1-CTGF fibrotic pathways in fibro-proliferative disorders, but has not been well studied in response to RV afterload.[20] In addition, LV RhoA was increased with PAB and decreased with losartan. In PAH, most attention has been placed on the vasoconstriction effects of the RhoA-ROCK pathway through modulation of NO and other mechanisms.[21,22] Although direct myocardial effects of the RhoA-ROCK pathway have been described, largely in relation to heart failure from myocardial infarction[23]; ours is the first study to demonstrate its direct role in the biochemical cross talk associated with adverse ventricular interactions secondary to RV afterload. While imperfect, as with any animal model, our pure PAB mechanical model allows differentiation of the cardiac role of RhoA-ROCK without the confounding effects of pharmacologically induced pulmonary vascular disease, where RhoA-ROCK is also central in mediating vascular injury. Our preliminary findings may be clinically relevant given the potential to inhibit the RhoA-ROCK pathway.[21]

ET1 is a powerful signaling molecule in chronic heart failure and in PAH its role as a vasoconstrictor is well recognized. In the current study, with the increase in ET1 mRNA expression, there was concomitant increase in ETRB, but not ETRA expression with PAB, and reversal with losartan. This was more marked in the RV, despite ET1 mRNA levels being markedly increased in both ventricles. In normal fibroblasts ET1 acts downstream of TGFβ1 to induce fibrosis.[24] Our results support this pathway, as ET1 levels were reduced to sham levels with the addition of angiotensin receptor blockade. Our results would suggest that they may also have a role in preventing biochemical crosstalk leading to biventricular fibrosis[25] beyond their current use as vasodilators in PAH.

The extra-cellular matrix plays a central role in systolic and diastolic ventricular dysfunction. MMPs, key determinants of the extra-cellular matrix milieu and fibrous degradation, have been found to be excessively activated in rodent PAH models and RV failure.[26] Pertinent to our results, TGFβ1 may directly promote extra-cellular matrix gene expression and deposition by suppressing MMP expression.[27] In the pressure-loaded RV, an imbalance between MMPs and tissue proteinase inhibitors may further promote fibrosis. We found markedly increased MMP2 levels in the RV and MMP9 levels in the LV with PAB, and both were reduced following losartan. These data suggest that Ang II mediates upregulation of MMPs and that these may have a role in mediating ventricular-ventricular interactions and adverse biventricular remodeling in PAH. Moreover, ET1 may promote mast cell degradation to influence MMP expression and this requires further study as a possible mechanism in our model.[28] Our finding of reduced LV MMP9 signaling after losartan is consistent with attenuated myocardial oxidative stress, which is itself a stimulator of

adverse RV remodeling in pressure afterload.[29]

Clinical Implications

The potential therapeutic implications of our findings are speculative, but intriguing. Recapitulating the beneficial effects, we previously showed with aortic banding in RV afterload to harness ventricular-ventricular interactions using losartan is appealing as systemic vasoconstriction in patients with PAH is not easily achieved, nor would it be readily adopted by clinicians and patients. Conversely, losartan is widely used in clinical practice and has a relatively good safety profile. Furthermore, the amelioration of biventricular fibrosis in our rabbit model seemed more potent with losartan than with aortic banding. Thus it may be possible to modify RV and LV fibrotic and apoptotic responses associated with increased TGFβ1 signaling via angiotensin-II using an angiotensin receptor blocker, in the same way as has been shown in models of LV disease. Likewise, our observations regarding the pro-fibrotic responses within the RV and LV also raise the possibility of using other agents to modify biventricular responses. Endothelin blockade is already widely used in patients with advanced pulmonary hypertension, but it might be argued that if it were to have a beneficial effect on RV and LV remodeling, it would need to be given earlier in the course of the disease.

The ventricular-ventricular interactions demonstrated in this study are not limited to PAH and likely affect other congenital and acquired conditions. In tetralogy of Fallot (TOF) for example, LV function influences RV function and clinical outcomes.[30] Regional and global abnormalities of RV and LV function and interactions in TOF are interrelated and are associated with abnormal mechanoelectric interactions and arrhythmia. We recently demonstrated reduced LV myocardial performance in children after TOF repair related to RV dilatation and pulmonary regurgitation.[31] This is interesting as, similar to our PAH models, TOF patients have LV and RV fibrosis.[32] As for PAH, TOF is considered a 'RV disease', yet increasingly LV dysfunction is recognized as a major risk factor for adverse outcomes.[33] Similarly, biochemical cross talk may be crucial in mediating biventricular injury and fibrosis. Therefore, the implications of geometric and biochemical cross talk, and their attenuation using pharmacotherapy, demonstrated in the current study may potentially extend to a wide spectrum of congenital and acquired heart disease.

Study limitations

In our model, as with many others, RV pressures were at systemic levels for only 2-3 weeks, and no animal displayed overt right heart failure. Consequently, our model may not adequately reflect the effects of truly 'chronic' RV overload. Nevertheless, our aim was not to study 'end-stage' responses, and despite the relatively brief hemodynamic burden the differences between the groups were highly significant, and the model was sufficient to study the development/ attenuation of myocyte hypertrophy, fibrosis and apoptosis. We did not evaluate whether adverse myocardial remodeling in response to pressure load and its reversal with losartan, is characterized by a maladaptive hypertrophy with changes in phosphodiesterase type 5 (PDE5a) expression[34], myosin heavy chain isoform switch or other markers of pathological hypertrophy such as calcineurin activation.[35] RV hypertrophy in response to afterload is usually 'pathological'.[36] These maladaptive hypertrophic responses have been characterized by others, and in this study we focused on the amelioration of adverse ventricular-ventricular interactions through of TGFβ1/ CTGF modulation. Although one study found that progressive PAB does not induce RV failure,[37] in that study RV pressure was only ~60% of systemic, a level that allows adaptation and usually does not induce clinical symptoms in patients with pulmonary stenosis. Likewise, even if contractility increases with PAB, RV stroke volume and cardiac output may still fall.[38] While it is clear that it is not pressure alone that induces RV failure[39], similar murine models with systemic RV pressure levels have shown RV failure, RV dilation, decreased RV wall motion, elevated RV end-diastolic pressure, decreased cardiac output, clinical evidence of right heart failure, and decreased survival.[40] The presence of myocyte hypertrophy, fibrosis and apoptosis in our rabbit RV afterload model is consistent with pathological ventricular changes. Furthermore, the presence of LV fibrosis suggests pathological changes as a result of ventricular-ventricular interactions. This result differs from other studies, where there was no LV fibrosis, after PAB.[39] Some myocardial patterning changes in other models may be related to the conditions inducing PAH rather than to the afterload itself. In this respect our model of pure mechanical RV afterload may have been advantageous.

Multiple pathways may be activated in RV hypertrophy and maladaptation, including MAPK, ERK and JNK.[8] We did not perform an exhaustive investigation all of these, but rather concentrated on the central signaling pathways around our most striking observed results. Finally, we demonstrated these effects in one model, and therefore cannot totally exclude that effects are model specific.

Conclusion

In summary, we have shown that in isolated RV afterload, adverse ventricular-ventricular interactions lead to LV as well as RV fibrosis and apoptosis mediated by biochemical crosstalk through the TGFβ1, CTGF and ET1 pathways. Our results suggest that biventricular fibrosis, apoptosis, hypertrophy and molecular maladaptive responses to increased RV afterload can be attenuated by angiotensin receptor blockade using losartan.

References

1. Apitz C, Honjo O, Humpl T, et al. Biventricular structural and functional responses to aortic constriction in a rabbit model of chronic right ventricular pressure overload. J Thorac Cardiovasc Surg 2012;144:1494-501.
2. Sun M, Chen M, Dawood F, et al. Tumor necrosis factor-alpha mediates cardiac remodeling and ventricular dysfunction after pressure overload state. Circulation 2007;115:1398-407.
3. Sun M, Opavsky MA, Stewart DJ, et al. Temporal response and localization of integrins beta1 and beta3 in the heart after myocardial infarction: regulation by cytokines. Circulation 2003;107:1046-52.
4. Gan CT, Lankhaar JW, Marcus JT, et al. Impaired left ventricular filling due to right-to-left ventricular interaction in patients with pulmonary arterial hypertension. Am J Physiol Heart Circ Physiol 2006;290:H1528-33.
5. Brookes C, Ravn H, White P, Moeldrup U, Oldershaw P, Redington A. Acute right ventricular dilatation in response to ischemia significantly impairs left ventricular systolic performance. Circulation 1999;100:761-7.
6. Shehata ML, Lossnitzer D, Skrok J, et al. Myocardial delayed enhancement in pulmonary hypertension: pulmonary hemodynamics, right ventricular function, and remodeling. AJR Am J Roentgenol 2011;196:87-94.
7. Freed BH, Gomberg-Maitland M, Chandra S, et al. Late gadolinium enhancement cardiovascular magnetic resonance predicts clinical worsening in patients with pulmonary hypertension. J Cardiovasc Magn Reson 2012;14:11.
8. Leask A. Potential therapeutic targets for cardiac fibrosis: TGFbeta, angiotensin, endothelin, CCN2, and PDGF, partners in fibroblast activation. Circ Res 2010;106:1675-80.
9. Kreymborg K, Uchida S, Gellert P, et al. Identification of right heart-enriched genes in a murine model of chronic outflow tract obstruction. J Mol Cell Cardiol 2010;49:598-605.
10. Huntgeburth M, Tiemann K, Shahverdyan R, et al. Transforming growth factor beta(1) oppositely regulates the hypertrophic and contractile response to beta-adrenergic stimulation in the heart. PLoS One 2011;6:e26628.
11. Chen MM, Lam A, Abraham JA, Schreiner GF, Joly AH. CTGF expression is induced by TGF- beta in cardiac fibroblasts and cardiac myocytes: a potential role in heart fibrosis. J Mol Cell Cardiol 2000;32:1805-19.
12. Mori T, Kawara S, Shinozaki M, et al. Role and interaction of connective tissue growth factor with transforming growth factor-beta in persistent fibrosis: A mouse fibrosis model. J Cell Physiol 1999;181:153-9.
13. Schultz Jel J, Witt SA, Glascock BJ, et al. TGF-beta1 mediates the hypertrophic cardiomyocyte growth induced by angiotensin II. J Clin Invest 2002;109:787-96.
14. Hilfiker A, Hilfiker-Kleiner D, Fuchs M, et al. Expression of CYR61, an angiogenic immediate early gene, in arteriosclerosis and its regulation by angiotensin II. Circulation 2002;106:254-60.
15. Iwanciw D, Rehm M, Porst M, Goppelt-Struebe M. Induction of connective tissue growth factor by angiotensin II: integration of signaling pathways. Arterioscler Thromb Vasc Biol 2003;23:1782-7.
16. Bergestuen DS, Gravning J, Haugaa KH, et al. Plasma CCN2/connective tissue growth factor is associated with right ventricular dysfunction in patients with neuroendocrine tumors. BMC Cancer

2010;10:6.
17. Sisco M, Kryger ZB, O'Shaughnessy KD, et al. Antisense inhibition of connective tissue growth factor (CTGF/CCN2) mRNA limits hypertrophic scarring without affecting wound healing in vivo. Wound Repair Regen 2008;16:661-73.
18. Liu Q, Mao H, Nie J, et al. Transforming growth factor {beta}1 induces epithelial-mesenchymal transition by activating the JNK-Smad3 pathway in rat peritoneal mesothelial cells. Perit Dial Int 2008;28 Suppl 3:S88-95.
19. Nakerakanti SS, Kapanadze B, Yamasaki M, Markiewicz M, Trojanowska M. Fli1 and Ets1 have distinct roles in connective tissue growth factor/CCN2 gene regulation and induction of the profibrotic gene program. J Biol Chem 2006;281:25259-69.
20. Samarakoon R, Overstreet JM, Higgins PJ. TGF-beta signaling in tissue fibrosis: Redox controls, target genes and therapeutic opportunities. Cell Signal 2012;25:264-268.
21. Abe K, Shimokawa H, Morikawa K, et al. Long-term treatment with a Rho-kinase inhibitor improves monocrotaline-induced fatal pulmonary hypertension in rats. Circ Res 2004;94:385-93.
22. Xu EZ, Kantores C, Ivanovska J, et al. Rescue treatment with a Rho-kinase inhibitor normalizes right ventricular function and reverses remodeling in juvenile rats with chronic pulmonary hypertension. Am J Physiol Heart Circ Physiol 2010;299:H1854-64.
23. Kobayashi N, Horinaka S, Mita S, et al. Critical role of Rho-kinase pathway for cardiac performance and remodeling in failing rat hearts. Cardiovasc Res 2002;55:757-67.
24. Shi-wen X, Kennedy L, Renzoni EA, et al. Endothelin is a downstream mediator of profibrotic responses to transforming growth factor beta in human lung fibroblasts. Arthritis Rheum 2007;56:4189-94.
25. Clozel M, Salloukh H. Role of endothelin in fibrosis and anti-fibrotic potential of bosentan. Ann Med 2005;37:2-12.
26. Umar S, Hessel M, Steendijk P, et al. Activation of signaling molecules and matrix metalloproteinases in right ventricular myocardium of rats with pulmonary hypertension. Pathol Res Pract 2007;203:863-72.
27. Leask A. Targeting the TGFbeta, endothelin-1 and CCN2 axis to combat fibrosis in scleroderma. Cell Signal 2008;20:1409-14.
28. Murray DB, Gardner JD, Brower GL, Janicki JS. Endothelin-1 mediates cardiac mast cell degranulation, matrix metalloproteinase activation, and myocardial remodeling in rats. Am J Physiol Heart Circ Physiol 2004;287:H2295-9.
29. Awad AE, Kandalam V, Chakrabarti S, et al. Tumor necrosis factor induces matrix metalloproteinases in cardiomyocytes and cardiofibroblasts differentially via superoxide production in a PI3Kgamma-dependent manner. Am J Physiol Cell Physiol 2010;298:C679-92.
30. Geva T, Sandweiss BM, Gauvreau K, Lock JE, Powell AJ. Factors associated with impaired clinical status in long-term survivors of tetralogy of Fallot repair evaluated by magnetic resonance imaging. J Am Coll Cardiol 2004;43:1068-74
31. Fernandes FP, Manlhiot C, Roche SL, et al. Impaired left ventricular myocardial mechanics and their relation to pulmonary regurgitation, right ventricular enlargement and exercise capacity in asymptomatic children after repair of tetralogy of fallot. J Am Soc Echocardiogr 2012;25:494-503.
32. Babu-Narayan SV, Kilner PJ, Li W, et al. Ventricular fibrosis suggested by cardiovascular magnetic resonance in adults with repaired tetralogy of fallot and its relationship to adverse

markers of clinical outcome. Circulation 2006;113:405-13.
33. Broberg CS, Aboulhosn J, Mongeon FP, et al. Prevalence of left ventricular systolic dysfunction in adults with repaired tetralogy of fallot. Am J Cardiol 2011;107:1215-20.

34. Nagendran J, Archer SL, Soliman D, et al. Phosphodiesterase type 5 is highly expressed in the hypertrophied human right ventricle, and acute inhibition of phosphodiesterase type 5 improves contractility. Circulation 2007;116:238-48.
35. Bartelds B, Borgdorff MA, Smit-van Oosten A, et al. Differential responses of the right ventricle to abnormal loading conditions in mice: pressure vs. volume load. Eur J Heart Fail 2011;13:1275-82.
36. Nagendran J, Michelakis ED. Mitochondrial NOS is upregulated in the hypoxic heart: implications for the function of the hypertrophied right ventricle. Am J Physiol Heart Circ Physiol 2009;296:H1723-6.
37. Faber MJ, Dalinghaus M, Lankhuizen IM, et al. Right and left ventricular function after chronic pulmonary artery banding in rats assessed with biventricular pressure-volume loops. Am J Physiol Heart Circ Physiol 2006;291:H1580-6.
38. Leeuwenburgh BP, Helbing WA, Steendijk P, Schoof PH, Baan J. Biventricular systolic function in young lambs subject to chronic systemic right ventricular pressure overload. Am J Physiol Heart Circ Physiol 2001;281:H2697-704.
39. Bogaard HJ, Natarajan R, Henderson SC, et al. Chronic pulmonary artery pressure elevation is insufficient to explain right heart failure. Circulation 2009;120:1951-60.
40. Urashima T, Zhao M, Wagner R, et al. Molecular and physiological characterization of RV remodeling in a murine model of pulmonary stenosis. Am J Physiol Heart Circ Physiol 2008;295:H1351-H1368.

Appendix.

PCR primers

Endothelin-1 (ET-1) (Forward: 5'-ACTTCTGCCACCTGGACATCA-3', Reverse: 5'-ACGCTGCCCTGGTAGGAAAT-3'),

endothelin receptor type A (ENDRA) (Forward: 5'-GCTTCTTGCTGCTCATGG ATTAC-3', Reverse: 5'- CCGAGGTCATCAGGCTCTTG-3'),

endothelin receptor type B (ENDRB) (Forward: 5'-CTGGCCATTTGGAGCTGAGA-3', Reverse: 5'-TTTGGAACCCCAATTCCTTTAA-3'),

matrix metalloproteinase-2 (MMP-2) (Forward: 5'-AGGACTACGACCGCGACAAG-3', Reverse: 5'- TGTTGCCCAGGAAGGTGAAG -3'),

matrix metalloproteinase-9 (MMP-9) (Forward: 5'-CTTCCAACTTTGA CAGCGACA-3', Reverse: 5'-GGAGTGATCCAAGCCCAGTG-3'),

TGF-β (Forward: 5'-AGGGCTACCACGCCAACTT-3', Reverse: 5'-CCGGGTTGTGCTGGTTGTAC-3'),

connective tissue growth factor (CTGF) (Forward: 5'-CCCTGCGTCTTCGGTGGC-3', Reverse: 5'-AGGCAGTTGGCTCGCATCAT-3'),

GAPDH (Reverse: 5'-AGGCCGTGGGCAAGGT-3', Reverse: 5'-CCTCGGATG CCTGCTTCA-3'). Fli1 (Forward: 5' – CCACCAACGAGAGAAGAGTCATC-3', Reverse: 3' TCTCCATCAAGCCGTACTCCTT-5'), ETS1 (Forward: 5'-GGACGTGAA ACCGTATCAAGTGA-3', Reverse: 3'-CTGGGCGTGCTCGATACC- 5'), RhoA (Forward: 5'-AGCAGGGCAGGAAGACTATGAT -3', Reverse: 3'-TGGAG AGCACATGAGGATGAC-5'), CDC42 (Forward: 5'-TGACCCCTCTA CTATTGAGAAACTTG-3', Reverse: 3'- ACTCCACATACTTGACAGCCTTCA-5'),

Rac1 (Forward: 5'-GCCTGCTCATCTGCTACACAAC-3', Reverse: 3'- GGGCA CTGT AATTGTCGAACAC-5').

Supplemental material

Given, the marked increase in TGFβ and CTGF with PAB and their amelioration with losartan, we further investigated up/downstream molecular signaling pathways of TGFβ /CTGF (**Figure**). RV Fli1 mRNA trended to being increased with PAB, although it did not reach statistical significance (PAB 1.32±0.62 vs. sham 1.07± 0.44; p=0.06). With the addition of losartan, RV Fli1 mRNA decreased to sham levels (losartan 1.02±0.61 vs. sham 1.07± 0.44; p=0.88). RV mRNA levels of Ets (sham 1.04±0.33; PAB 0.94±0.28, p>0.05 vs. sham; losartan 1.23±0.46, p>0.05 vs sham and PAB), RhoA (sham 1.08±0.44; PAB 1.12±0.48, p>0.05 vs. sham; losartan 0.89±0.44, p>0.05 vs sham and PAB), CDC42 (sham 1.03±0.31; PAB 0.92±0.28 p>0.05 vs. sham; losartan 1.01±0.27, p>0.05 vs sham and PAB) and Rac1 (sham 1.07± 0.49; PAB 0.93± 0.25, p>0.05 vs. sham; losartan 1.13±0.34, p>0.05 vs sham and PAB) were unchanged following PAB or losartan.

LV mRNA levels of Fli1 (sham 1.04±0.32; PAB 1.34±0.31, p=0.1 vs. sham); (losartan 0.70±0.23, p<0.01 vs. sham) and RhoA (sham 1.07±0.45, PAB 1.30±0.32, p=0.3 vs. sham), (losartan 0.65±0.16, p=0.005) were increased with PAB and significantly decreased to below sham levels with addition of losartan. Ets1 (sham 1.05±0.38; PAB 0.95±0.28; losartan 0.85±0.28), CDC42 (sham1.01±0.15, PAB 1.13±0.26, losartan 0.87±0.18), and Rac1 (sham 1.01±0.14, PAB 1.15±0.22, losartan 0.96±0.25) were unchanged with PAB and losartan.

Chapter 8

The role of β1integrin in mediating adverse mechanical to molecular RV-LV interactions in RV pressure loading

Experimental right ventricular hypertension induces regional β1integrin mediated transduction of hypertrophic and pro-fibrotic right and left ventricular signaling

Authors
Mei Sun, MD, PhD; Ryo Ishii, MD; Kenichi Okumura, MD, PhD; Adrienn Krauszman; Siegfried Breitling, PhD; Olga Gomez, MD; Aleksander Hinek, MD, PhD; Stellar Boo; Boris Hinz, PhD; Kim Connelly, MD; Wolfgang M. Kuebler, MD; Mark K. Friedberg, MD

(adapted from) J Am Heart Assoc 2018; 7(7):pii. e007928

Abstract

Background: Development of right ventricular (RV) hypertension eventually contributes to right (RV) and left (LV) ventricular myocardial fibrosis and dysfunction. The molecular mechanisms are not fully elucidated.

Methods and Results: Pulmonary artery banding (PAB) was used to induce RV hypertension in rats *in vivo*. Then, we evaluated cardiac function and regional remodeling 6-weeks after PAB. To further elucidate mechanisms responsible for regional cardiac remodeling, we also mimicked RV hypertensive stress by cyclic mechanical stretching applied to confluent cultures of cardiac fibroblasts, isolated from the RV free-wall, septal hinge-points and LV free-wall. Echocardiography and catheter evaluation demonstrated that PAB-rats developed RV hypertension with leftward septal displacement, LV compression and increased LV end-diastolic pressures. Picro-Sirius Red staining indicated that PAB induced marked RV fibrosis and dysfunction with prominent fibrosis and elastin deposition at the septal hinge-points; but less LV fibrosis. These changes were associated with proportionally increased expressions of integrinβ1 and pro-fibrotic signaling proteins including phosphor-Smad2/3 and TGF-β1. Moreover, mechanically stretched fibroblasts also expressed significantly increased levels of α-smooth muscle actin, integrinβ1, transforming growth factor (TGF)-β1, collagen-I deposition and wrinkle formation on gel assays, consistent with myofibroblast transformation. These changes were not observed in parallel cultures of mechanically stretched fibroblasts, pre-incubated with the integrin inhibitor (BTT-3033).

Conclusions: Experimentally-induced RV hypertension triggers regional RV, hinge-point and LV integrin β1-dependent mechano-transduction signaling pathways that eventually trigger myocardial fibrosis via TGF-β1 signaling. Reduced LV fibrosis and preserved global function, despite geometrical and pressure aberrations, suggest a possible elastin-mediated protective mechanism at the septal hinge-points.

Clinical perspective

What is new?

Isolated right ventricular (RV) hypertension leads to geometrical changes which promote regional RV and septal hinge-point integrinβ1 and pro-fibrotic signaling. However, despite LV geometrical distortion and increased end-diastolic pressures, mechanical-molecular remodeling is attenuated in the LV suggesting a possible mechano-transduction adaptive mechanism mediated by integrinβ1, possibly through upregulation of elastin. Thus, β1integrins

may mediate co-existent adaptive and maladaptive mechano-transduction mechanisms, and the balance between these may determine biventricular function in RV pressure-loading.

What are the clinical implications?

In RV pressure-loading, treatments modulating integrinβ1 expression and function; or those increasing elastin production and decreasing RV and LV fibrosis may be beneficial. Furthermore, there may a therapeutic window before more extensive development of LV fibrosis and dysfunction.

Introduction

The exact prevalence of pediatric heart failure is largely unknown but it is increasing. Development of progressive right ventricular (RV) hypertension initially triggers RV dysfunction, and if persistent, eventually transduces to the LV myocardium, causing its dysfunction and increasing mortality.[1-6] However, the molecular mechanisms of this pathologic phenomenon are not yet fully elucidated. Observations in human cases of pulmonary arterial hypertension have shown the development of peculiar fibrosis at the septal hinge-points which is associated with RV and pulmonary hemodynamics and clinical outcomes.[7, 8] We recently demonstrated, in an experimental model of Pulmonary Artery Banding (PAB) induced RV hypertension, marked upregulation of pro-fibrotic signaling and severe collagenous fibrosis at the septal hinge-points; hypothesizing that this mechanically stressed region, where the RV and LV adjoin, plays a pivotal role in mediating, or possibly mitigating, LV injury secondary to RV hypertension[9].

The integrin trans-membrane glycoprotein receptors, and their molecular cross-talk with TGF-β1 pathways have previously been recognized in the LV as translating pressure-stress into biochemical signaling (mechano-transduction) in various clinical and experimental models[10-12]. Integrins are also major regulators of intracellular pro-fibrotic signaling including connective tissue growth factor (CTGF) and transforming growth factor (TGF)-β1. Importantly, we have recently demonstrated in an experimental PAB model that triggering of TGF-β1 signaling pathways preceded generation of RV and LV fibrosis and their ultimate dysfunction in response to excessive RV pressure-load; suggesting that β1integrins and other mechano-transduction pathways may play a pivotal role in triggering RV and LV fibrosis in response to RV hypertension.[13-17]

However, our experiments showed that while LV geometry and pressure are substantially affected by RV hypertension, the LV free-wall was substantially less affected by collagenous fibrosis compared to the RV and septal hinge-regions.[9] This suggests the presence of a possible adaptive mechano-transduction mechanism to reduce LV myocardial remodeling and maintain LV function.

Consequently, the aim of this study was to investigate regional β1integrin mechano-transduction in RV hypertension and its relation to the development of RV and LV fibrosis. Here, we hypothesized that regional integrin β1A+D expression mediates RV and LV fibrosis secondary to RV hypertension.

Methods

In Vivo Pulmonary Artery Banding Model

Animal experiments were approved by the institutional animal ethics committee. Thirty-six male Sprague-Dawley rats (200g body weight) were randomized to either sham (n=10) surgery (thoracotomy) or to PAB (n=26). Anesthesia was induced by intraperitoneal pentobarbital sodium (60 mg/kg). After intubation, animals were mechanically ventilated using a volume-controlled respirator and oxygen-enriched room air. Positive end-expiratory pressure was maintained at 4 cm H_2O. Through a left thoracotomy the pulmonary artery (PA) was separated from aorta. Then, an 18-gauge needle was placed under the PA, and a silk suture tied around the needle and vessel. Subsequent removal of the needle produced a fixed and standardized external PA constriction, proportional to the needle diameter. Both groups, sham and PAB rats, were then maintained for the following 6-weeks when the PAB animals developed permanent PA constriction leading to RV pressure overload.

Assessment of Cardiac Function

1) *Echocardiography*

Rats from both experimental groups were monitored at time of PAB placement and at the terminal experiment using a Vivid E9 ultrasound system with a 12-MHz phased-array transducer (GE Healthcare, Wauwatosa, WI) achieving two-dimensional (2D) frame rates of 275 frames/second. After 6-weeks, at the terminal experiment, before sacrifice, 2-dimensional, M-mode, color Doppler, and conventional pulsed Doppler images were obtained with simultaneous electrocardiogram. Digitally recorded images were stored for offline analysis with the EchoPac, version 8.0, GE Health-care, Wauwatosa, WI system.

Interventricular septum and LV free-wall thickness and shortening fraction were measured by M-mode from a short-axis view at the papillary muscle level. The LV eccentricity index (EC), defined as the ratio between the LV antero-posterior and septo-lateral dimensions,[18] was measured at end-systole and end-diastole as an index of RV hypertension severity and geometric distortion of the LV caused by leftward septal-shift **(Figure 1).** RV functional parameters included fractional area change (FAC), tricuspid annular plane systolic excursion (TAPSE) and RV myocardial performance index (MPI).

2) *Hemodynamic measurements*

After 6-weeks, RV and LV hemodynamics were assessed immediately following echocardiography. A 2F high-fidelity pressure-tipped catheter (Millar Instruments, Inc, Houston, Tx) was inserted into the RV and LV through the apex. The maximal rate of ventricular pressure rise (dp/dt_{max}) was recorded as an index of systolic function. Ventricular relaxation was reflected by Tau-

the time constant of mono-exponential decay of ventricular pressure during isovolumic relaxation.

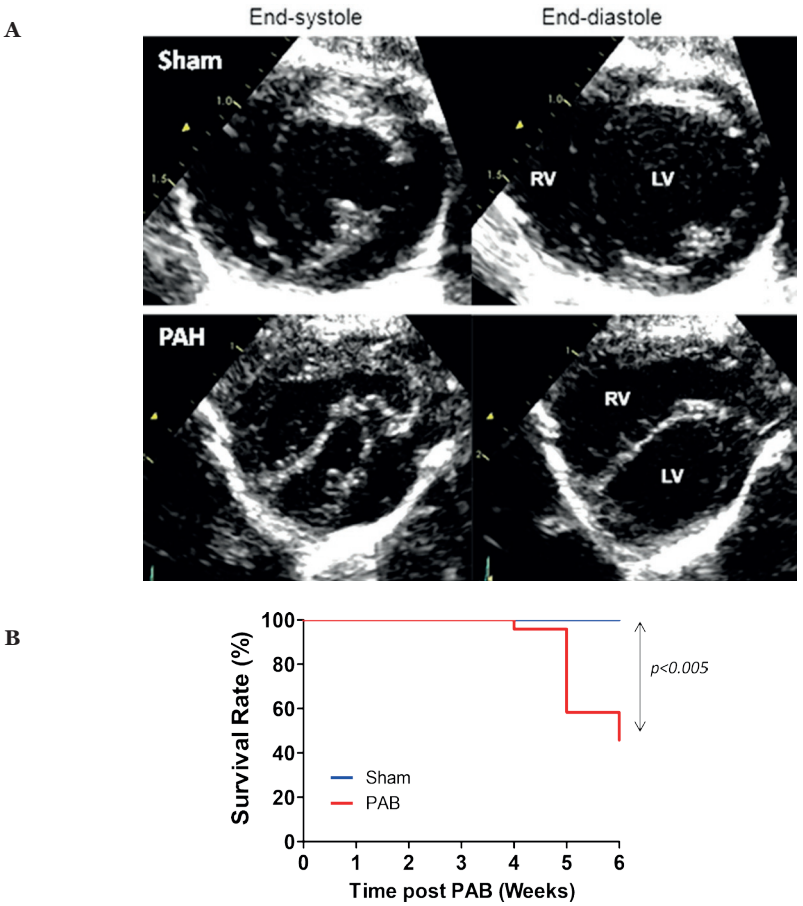

Figure 1

*A: Representative Echocardiography indicating that raising the right ventricular (RV) pressure-load induces right ventricular dilatation, septal flattening and LV compression. Septal flattening changes geometry at the septal-hinge point regions and left ventricle (LV). Short-axis view obtained at the papillary muscle level at end-systole and end-diastole in a sham (A) and PAH (B) rat. The sham rat shows a circular LV with normal round interventricular septal curvature and position throughout the cardiac cycle; while in PAH the RV is markedly enlarged, the LV flattened and 'D-shaped' throughout the cardiac cycle, with the interventricular septum displaced leftward in systole and flattened into end-diastole. B. Kaplan-Meier survival curves in sham (n=8) and PAB (n=26) 6-weeks rats. **P<0.005 vs. sham. The median survival in PAB is n=6.*

Histochemical detection of collagen-I and hydroxyproline as markers of fibrosis

Five mm thick transverse sections of the hearts from both experimental groups (sacrificed after 6-weeks) were fixed in 10% formalin for 24-hours; dehydrated and embedded in paraffin. Then, 4-μm microtome sections were prepared (Leica Microsystems A/S, Herlev, Denmark) and subjected to histochemical staining with Picrosirius Red (PSR) to visualize interstitial collagen, as previously described[19]. The proportional comparison of areas occupied by PSR-positive collagen versus the entire visual field was quantified morphometrically.

We also quantified hydroxyproline content in the heart tissues, using a commercial kit according to the manufacturer's protocol (Sigma Aldrich, St. Louis, MO). Briefly, the RV, LV and septal hinge-point regions of sham and PAB hearts were dissected separately, weighed, homogenized in sterile water and hydrolyzed in 12N HCl at 120°C for 3h. Then, hydrolyzed samples were incubated with 4-(Dimethylamino) benzaldehyde (DMAB) for 90 min at 60° C, and the absorbance of oxidized hydroxyproline was determined photometrically at 560 nm.

Detection of elastin deposition by Movat pentachrome staining

Cryostat sections (5 μm) were fixed in Bouin's solution for 30 min, followed by staining with Alcian Blue solution for 30 min. Slides were then washed in running water for 3 min and incubated with ammonium hydroxide in 95% alcohol (pH above 8) for 2 h. After washing with running water and rinsing in 70% alcohol, the slides were incubated with Weigert–Hart Resorcin solution for 3 h at 58°C and then stained with Weigert's haematoxylin for 15-minutes. Next, they were rinsed with running water and stained with Woodstain Scarlet Fuchsin solution for 5-minutes, followed by rinsing in 0.5% aqueous glacial acetic acid. Slides were then rinsed thoroughly in 3-changes of absolute alcohol and incubated with alcoholic saffron for 15-minutes. This was followed by washing with 4-changes of absolute alcohol. Finally, the slides were washed with several changes of xylene and then mounted in Permount[20].

Western Blot Analysis

Protein was extracted from heart tissue in *in vivo* experiments as well as from cultured fibroblasts with lysis buffer and diluted 1:1 with 2× SDS sample buffer (Invitrogen Canada Inc). Equal amounts of protein (20 μg) were loaded in each lane of Novex™ 4-12% Tris-Glycinegel (Invitrogen Canada Inc). Proteins were separated by electrophoresis and transferred from the gel to a nitrocellulose membrane with an electro-blotting apparatus. Membranes were incubated with 5% non-fat dry milk for 1-hour to decrease non-specific sites and then incubated with primary antibodies, to integrinβ1A and β1D that were generated in our

laboratory and used in previously published studies[21]; α-integrins 1, 2, 10 and 11(Santa Cruz,Inc); Focal Adhesion Kinase (FAK), phosphor-FAK and Integrin Linked Kinase (ILK), Erk and phosphor-Erk (Cell Signaling Technology); TGF-β1 and CTGF (Abcam, Inc); Smad2/3 and phosphor-Smad 2 and 3 (Cell Signaling Technology) overnight at 4°C. Samples were then washed and incubated with peroxidase-conjugated secondary antibody and detected by an ECL detection Kit (Bio-Rad, Canada).

Immunohistochemistry and immunofluorescence

Cryostat sections (5μm), fixed in 4% paraformaldehyde/PBS, were incubated with 0.3% hydrogen peroxide and 10% BSA for 15 minutes and then were incubated with primary antibodies recognizing ANNP (natriuretic peptides A preproprotein) at 4°C overnight. The sections were then incubated with a matching biotinylated secondary antibody (Vector, Burlingame, Calif) for 45-minutes at room temperature. Negative controls were performed for all immunological staining by omission of the primary antibody. Similar procedures were followed for fibroblast proliferation using antibodies to vimentin and Ki67. Wheat germ agglutinin (WGA) was additionally used to visualize cardiomyocyte cell membranes. Sections were then incubated with appropriate secondary or fluorescein-conjugated secondary antibodies for 60-minutes at room temperature. Negative controls were performed for all immunological staining by omission of the primary antibody. Nuclei were counterstained with 4', 6-diamidino-2-phenylindole Dilactate (DAPI).

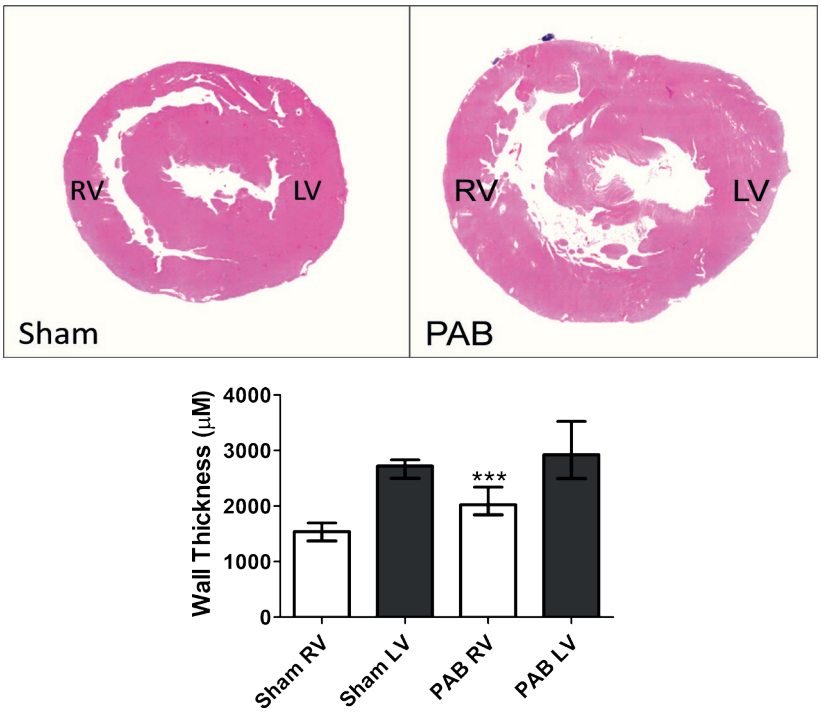

Figure 2

*Representative H&E-stained histologic morphometry of rat hearts 6-weeks after sham and PAB procedures. H&E-stained heart cross-sections derived from sham and PAB animals (Upper panel). Morphometric quantification indicated that PAB induced a significantly increased RV free-wall thickness vs. shams, while LV free-wall thickness was similar between groups. Values are expressed as medians and interquartile range (IQR) (n=5), ***p<0.0001 vs. sham.*

Primary cardiac fibroblast cultures

To evaluate the effect of mechanical stress in fibroblasts isolated from RV hypertensive animals we isolated cardiac fibroblasts from a Sugen-hypoxia rat model. For these experiments pulmonary hypertension was induced in male Sprague-Dawley rats (200 g BW) with subcutaneous Sugen5416 (20mg/kg) followed by chronic hypoxia (10% O_2) for 3-weeks. Rats were then kept at 3-weeks of normoxia before sacrifice. Control animals were placed in room air for the same duration.

Region-specific primary cardiac fibroblasts were isolated by collagenase digestion from dissected fragments of the RV free-wall, LV free-wall and septal hinge-points (**Figure 3**) derived from 200-250g adult healthy and pulmonary

hypertensive (Sugen-hypoxia) male Sprague-Dawley rats. Isolated cells were re-suspended in fresh medium consisting of DMEM with 10% FBS and plated on 100 mm² culture dishes at 37°C with 5% CO_2 for 2-hours. Non-adherent cells were washed out and the adherent cells (95% fibroblasts) were incubated in medium containing 10% FBS and 1% antibiotics. The cells were passaged 3-times (P1–P3) for all experiments and used for quantitative assessment of protein expression and immunofluorescence analyses.

Mechanical stretch of cardiac region-specific fibroblasts

To explore the possibility that integrin-β1 plays a crucial role in RV-LV mechano-transduction, we mimicked the mechanical stretch induced by RV hypertension in cardiac fibroblasts plated on membranes of the stretch apparatus (Flexcell 4000; Hillsborough, NC). Cells were plated at a density of 0.5×10^6 cells/well in DMEM medium and maintained at 37°C in humid air with 5% CO_2. When cells were ~80% confluent, the culture medium was changed to 2% serum DMEM and separate cultures were maintained in the presence and absence of integrinβ1 inhibitor (BTT3033, 10μM, Tocris Bioscience). Stretched cell-cultures were exposed to cyclic 20% equiaxial stretch at 1.7 Hz for 24-hours in a Flexcell FX-4000 strain unit equipped with loading posts. Non-stretched fibroblasts were cultured on the same stretch-chambers in the same incubator.

After treatment, cells on stretch membranes were washed twice with PBS and fixed in 4% paraformaldehyde in PBS or cold methanol for 15-minutes and blocked in 10% normal BSA in PBS for 15-minutes, before they were incubated with primary antibodies recognizing collagen type-I, integrinβ1A, TGF-β1, α-SMA and ki-67 respectively, at 4°C overnight. This step was followed by 45-minute-long incubation with the appropriate secondary antibodies conjugated with green FITC or red TRITC (Sigma). Nuclei were counterstained with a blue DAPI. Secondary antibodies alone were used as an additional control. The cells were washed twice with PBS, the wells separated with a scalpel and mounted on slides with cover slips. All cultures were examined with a Nikon Eclipse E1000 microscope attached to a cooled charge-coupled device camera (Retiga EX; QImaging, Surrey, BC, Canada).

Isolated cardiac fibroblast contraction assays

To evaluate the functional properties of active (myo)fibroblasts, cells were obtained from 3 different regions in the heart (RV, LV, septal hinge-points) and cultured on stretchable substrates. Cells were subjected to 24-hour stretching or no-stretching conditions in the presence or absence of the integrin inhibitor BTT.

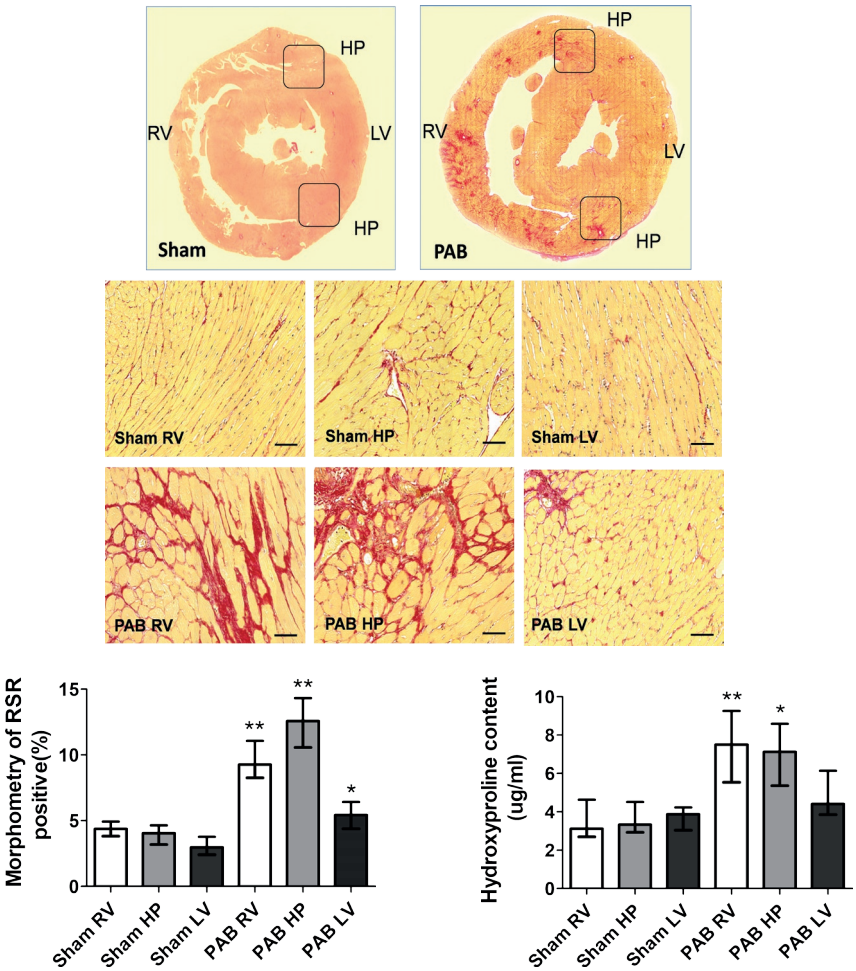

Figure 3

*Representative Picrosirius red (PSR) staining of rat hearts 6 weeks after sham and pulmonary artery banding (PAB) procedures. PSR staining demonstrates that PAB-induced right ventricular (RV) pressure load is associated with a remarkable accumulation of PSR-positive collagen and myocyte hypertrophy in the RV and septal hinge-point (HP) regions. In contrast, the left ventricle (LV) displays only disseminated foci of PSR-positive material (top panel). Low magnification of heart histological cross-sections derived from sham and PAB animals and stained with PSR (middle panels). Higher magnification of representative sections derived from the RV, hinge-point (HP), and LV heart regions (bottom panels). Bars=50 lm. The bar graphs depict morphometric quantification of the areas occupied by PSR-positive collagen, as well as values of hydroxyproline content. Values are expressed as medians and interquartile range (n=5). *P<0.05, **P<0.005 vs sham.*

Cells were then trypsinized and re-seeded onto deformable silicone substrates coated with gelatin (2μg/cm^2).[22] Cell force transmission to these substrates results in surface distortions ("wrinkles") that are visible as white lines in phase contrast micrographs.[23] After attachment overnight and development of wrinkles due to cell contraction, 20-images were taken per condition (12-conditions in total) and wrinkle area quantified per cell after thresholding images for bright lines. After elimination of technically inadequate points, 18-19 data points were analyzed per condition.

Statistical Analysis

Statistical analyses were performed with GraphPad Prism 5.0. Survival between groups was analyzed using Kaplan-Meier survival analysis. For non-normally distributed data, the Mann–Whitney or Kruskal–Wallis test were applied to test for significance. Values are expressed as medians and interquartile range (IQR). Statistical significance is recognized at $p<0.05$.

Results

Echocardiography and Hemodynamics

Sham rats showed a circular LV with round interventricular septal curvature and position throughout the cardiac cycle. In PAB rats, the RV was significantly enlarged, and the LV was flattened and geometrically distorted with a 'D-shaped' configuration throughout the cardiac cycle, where the interventricular septum was displaced leftward in systole and flattened through to end-diastole (**Figure 1A).** Echocardiographic and hemodynamic parameters are summarized in **(Table 1 and 2).** They show that RV peak systolic and end-diastolic pressures were increased in the PAB group vs. controls, with increased LV systolic and diastolic eccentricity-index and smaller LV end-diastolic diameter. The eccentricity-index was increased in systole, but did not reach statistical significance (due to a large standard deviation). Of 26 PAB rats who entered the protocol, the survival rate was 100% after 3-weeks, 88% after 4-weeks, 53% after 5-weeks and 42% after 6-weeks after PAB versus 100% in sham controls (**Figure 1B**). Of these, 5 PAB rats with complete imaging, hemodynamic, histologic and molecular data were analyzed.

Regional cardiac hypertrophy and fibrosis

Given markedly altered heart geometry following PAB, with septal flattening and displacement at the septal hinge-point regions, we also evaluated regional heart morphology and changes in expression of integrinβ1 pathway and profibrotic signaling components. The histologic assessment and morphometry of serial,

H&E-stained transverse sections indicated that PAB induced a significantly increased RV free-wall thickness vs. shams, while LV free-wall thickness was similar between groups (**Figure 2**).

We then established that the RV free wall and hinge-point regions of PAB rats demonstrated heightened deposition of PSR-positive collagen-I, as compared to sham controls. This finding was additionally confirmed by the fact that tissue fragments dissected from these regions demonstrated higher concentrations of hydroxyproline. Histochemical analysis also showed that the LV of PAB rats demonstrated increased collagen-1 fibrosis, but significantly less as compared to the RV and septal hinge-point regions; and mostly limited to perivascular areas (**Figure 3)**

Table 1. Comparison of echocardiographic measurements in pulmonary artery band (PAB)-rats vs. shams

	Sham (n=8)	PAB (n=5)
HR (bpm)		
Median	341.1	264*
Interquartile range	320.4-373.4	244.5-346.5
RV parameter:		
RVEDD (cm)		
Median	0.25	0.54 **
Interquartile range	0.24-0.2625	0.515-0.62
RVESD (cm)		
Median	0.155	0.49 **
Interquartile range	0.12-0.19	0.37-0.515
RV FAC (%)		
Median	44	21**
Interquartile range	37.5-47	18-22
TAPSE (cm)		
Median	0.28	0.09 **
Interquartile range	0.2425-0.3075	0.065-0.155
RV-MPI		
Median	0.13	0.59 **
Interquartile range	0.02-0.31	0.475-0.645
LV parameter:		
LV end-systolic ECC		
Median	1.095	2.22
Interquartile range	1.06-1.163	0.73-2.545
LV end-diastolic ECC		
Median	1.065	1.57
Interquartile range	1.045-1.113	1.075-1.585
LVPW (cm)		
Median	0.15	0.11
Interquartile range	0.13-0.17	0.09-0.145
IVS (cm)		
Median	C0.135	0.13
Interquartile range	0.1275-0.1525	0.085-0.155
LVEDD (cm)		
Median	0.885	0.71
Interquartile range	0.7175-0.6225	0.645-0.92
LVESD (cm)		
Median	0.55	0.61
Interquartile range	0.485-0.66	0.385-0.645
LV SF (%)		
Median	33.5	28
Interquartile range	27-39	20-42

Caption on next page

*Quantification of the echocardiograms and presented as the LV eccentricity index. These geometrical LV changes are expected to induce increased mechanical stress at the RV and septal hinge-point regions and mimic findings in human RV hypertension. HR= heart rate, bpm= beats per minute, LV= left ventricle, RV= right ventricle, IVS= interventricular septum. 2D measurements: ECC= eccentricity index, FAC= fractional area change. M-mode measurements: PW= posterior wall, SF= shortening fraction, TAPSE=tricuspid systolic annular excursion. Pulsed-Doppler measurements: MPI= myocardial performance index. *p<0.05, **p<0.01 vs. shams.*

To further evaluate the effect of PAB on extra-cellular matrix (ECM) composition, we also evaluated regional changes in myocardial elastin content. In comparison to sham controls, Movat's staining in PAB rats showed increased elastin content in the RV and most prominently at the septal hinge-points, but much less in LV **(Figure 4).**

Table 2. Comparison of Invasive hemodynamic parameters in pulmonary artery band (PAB) rats vs. shams

	Sham (n=8)	PAB (n=5)
HR (bpm)		
Median	343.6	270 **
Interquartile range	325.1-391.5	262-315
RV parameters :		
RV peak systolic pressure (mmHg)		
Median	19	55 **
Interquartile range	18.25-22.5	52.5-79
RV end-diastolic pressure (mmHg)		
Median	1.3	6 **
Interquartile range	1.1-3.475	4-6.5
RV dP/dT max (mmHg/s)		
Median	995	2895 *
Interquartile range	889.3-1455	1413-3293
RV Tau (ms)		
Median	10.5	19 *
Interquartile range	5.25-15.75	14.5-21.5
LV parameters :		
LV peak systolic pressure (mmHg)		
Median	77	110
Interquartile range	64.5-92	66-117
LV end-diastolic pressure (mmHg)		
Median	4.35	7 *
Interquartile range	3.073-4.448	5-13
LV dP/dT max (mmHg/s)		
Median	3495	6454
Interquartile range	2456-3425	3170-6211
LV Tau (ms)		
Median	8	20 *
Interquartile range	8-10.5	11-23.5

*Comparison of hemodynamic parameters in PAB-rats vs. sham. RV peak systolic and end-diastolic pressures were increased in the PAB group vs. sham with increased systolic and diastolic eccentricity-index and smaller LV end-diastolic diameter. In PAB rats, eccentricity-index increased in systole, but did not reach statistical significance (due to a large standard deviation). HR= heart rate, bpm= beats per minute, RV= right ventricle, LV= left ventricle *p<0.05, **p<0.01 vs. sham rats.*

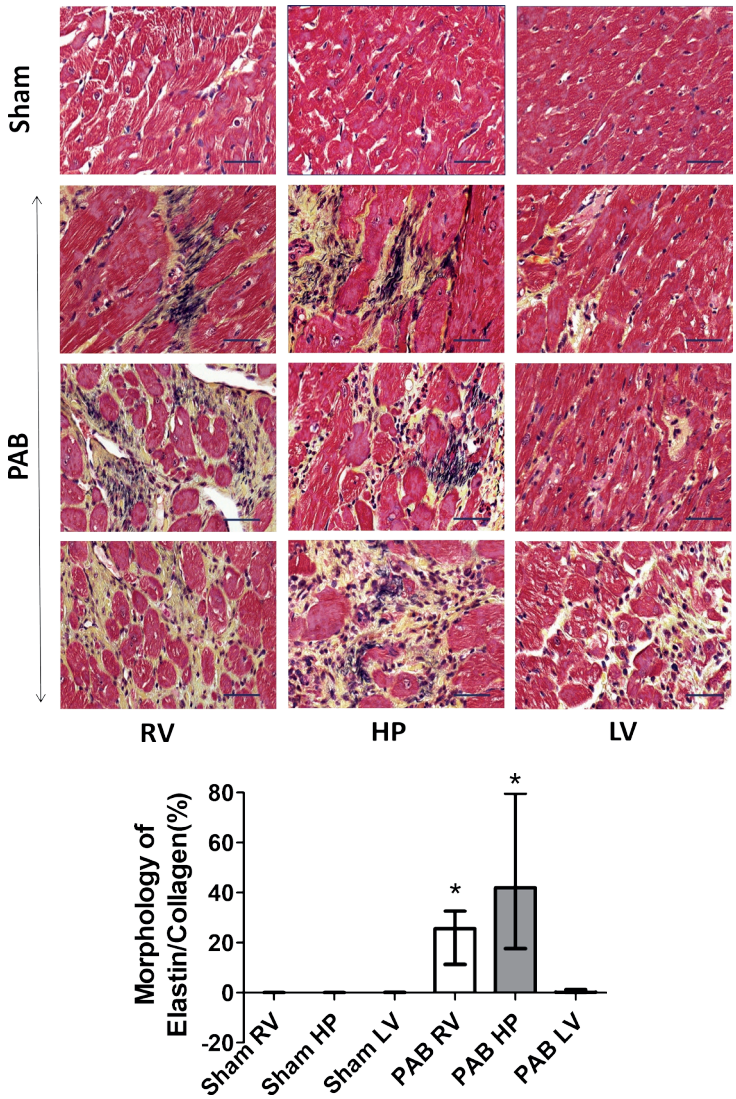

Figure 4. Representative Movat's staining of rat hearts 6-weeks after sham and PAB procedures.

Movat's staining depicting collagen-I (yellow) and elastin (black) marking differences in regional cardiac fibrosis and extra-cellular matrix composition in fragments dissected from the right ventricle (RV), hinge-point (HP) and left ventricle (LV) heart regions of sham and PAB rats ***(Upper panel)****. Note the increased elastin deposition most prominently at the septal HP. Scale bars = 50 μm. The bar graphs depict morphometric quantification of areas occupied by Movats-positive elastin and collagen* ***(Lower panel)****. Values are expressed as medians and interquartile range (IQR) (n=5), *p<0.05 vs. sham.*

Further immune-histochemical studies showed that all cardiac regions in PAB rats had increased numbers of interstitial cardiac fibroblasts, marked by the presence of immune-detected vimentin and increased number of co-localized with the presence of Ki67 proliferative antigen (**Figure 5A**). Interestingly, detection of fluorescent WGA, which marks the cell membranes of cardiomyocytes (**Figure 5B**) and H&E staining (**Figure 5C**), in parallel sections, additionally demonstrated that in PAB rats, individual RV and hinge-point cardiomyocytes showed significant hypertrophy, while LV cardiomyocytes hypertrophied, but less than RV and hinge-point cells (**Figure 5D**). Furthermore, NPPA, a sensitive marker for local stress, displayed granular cytoplasmic expression in cardiac muscle of PAB rats more at the HP and RV regions, the LV showed only a mild increase in immune-positive NPPA staining(**Figure 5E**).

A

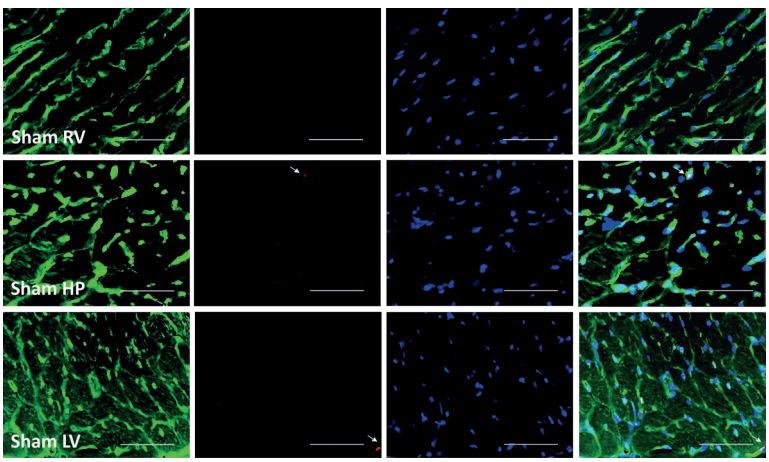

B

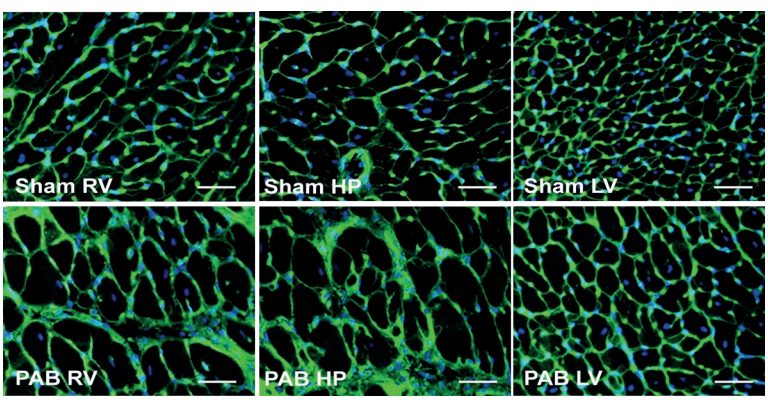

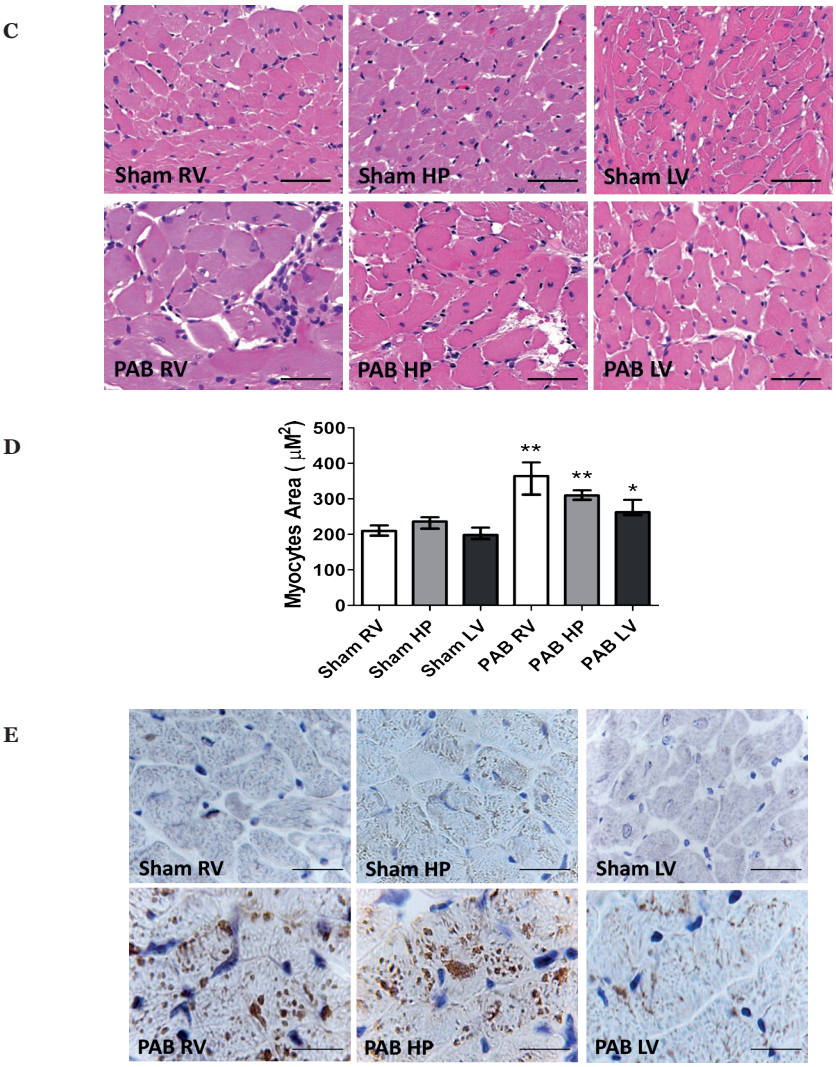

Figure 5. Representative micrographs of transversal sections of rat hearts sham and 6 weeks PAB procedures.

A: *Immunofluorescent detection of vimentin-positive fibroblasts (green) and those displaying the presence of Ki67 proliferative antigen (red). Cell nuclei were stained blue, with DAPI. Scale bars =15 μm.* ***B:*** *Wheat germ agglutinin (WGA) interacting with cardiac myocyte cell membranes, detected with green FITC staining. Scale bar: = 20 μm.* ***C:*** *Haemotoxylin and Eosin staining for cardiomyocyte cross-sectional area. Scale bar: = 20 μm.* ***D:*** *The bar graphs depict morphometric assessment of cardiac myocyte areas (n = 5, 200 cells per section). Values are expressed as medians and interquartile range (IQR). **P<0.001 vs. sham; *P<0.05 vs. sham* ***E:*** *Immunohistochemical staining of NPPA in cardiac muscle of sham and PAB rats. Scale bar: = 50 μm.*

Regional expression of diverse integrins

Given the varying regional hypertrophy and fibrosis following PAB we evaluated whether varying levels of regional mechano-transduction molecules would diversely modulate downstream signaling pathways, likely engaging activation of different integrins; including the collagen binding α1 and 11integrins. Indeed, while we observed rather similar levels of PAB-induced increases in β1A- and α1 integrin protein expression (detected by Western blots) in all regions, levels of β1D- and α11 integrin were even higher in the septal hinge-point regions (**Figure 6)**. Moreover, integrinβ1A (detected by immune-fluorescence) could be localized to interstitial fibroblasts, myofibroblasts and smooth muscle cells in those regions, but not to the cardiomyocytes (data not shown)**.** In contrast, integrin β1D was predominantly expressed at the cardiomyocyte cell membrane.

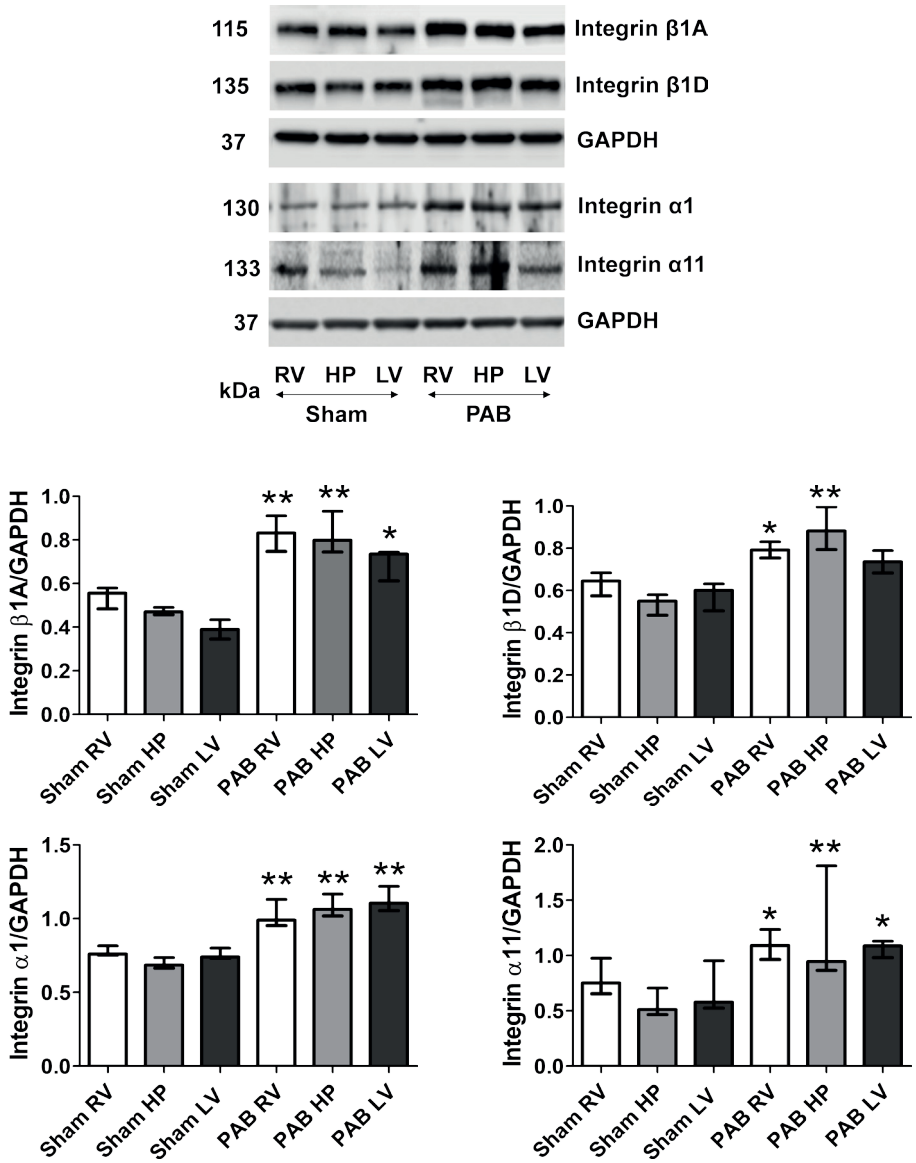

Figure 6. Right ventricular (RV) pressure-load diversely up-regulates levels of indicated integrins in heart regions 6 weeks after sham and PAB procedures. *Representative Western blots detecting indicated integrins and their quantitative assessments in the RV, HP and LV regional of sham and PAB rats. Values are expressed as medians and interquartile range (IQR) (n=5) **p< 0.001 vs. sham; *p<0.05 vs. sham*

Assessment of integrin-induced downstream signaling and pro-fibrotic signaling

Given the biventricular increase in integrinβ1 signaling following PAB, we also assessed 3 major components of downstream integrin-mediated signaling. We established that expression of phosphorylated focal adhesion kinase (FAK), integrin-linked kinase (ILK) and phosphorylated ERK were significantly increased in the RV free-wall and septal hinge-point regions, as compared to their counterparts in sham controls. Meaningfully, these proteins were only slightly unregulated in the LV of PAB rats (**Figure 7A**). Moreover, we also found that the RV and septal hinge-points of PAB hearts demonstrated heightened protein expression of the pro-fibrotic signaling pathway components TGF-β1, Smad-2, Smad-3, phosphor-Smad-2/3and CTGF. These results are consistent with activation of TGF-β1. However, expression of these proteins was only mildly elevated in the LV **(Figure 7B).**

A

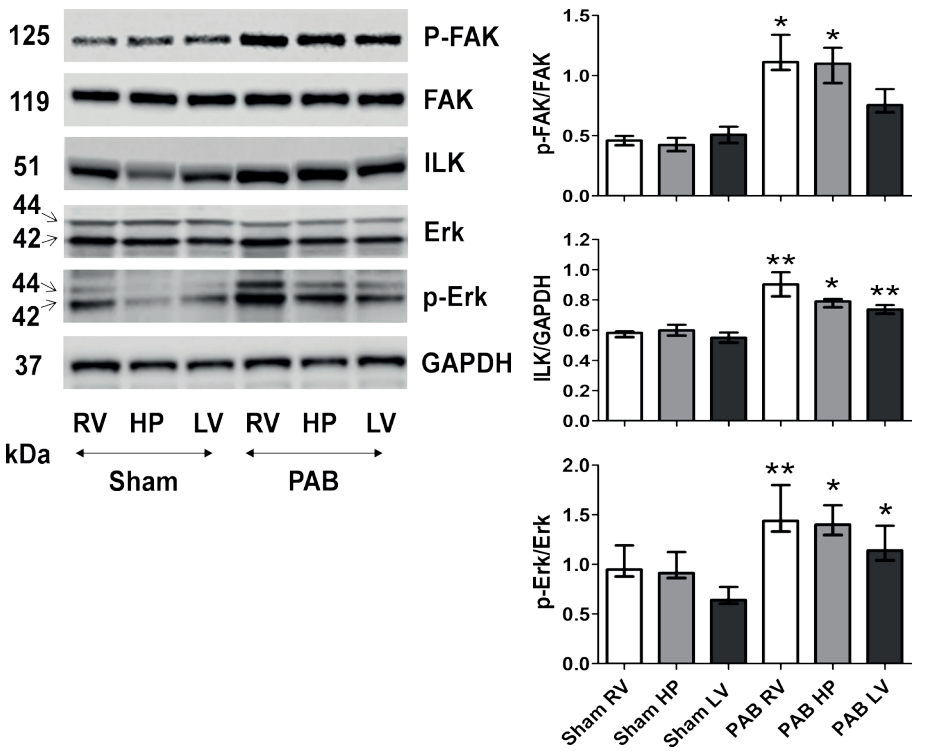

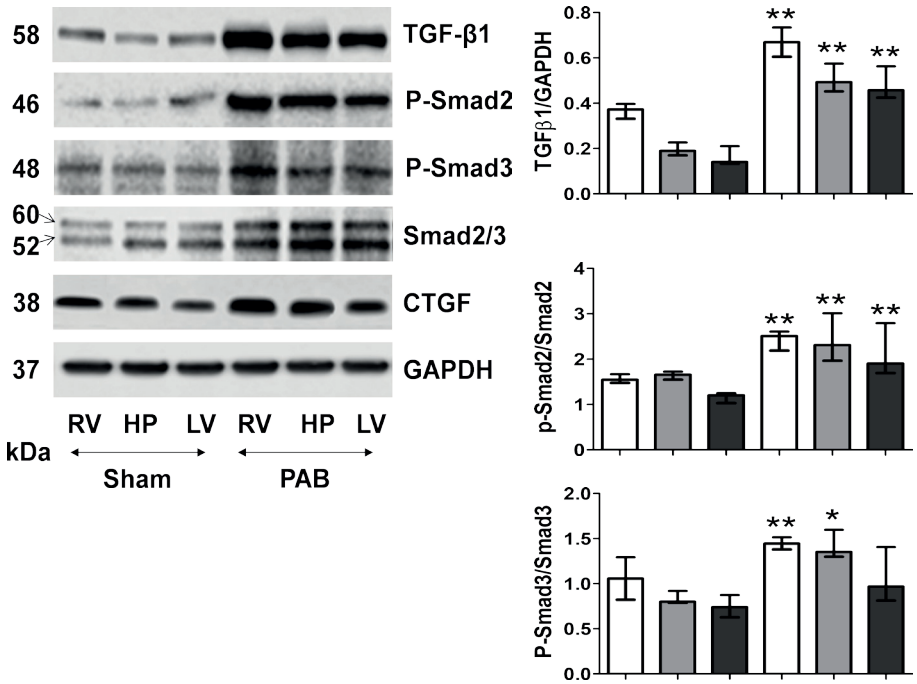

Figure 7. Application of PAB induces a diverse up-regulation in activity of the integrin-dependent signals that consequently trigger pro-fibrotic pathway 6-weeks after sham and PAB procedures.

A: *Representative Western blots detecting basic regional expression of protein levels and phosphorylation rates of the integrin-induced down-stream signaling pathway components (FAK, ILK, Erk). Values are expressed as medians and interquartile range (IQR) (n=5). **p< 0.001 vs. sham; *p<0.05 vs. sham.* ***B:*** *Representative Western blots detecting basic regional expression of protein levels and phosphorylation rates of pro-fibrotic components TGF-β1, Smad 2, Smad 3 and CTGF in sham and PAB-exposed hearts. Quantification analyses (n=5). ***p<0.0001 vs. sham; **p< 0.001 vs. sham; *p<0.05 vs. sham. Values are expressed as medians and interquartile range (IQR).*

Integrins upregulate TGF-β1 expression and collagen type-I deposition in RV, LV and hinge-point region fibroblasts in response to *in vitro* mechanical stress

Given our above-mentioned data acquired from *in vivo* experiments, we next studied the possible effects of mechanical stress on confluent cultures of normal cardiac fibroblasts, derived from control (healthy rats) and in cardiac fibroblasts isolated from the RV, HP and LV from sugen-hypoxia induced pulmonary hypertensive rats (PH). Fibroblasts that were plated on membranes of the stretch apparatus chamber (Flexcell FX-4000) and kept for 24-hours in the presence or absence of cyclic 20% equiaxial stretch at 1.7 Hz, as described above. All cultures were also kept in the presence or absence of the integrin inhibitor BTT 3033. We first found that primary cultures of cardiac fibroblasts isolated from 3 myocardial regions of normal rats showed no morphologic differences (data not shown). However, we observed that 24 hours culture of fibroblasts isolated from all 3 myocardial regions significantly up-regulated their production of collagen type-I in response to mechanical stress, as compared to non-stretched controls **(Figure 8A, C)**. Non-stretched and stretched cells from the RV and HP regions from pulmonary hypertensive rats, showed increased collagen production with no further increase in response to stretch. Collagen production in cell cultures isolated from the LV in pulmonary hypertensive animals showed significant up-regulation of collagen type-I production in response to mechanical stress **(Figure 8B, C)**. Addition of the integrin inhibitor (BTT-3033) completely suppressed collagen production in response to mechanical-stretch in both control and pulmonary hypertension rats **(Figure 8A, B, C)**. Since, BTT-3033 also inhibited collagen-1 production in non-stretched cultures, this suggests that even basal production of collagen in the heart could be modulated by integrin signaling.

A

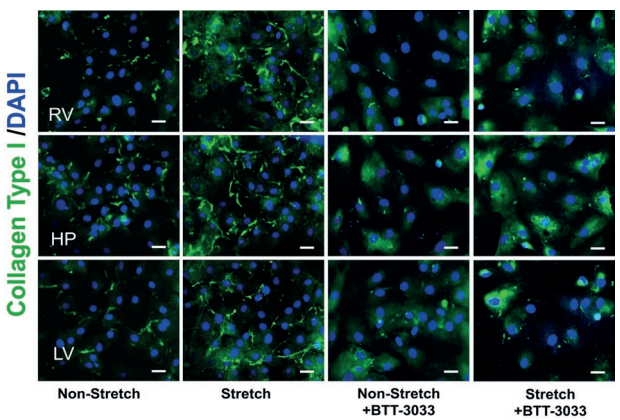

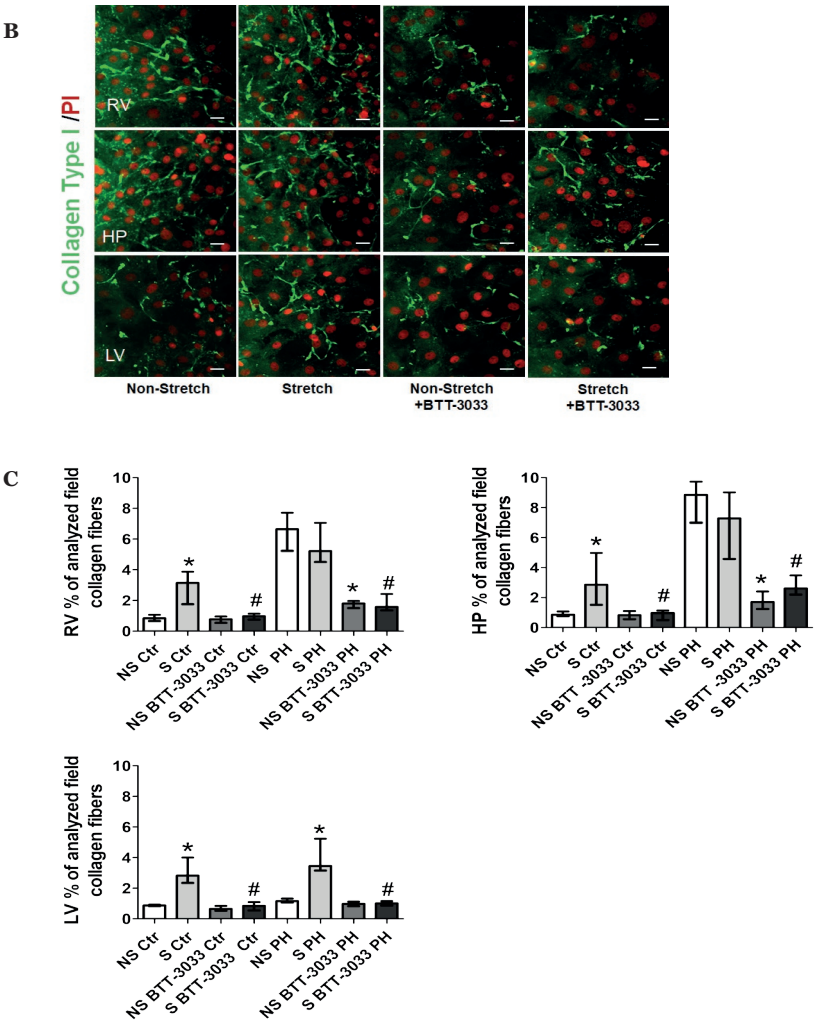

Figure 8. 24-hour long cyclic mechanical stretch of cultured cardiac fibroblasts isolated from the indicated heart regions.

A: *From control rats, induced a strong up-regulation of immune-detected collagen-I deposition, as compared to the non-stretched counterparts. This phenomenon has been suppressed in parallel cultures exposed to integrin inhibitor (BTT-3033) (upper panels).* ***B:*** *From pulmonary hypertension rats, indicated strong immune-detected collagen-I deposition in stretched and non-stretched cells of RV and HP regions, but not in LV.* ***C:*** *Representative fields of cardiac fibroblasts immune-stained with collagen type-I (Green) and nuclear DAPI staining (blue)/PI (red). Scale bar: = 50 μm. The bar graph represents the quantification data of the percentage of analyzed collagen fibers per field. Values are expressed as medians and interquartile range (IQR). *p<0.05 vs. NS (non-stretch) group; #p<0.05 vs. S (stretch) group (n=4).*

Results of the next series of experiments, in which we tested RV-derived fibroblasts, provided more details on RV integrin β1-dependent pro-fibrotic signaling. First, they demonstrated that cultures of RV-derived fibroblasts, stretched for 24-hours contained more pronounced immune-staining of antibodies to integrinβ1. They also contained more α-SMA-positive cells that could be defined as myofibroblasts and displayed more pronounced expression of TGF-β1 as well as increased wrinkles in gel assays, suggesting myofibroblast activity (**Figure 9, 10**). Moreover, stretched cultures of cardiac fibroblasts also demonstrated higher expression of immune-detected CTGF than non-stretched controls. We also found that 24 hour-long treatment with the integrin inhibitor BTT-3033 markedly decreased their expression of integrinβ1, α-SMA and TGF-β1 in both non-stretched and stretched cultures and contractile function in gel wrinkle assays. Meaningfully, treatment with BTT-3033 did not diminish the stretch-induced up-regulation in CTGF expression. This latest observation indicates that mechanical forces might also induce parallel pro-fibrotic pathways, containing CTGF, but not dependent on the prior activation of integrinβ1. The additional quantitative assessments of Western blots, detecting components of pro-fibrotic pathways, confirmed immuno-histochemistry results **(Figure 10).**

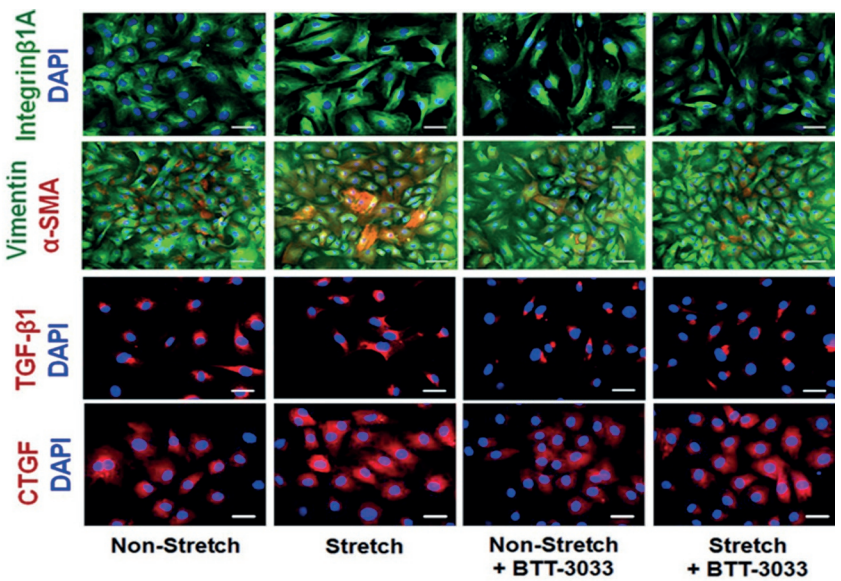

Figure 9. Representative micrographs depicting cultures of cardiac fibroblasts isolated from RV that were either kept still or subjected to 24-hour long mechanical stretching in the presence or absence of integrin inhibitor (BTT-3033).

The parallel cultures were immune-stained with specific antibodies recognizing integrin β1A (green), vimentin (green), α-SMA (red) TGF-β1 (red) and CTGF (red), combined with blue DAPI nuclear staining. Scale bars = 50μm.

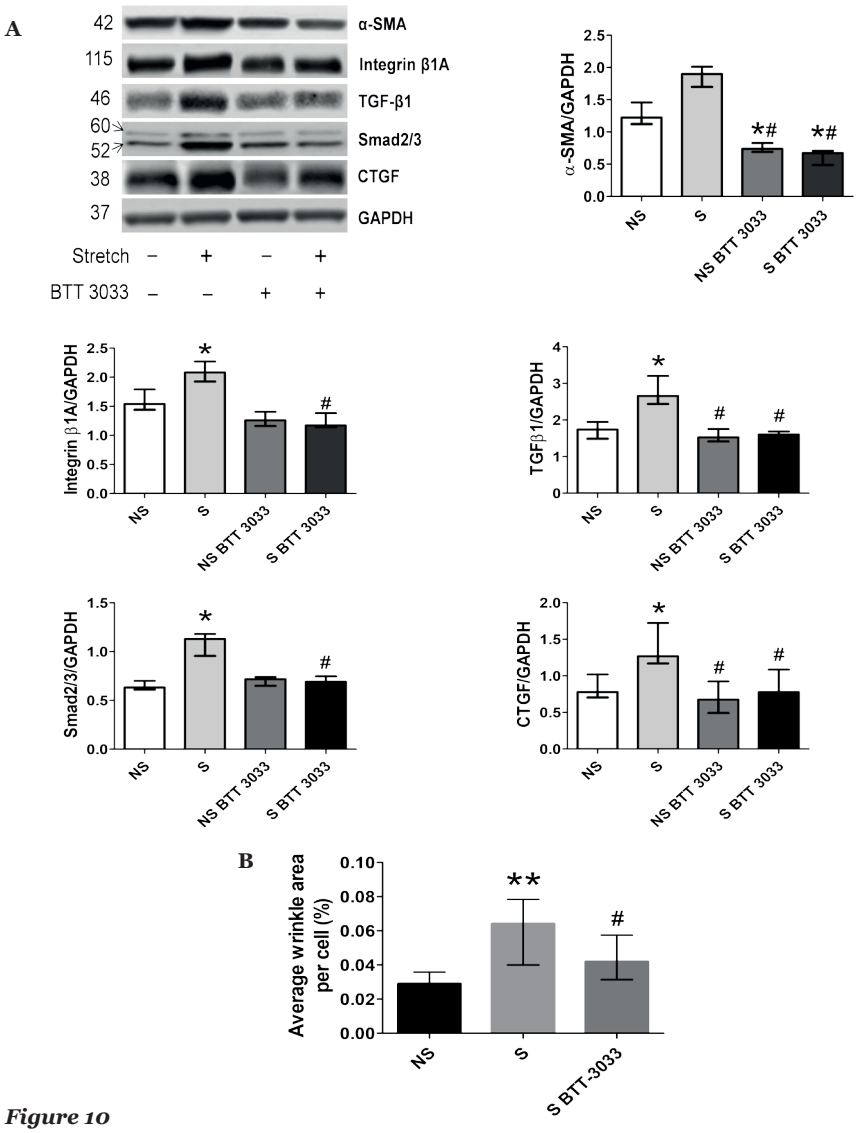

Figure 10

*Western blot assessment of pro-fibrotic pathway components in RV cardiac fibroblasts cultures. A: Cyclic mechanical stretch of cultured cardiac fibroblasts causes up-regulation in the net expressions of their α-SMA, integrin-β1 and pro-fibrotic signaling pathway components; TGF-β1, Smad 2/3 and CTGF. Western blots with indicated antibodies were assessed by densitometry and normalized against the GAPDH-positive bands (n=4). *p<0.05 vs. NS (non-stretch) group; #p<0.05 vs. S (Stretch) group. Values are expressed as medians and interquartile range (IQR). B: Percentage of analyzed collagen fibers and average cell surface wrinkles visible area to indicate cell contraction in gel assays. ***p<0.0005 vs. NS (non-stretch) group; ##p<0.005 vs. S (stretch) group (n=5). Values are expressed as medians and interquartile range (IQR).*

Discussion

The mechano-transduction of RV hypertension to ECM remodeling and fibrosis, and the transmission of these effects to the LV are inadequately characterized. In this study, we show that integrinβ1A+D, in association with the fibrillar collagen binding integrins α1 and α11, appear to transduce the mechanical stress of RV hypertension to regional RV and septal hinge-point TGF-β1 signaling and myocardial fibrosis. In contrast, although LV geometry was substantially distorted by the hypertensive RV and LV pressures elevated, in the experimental time-frame of 6-weeks, the LV developed only mild fibrosis and maintained overall good systolic function. These results suggest the possibility of a hitherto undescribed adaptive regional mechano-transduction mechanisms which may reduce LV dysfunction in the time frame produced by this experiment, through buffering effects at the septal hinge-points. These findings also suggest the possibility of a therapeutic window before extensive LV fibrosis and dysfunction ensue.

Regional mechano-transduction in isolated RV hypertension

Given the prominent *in vivo* findings of RV and septal hinge-point region fibrosis; and in cardiac fibroblast cell cultures of pro-fibrotic signaling, and by the reduction of collagen deposition with integrinβ1 pharmacological inhibition *in vitro*, our results suggest that RV hypertension and altered regional hinge-point geometry, secondary to septal shift, induces a mechanical-molecular wavefront of 'outside in' integrin signaling that triggers regional myocardial fibrosis through the TGF-β1 pathway in the RV and septal hinge-points and to a lesser degree in the LV. The marked regional activation and phosphorylation of Smad-2/3 and upregulation of collagen-binding integrins, also suggest a positive feedback loop whereby geometrical change and mechanical wall stress induces regional Smad2/3 activation leading to RV and hinge-point fibrosis. Collagens may then bind to and activate collagen-binding integrins, leading to excessive myocardial stiffness in these regions.[24] Integrinβ1A was predominantly detectable in cardiac fibroblasts and myofibroblasts; and upregulation of regional integrinβ1A and β1D expression was concomitant with regional changes in geometry (and hence wall stress) as seen on echocardiography, ECM remodelling, collagen deposition and myocyte hypertrophy.[21] Immuno-histochemistry staining of p-Smad2/3 is congruent for activation of TGF-β1 in these regions of remodeled myocardium. Downstream integrin signaling through molecules such as ILK, FAK and Erk[25] paralleled these findings with highest expression in the RV, followed by the septal hinge-points and relatively lower expression in the LV free-wall.

Our *in vitro* experiments further delineated this pathway demonstrating that mechanical stretch induced aggregation of integrinβ1 on the cell surface. This distribution change may allow 'outside-in' signalling, as the integrin β1A+D extra-cellular domains may allow interactions between (myo)fibroblasts and/or

myocytes and the ECM to 'sense' the mechanical wall stress of RV hypertension, septal shift, altered geometry and increased fibrillar collagen, to trigger RV and septal hinge-point biochemical signaling and ECM remodeling.[26, 27] We previously identified the TGF-β1 pathway as a central mediator of fibrosis in RV pressure-load.[13] TGF-β1 binds integrinβ1 which reciprocally activates latent TGF-β1 and its pro-fibrotic signaling.[28-30] Consistent with our *in vitro* results, integrinβ1 inhibition in fibroblasts blocks TGF-β1 activation and prevents fibrosis.[31, 32] Activated TGF-β1 induces collagen-type I production through signaling cascades (e.g. Smad2/3) which are active in our models.[33-36] This was supported by our *in vitro* experiments that showed that blocking integrins decreased contractile activity of stretched fibroblasts. FAK phosphorylation with upregulation of Erk, may present an interesting link in RV hypertension between integrinβ1 upregulation and fibrosis through TGFβ1 and endothelin-1 signaling.[13, 15, 16,28, 29]

CTGF is also upregulated by integrinβ1, which is reciprocally upregulated by CTGF and TGF-β1.[34-36] Our *in vitro* experiments show that integrinβ1 inhibition suppresses mechanical stretch mediated TGF-β1 expression and collagen type-I production in regionally derived fibroblasts. This reciprocal interaction and canonical 'inside-out' integrin signaling may be active during isolated RV hypertension. Nonetheless, CTGF remained elevated with integrinβ1 inhibition suggesting that alternative pathways are active and need further delineation. CTGF also strongly upregulates elastin production, although not through integrin signaling. This suggests that therapies targeting mechano-transduction pathways to decrease collagen, while increasing elastin, may be feasible to produce a more compliant myocardium.

Despite the concomitant development of distorted LV geometry and markedly increased LV diastolic pressures, fibrosis was only mild in the LV free-wall and predominantly in a perivascular distribution. Likewise, LV systolic function was maintained. Together with increased collagen-I deposition at the septal hinge-points, we also observed increased septal hinge-point deposition of extra-cellular matrix elastin. Elastin is significantly more compliant than collagen and may attenuate the increased stiffness induced by excess collagen-I deposition[37-39]. Likewise, expression of the stress marker NPPA was increased at the septal hinge-points[40]. Taken together, our results suggests that the septal hinge-points regions, where the RV and LV adjoin, while sustaining extensive stress and fibrosis, may also act as more compliant, elastin-rich buffer-zones that attenuate LV free-wall injury. This possible adaptive mechanism has not been previously described; and may act to maintain LV function as we observed overall good LV function in this study. Preserved LV systolic function may also represent an early stage of pathology in which 6-weeks of PAB allows the aforementioned compensatory remodelling of the mechanically stressed heart that postpones fibrotic hypertrophy of the LV and ultimately heart failure.

Nonetheless, impaired RV and LV diastolic dysfunction was evident by delayed relaxation (prolonged Tau) and increased RV and LV end-diastolic pressures. These are important findings as end-diastolic pressures correlate with adverse outcomes in human cardiac disease[41]. RV diastolic dysfunction may be worsened by increased RV hypertrophy and fibrosis[42, 43] which is consistent with our own previous results and other studies[44-46]. While LV diastolic impairment may result from its geometrical compression by the hypertensive RV there may be some contribution of increased LV collagen deposition. Consequently, treatments addressing RV and LV fibrosis may be beneficial[47]. In parallel to fibrosis, our *in vivo* and *in vitro* results suggest that in response to pressure-stress, and mediated by integrinβ1A+D signaling, the pressure-stressed myocardium upregulates pro-hypertrophic factors such as TGF-β1 and endothelin-1,[48, 49] most prominently in the RV and septal hinge-points and less in the LV.[50, 51] Accordingly, LV myocytes were less hypertrophied than in the RV and septal hinge-point regions, there was less cell proliferation in the LV; and gross LV wall thickness in PAB rats was not increased compared to sham controls. Taken together, our results suggest that β1integrins may mediate co-existent adaptive and maladaptive mechano-transduction mechanisms, and that the balance between these may determine biventricular function, as frequently occurs in biological systems. Consistent with our previous studies in animal models, we found increased LV myocyte hypertrophy and no decrease in LV mass. These findings are discrepant with those of Hardziyenka et al. who found LV myocyte atrophy and decreased LV free-wall mass in chronic thrombo-embolic pulmonary hypertension and in a rat model of LV failure[52]. While the reason for these discrepant results is not apparent, the increased LV pressures resulting from left septal shift may have led to a mild LV hypertrophic response. Our RV results are also more severe than the adaptive changes seen in other studies using a PAB model; but similar to those where PAB caused severe constriction[6].[43]

Study limitations

Our findings are limited to RV hypertension induced by PAB and may not automatically apply to pulmonary arterial hypertension. We did not investigate the time course of development of RV and LV fibrosis and hence ultimate development of LV fibrosis and the possibility of a therapeutic window remain conjectures. We did not demonstrate whether blocking elastin production at the septal hinge-points increases LV fibrosis. There was low variation in fibrosis levels between individual animals and consequently we could not demonstrate an association between the degree of fibrosis and the severity of RV dysfunction, an association previously found in other papers[42]. We have previously demonstrated apoptosis in our models as a mechanism of myocardial dysfunction[9]. This analysis was not repeated in these experiments. We did not

directly measure regional myocardial compliance. Histological study of fibrosis and integrin signaling pathways in human tissue from pulmonary hypertension patients would increase the clinical translation of our experimental findings and this constitutes a topic worthy of future study.

Conclusion

In conclusion, isolated RV hypertension displaces the interventricular septum, leading to geometrical changes which promote RV and septal hinge-point integrinβ1 and profibrotic signaling, leading to increased fibrosis in these regions. Despite LV geometrical distortion and markedly increased end-diastolic pressures, this mechanical-molecular remodeling was attenuated in the LV in association with increased septal hinge-point elastin deposition suggesting a possible mechano-transduction adaptive mechanism. Future studies should investigate whether these results allow for a therapeutic window before more extensive development of LV fibrosis and dysfunction.

References

1. Badesch DB, Champion HC, Sanchez MA, Hoeper MM, Loyd JE, Manes A, McGoon M, Naeije R, Olschewski H, Oudiz RJ, Torbicki A. Diagnosis and assessment of pulmonary arterial hypertension. *J Am Coll Cardiol*. 2009;54;S55-66.
2. Belenkie I, Horne SG, Dani R, Smith ER, Tyberg JV. Effects of aortic constriction during experimental acute right ventricular pressure loading. Further insights into diastolic and systolic ventricular interaction. *Circulation*. 1995;92;546-554.
3. Mitchell JR, Whitelaw WA, Sas R, Smith ER, Tyberg JV, Belenkie I. RV filling modulates LV function by direct ventricular interaction during mechanical ventilation. *Am J Physiol Heart Circ Physiol*. 2005;289;H549-557.
4. Damiano RJ, Jr., La Follette P, Jr., Cox JL, Lowe JE, Santamore WP. Significant left ventricular contribution to right ventricular systolic function. *Am J Physiol*. 1991;261;H1514-1524.
5. Hirata M, Ousaka D, Arai S, Okuyama M, Tarui S, Kobayashi J, Kasahara S, Sano S. Novel Model of Pulmonary Artery Banding Leading to Right Heart Failure in Rats. *Biomed Res Int*.2015;753210.
6. Bogaard HJ, Natarajan R, Henderson SC, Long CS, Kraskauskas D, Smithson L, Ockaili R, McCord JM, Voelkel NF. Chronic pulmonary artery pressure elevation is insufficient to explain right heart failure. *Circulation*. 2009;120;1951-1960.
7. Sanz J, Dellegrottaglie S, Kariisa M, Sulica R, Poon M, O'Donnell TP, Mehta D, Fuster V, Rajagopalan S. Prevalence and correlates of septal delayed contrast enhancement in patients with pulmonary hypertension. *Am J Cardiol*. 2007;100;731-735.
8. Freed BH, Gomberg-Maitland M, Chandra S, Mor-Avi V, Rich S, Archer SL, Jamison EB, Jr., Lang RM, Patel AR. Late gadolinium enhancement cardiovascular magnetic resonance predicts clinical worsening in patients with pulmonary hypertension. *J Cardiovasc Magn Reson.2012;* 14:11.
9. Nielsen EA, Okumura K, Sun M, Hjortdal VE, Redington AN, Friedberg MK. Regional septal hinge-point injury contributes to adverse biventricular interactions in pulmonary hypertension. *Physiol Rep* 2017; 5:pii: e13332. doi: 10.14814/phy2.13332
10. Henderson NC, Sheppard D. Integrin-mediated regulation of TGFbeta in fibrosis. *Biochim Biophys Acta*. 2013;1832:891-896.
11. Hynes RO. Integrins: bidirectional, allosteric signaling machines. *Cell*. 2002;110:673-687.
12. Ross TD, Coon BG, Yun S, Baeyens N, Tanaka K, Ouyang M, Schwartz MA. Integrins in mechanotransduction. *Curr Opin Cell Biol*. 2013;25:613-618.
13. Apitz C, Honjo O, Friedberg MK, Assad RS, Van Arsdell G, Humpl T, Redington AN. Beneficial effects of vasopressors on right ventricular function in experimental acute right ventricular failure in a rabbit model. *Thorac Cardiovasc Surg*. 2012;60:17-23.
14. Ruwhof C, van der Laarse A. Mechanical stress-induced cardiac hypertrophy: mechanisms and signal transduction pathways. *Cardiovasc Res*. 2000;47:23-37.
15. Friedberg MK, Cho MY, Li J, Assad RS, Sun M, Rohailla S, Honjo O, Apitz C, Redington AN. Adverse biventricular remodeling in isolated right ventricular hypertension is mediated by increased transforming growth factor-beta1 signaling and is abrogated by angiotensin receptor blockade. *Am J Respir Cell Mol Biol*.49:1019-1028.
16. Nielsen EA, Sun M, Honjo O, Hjortdal VE, Redington AN, Friedberg MK. Dual Endothelin

Receptor Blockade Abrogates Right Ventricular Remodeling and Biventricular Fibrosis in Isolated Elevated Right Ventricular Afterload. *PLoS One*. 2016 11:e0146767.
17. Blyth KG, Groenning BA, Martin TN, Foster JE, Mark PB, Dargie HJ, Peacock AJ. Contrast enhanced-cardiovascular magnetic resonance imaging in patients with pulmonary hypertension. *Eur Heart J*. 2005;26:1993-1999.
18. Ryan JJ, Archer SL. The right ventricle in pulmonary arterial hypertension: disorders of metabolism, angiogenesis and adrenergic signaling in right ventricular failure. *Circ Res*.2014;115:176-188.
19. Sun M, Dawood F, Wen WH, Chen M, Dixon I, Kirshenbaum LA, Liu PP. Excessive tumor necrosis factor activation after infarction contributes to susceptibility of myocardial rupture and left ventricular dysfunction. *Circulation*. 2004;110:3221-3228.
20. Sun M, Chen M, Liu Y, Fukuoka M, Zhou K, Li G, Dawood F, Gramolini A, Liu PP. Cathepsin-L contributes to cardiac repair and remodelling post-infarction. *Cardiovasc Res*.2011;89:374-383.
21. Sun M, Opavsky MA, Stewart DJ, Rabinovitch M, Dawood F, Wen WH, Liu PP. Temporal response and localization of integrins beta1 and beta3 in the heart after myocardial infarction: regulation by cytokines. *Circulation*. 2003;107:1046-1052.
22. Modarressi A, Pietramaggiori G, Godbout C, Vigato E, Pittet B, Hinz B. Hypoxia impairs skin myofibroblast differentiation and function. *J Invest Dermatol*. 2010;130:2818-2827.
23. Hinz B, Celetta G, Tomasek JJ, Gabbiani G, Chaponnier C. Alpha-smooth muscle actin expression upregulates fibroblast contractile activity. *Mol Biol Cell*. 2001;12:2730-2741.
24. Talior-Volodarsky I, Arora PD, Wang Y, Zeltz C, Connelly KA, Gullberg D, McCulloch CA. Glycated Collagen Induces alpha11 Integrin Expression Through TGF-beta2 and Smad3. *J Cell Physiol*. 2015;230:327-336.
25. Chen C, Li R, Ross RS, Manso AM. Integrins and integrin-related proteins in cardiac fibrosis. *J Mol Cell Cardiol*. 2016;93:162-174.
26. Hsueh WA, Law RE, Do YS. Integrins, adhesion, and cardiac remodeling. *Hypertension*. 1998;31:176-180.
27. MacKenna D, Summerour SR, Villarreal FJ. Role of mechanical factors in modulating cardiac fibroblast function and extracellular matrix synthesis. *Cardiovasc Res*. 2000;46:257-263.
28. Schultz-Cherry S, Chen H, Mosher DF, Misenheimer TM, Krutzsch HC, Roberts DD, Murphy-Ullrich JE. Regulation of transforming growth factor-beta activation by discrete sequences of thrombospondin 1. *J Biol Chem*. 1995;270:7304-7310.
29. Annes JP, Munger JS, Rifkin DB. Making sense of latent TGFbeta activation. *J Cell Sci*. 2003;116:217-224.
30. Sarrazy V, Koehler A, Chow ML, Zimina E, Li CX, Kato H, Caldarone CA, Hinz B. Integrins αvβ5 and αvβ3 promote latent TGF-beta1 activation by human cardiac fibroblast contraction. *Cardiovasc Res*.2014;102:407-417.
31. Henderson NC, Arnold TD, Katamura Y, Giacomini MM, Rodriguez JD, McCarty JH, Pellicoro A, Raschperger E, Betsholtz C, Ruminski PG, Griggs DW, Prinsen MJ, Maher JJ, Iredale JP, Lacy-Hulbert A, Adams RH, Sheppard D. Targeting of αv integrin identifies a core molecular pathway that regulates fibrosis in several organs. *Nat Med*. 2013;19:1617-1624.
32. Liu S, Xu SW, Blumbach K, Eastwood M, Denton CP, Eckes B, Krieg T, Abraham DJ, Leask A. Expression of integrin beta1 by fibroblasts is required for tissue repair in vivo. *J Cell Sci*. 2010;123:3674-3682.

33. Leask A. Potential therapeutic targets for cardiac fibrosis: TGFbeta, angiotensin, endothelin, CCN2, and PDGF, partners in fibroblast activation. *Circ Res*. 2010;106:1675-1680.
34. Hu X, Li N, Tao K, Fang X, Liu J, Wang Y, Wang H, Shi J, Ji P, Cai W, Bai X, Zhu X, Han J, Hu D. Effects of integrin αvβ3 on differentiation and collagen synthesis induced by connective tissue growth factor in human hypertrophic scar fibroblasts. *Int J Mol Med*. 2014;34:1323-1334.
35. Sonnylal S, Shi-Wen X, Leoni P, Naff K, Van Pelt CS, Nakamura H, Leask A, Abraham D, Bou-Gharios G, de Crombrugghe B. Selective expression of connective tissue growth factor in fibroblasts in vivo promotes systemic tissue fibrosis. *Arthritis Rheum*. 2010;62:1523-1532.
36. Lee CH, Shah B, Moioli EK, Mao JJ. CTGF directs fibroblast differentiation from human mesenchymal stem/stromal cells and defines connective tissue healing in a rodent injury model. *J Clin Invest*.120(9):3340-3349.
37. Rodgers UR, Weiss AS. Cellular interactions with elastin. *Pathol Biol*. 2005;53:390-398.
38. Steed MM, Tyagi SC. Mechanisms of cardiovascular remodeling in hyperhomocysteinemia. *Antioxid Redox Signal*. 2011;15:1927-1943.
39. Henderson BC, Sen U, Reynolds C, Moshal KS, Ovechkin A, Tyagi N, Kartha GK, Rodriguez WE, Tyagi SC. Reversal of systemic hypertension-associated cardiac remodeling in chronic pressure overload myocardium by ciglitazone. *Int J Biol Sci*. 2007;3:385-392.
40. Sergeeva IA, Christoffels VM. Regulation of expression of atrial and brain natriuretic peptide, biomarkers for heart development and disease. *Biochim Biophys Acta*. 2013;1832:2403-2413.
41. Burkett DA, Slorach C, Patel SS, Redington AN, Ivy DD, Mertens L, Younoszai AK, Friedberg MK. Impact of Pulmonary Hemodynamics and Ventricular Interdependence on Left Ventricular Diastolic Function in Children With Pulmonary Hypertension. *Circ Cardiovasc Imaging*. 2016;9:pii: e004612. doi: 10.1161/CIRCIMAGING.116.004612.
42. Rain S, Andersen S, Najafi A, Gammelgaard Schultz J, da Silva Goncalves Bos D, Handoko ML, Bogaard HJ, Vonk-Noordegraaf A, Andersen A, van der Velden J, Ottenheijm CA, de Man FS. Right Ventricular Myocardial Stiffness in Experimental Pulmonary Arterial Hypertension: Relative Contribution of Fibrosis and Myofibril Stiffness. *Circ Heart Fail*. 2016;9:pii: e002636. doi:10.1161/CIRCHEARTFAILURE.115.002636.
43. Mendes-Ferreira P, Santos-Ribeiro D, Adao R, Maia-Rocha C, Mendes-Ferreira M, Sousa-Mendes C, Leite-Moreira AF, Bras-Silva C. Distinct right ventricle remodeling in response to pressure overload in the rat. *Am J Physiol Heart Circ Physiol*. 2016;311:H85-95.
44. Okumura K, Kato H, Honjo O, Breitling S, Kuebler WM, Sun M, Friedberg MK. Carvedilol improves biventricular fibrosis and function in experimental pulmonary hypertension. *J Mol Med)*.2015;93:663-674.
45. Bogaard HJ, Natarajan R, Mizuno S, Abbate A, Chang PJ, Chau VQ, Hoke NN, Kraskauskas D, Kasper M, Salloum FN, Voelkel NF. Adrenergic receptor blockade reverses right heart remodeling and dysfunction in pulmonary hypertensive rats. *Am J Respir Crit Care Med*. 2010;182:652-660.
46. Borgdorff MA, Koop AM, Bloks VW, Dickinson MG, Steendijk P, Sillje HH, van Wiechen MP, Berger RM, Bartelds B. Clinical symptoms of right ventricular failure in experimental chronic pressure load are associated with progressive diastolic dysfunction. *J Mol Cell Cardiol*. 2015;79:244-253.
47. Handoko ML, de Man FS, Allaart CP, Paulus WJ, Westerhof N, Vonk-Noordegraaf A. Perspectives on novel therapeutic strategies for right heart failure in pulmonary arterial hypertension: lessons from the left heart. *Eur Respir Rev*. 2010;19:72-82.

48. Ayca B, Sahin I, Kucuk SH, Akin F, Kafadar D, Avsar M, Avci, II, Gungor B, Okuyan E, Dinckal MH. Increased Transforming Growth Factor-beta Levels Associated with Cardiac Adverse Events in Hypertrophic Cardiomyopathy. *Clin Cardiol*. 2015;38:371-377.
49. Olson AK, Ledee D, Iwamoto K, Kajimoto M, O'Kelly Priddy C, Isern N, Portman MA. C-Myc induced compensated cardiac hypertrophy increases free fatty acid utilization for the citric acid cycle. *J Mol Cell Cardiol*. 2013;55:156-164.
50. Sadoshima J, Izumo S. The cellular and molecular response of cardiac myocytes to mechanical stress. *Annu Rev Physiol*. 1997;59:551-571.
51. Schultz Jel J, Witt SA, Glascock BJ, Nieman ML, Reiser PJ, Nix SL, Kimball TR, Doetschman T. TGF-beta1 mediates the hypertrophic cardiomyocyte growth induced by angiotensin II. *J Clin Invest*. 2002;109:787-796.
52. Hardziyenka M, Campian ME, Reesink HJ, Surie S, Bouma BJ, Groenink M, Klemens CA, Beekman L, Remme CA, Bresser P, Tan HL. Right ventricular failure following chronic pressure overload is associated with reduction in left ventricular mass: evidence for atrophic remodeling. *J Am Coll Cardiol*.57:921-928.

Chapter 9

The stressed right ventricle in repaired tetralogy of Fallot: Dyssynchronous activation induces regional disparities in stress and function

Relative impact of right ventricular electro-mechanical dyssynchrony versus pulmonary regurgitation on right ventricular dysfunction and exercise intolerance in patients after repair of tetralogy of Fallot.

Authors
Joost Lumens, PhD, Chun-Po Steve Fan, PhD, John Walmsley, PhD, Deane Yim, MD, Cedric Manlhiot, PhD, Andreea Dragulescu, MD, Lars Grosse-Wortmann, MD, Luc Mertens, MD, PhD, Frits W. Prinzen, PhD, Tammo Delhaas, MD, PhD, Mark K. Friedberg, MD

Chun-Po Steve Fan, John Walmsley and Deane Yim contributed equally to this work

(adapted from) J Am Heart Assoc. 2019 Jan 22; 8(2): e010903

Abstract

Background: The relative impact of right ventricular (RV) electro-mechanical dyssynchrony versus pulmonary regurgitation (PR) on exercise capacity and RV function after tetralogy of Fallot repair (rTOF) is unknown. We aimed to delineate the relative effects of these factors on RV function and exercise capacity.

Methods and Results: We retrospectively analyzed 81 rTOF children using multivariable regression. Predictor parameters were electrocardiogram QRS duration reflecting electro-mechanical dyssynchrony and PR severity by cardiac magnetic resonance (CMR). The outcome parameters were exercise capacity (% predicted peak oxygen consumption (VO_2)) and CMR ejection-fraction (RVEF). To understand the relative effects of RV dyssynchrony versus PR on exercise capacity and RV function, virtual patient simulations were performed using a closed-loop cardiovascular system model (Circadapt), covering a wide spectrum of disease severity.

Eighty-one rTOF patients (median (IQR) age 14.48 (11.55 – 15.91) years) were analyzed. All had prolonged QRS duration (144 (123–152) msec), at least moderate PR (40% (29–48)), reduced exercise capacity (79% (68–92) predicted peak VO_2) and reduced RVEF (48% (44–52)). Longer QRS duration, more than PR, was associated with lower VO_2 and lower RVEF. In a multivariable regression analysis VO_2 decreased with both increasing QRS duration and PR severity. CircAdapt modeling showed that RV dyssynchrony exerts a stronger limiting effect on exercise capacity and on RVEF than does PR, regardless of contractile function.

Conclusions: In both patient data and computer simulations, RV dyssynchrony, more than PR, appears to be associated with reduced exercise capacity and RV systolic dysfunction in patients after TOF repair.

Clinical Perspective

What is new?

A significant proportion of patients with repaired tetralogy of Fallot have electro-mechanical dyssynchrony which may substantially impact RV function and exercise capacity more than the severity of PR.

What are the clinical implications?

Many patients with rTOF and RV dysfunction may benefit from cardiac resynchronization therapy. Addressing RV electro-mechanical dyssynchrony may become a central therapeutic goal in repaired tetralogy of Fallot, in addition to, or independently of, pulmonary valve replacement.

Background

Surgically repaired Tetralogy of Fallot (rTOF) is the most prevalent cyanotic congenital heart disease. While surgery in infancy has led to improved life expectancy and quality of life, residual lesions that result from surgical repair are common. These impact right ventricular (RV) size and function and affect symptoms, exercise capacity, and long-term outcomes.[1-4]

There are multiple, often co-existing, reasons for progressive RV dysfunction in rTOF.[3] Among these, chronic volume loading resulting from chronic pulmonary regurgitation (PR) is thought to cause progressive RV dilation and dysfunction.[2,5,6] Consequently, several studies and guideline documents recommend replacing the pulmonary valve in patients with symptoms or in severely dilated RVs prior to development of irreversible RV remodeling.[7] The current indications and timing for pulmonary valve replacement remain controversial and continue to be actively debated. Current practice in many centers include replacing the pulmonary valve in asymptomatic patients, when the RV is enlarged beyond an end diastolic volume of 150-170 ml/m^2 or an end-systolic volume >90 ml/m^2.[7] While pulmonary valve replacement leads to decreased RV volumes and subjective improvement in many patients, there is no conclusive evidence to show that it improves key clinical outcomes such as exercise capacity, RV systolic function and mortality.[8,9] Therefore, other factors may be important contributors to the progressive RV dysfunction commonly observed in this population.

Among the possible other etiological factors for RV dysfunction, electro-mechanical abnormalities have been shown to be important.[10,11] After surgical TOF repair, over 90% of patients develop right bundle branch block (RBBB) and a prolonged QRS duration has been recognized as a major risk factor for ventricular arrhythmia and mortality.[11] We described that RBBB-induced electro-mechanical dyssynchrony is associated with RV dysfunction.[12] Accordingly, resynchronizing the dysfunctional RV could improve its hemodynamics, work and efficiency.[13] However, the relative contribution of electro-mechanical dyssynchrony versus PR on RV function and exercise capacity is currently unknown. This knowledge gap is highly relevant as it is likely to influence patient management in terms of deciding between pulmonary valve replacement (PVR) versus cardiac resynchronization therapy (CRT). Resynchronization of the dysfunctional sub-pulmonary RV in rTOF is not yet routine therapy, but may be helpful in a portion of patients where RV electro-mechanical dyssynchrony underlies RV dysfunction and reduced exercise capacity.[14,15] Consequently, the aim of this study was to investigate the relative influence of PR versus electro-mechanical dyssynchrony on RV function and exercise capacity in rTOF. We hypothesized that electro-mechanical dyssynchrony is more strongly associated with RV dysfunction and exercise intolerance than PR.

Methods

Study design

The data, analytic methods, and study materials will not be made available to other researchers for purposes of reproducing the results or replicating the procedure. To address the above research question, we used a dual approach using statistical analysis of patient data followed by computer modeling. We performed a clinically based, retrospective, cross-sectional statistical analysis of 81 children who had undergone surgical repair of TOF in early childhood to explore how QRS duration and PR are related to exercise capacity and RV function. We then performed virtual patient simulations covering a wide spectrum of disease severity to generate hypotheses about the relative mechanistic effect of RV dyssynchrony versus PR on exercise capacity and RV systolic function under tightly controlled and standardized circumstances. For this step, we used the Circadapt model of the human heart and circulation, which has been shown to contribute to physiological understanding of both RV function and electro-mechanical dyssynchrony.[16-18]

Study population for the clinical analysis

We performed a retrospective cross-sectional analysis of data from patients whose data was collected between January 2007 and December 2014. The study was approved by the institutional research ethics board of the Hospital for Sick Children (Toronto, Ontario, Canada). Patients provided informed consent. A departmental database was used to screen for eligible patients (aged <18 years) after TOF repair who had cardiac magnetic resonance (CMR) imaging. Patients who had a primary diagnosis of an atrioventricular septal defect with TOF or with more than minor (potentially hemodynamically significant) residual intra-cardiac shunts were excluded. Furthermore, to obtain a relatively homogeneous cohort in terms of volume-loading as the predominant lesion, we excluded patients with moderate or severe RV outflow tract (RVOT) obstruction, defined as a Doppler-echocardiography outflow gradient >40mmHg[19], within 6-months of CMR. Likewise, to avoid the major confounder of pacing-induced dyssynchrony, patients with active pacemakers were excluded. As patients with repaired TOF/ absent pulmonary valve face the same clinical issues, and the influence of PR versus RBBB-dyssynchrony is relevant to this population, we included these patients in the analysis.

Cardiac Magnetic Resonance

Cardiac Magnetic Resonance (CMR) was used to quantify RV volumes, RV ejection fraction (RVEF) and pulmonary regurgitation. CMR was performed on a 1.5 Tesla scanner ('Avanto', Siemens Medical Systems, Erlangen, Germany). The clinical protocol included short-axis cine imaging for quantification of

biventricular volumes and ejection fractions, as well as main pulmonary artery phase contrast flow velocity mapping for estimation of the PR volume and fraction. Ventricular volumes, mass and flow quantification were performed using commercially available software (QMass Version 7.6 and QFlow Version 5.6, Medis Medical Imaging Systems, Leiden, the Netherlands).

Clinical parameters

Demographic and clinical data were collected from the medical record. Patients had cardiopulmonary exercise testing (CPET) and a 12-lead body surface electrocardiogram (ECG) within 6-months of CMR. CPET was performed using a modified Bruce protocol. Peak oxygen consumption (peak VO_2) and the percentage of predicted peak oxygen consumption were recorded. The duration of the QRS complex was considered to be the continuous ECG parameter reflecting RV electro-mechanical dyssynchrony because all patients had a RBBB configuration on the ECG.

Outcomes

The outcome variables were peak VO_2, which we also expressed as percent of predicted VO_2 (as commonly done in clinical practice) and RVEF, evaluated by CMR, as a measure of RV global systolic function. VO_2 was normalized according to published data.[20] We also analyzed the relationship of PR and RBBB to RV end-systolic (RVESV) and end-diastolic (RVEDV) volumes indexed to body surface area as parameters of RV remodeling.

Independent variables

QRS duration and PR fraction were the 2 independent variables of interest. Age, sex, body surface area and heart rate were considered as covariates.

Statistical Methods

Descriptive analysis

Continuous variables were summarized in terms of median and interquartile range (IQR); dichotomous variables were summarized by frequencies and proportions. We also assessed correlations between QRS duration, PR fraction and the outcome variables of interest using Spearman's correlation. The 95% confidence intervals (CIs) of correlation coefficients were constructed using Fisher's z-transformation.

Multivariable regression analysis

The association between QRS duration, PR fraction and peak VO_2 was modelled using multivariable linear regression. The non-linear association between an outcome variable and QRS duration and PR fraction was quantified using restricted cubic splines. The models included interactions between QRS duration and PR fraction, but these were restricted to linear-linear and linear-nonlinear interactions because of the limited sample size. Two regression models, namely unadjusted and covariate-adjusted models, were used to examine the associations. The unadjusted models included only the independent variables of interest (QRS duration and PR fraction); whereas the adjusted model further included the aforementioned clinical covariates.

The proportion of missing values in all variables considered in the study varied between 1 and 20%. Following the recommendation by Harrell[21], twenty imputed datasets were constructed using a flexible additive regression spline model. Missing values in continuous variables were then imputed using predictive mean matching.[21] The final regression models were obtained by applying Rubin's rules to combine the regression results across multiply imputed datasets. Diagnostic assessment of the final model was performed by inspecting residual plots.

We used heat maps to summarize predicted outcomes with respect to the independent variables of interest using both unadjusted and adjusted models. The estimated regression equations for the heat maps are included in the Appendix. Furthermore, the association was also adjusted for age, sex, BSA and heart rate. The association plots were created with average values for continuous covariates and for male gender. All analyses were conducted using R v3.4.1 with the rms package.

Virtual patient simulations

Reference rTOF simulation

The CircAdapt model is a closed-loop cardiovascular system model featuring contractile atria and ventricles, and lumped representations of the systemic and pulmonary circulations, separated by the four cardiac valves.[22-24] Structural adaptation to changes in hemodynamic loading can be simulated by varying the structure of the cardiovascular system, i.e. mass, size and passive stiffness of cardiac and vascular walls, through physiological adaptation rules.[25] For this study, resting conditions were taken to be a cardiac output (CO) of 5.4 L/min with a heart rate (HR) of 76 beats per minute, being the average values measured in the rTOF patient cohort. Note that the CO of 5.4 L/min is the effective systemic blood flow, which equals the output of the left ventricle, as the aortic and mitral valves are assumed to be competent. Mean arterial pressure was allowed to stabilize at 92 mmHg through changes in systemic vascular resistance and circulating blood volume in all simulations. Two reference simulations were used in this study, one with healthy RV myocardium (the default CircAdapt model), and one with right atrial (RA) and RV myocardial dysfunction. The latter was created by reducing the RV and right atrial myocardial contractility to 50% of the healthy value, so that RV ejection fraction (RVEF) was in the range measured in the rTOF patient cohort (44-52%, **Table 1**), given a simulated PR fraction of 40% (i.e. the median value of the patient cohort, **Table 1**). RA dysfunction was induced as the RA has been shown to be dysfunctional in association with RV dysfunction in rTOF.[26,27] Varying combinations of both PR and RV electro-mechanical dyssynchrony were then imposed on these two reference simulations as described below, yielding two sets of 100 rTOF simulations. For each simulation, RVEF was quantified as the change in RV volume during systole divided by end-diastolic volume, as in the patients.

Simulating PR

CircAdapt treats flow across the valve as being unsteady and non-viscous with a non-linear flow profile. The Bernoulli equation is used to relate flow velocity and valve area to pressure drop across the valve, with inertial effects on acceleration and deceleration due to blood mass included. In the standard CircAdapt model, the pulmonary valve begins to close once pulmonary arterial pressure exceeds RV pressure, with the valve's effective regurgitant orifice area (EROA) being 0 cm^2 when the valve is closed, preventing backward flow. Valvular regurgitation can be simulated in the CircAdapt model by setting the EROA to be non-zero, mimicking a hole in the valve through which retrograde flow can occur when pulmonary arterial pressure exceeds RV pressure (**Supplementary Figure 1)**. Retrograde flow uses the same equations as forward flow. Computational details are provided in the Appendix. In this study, the effective opening area of the pulmonary valve was 4.7 cm^2. We used ten effective regurgitant orifice areas (EROAs) ranging from 0 cm^2 (no PR) up to 2.25 cm^2 (severe PR) in steps

of 0.25cm2.

Simulating Electro-Mechanical Dyssynchrony

Electro-mechanical dyssynchrony was introduced into the RV of the CircAdapt model by dividing the RV free wall into five equally-sized segments that can mechanically interact both with one another, and with the LV free wall and septum.[24] This methodology has previously been shown to produce realistic simulations of the dyssynchronously activated heart for both LV and RV stresses and strains as well as system-level hemodynamics.[17,28] Dispersion in onset of contraction (i.e. sarcomeric force generation) within these RV free wall segments was introduced to simulate varying degrees of RBBB by delaying their activation relative to the LV free wall and septum. One RV segment was activated simultaneously with the LV, and the remaining four RV segments were activated at 25%, 50%, 75% and 100% of the maximum delay in the RV free wall (**Supplemental Figure 2**). Nine different maximum delays were used to simulate varying severities of RBBB, ranging from synchronous contraction (no RV delay) to severe contractile dyssynchrony (180 ms delay in the latest activated RV segment), in steps of 20ms.

Modelling Exercise Capacity

Exercise can be simulated in CircAdapt by simultaneously increasing heart rate (HR) and cardiac output (CO). Exercise levels are achieved while increasing the circulating blood volume in the cardiovascular system, with mean arterial pressure maintained at 92 mmHg through changes in systemic vascular resistance (**Supplemental Methods**). We hypothesized that increased central venous pressure (i.e. mean vena cava pressure) is a limiting factor for the cardiovascular system's ability to perform exercise. To quantify exercise capacity and allow comparison between simulations, we assumed that it is impossible to perform exercise when mean pressure in the *vena cava* exceeds 25 mmHg. This threshold was chosen as it is significantly in excess of the 15mmHg RA pressure reported by Stickland et al. at near-peak exercise.[29] Sensitivity of results was tested against other pressure thresholds. For each of the virtual rTOF patient simulations described above, CO and HR were gradually increased from rest until the pre-defined threshold pressure was reached, with exercise capacity defined to be this threshold-reaching CO ($CO_{max\text{-}exc}$). We used a fixed HR-CO relationship from the literature to determine the HR for a given CO (**Supplemental Figure 3**).

Results

Clinical cohort

Eighty-one rTOF patients at a median (IQR) age of 14.48 (11.55 – 15.91) years were analyzed. The average age at time of repair was 0.95±0.78 years. Their clinical characteristics are shown in **Table 1**. All patients had prolonged QRS in a RBBB pattern and moderate PR (**Table 1**).

Table 1. Clinical characteristics of the patient cohort

Clinical characteristic	N	Median (Interquartile range)
Age (years)	81	14.48 (11.55 – 15.91)
Sex (number)	81	
Female		34 (42%)
Male		47 (58%)
Height (centimeters)	76	155.0 (143.4 – 166.0)
Weight (kilograms)	76	47.0 (34.8 – 66.0)
Body surface area (meter^2)	79	1.46 (1.19 – 1.69)
Heart rate at CMR (bpm)	80	76 (68 – 85)
QRS duration (milliseconds)	72	144 (123 – 152)
Pulmonary regurgitation fraction (%)	76	40 (29 – 48)
Years between repair and CMR	75	13.0 (10.6 – 15.1)

bpm = beats per minute, CMR=cardiac magnetic resonance

The median time between CPET and CMR was 1.9 months. ECG and CMR were done on the same day in the vast majority of patients.

The outcome variables of interest are presented in **Table 2**. rTOF patients had overall mildly to moderately reduced exercise capacity and mildly reduced RVEF.

Table 2. Outcome variables summarized as medians and interquartile ranges.

Clinical characteristics	N	Median (interquartile range)
Peak VO2 (ml/min/m²)	65	35.0 (29.0 – 41.8)
Percent predicted peak VO2 (%)	65	79 (68 – 92)
RV ejection fraction (%)	80	48 (44 – 52)
Cardiac Index (l/min/m²)	79	3.67 (3.28 – 4.22)

VO_2 = oxygen consumption; ml=milliliters; min=minute; m=meter
RV=right ventricle
l=liters

Association between QRS duration versus PR on exercise capacity

Figure 1 shows the predicted peak VO_2 without and with covariate adjustment in this patient cohort.

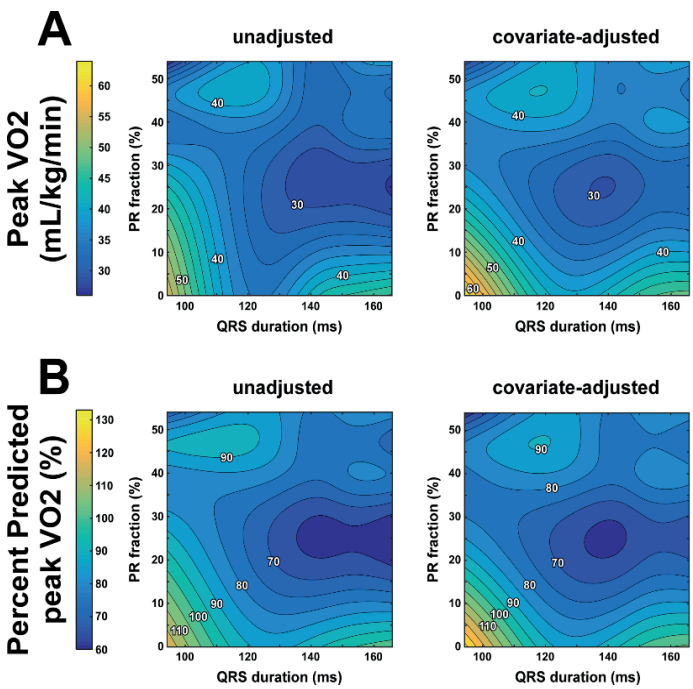

Figure 1

Predicted exercise capacity as function of right ventricular (RV) dyssynchrony and pulmonary regurgitation (PR) in the clinical rTOF patient cohort. Exercise capacity is represented by peak VO_2, while QRS duration is taken as a surrogate of RV dyssynchrony. Predicted peak VO_2 values are presented without (left panel) as well as with (right panel) adjustment for covariates.

In both heat maps, especially in that unadjusted for covariates, the association of prolonged QRS duration with predicted peak VO_2 appeared to be stronger than that of PR severity. That is, moving from left to right on the heat map (increasing QRS duration) is on average associated with a lower peak VO_2; while moving from bottom to top on the heat map (increasing PR fraction) is not substantially associated with peak VO_2. Nonetheless, other factors likely impact exercise capacity, as the heat maps also show a wide distribution of for example a VO_2 of 40 ml/kg/min. This distribution is likely also impacted by the relatively low number of patients available for analysis.

Figure 2 shows the statistically predicted RVEF with QRS duration and PR with and without covariate adjustment.

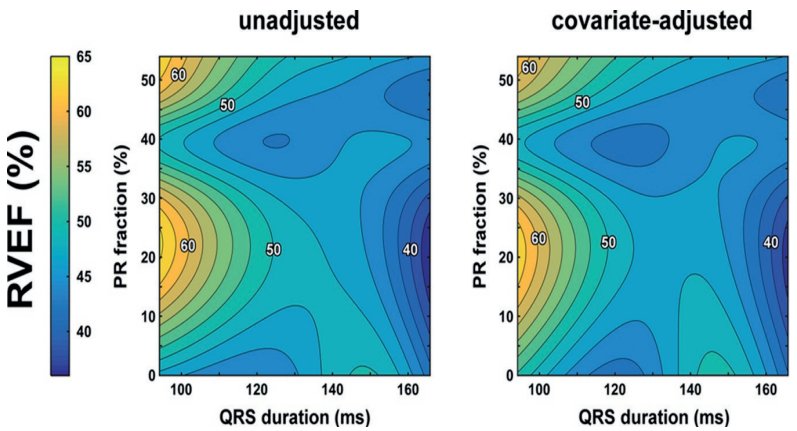

Figure 2

Predicted resting right ventricular (RV) systolic function as function of right ventricular (RV) dyssynchrony and pulmonary regurgitation (PR) in the clinical rTOF patient cohort. RV systolic function is represented by RV ejection fraction (RVEF), while QRS duration is taken as a surrogate of RV dyssynchrony. Predicted resting RVEF values are presented without (left panel) as well as with (right panel) adjustment for covariates.

The patterns with and without covariate adjustment were similar. As described above for peak VO_2, in both heat maps the association of progressively increasing QRS duration on RVEF is stronger than that of PR severity in both heat maps. That is, moving from left to right on the heat map (increasing QRS duration) is associated with a lower RVEF; while moving from bottom to top on the heat map (increasing PR fraction) does not substantially impact RVEF.

Pairwise Correlation Analyses

Figure 3 shows the pairwise correlations between QRS duration, PR fraction and the outcome variables of interest.

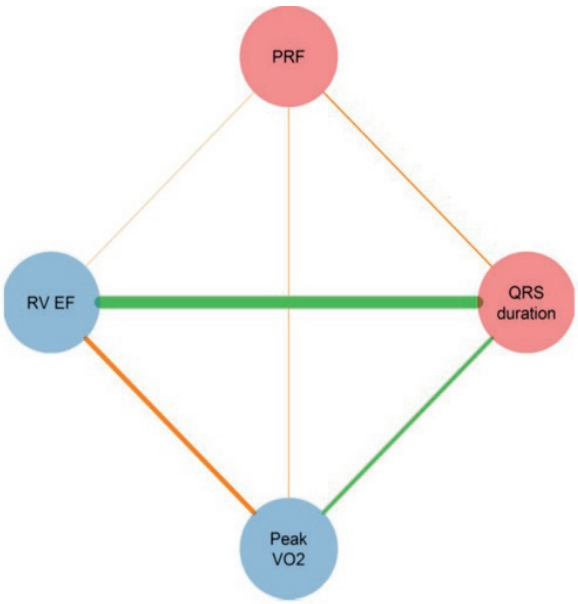

Independent Variable	Dependent Variable	Correlation [95% CI]	P-value
Pulmonary regurgitation fraction	QRS duration	0.079 [-0.149, 0.326]	0.52
	Peak VO2	0.036 [0.228, 0.299]	0.78
	RV EF	0.021 [-0.209, 0.230]	0.86
QRS duration	Peak VO2	-0.194 [-0.401, 0.040]	0.135
	RV EF	-0.559 [-0.714, -0.367]	<0.001
Peak VO2	RV EF	0.228 [-0.049, 0.448]	0.067

The table summarizes the pairwise correlation among all pairs. The 95% CI and p-value were based on Fisher's transformation

Figure 3

Univariable correlations of the outcome parameters in the clinical cohort. Circles and edges represented variables and pairwise Spearman's correlation, respectively. Red circles represented independent variables (i.e. pulmonary regurgitation and QRS duration); blue circles represented the outcome variables. Orange edges show a positive correlation between two variables; green edges show negative one. The thicker an edge is, the stronger the correlation is.

There was a moderate negative correlation between QRS duration and RVEF such that a longer QRS duration was associated with a lower RVEF (p= -0.56, p< 0.001). There was no significant pairwise correlation between QRS duration and peak VO_2 (p= -0.19, p= 0.135). PR fraction did not correlate at all with RVEF or peak VO_2 (p-values > 0.5).

Virtual patient simulation study

Effect on Cardiac Output as a Measure of Exercise Capacity

Figure 4 enables direct comparison of the simulated effects of PR versus RV dyssynchrony on exercise capacity in the virtual rTOF patient cohorts with normal and decreased myocardial contractility (panels A and B, respectively). The upper half of this figure illustrates how CVP increases with CO during exercise in four representative virtual patients, i.e. one without both PR and RV dyssynchrony (gray line), one with RV dyssynchrony alone (red line), one with PR alone (blue line), and one with both PR and RV dyssynchrony (purple line). The lower half of the figure presents continuous heat maps of exercise capacity ($CO_{max\text{-}exc}$) as function of RV dyssynchrony and PR, with the four representative virtual patients marked by circles.

In general, these data suggest that RV dyssynchrony exerts a stronger limiting effect on exercise capacity than PR, regardless of myocardial contractile function. RV dyssynchrony alone (red line) was associated with a leftward-shift of the central venous pressure-CO curve, with CVP reaching the exercise-limiting threshold value at 30% lower CO than the virtual patient without PR and RV dyssynchrony and normal contractility (panel A). Conversely, PR alone (blue line) had less effect on exercise capacity, with $CO_{max\text{-}exc}$ being only 5% lower that the virtual patient without PR and RV dyssynchrony and normal contractility. The limiting effect of PR and RV dyssynchrony on exercise capacity were additive, with $CO_{max\text{-}exc}$ being decreased by 36% in the virtual patient with both right heart pathologies, but normal contractility. RV contractile dysfunction had a profound exercise-limiting effect, as the 50% right heart decrease in contractility lowered $CO_{max\text{-}exc}$ by 25% in absence of PR and RV dyssynchrony (gray lines in panel A versus B). In the virtual patients with contractile dysfunction (panel B), the relative effects on exercise capacity of RV dyssynchrony alone (27% decrease of $CO_{max\text{-}exc}$), PR alone (12% decrease of $CO_{max\text{-}exc}$), and both pathologies combined (36% decrease of $CO_{max\text{-}exc}$) were similar to those observed in the virtual patients with normal contractility. Different CVP thresholds produced quantitatively similar relationships between exercise capacity, PR, and RBBB, demonstrating that the relationship is insensitive to the choice of threshold (**Supplemental Figures 4 and 5**).

Effect on RV global systolic function and remodeling

The effects of PR versus RV dyssynchrony on RV volumes and global systolic function (i.e. RVEF) is shown in **Figure 5**.

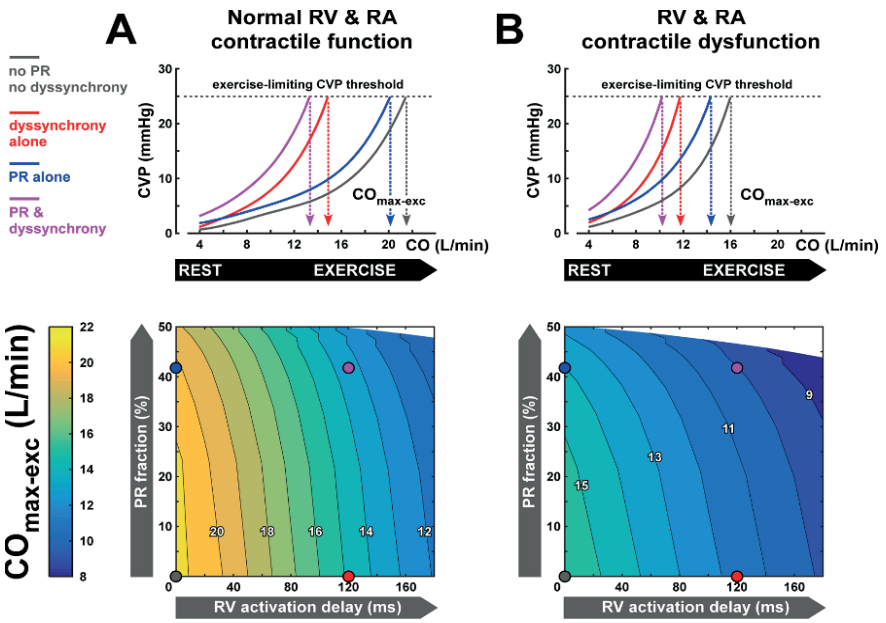

Figure 4

Exercise capacity as function of right ventricular (RV) dyssynchrony and pulmonary regurgitation (PR) in the virtual rTOF patient cohorts with normal (panel A) and decreased (panel B) contractile function of the RV and right atrial (RA) myocardium. The upper panels show how CVP rises with CO during exercise in four representative virtual rTOF patients. Those virtual patients are marked by circles in the heat plots showing continuous effects of RV dyssynchrony and PR on exercise capacity. Simulated exercise capacity is defined as the virtual patient's cardiac output ($CO_{max\text{-}exc}$) associated with the exercise-limiting central venous pressure (CVP) threshold. In general, RV dyssynchrony and contractile dysfunction are more limiting for exercise capacity than PR.

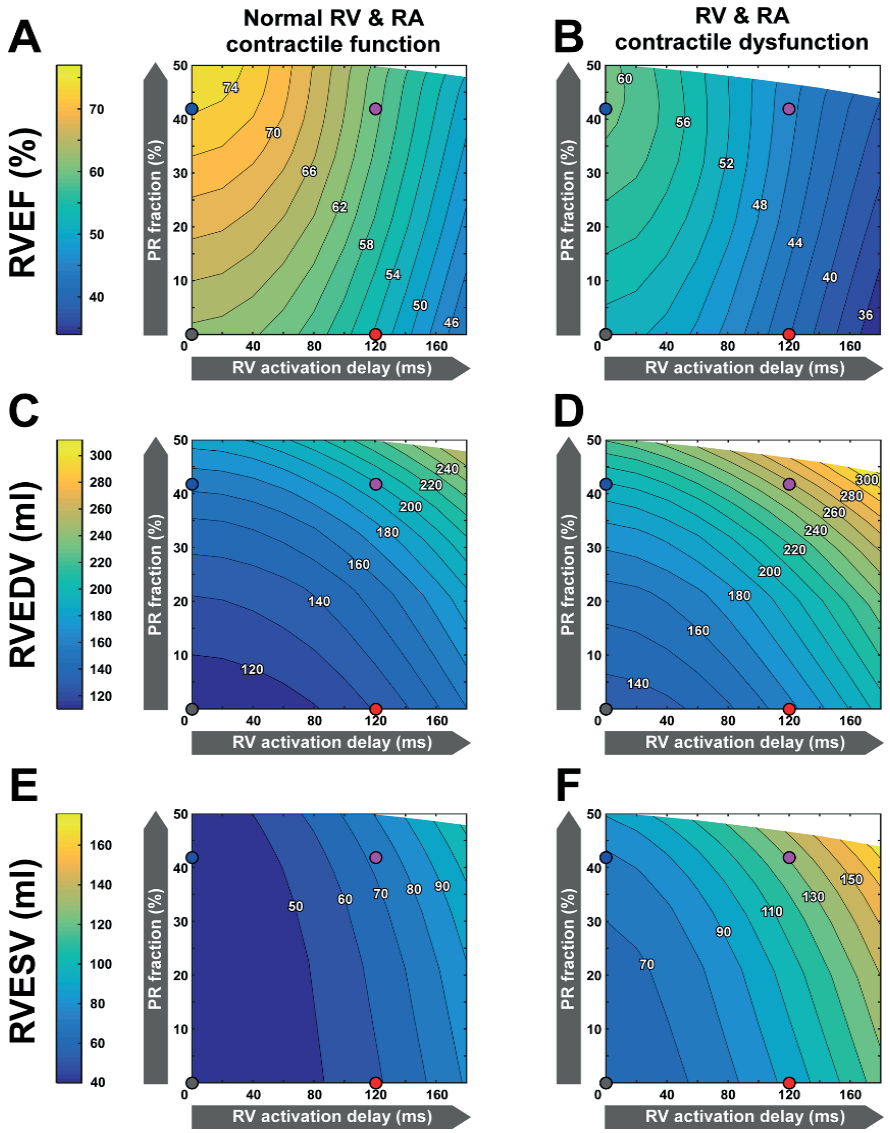

Figure 5

Resting right ventricular (RV) systolic function (Panels A,B) and end diastolic (Panels C,D) and end systolic (Panels E,F) volumes as a function of right ventricular (RV) dyssynchrony and pulmonary regurgitation (PR) in the virtual rTOF patient cohorts with normal (Panels A,C,E) and decreased (Panels B, D, F) contractile function of the RV and right atrial (RA) myocardium. Simulated RV systolic function is represented by the virtual patient's RV ejection fraction (RVEF).

RVEF decreased with increasing RV dyssynchrony, but increased with PR severity, regardless of myocardial contractile function (**Panels A,B)**. PR and RV delay cause a similar increase in RVEDV (**Panels C,D)**, while RVESV increased more strongly with RV activation delay than with PR (**Panels E,F)**.

RVEF decreased with increasing RV dyssynchrony, but increased with PR severity, regardless of myocardial contractile function (**Figure 5A,B)**. An RV activation delay of 120 ms alone reduced RVEF from 63% to 54% in the virtual patients with normal contractility and from 53% to 42% in those with RV and RA contractile dysfunction. In contrast, PR alone increased RVEF to supra-normal or normal values in the virtual patients with normal and decreased contractility, respectively (**Figure 5A,B)**.

PR and RV delay cause a similar increase in RVEDV (**Figure 5C,D)**, while RVESV increased more strongly with RV activation delay than with PR (**Figure 5E,F)**. The latter is most likely due to the fact that RV dyssynchrony impairs RV systolic function, while PR does so less.

Relation of hemodynamics with PR or RBBB to exercise level
Figure 6 illustrates how PR fraction and RV dp/dt max change with increasing exercise intensity in the same sample of four representative virtual patients.

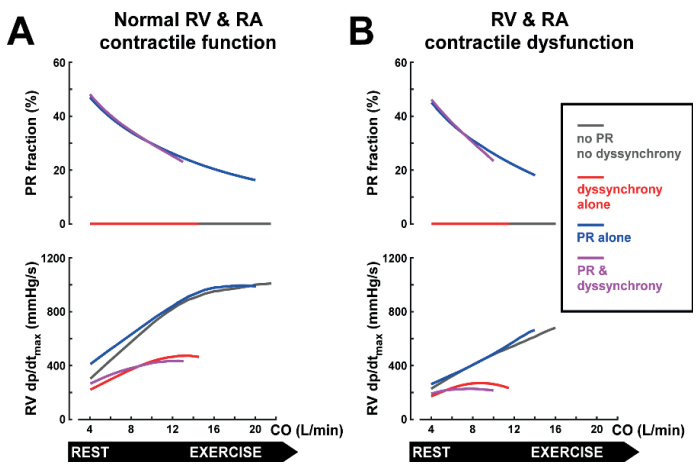

Figure 6

Valvular regurgitation (top) and global RV contractility (bottom) as functions of exercise level in virtual rTOF patients with normal (panel A) and decreased (panel B) contractile function of the RV and right atrial (RA) myocardium. The four representative virtual rTOF patients are the same as in Figures 4 and 5. Lines are plotted until $CO_{max\text{-}exc}$ is reached. The pathological consequences of PR, as quantified by PR fraction, decrease with exercise level (top), whereas RV dyssynchrony reduces RV global contractility and this effect becomes more pronounced as exercise level increases.

Panel A (top) shows that, with normal contractility, the PR fraction decreases as the exercise level increases in the virtual patient with PR only (blue line). The additional presence of RV dyssynchrony (purple line) does not significantly affect this reduction. **Panel A** (bottom) shows that the increase in RV dp/dt_{max} during exercise is similar in the PR-only case (blue line) and the no pathology case (grey line). **Panel B** shows that the results are qualitatively similar when RV contractile dysfunction is present, although the RV dp/dt_{max} is reduced and lower values of $CO_{max\text{-}exc}$ are reached. These simulation results strongly suggest that the relatively small compromising effect of PR on exercise capacity is due to a diminishing PR fraction as HR increases with exercise intensity, while systolic RV function is maintained. In contrast, the virtual patients with dyssynchrony (**Panel A**, red and purple lines) show reduced RV dp/dt_{max} at rest in comparison with the no pathology and PR-only simulations. Furthermore, increasing exercise level results in less increase in RV dp/dt_{max} in the virtual patients with dyssynchrony as compared to the ones without, causing the difference in systolic RV function between the two to increase with exercise intensity. This effect was further exacerbated by the presence of RV contractile dysfunction, which severely reduces the increase in RV dp/dt_{max} when dyssynchrony was present (**Panel B**). Therefore, in contrast to the effects of PR alone, the limiting effect of RV dyssynchrony on RV contractility is large at all levels of exercise and worsens as exercise level increases.

Discussion

In this unique exploratory study incorporating clinical observation and computer modeling, we compared the pathophysiological contributions and associations of RV volume-loading from PR versus those of RBBB-dyssynchrony on RV (dys)function and exercise capacity in patients after TOF repair. The integrative modelling approach was instrumental in relating cardiac function to exercise capacity in a complex population with co-existing and incompletely characterized pathologies (i.e. RBBB and PR). The mechanistic nature of this approach suggests that our results may have applicability beyond rTOF, and that the relation between bundle-branch block and exercise capacity in other patient populations merits further investigation.

The main result of this study is that dyssynchrony in patients with rTOF, reflected by the duration of the QRS complex, appears to be substantially more associated with reduced exercise capacity and RV systolic dysfunction compared to PR in these patients. Computer modelling leads us to hypothesize that the association of prolonged QRS in an RBBB pattern with reduced exercise capacity observed in the patients is a direct mechanistic consequence of RV dyssynchrony. Alleviation of RV volume loading by PVR is currently a central therapeutic

goal of rTOF management; yet, although RV dyssynchrony is common in this population, CRT is not commonly considered and is not a routine therapy. Thus, our results may have important implications for future investigations into the relative merits of CRT and/ or PVR for improving outcomes in rTOF patients.

Effect of PR on RV function and exercise capacity

Previous studies have shown reduced RV function in rTOF, which is most commonly attributed to volume-loading and RV remodeling from PR.[30] Consequently, pulmonary valve replacement has been recommended as the primary treatment for RV dilatation, remodeling and/or dysfunction in this setting.[7]

However, previous studies have shown varying results when investigating the relationship between reduction of PR through pulmonary valve replacement and RV function. Our group recently found in a pre-operative pediatric TOF-cohort that RV end-diastolic volumes correlated with RV myocardial strain and that those patients with larger pre-operative RV volumes had lower RV strain post-operatively.[31] We also found that following pulmonary valve replacement, an increase in global RV strain beyond pre-operative values may suggest positive RV remodeling and adaptation. These results differ from other studies where 6-months after surgical pulmonary valve replacement strain did not improve.[31,32] Eyskens found a moderate correlation between the PR% and RV strain.[33] In contrast, Frigiola found that RV strain was reduced to a similar degree regardless of the severity of PR.[30] When evaluating global function, most studies have not found an improvement in RVEF following pulmonary valve replacement[9], which is consistent with our current results that the severity of PR was not associated with RVEF. While some studies have found improvement in exercise capacity following pulmonary valve replacement, those patients had predominantly pressure-loaded RVs and only mild PR.[34] Our findings are consistent with empirical findings that pulmonary valve replacement does not lead to improved global RV function or exercise capacity in the chronically volume-loaded RV.[19] As RV dysfunction is a risk factor for death, our results are also consistent with studies where alleviation of PR by pulmonary valve replacement was not associated with a reduced rate of death or sustained VT.[9,35] In fact, one recent multi-center study, suggested that there may even be a detrimental effect for inappropriate pulmonary valve replacement in subjects not meeting consensus criteria for pulmonary valve replacement.[35] RV remodeling, beyond RV volume per se, likely determines RV function and response to PVR; and recent studies have suggested that RVESV, possibly representing systolic function, is associated with adverse outcomes.[35] The question remains whether a more aggressive approach and early prevention of PR, prior to the development of irreversible RV remodeling and dysfunction, ultimately improves exercise tolerance and outcomes.[7]

Effect of Dyssynchrony on RV Function and Exercise Capacity

Electrophysiological markers have long been identified as risk factors for adverse outcomes in rTOF. In landmark studies, Gatzoulis identified a prolonged QRS duration as a major risk factor for sudden death in rTOF patients, although the more recent INDICATOR cohort study failed to confirm this result.[2,11,36] While some studies have not found a link between RV dyssynchrony and clinical outcomes, they used relatively non-specific markers of mechanical dispersion.[28,37,38] Recently, QRS duration>160 msec, in addition to RV volumes, has been found to predict adverse outcomes.[35] We recently identified specific mechanical patterns of RBBB-induced mechanical dyssynchrony associated with RV inefficiency and dysfunction[12]; and others have subsequently shown that acutely resynchronizing the dyssynchronous sub-pulmonary RV can increase its function and mechanical efficiency.[13] Moreover, we previously found that increased mechanical dyssynchrony, which is a consequence of RBBB-induced QRS prolongation, correlates with decreased exercise capacity in rTOF[39], and that mechanical dyssynchrony worsens during exercise, possibly explaining reduced exercise capacity in this population through a negative feedback loop.[40] Similarly, a large magnetic resonance study recently found increased mechanical delay, in association with prolonged QRS duration, that were associated with lower exercise peak oxygen consumption and worse RV and LV global function.[41] Those results are concordant with the results of the current study, in which we found that a longer QRS duration is associated with decreased RV global function and worse exercise tolerance suggesting that narrowing the QRS via pacing may be an effective treatment to improve exercise capacity. Moreover, our modeling results suggest that, when RV contractility is reduced, critical thresholds that would correspond to severe exercise intolerance, are reached much more quickly when QRS duration is prolonged. This finding suggests that the effect of a prolonged QRS on exercise capacity is particularly important when RV contractility is decreased. These simulations also suggest that underlying myocardial failure (i.e. difference between panels A and B in Figure 4) may be an important confounder in the patient data. These simulations strongly suggest that inter-individual differences in myocardial contractile strength/failure is one of the confounders that we do not measure/quantify in the patients and may therefore cause some of the variability in the patient heat plots for peak VO_2.

The clinical translation of our findings may not be straightforward as at least one study found that RV pacing may not narrow the QRS complex, and consequently does not lead to hemodynamic improvement.[42] However, the same group found both in experimental models and in a small number of adults with rTOF, that cardiac resynchronization therapy via biventricular pacing improved RV and LV function by improving electro-mechanical dyssynchrony as manifested by a reduced QRS duration and electrical mapping-activation studies.[43] In these animals and in patients, PR was left untreated. These results are consistent with our findings that QRS duration, more than PR fraction is associated with RV

dysfunction and consequently exercise intolerance. Moreover, a recent study has demonstrated that acute RV free wall pacing with fusion with native activation can both shorten the QRS complex and improve hemodynamic parameters in children with rTOF, at least within 24h of surgery.[44]

Gatzoulis et al. found that QRS duration was related to RV dilatation and one study found a reduction in QRS duration following PVR.[36] This is in contrast to our current results, stemming from both modeling and observational data. It is also in contrast to our prior studies where QRS duration was not associated with RV size.[39] The differences in results may relate to the different ages of the cohorts and differences in era and surgical management as we do not exclude the idea that in very dilated and scarred ventricles, more common in older patients managed in previous years, distal conduction disease may progress and potentially contribute to progressive dyssynchrony.

Agreement between Computer Modeling and Empirical Data

Predictions afforded by modeling could not and cannot be entirely validated. Moreover, specifically in our study, the cross-sectional retrospective observational design cannot validate the modeling results. Nonetheless, as an exploratory study, the clinical observations and empirical statistical associations were consistent with the predicted effects from computer modeling. Furthermore, the computer model allowed us to hypothesize a mechanistic explanation for our clinical findings. The combined approach of using computer modeling alongside clinical observations has been contributory in LV pathologies[18,28], but is much less characterized for the RV.[17] Our group has combined computer modeling with clinical observations to understand mechanisms of RV dysfunction and to assist with clinical decision making in other diseases.[45,46] As a future perspective, the combination of modeling with clinical data such as imaging may be very useful to understand which patients with rTOF have mechanical dyssynchrony amenable to resynchronization and are, hence, most likely to benefit from electrical rather than, or possibly together with, hemodynamic therapy.[12,17]

Limitations

In the clinical cohort, the range of PR was relatively narrow and the number of patients with severe PR was limited. This limits our ability to corroborate the computer modeling of severe PR. Likewise, by design we excluded patients with moderate to severe RVOT obstruction. Therefore, our results may not apply to patients with mixed pressure and volume loading and this should be studied in the future. We could not evaluate the 'hard' clinical outcomes of sustained ventricular tachycardia or death as these are uncommon in children and cannot be modeled in a computer model based on hemodynamics. Therefore, reduced exercise tolerance, the most prominent clinical outcome parameter in childhood and adolescence, was chosen as the independent clinical outcome. It would be pertinent to study regional wall motion abnormalities by echocardiography as the mechanical correlate of RBBB dyssynchrony that determines RV dysfunction and exercise capacity.[12,40] This will be the topic of future investigations and in this initial study we chose to focus on QRS duration as it is the primary, and most quantifiable and clinically applicable parameter of RBBB dyssynchrony. In the future it would also be interesting to further model effects of regional RV dysfunction on clinical outcomes.

Conclusion

In conclusion, in both patient data and computer simulations, RV dyssynchrony, more than PR, appears to be associated with reduced exercise capacity and RV systolic dysfunction in patients after TOF repair. Computer modelling allowed us to hypothesize that this association between QRS prolongation and reduced exercise capacity may be causative. Based on previous literature and our current results, both PR and RV dyssynchrony appear to impact RV function and exercise tolerance; and the question in the individual patient is what is the balance between these factors. Our results suggest that in many cases RV resynchronization might be helpful after repair of tetralogy of Fallot. These results have important implications for future investigations and subsequently the management goals of this important population.

Table 3. Clinical characteristics of the patient cohort

Clinical characteristic	N	Median (Interquartile range)
Age (years)	81	14.48 (11.55 – 15.91)
Sex (number)	81	
Female		34 (42%)
Male		47 (58%)
Height (centimeters)	76	155.0 (143.4 – 166.0)
Weight (kilograms)	76	47.0 (34.8 – 66.0)
Body surface area (meter^2)	79	1.46 (1.19 – 1.69)
Heart rate at CMR (bpm)	80	76 (68 – 85)
QRS duration (milliseconds)	72	144 (123 – 152)
Pulmonary regurgitation fraction (%)	76	40 (29 – 48)
Years between repair and CMR	75	13.0 (10.6 – 15.1)

bpm = beats per minute, CMR=cardiac magnetic resonance

Table 4. Outcome variables summarized as medians and interquartile ranges

Clinical characteristics	N	Median (interquartile range)
Peak VO2 (ml/min/m^2)	65	35.0 (29.0 – 41.8)
Percent predicted peak VO2 (%)	65	79 (68 – 92)
RV ejection fraction (%)	80	48 (44 – 52)
Cardiac Index (l/min/m^2)	79	3.67 (3.28 – 4.22)

VO_2 = oxygen consumption; ml=milliliters; min=minute; m=meter
RV=right ventricle
l=liters

References

1. Orwat S, Diller GP, Kempny A, Radke R, Peters B, Kuhne T, Boethig D, Gutberlet M, Dubowy KO, Beerbaum P, Sarikouch S, Baumgartner H, German Competence Network for Congenital Heart Defects I. Myocardial deformation parameters predict outcome in patients with repaired tetralogy of Fallot. *Heart*. 2016; 102:209-215.
2. Valente AM, Gauvreau K, Assenza GE, Babu-Narayan SV, Schreier J, Gatzoulis MA, Groenink M, Inuzuka R, Kilner PJ, Koyak Z, Landzberg MJ, Mulder B, Powell AJ, Wald R, Geva T. Contemporary predictors of death and sustained ventricular tachycardia in patients with repaired tetralogy of Fallot enrolled in the INDICATOR cohort. *Heart*. 2014; 100:247-253.
3. Geva T. Repaired tetralogy of Fallot: the roles of cardiovascular magnetic resonance in evaluating pathophysiology and for pulmonary valve replacement decision support. *Journal of cardiovascular magnetic resonance: official journal of the society for Cardiovascular Magnetic Resonance*. 2011; 13:9.
4. Larios G, Friedberg MK. Imaging in repaired tetralogy of Fallot with a focus on recent advances in echocardiography. *Current opinion in cardiology*. 2017; 32:490-502.
5. Knauth AL, Gauvreau K, Powell AJ, Landzberg MJ, Walsh EP, Lock JE, del Nido PJ, Geva T. Ventricular size and function assessed by cardiac MRI predict major adverse clinical outcomes late after tetralogy of Fallot repair. *Heart*. 2008; 94:211-216.
6. Geva T, Sandweiss BM, Gauvreau K, Lock JE, Powell AJ. Factors associated with impaired clinical status in long-term survivors of tetralogy of Fallot repair evaluated by magnetic resonance imaging. *Journal of the American College of Cardiology*. 2004; 43:1068-1074.
7. Tretter JT, Friedberg MK, Wald RM, McElhinney DB. Defining and refining indications for transcatheter pulmonary valve replacement in patients with repaired tetralogy of Fallot: Contributions from anatomical and functional imaging. *International Journal of Cardiology*. 2016; 221:916-925.
8. Geva T, Gauvreau K, Powell AJ, Cecchin F, Rhodes J, Geva J and del Nido P. Randomized trial of pulmonary valve replacement with and without right ventricular remodeling surgery. *Circulation*. 2010; 122(11 Suppl):S201-S208.
9. Harrild DM, Berul CI, Cecchin F, Geva T, Gauvreau K, Pigula F, Walsh EP. Pulmonary valve replacement in tetralogy of Fallot: impact on survival and ventricular tachycardia. *Circulation*. 2009; 119:445-451.
10. Vogel M, Sponring J, Cullen S, Deanfield JE, Redington AN. Regional wall motion and abnormalities of electrical depolarization and repolarization in patients after surgical repair of tetralogy of Fallot. *Circulation*. 2001; 103:1669-1673.
11. Gatzoulis MA, Balaji S, Webber SA, Siu SC, Hokanson JS, Poile C, Rosenthal M, Nakazawa M, Moller JH, Gillette PC, Webb GD, Redington AN. Risk factors for arrhythmia and sudden cardiac death late after repair of tetralogy of Fallot: a multicentre study. *Lancet*. 2000; 356:975-981.
12. Hui W, Slorach C, Dragulescu A, Mertens L, Bijnens B, Friedberg MK. Mechanisms of right ventricular electromechanical dyssynchrony and mechanical inefficiency in children after repair of tetralogy of fallot. *Circulation Cardiovascular imaging*. 2014; 7:610-618.
13. Janousek J, Kovanda J, Lozek M, Tomek V, Vojtovic P, Gebauer R, Kubus P, Krejcir M, Lumens J, Delhaas T, Prinzen F. Pulmonary Right Ventricular Resynchronization in Congenital Heart Disease: Acute Improvement in Right Ventricular Mechanics and Contraction Efficiency.

Circulation Cardiovascular imaging. 2017; 10:e0006424.
14. Kubus P, Materna O, Tax P, Tomek V, Janousek J. Successful permanent resynchronization for failing right ventricle after repair of tetralogy of Fallot. *Circulation*. 2014; 130:e186-190.
15. Friedberg MK. Another Step in the Right Direction: Resynchronizing the Dyssynchronous Right Ventricle Improves Its Efficiency and Function. *Circulation Cardiovascular imaging*. 2017; 10:e006905.
16. Lumens J, Delhaas T. Cardiovascular modeling in pulmonary arterial hypertension: focus on mechanisms and treatment of right heart failure using the CircAdapt model. *The American journal of cardiology*. 2012; 110(6 Suppl):39S-48S.
17. Walmsley J, van Everdingen W, Cramer MJ, Prinzen FW, Delhaas T, Lumens J. Combining computer modelling and cardiac imaging to understand right ventricular pump function. *Cardiovascular research*. 2017; 113:1486-1498.
18. Lumens J, Ploux S, Strik M, Gorcsan J 3rd, Cochet H, Derval N, Strom M, Ramanathan C, Ritter P, Haissaguerre M, Jais P, Arts T, Delhaas T, Prinzen FW, Bordachar P. Comparative electromechanical and hemodynamic effects of left ventricular and biventricular pacing in dyssynchronous heart failure: electrical resynchronization versus left-right ventricular interaction. *Journal of the American College of Cardiology*. 2013; 62:2395-2403.
19. Coats L, Khambadkone S, Derrick G, Hughes M, Jones R, Mist B, Pellerin D, Marek J, Deanfield JE, Bonhoeffer P, Taylor AM. Physiological consequences of percutaneous pulmonary valve implantation: the different behaviour of volume- and pressure-overloaded ventricles. *European heart journal*. 2007; 28:1886-1893.
20. Washington RL, van Gundy JC, Cohen C, Sondheimer HM, Wolfe RR. Normal aerobic and anaerobic exercise data for North American school-age children. *The Journal of pediatrics*. 1988; 112:223-233.
21. Harrell F. Regression Modeling Strategies: with applications to linear models, logistic and orginal regression and survival analysis. 2nd ed. *Switzerland: Springer International Publishing*; 2015.
22. Lumens J, Delhaas T, Kirn B, Arts T. Three-wall segment (TriSeg) model describing mechanics and hemodynamics of ventricular interaction. *Annals of biomedical engineering*. 2009; 37:2234-2255.
23. Arts T, Delhaas T, Bovendeerd P, Verbeek X, Prinzen FW. Adaptation to mechanical load determines shape and properties of heart and circulation: the CircAdapt model. *American journal of physiology Heart and circulatory physiology*. 2005; 288:H1943-1954.
24. Walmsley J, Arts T, Derval N, Bordachar P, Cochet H, Ploux S, Prinzen FW, Delhaas T, Lumens J. Fast Simulation of Mechanical Heterogeneity in the Electrically Asynchronous Heart Using the MultiPatch Module. *PLoS computational biology*. 2015; 11:e1004284.
25. Arts T, Lumens J, Kroon W, Delhaas T. Control of whole heart geometry by intramyocardial mechano-feedback: a model study. *PLoS computational biology*. 2012; 8:e1002369.
26. Kutty S, Shang Q, Joseph N, Kowallick JT, Schuster A, Steinmetz M, Danford DA, Beerbaum P, Sarikouch S. Abnormal right atrial performance in repaired tetralogy of Fallot: A CMR feature tracking analysis. *International journal of cardiology*. 2017; 248:136-142.
27. Riesenkampff E, Al-Wakeel N, Kropf S, Stamm C, Alexi-Meskishvili V, Berger F, Kuehne T. Surgery impacts right atrial function in tetralogy of Fallot. *The Journal of thoracic and cardiovascular surgery*. 2014; 147:1306-1311.

28. Lumens J, Tayal B, Walmsley J, Delgado-Montero A, Huntjens PR, Schwartzman D, Althouse AD, Delhaas T, Prinzen FW, Gorcsan J 3rd. Differentiating Electromechanical From Non-Electrical Substrates of Mechanical Discoordination to Identify Responders to Cardiac Resynchronization Therapy. *Circulation Cardiovascular imaging*. 2015; 8:e003744.
29. Stickland MK, Welsh RC, Petersen SR, Tyberg JV, Anderson WD, Jones RL, Taylor DA, Bouffard M, Haykowsky MJ. Does fitness level modulate the cardiovascular hemodynamic response to exercise? *Journal of applied physiology*. 2006; 100:1895-1901.
30. Frigiola A, Redington AN, Cullen S, Vogel M. Pulmonary regurgitation is an important determinant of right ventricular contractile dysfunction in patients with surgically repaired tetralogy of Fallot. *Circulation*. 2004; 110(11 Suppl 1):II153-II157.
31. Yim D, Mertens L, Morgan CT, Friedberg MK, Grosse-Wortmann L, Dragulescu A. Impact of surgical pulmonary valve replacement on ventricular mechanics in children with repaired tetralogy of Fallot. *The international journal of cardiovascular imaging*. 2017; 33:711-720.
32. Knirsch W, Dodge-Khatami A, Kadner A, Kretschmar O, Steiner J, Bottler P, Kececioglu D, Harpes P, Valsangiacomo Buechel ER. Assessment of myocardial function in pediatric patients with operated tetralogy of Fallot: preliminary results with 2D strain echocardiography. *Pediatric cardiology*. 2008; 29:718-725.
33. Eyskens B, Brown SC, Claus P, Dymarkowski S, Gewillig M, Bogaert J and Mertens L. The influence of pulmonary regurgitation on regional right ventricular function in children after surgical repair of tetralogy of Fallot. *European journal of echocardiography : the journal of the Working Group on Echocardiography of the European Society of Cardiology*. 2010; 11:341-345.
34. Batra AS, McElhinney DB, Wang W, Zakheim R, Garofano RP, Daniels C, Yung D, Cooper DM, Rhodes J. Cardiopulmonary exercise function among patients undergoing transcatheter pulmonary valve implantation in the US Melody valve investigational trial. *American heart journal*. 2012; 163:280-287.
35. Bokma JP, Geva T, Sleeper LA, Babu Narayan SV, Wald R, Hickey K, Jansen K, Wassall R, Lu M, Gatzoulis MA, Mulder BJ, Valente AM. A propensity score-adjusted analysis of clinical outcomes after pulmonary valve replacement in tetralogy of Fallot. *Heart*. 2018; 104:738-744.
36. Gatzoulis MA, Till JA, Somerville J, Redington AN. Mechanoelectrical interaction in tetralogy of Fallot. QRS prolongation relates to right ventricular size and predicts malignant ventricular arrhythmias and sudden death. *Circulation*. 1995; 92:231-237.
37. Moon TJ, Choueiter N, Geva T, Valente AM, Gauvreau K, Harrild DM. Relation of biventricular strain and dyssynchrony in repaired tetralogy of fallot measured by cardiac magnetic resonance to death and sustained ventricular tachycardia. *The American journal of cardiology*. 2015; 115:676-680.
38. Jing L, Wehner GJ, Suever JD, Charnigo RJ, Alhadad S, Stearns E, Mojsejenko D, Haggerty CM, Hickey K, Valente AM, Geva T, Powell AJ, Fornwalt BK. Left and right ventricular dyssynchrony and strains from cardiovascular magnetic resonance feature tracking do not predict deterioration of ventricular function in patients with repaired tetralogy of Fallot. *Journal of cardiovascular magnetic resonance: official journal of the Society for Cardiovascular Magnetic Resonance*. 2016; 18:49.
39. Friedberg MK, Fernandes FP, Roche SL, Slorach C, Grosse-Wortmann L, Manlhiot C, Fackoury C, McCrindle BW, Mertens L, Kantor PF. Relation of right ventricular mechanics to exercise tolerance in children after tetralogy of Fallot repair. *American heart journal*. 2013;

165:551-557.
40. Roche SL, Grosse-Wortmann L, Redington AN, Slorach C, Smith G, Kantor PF, Friedberg MK. Exercise induces biventricular mechanical dyssynchrony in children with repaired tetralogy of Fallot. *Heart*. 2010; 96:2010-2015.
41. Kalaitzidis P, Orwat S, Kempny A, Robert R, Peters B, Sarikouch S, Beerbaum P, Baumgartner H, Diller GP, Competence Network for Congenital Heart Defects D. Biventricular dyssynchrony on cardiac magnetic resonance imaging and its correlation with myocardial deformation, ventricular function and objective exercise capacity in patients with repaired tetralogy of Fallot. *International journal of cardiology*. 2018; 264:53-57.
42. Bordachar P, Iriart X, Chabaneix J, Sacher F, Lafitte S, Jais P, Haissaguerre M, Clementy J, Dos Santos P, Thambo JB. Presence of ventricular dyssynchrony and haemodynamic impact of right ventricular pacing in adults with repaired Tetralogy of Fallot and right bundle branch block. *Europace: European pacing, arrhythmias, and cardiac electrophysiology: journal of the working groups on cardiac pacing, arrhythmias, and cardiac cellular electrophysiology of the European Society of Cardiology*. 2008; 10:967-971.
43. Thambo JB, Dos Santos P, De Guillebon M, Roubertie F, Labrousse L, Sacher F, Iriart X, Lafitte S, Ploux S, Jais P, Roques X, Haissaguerre M, Ritter P, Clementy J, Narayan SM, Bordachar P. Biventricular stimulation improves right and left ventricular function after tetralogy of Fallot repair: acute animal and clinical studies. *Heart rhythm*. 2010; 7:344-350.
44. Vojtovic P, Kucera F, Kubus P, Gebauer R, Matejka T, Tlaskal T, Lozek M, Kovanda J, Janousek J. Acute right ventricular resynchronization improves haemodynamics in children after surgical repair of tetralogy of Fallot. *Europace: European pacing, arrhythmias, and cardiac electrophysiology: journal of the working groups on cardiac pacing, arrhythmias, and cardiac cellular electrophysiology of the European Society of Cardiology*. 2018; 20:323-328.
45. Palau-Caballero G, Walmsley J, Van Empel V, Lumens J, Delhaas T. Why septal motion is a marker of right ventricular failure in pulmonary arterial hypertension: mechanistic analysis using a computer model. *American journal of physiology Heart and circulatory physiology*. 2017; 312:H691-H700.
46. van Everdingen WM, Walmsley J, Cramer MJ, van Hagen I, De Boeck BWL, Meine M, Delhaas T, Doevendans PA, Prinzen FW, Lumens J, Leenders GE. Echocardiographic Prediction of Cardiac Resynchronization Therapy Response Requires Analysis of Both Mechanical Dyssynchrony and Right Ventricular Function: A Combined Analysis of Patient Data and Computer Simulations. *Journal of the American Society of Echocardiography: official publication of the American Society of Echocardiography*. 2017; 30:1012-1020 e2.

Supplementary figures

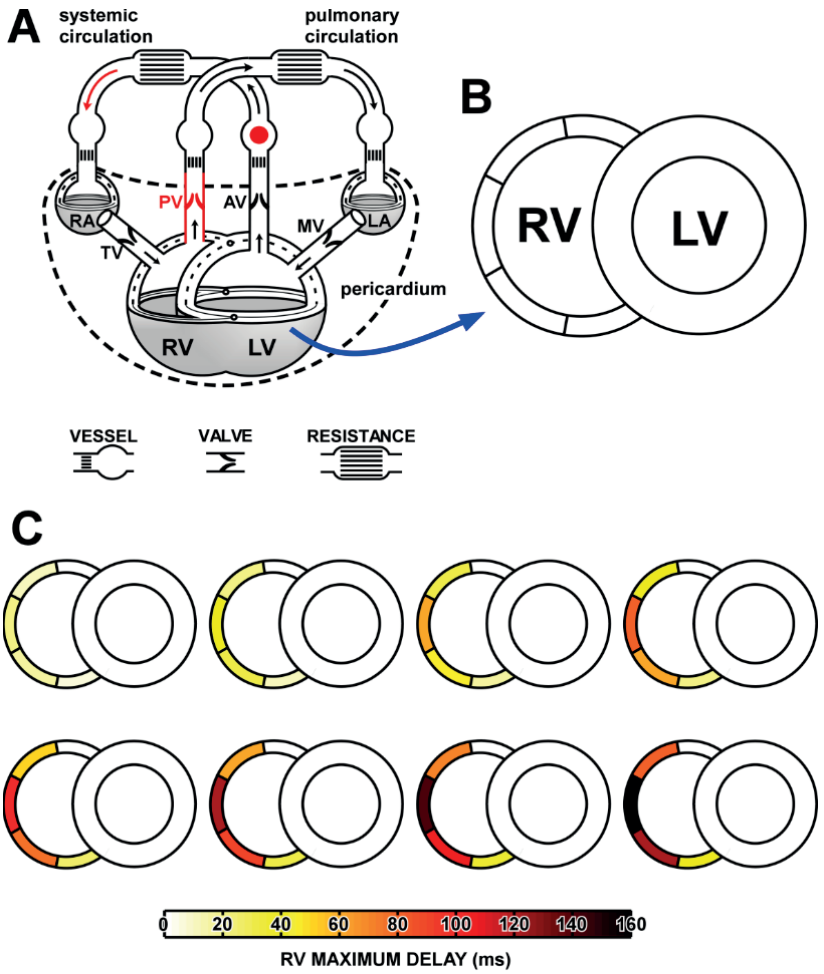

Supplementary Figure 1

Panel A shows a schematic diagram of the CircAdapt model, modified from Lumens et al. Ann Biomed Eng. 2009;37(11):2234-55, with permission. Red has been used to highlight key parts of the model for this study referred to in the supplemental methods, being the pulmonary valve, pressure control in the aorta, and systemic venous return. Panel B shows a schematic of the ventricles in the synchronous case, with location in the model indicated by the blue arrow. Note that the LV is always synchronously activated in this study. Panel C shows the remaining eight activation patterns, with progressively increasing delay within the RV free wall. The colour bar indicates the magnitude of the delay in each segment. RV segments are activated at 0%, 25%, 50%, 75% and 100% of the latest RV activation time in each case.

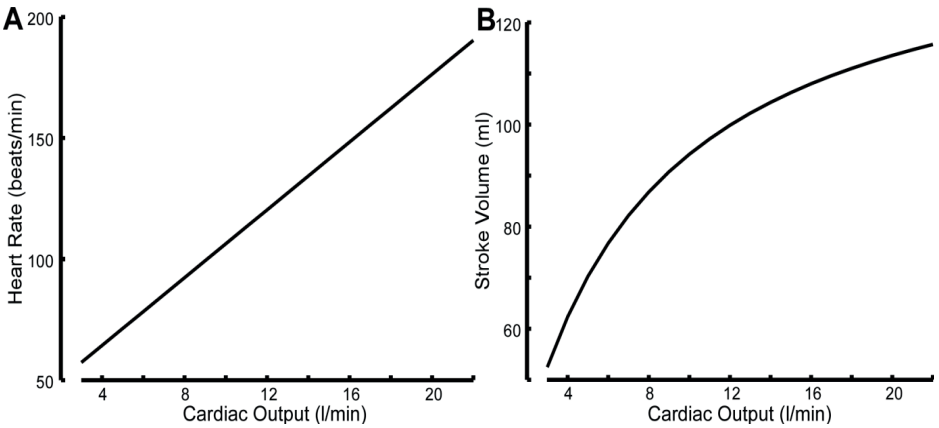

Supplementary Figure 2

Heart rate – LV cardiac output relationship used in this study (Panel A). The corresponding stroke volume – cardiac output relationship is shown in Panel B. This relationship is based on linear interpolation of data recorded in healthy adults from WF Boron and EL Boulpaep, Medical Physiology, Elsevier Science 2003.

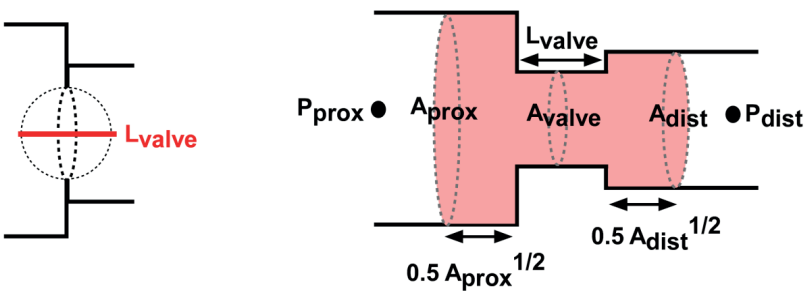

Supplementary Figure 3

Definitions used in the text for the simulation of valvular function. The pink area indicates the total volume of blood considered in the inertance of the valve.

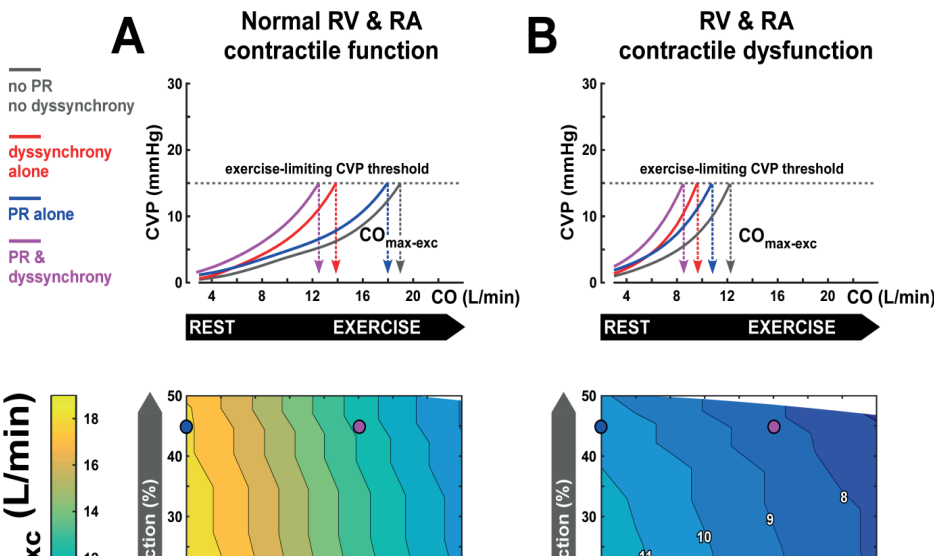

Supplementary Figure 4

Exercise capacity (using 15 mmHg as the pressure threshold) as function of right ventricular (RV) dyssynchrony and pulmonary regurgitation (PR) in the virtual rTOF patient cohorts with normal (panel A) and decreased (panel B) contractile function of the RV and right atrial (RA) myocardium. The upper panels show how CVP rises with CO during exercise in four representative virtual rTOF patients. Those virtual patients are marked by circles in the heat plots showing continuous effects of RV dyssynchrony and PR on exercise capacity. Simulated exercise capacity is defined as the virtual patient's cardiac output ($CO_{max\text{-}exc}$) associated with the exercise-limiting central venous pressure (CVP) threshold. In general, RV dyssynchrony and contractile dysfunction are more limiting for exercise capacity than PR.

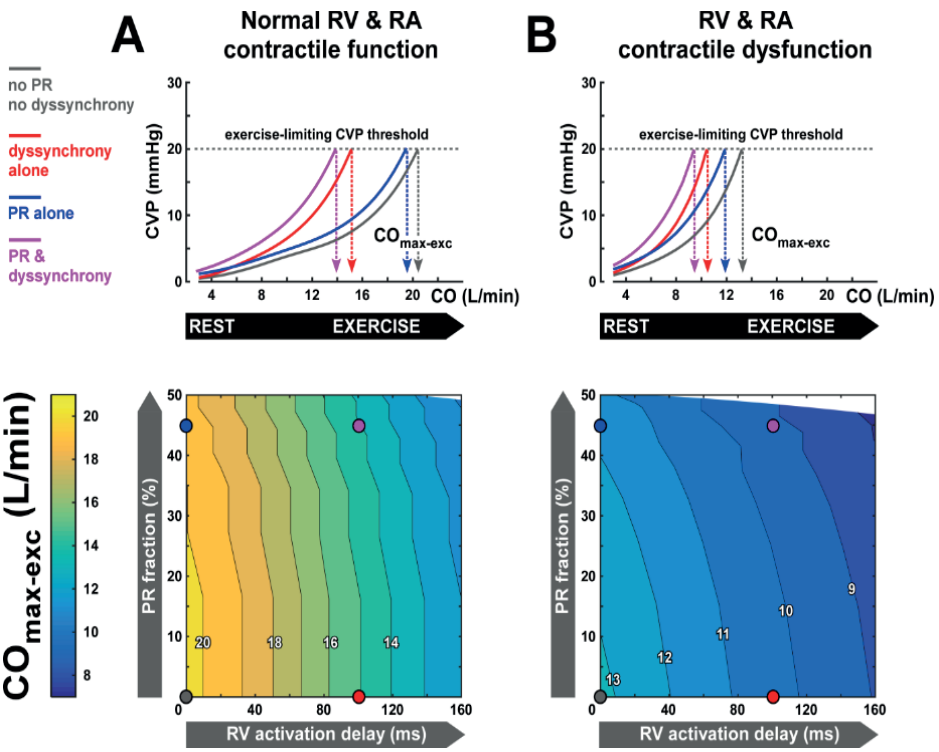

Supplementary figure 5

Exercise capacity (using 20 mmHg as the pressure threshold) as function of right ventricular (RV) dyssynchrony and pulmonary regurgitation (PR) in the virtual rTOF patient cohorts with normal (panel A) and decreased (panel B) contractile function of the RV and right atrial (RA) myocardium. The upper panels show how CVP rises with CO during exercise in four representative virtual rTOF patients. Those virtual patients are marked by circles in the heat plots showing continuous effects of RV dyssynchrony and PR on exercise capacity. Simulated exercise capacity is defined as the virtual patient's cardiac output ($CO_{max-exc}$) associated with the exercise-limiting central venous pressure (CVP) threshold. In general, RV dyssynchrony and contractile dysfunction are more limiting for exercise capacity than PR.

Chapter 10

Summary and Clinical Implications

A testament to the progress made in pediatric cardiology and cardiac surgery is the extraordinary improvement in survival in patients with congenital heart disease (CHD) with a nearly 30% reduction in mortality from the 1980s to the early 2000s. This is mostly attributed to improved outcomes in infants with severe forms of CHD such as right sided obstructive lesions and single ventricles and a resulting dramatic increase in adults living with repaired CHD, now representing 1.4 million individuals in the U.S. alone. These improved outcomes have led to an increasing number of infants, children and adults with heart failure. In particular, RV failure is an important determinant of clinical status and outcomes in children and adults with various types of CHD. As discussed earlier in this thesis, the RV is at risk for failure from a variety of causes including reduced contractile function (e.g. arrhythmogenic right ventricular cardiomyopathy and Ebstein anomaly), increased pressure-loading (e.g. RV-pulmonary artery (PA) conduit stenosis after repair of truncus arteriosus or pulmonary atresia and pulmonary hypertension), increased volume-loading (e.g. pulmonary regurgitation (PR) after repair of tetralogy of Fallot (rTOF)), electro-mechanical dyssynchrony (i.e. incoordinate contraction between different segments of the ventricle) induced by right bundle branch block (e.g. rTOF), increased myocardial fibrosis (e.g. rTOF), abnormal coronary perfusion (e.g. pulmonary atresia with intact ventricular septum, pulmonary hypertension), restricted filling capacity (e.g. Fontan circulation), inefficient energy transfer between the ventricle and the vasculature (e.g. pulmonary hypertension , Fontan circulation) and adverse interactions between the RV and LV (e.g pulmonary hypertension, hypoplastic left heart syndrome (HLHS)). In many instances the co-existence of multiple factors may lead to RV failure, such as in the systemic RV with tricuspid regurgitation.

In **Chapter 3**, I used the known differences in clinical course and outcomes between pediatric pulmonary hypertension versus RV pressure loading to understand differences in the RV response to these two pressure-loading conditions. Using echocardiography, we found that children with PAH demonstrate adverse global and regional RV remodeling and mechanics compared to those with PS. The mechanisms we observed of RV systolic dysfunction in PAH included decreased longitudinal strain (deformation), usually the dominant contraction vector of the normal RV, decreased or absent transverse shortening, which reflects a loss of the bellows action of the normal RV and post-systolic shortening, reflecting contractile inefficiency and increased segmental interactions. As detailed below, some of these markers, such as inefficient transverse shortening and post-systolic shortening, are not routinely used in current clinical practice, but may be useful to identify children at risk of RV failure and hence at risk of morbidity and mortality. Echocardiographic markers of RV dysfunction have been found by our group and others in other high-risk situations such as hypoplastic left heart syndrome (HLHS).
In a recent study we identified RV remodeling and decreased RV fractional

area of change (a surrogate of ejection fraction) to be powerful predictors of outcome.[1] Additionally, a more direct assessment of RV myocardial function via echocardiography strain imaging may be beneficial in assessment of HLHS. In a small study of 35 infants with HLHS during the first 6 months of life, RV strain analysis was found to identify at-risk HLHS infants with interstage strain values being worse in infants with HLHS who had a poor cardiac outcome as defined by cardiac death, heart transplantation, or persistent moderate or greater RV dysfunction.[2] Similarly, when assessed before the bidirectional cavopulmonary anastomosis, children with good RV function by echocardiographic measures such as RV fractional area change (a surrogate for ejection fraction) and RV strain had a low likelihood of death or heart transplantation.[3] In HLHS patients with normal RV fractional area change values, reduced strain may improve prediction of clinical outcomes.[3] Similarly, we found that longitudinal assessment of strain in children with PAH predicts clinical outcomes.[4]

The contractile dysfunction in PAH we observed by echocardiography may stem from the unique molecular responses of the stressed RV myocardium. As detailed in Chapter 2, investigators have highlighted differences in the mechanisms of right vs. left ventricular failure.[5] Indeed, data from animal models of RV stress mimicking residual lesions after repair of tetralogy of Fallot have shown extracellular matrix and cytoskeletal remodeling, upregulation of genes regulating reactive oxygen species production and downregulation of antioxidant protection, angiogenesis, energy production and mitochondrial function more so than that seen in the LV under stress.[6] Similarly, deranged mitochondrial function, energetics and microcirculation leading to myocardial dysfunction have been described in the pulmonary hypertensive RV.[7] As some of the molecular pathways, such as those regulating angiogenesis, metabolism, and mitochondrial dynamics, are similarly deranged in the RV and pulmonary vasculature, there is the possibility of therapies that treat the RV and pulmonary circulation.[8] Interestingly, RV volume and pressure overload may demonstrate similar changes; however, pressure overload shows a more severe phenotype at the molecular level.[6]

The differences in the molecular response of the RV and LV could impact the effectiveness of the drugs used to treat heart failure. In **Chapter 7,** we described in preclinical models of RV pressure-loading, that treatment with losartan led to an improvement in fibrosis and cardiac hypertrophy.[9] However, the REDEFINE trial in adults with repaired tetralogy of Fallot suggested that renin-angiotensin-aldosterone inhibition using losartan is not beneficial for patients with mild RV failure.[10] However, the findings from the REDEFINE study may suggest that once RV fibrosis has developed, as the molecular correlate of RV dysfunction, that it cannot be reversed with angiotensin receptor blockers, but that institution of angiotensin receptor blockers prior to the development of fibrosis might be beneficial. It is also possible that longer-term administration of angiotensin

receptor blockers might be required to limit the slow progression of RV fibrosis in these patients.

Despite the differences in the RV and LV response to stress, as described in **Chapter 2**, and in **Chapters 3-5** our studies demonstrate that RV remodeling leads not only to RV, but also LV dysfunction. We have further shown that RV dysfunction in association with volume or pressure loading is associated abnormal LV in other conditions such as Ebstein anomaly and repaired tetralogy of Fallot.[11,12] These results show that adverse RV-LV interactions are important in diverse conditions and impact clinical outcomes. RV dysfunction in LVF more than doubles mortality through direct interaction or secondary to PV remodeling[13]. In RVF, there is a linear relation between RV and LV dysfunction; and sudden death is higher in patients with co-existing LV dysfunction.[14] An abnormal LV also affects the stressed RV. We have recently shown that LV size and septal thickness are associated with worse outcomes in children with HLHS.[1] This data provides additional risk factors for adverse outcomes when counseling parents. From the data presented in these chapters, it is apparent that events in one ventricle profoundly affect the other; and that LV and RV function and failure cannot be regarded separately.

In **Chapters 5 and 6**, we showed that temporal RV-LV interactions combine with geometrical RV-LV interactions to affect biventricular function and that these can be imaged effectively with echocardiography-providing a clinically relevant bedside tool to image RV-LV interactions. Imaging of these geometrical interactions do not account for the disparate timing of RV and LV events that substantially impact ventricular-ventricular interactions in pulmonary hypertension. Given its high temporal resolution and the ability of M-mode to simultaneously image the RV, interventricular septum and LV, it is useful to study event timing using M-mode and Doppler echocardiography. From the PSAX view, at the level of the mitral leaflet tips or LV papillary muscles, an M-mode cursor can be placed through the RV free-wall, interventricular septum and LV posterior-wall. With raw DICOM images, some software allows post-processing placement of an anatomical M-mode on the 2-D image positioned to afford best visualization of RV, septal and LV thickening and excursion; but provides lower frame-rates than regular M-mode, an important disadvantage for event-timing. On the M-mode trace, the timing of semi-lunar and atrio-ventricular valve opening and closure can be superimposed directly or as a schematic representation as timed from Doppler images obtained at similar heart rates sampled in the RV and LV outflows and inflows.

In **Chapter 5 and 6** we showed how RV pressure-loading leads to RV dysfunction characterized by prolonged isovolumic contraction, contraction and isovolumic relaxation. This prolongs RV systole and shortens RV diastole. These components may be imaged by flow or tissue Doppler. Normally, RV isovolumic

contraction and relaxation are very short. In pulmonary hypertension, as the (failing) RV myocardium struggles to mount adequate force in early systole, isovolumic contraction prolongs. This can be measured from the onset of the ECG QRS complex to onset of pulmonary ejection from a Doppler sample in the RV outflow tract or pulmonary artery. Next, RV contraction is blunted and prolonged as the RV needs more time to maintain output through the high resistance pulmonary vasculature. This can be observed as reduced longitudinal strain, with myocardial shortening (contraction) that extends into early LV diastole or delayed RV free-wall peak excursion on M-mode. Despite prolonged RV contraction, paradoxically, pulmonary ejection time is shortened with short acceleration time, measured as onset to peak pulmonary ejection from Doppler flow, and a short ejection-time with low stroke-volume given the increased distal resistance. Thus, despite prolonged RV contraction, which pushes the septum leftward for a long portion of the cardiac cycle, ejection is short. The consequences are inefficient RV contraction and impaired LV filling. From an imaging standpoint, inefficient RV contraction and adverse RV-LV interaction, can be visualized as prolonged TR duration (corresponding to prolonged RV contraction), short pulmonary ejection and low pulmonary velocity time integral (corresponding to low stroke-volume) and impaired LV filling with short mitral filling and often reversed E/A ratio typical of delayed relaxation. As described in **Chapters 2, 4 and 5**, due to prolonged RV contraction, RV systole extends into early LV diastole. Peak RV shortening by 2-D speckle strain imaging occurs at time of mitral valve opening. These adverse interactions worsen LV filling. Because the RV continues to contract while the LV is relaxing, a sharp, early-diastolic leftward septal deflection can be seen on M-mode due to continuing high RV-pressures, while at the same time, LV pressures are falling in early diastole. Consequently, LV eccentricity index is maximal at this time. Thus, in pulmonary hypertension substantially impaired early LV filling can be imaged by conventional measures of LV diastolic filling and by LV diastolic strain-rate.

In **Chapter 7** I demonstrated how the adverse mechanics and RV-LV interactions RV pressure-loading described in **Chapters 2-5** translate into cardiomyocyte hypertrophy and myocardial fibrosis. As fibrosis is thought to worsen ventricular function in diverse cardiac conditions and constitutes a common final injury pathway in diverse organs (e.g. kidney, liver, skin, lung etc), there is an intense interest in fibrosis and anti-fibrotic therapy.

Tissue repair is fast because it mainly uses the extra-cellular matrix (ECM) to fix the damage as opposed to tissue or organ regeneration that restores the appropriate cell and ECM components.[15] Without controlled scarring, the myocardium would rupture after severe infarction or chronic overload. Similarly, in other organs, beneficial fibrotic tissue reduces pressure on chronically overloaded kidney glomeruli to maintain proper filter function and in the absence of stabilizing scar tissue, lung alveoli would tear under continuous breathing expansion. When

discussing myocardial injury, it is important to consider that "detrimental" fibrosis encompasses the same fundamental mechanisms and pathways that are involved in normal healing.[16] Both the normal healing and ultimately injurious fibrosis process is a highly regulated sequence of overlapping phases comprising hemostasis, inflammation, proliferation, and remodeling/maturation.[17] The ECM performs central functions at all stages, both as a reinforcing material and cell signaling instructor.[18] Thus, ECM remodeling and fibrosis are highly complex processes and therapeutically targeting a single component, of this complex system; which itself is just one component of the myocardium may be inadequate.

The main objective of losartan administration in my study (**Chapter 7**) was to demonstrate the importance of TGF-B1 signaling in mediating biventricular fibrosis in response to RV pressure loading. The results nonetheless demonstrate the potential to treat RV and LV myocardial fibrosis by targeting the TGFβ1 molecular axis. Likewise **Chapter 8** describes mechano-transduction pathways through β1integrin signaling that activate TGFβ1 signaling and may be a therapeutic target. In parallel, we also describe increased elastin deposition that may alleviate adverse RV-LV interactions through increased compliance and hence a new therapeutic avenue. Nonetheless, more specific targets are still needed.

In **Chapter 9**, 'The stressed right ventricle in repaired tetralogy of Fallot: Dyssynchronous activation induces regional disparities in stress and function' we explore additional factors that stress the RV, other than pressure or volume loading, specifically RV electro-mechanical dyssynchrony that stems from right bundle branch block. In adult left heart failure, a substantial portion of patients have la broad QRS that stems from left bundle branch block. This conduction delay to electrical activation of the LV free wall causes a complex pathophysiology of disparate contraction-relaxation between the late activated LV free wall and early activated septum which leads to disparate wall stress, regional activation of myocardial injury pathways and LV dysfunction. Consequently, a large number of such patients have greatly benefited from pacing therapy to 'overcome' the electrical conduction delay and mechanically resynchronize LV contraction with translation of these mechanical benefits to improved morbidity and mortality.

Although over 90% of rTOF patients have a broad QRS duration, mostly from RBBB, and while a wide QRS is thought to be a risk factor for increased morbidity and mortality in rTOF, electromechanical dyssynchrony has, to date, not been a substantial therapeutic target and overwhelming emphasis has been placed on the timing of pulmonary valve replacement to treat pulmonary regurgitation and RV volume loading. However, there are few conclusive data to show that PVR has reduced mortality or risk factors associated with mortality such as ventricular arrhythmia. Although, ventricular dilatation and remodeling, may be associated

with QRS widening, our study demonstrates that a broad QRS is as, or perhaps even more associated with RV dysfunction and exercise intolerance, than PR. This suggests that RBBB, as much as or more than PR should be a therapeutic target. Our results have strong implications for management of rTOF and at a minimum provide strong support for a clinical trial to evaluate the usefulness of RV cardiac resynchronization therapy in rTOF with RV dysfunction and heart failure symptoms.

Chapter 9, over and above the content findings of electromechanical dyssynchrony and its contribution to RV dysfunction in rTOF, presents a novel methodological approach that can be applied to a wide array of clinical problems. Consequently, this work is highly novel both in its implications for rTOF specifically and in its innovative approach using advanced statistical analysis on actual patient data combined with computer modeling to generate hypotheses, demonstrate pathophysiological mechanisms and potentially beneficial therapies across a spectrum of severity. The next natural step would be to apply this approach to specific patients contributing to a personalized medicine approach.

In summary, this thesis studies the pressure-loaded and dyssynchronous RV, both associated with regional inhomogeneities in RV wall stress and function that are associated with global RV dysfunction and adverse clinical status and outcomes. Moreover, the results of the studies presented in this thesis demonstrate that the pressure loaded RV impacts the LV, not only by septal shift and adverse hemodynamics, but also by temporal discordance of interventricular events. The biventricular geometrical aberrations, increased wall stress and dysfunction negatively impact the RV and LV, from regional tissue injury to global hemodynamics. Thus, our studies demonstrate a wide spectrum of associated abnormalities from adverse hemodynamics to myocardial pro-fibrotic signaling. These studies also translate the experimental and observational patient data to the bedside by providing non-invasive bedside tools, through echocardiography, to diagnose RV dysfunction and adverse RV-LV interactions, as well as suggesting novel therapeutic avenues to address them.

References (Clinical summary)

1. Son JS, James A, Fan CS, Mertens L, McCrindle BW, Manlhiot C, Friedberg MK. Prognostic value of serial echocardiography in hypoplastic left heart syndrome. Circ Cardiovasc Imaging. 2018; 11(7): e006983
2. Colquitt JL, Loar RW, Morris SA et al. Serial Strain Analysis Identifies Hypoplastic Left Heart Syndrome Infants at Risk for Cardiac Morbidity and Mortality: A Pilot Study. J Am Soc Echocardiogr. 2019; pii:S0894-7317(19)30006-30009 [Epub ahead of print]
3. Lin LQ, Conway J, Alvarez S, et al. Reduced Right Ventricular Fractional Area Change, Strain, and Strain Rate before Bidirectional Cavopulmonary Anastomosis is Associated with Medium-Term Mortality for Children with Hypoplastic Left Heart Syndrome. J Am Soc Echocardiogr. 2018; 31(7):831-842.
4. Okumura K, Humpl T, Dragulescu A, Mertens L, Friedberg MK. Longitudinal assessment of right ventricular myocardial strain in relation to transplant-free survival in children with idiopathic pulmonary hypertension. J Am Soc Echocardiogr. 2014; 27(12): 1344-1351
5. Friedberg MK, Redington AN. Right versus left ventricular failure: differences, similarities, and interactions. Circulation. 2014; 129(9):1033-1044
6. Reddy S, Bernstein D. Molecular mechanisms of right ventricular failure. Circulation. 2015; 132(18): 1734-1742
7. Ryan JJ, Archer SL. The right ventricle in pulmonary arterial hypertension: disorders of metabolism, angiogenesis and adrenergic signaling in right ventricular failure. Circ Res. 2014; 115(1):176-188
8. Ryan JJ, Huston J, Kutty S et al. Right ventricular adaptation and failure in pulmonary arterial hypertension. Can J Cardiol. 2015; 31(4):391-406
9. Friedberg MK, Cho MY, Li J et al. Adverse biventricular remodeling in isolated right ventricular hypertension is mediated by increased transforming growth factor-β1 signaling and is angiotensin receptor blockade. Am J Respir Cell Mol Biol. 2013; 49(6):1019-1028
10. Bokma JP, Winter MM, van Dijk AP et al. Effect of Losartan on right ventricular dysfunction: results from the double-blind, randomized REDEFINE trial (right ventricular dysfunction in tetralogy of Fallot: inhibition of the renin-angiotensin-aldosterone system) in adults with repaired tetralogy of Fallot. Circulation. 2018;137(14):1463-1471
11. Fujioka T, Kühn A, Sanchez-Martinez S et al. Impact of Interventricular Interactions on Left Ventricular Function, Stroke Volume, and Exercise Capacity in Children and Adults With Ebstein's Anomaly. JACC Cardiovasc Imaging. 2019;12(5):925-927.
12. Yim D, Mertens L, Morgan CT et al. Impact of surgical pulmonary valve replacement on ventricular mechanics in children with repaired tetralogy of Fallot. Int J Cardiovasc Imaging. 2017;33(5):711-720.
13. Ghio S, Gavazzi A, Campana C et al. Independent and additive prognostic value of right ventricular systolic function and pulmonary artery pressure in patients with chronic heart failure. J Am Coll Cardiol 2001; 37:183-188
14. Frigiola A et al. Biventricular response after pulmonary valve replacement for right ventricular outflow tract dysfunction: is age a predictor of outcome? Circ 2008; 118:S182-190
15. Gurtner GC, Werner S, Barrandon Y, Longaker MT. Wound repair and regeneration. Nature. 2008;453(7193):314–321

16. Pakshir P, Hinz B. The big five in fibrosis: marcophages, myofibroblasts, matrix, mechanics and miscommunication. Matrix Biol. 2018; 68-69:81-93
17. Chester D, Brown AC. The role of biophysical properties of provisional matrix proteins in wound repair. Matrix Biol. 2017;60–61:124–140.
18. Valiente-Alandi I, Schafer AE, Blaxall BC. Extracellular matrix-mediated cellular communication in the heart. J Mol Cell Cardiol. 2016;91:228-237

Chapter 11

Impact

From the work presented in this thesis as well as from other investigators, it is evident that various stressors can adversely affect the RV. These include increased pressure and volume loading and dyssynchronous activation, most typically from right bundle branch block. It is also evident from the results presented in this thesis that RV pressure loading triggers transforming growth factor beta and integrin molecular signaling leading to not only RV, but also LV myocardial fibrosis, in a regionally distinct pattern. These mechanical to molecular effects negatively impact ventricular function. Indeed, my thesis demonstrates that the stressed RV, particularly the pressure-loaded, and in particular the pulmonary hypertensive RV, affects not only RV function, but also the function of the neighboring LV. These adverse ventricular-ventricular interactions have important clinical implications in that we, and others, have shown that RV dysfunction is linked to clinically important outcomes and that the presence of biventricular dysfunction portrays worse outcomes.

The results of the studies presented in my thesis show that it is not only pressure loading per se that triggers RV dysfunction and adverse RV-LV interactions, but that the temporal aspects of these interactions and synchronous RV contraction and relaxation are central to effective RV function and physiological RV-LV interactions.

These results further our understanding of the mechanisms of RV and LV dysfunction in RV stress and also suggest potentially new therapeutic directions. My work suggests that the aspects of ventricular function detailed above are under-appreciated in clinical practice and under-utilized as therapeutic targets. For example, modestly increasing LV afterload is not a current therapeutic strategy in pulmonary hypertension and pharmacologically targeting RV fibrosis pathways is not a prevalent or current therapeutic strategy in RV pressure or volume loading; but based on my results, is expected to be beneficial to patients. Moreover, my work suggests that pulmonary valve replacement may be overutilized in repaired tetralogy of Fallot, and that regardless of pulmonary valve replacement, resynchronizing the dyssynchronous RV in these patients may be vastly underutilized. Likewise, the results agree with previous work by my supervisors that pacing the RV in pulmonary hypertension may be beneficial in addressing not only the regional distribution of RV wall stress, but also improve RV-LV interactions.

The pathophysiological mechanisms interrogated in this thesis also have bearings on how we diagnose RV dysfunction and hence ultimately how we manage patients. My work shows that adverse RV remodeling occurs at the RV apex and not only at the base. As current clinical assessment of the RV by echocardiography overwhelmingly focuses on the RV base (e.g. tricuspid annular plane systolic excursion (TAPSE) and tissue Doppler velocities (TDI)), my work suggests that changes in clinical assessment may be important to

detect adverse remodeling in the dysfunctional and failing RV. Moreover, as the myocardial fibers spiral at the cardiac apex to form a common apex to the RV and LV, apical dysfunction likely signifies biventricular dysfunction and adverse RV-LV interactions.

Currently, many of the aspects investigated in this thesis are considered separately in clinical practice, but the results presented in this thesis suggest that the parameters that affect RV function and RV-LV interactions are highly linked. My work suggests that pressure loading triggers RV dysfunction and also LV dysfunction that affects hemodynamic interactions and LV filling. Moreover, these adverse interactions extend beyond hemodynamics to induce tissue injury, in the form of biventricular fibrosis, predominantly at the high-stress septal hinge-point regions where the RV and LV anatomically join and interact. Integral to these adverse mechanical-molecular interactions in the RV and LV are the timing of events and the generation of asymmetrical RV work in both pressure-loading, particularly pulmonary hypertension, and RBBB induced electro-mechanical dyssynchrony in rTOF. These asymmetrical mechanics and injury cause stretching of the septum and leftward septal shift, producing inefficient RV function on the one hand and adverse RV-LV interactions on the other. Prolonged RV systole into LV diastole impairs LV filling and there is a temporal disconnect between RV and LV events that worsens biventricular systolic and diastolic function, in both pulmonary hypertension and in RBBB induced mechanical dyssynchrony. These abnormalities are greatly exaggerated by tachycardia and the dysfunctional or failing ventricle cannot summon sufficient reserve and cannot relax rapidly enough when heart rate increases. The asymmetrical RV mechanics leads to uneven wall stress within the RV, which imposes additional work on the already burdened RV free-wall and worsens myocardial fibrosis. Hence the chapters of this thesis indicate readily applied and simple measures to image this pathophysiology and its consequences for myocardial injury using echocardiography, that are not currently part of routine clinical practice.

At the same time, many questions remain unanswered. One of these is the precise relation between increased interstitial fibrosis and RV function. My data suggest a negative relationship between increased interstitial fibrosis and function: i.e. the more fibrosis, the greater the dysfunction. These data correlate with other experimental and clinical findings, but recent papers present different findings-showing increased fibrosis, that is not directly related to dysfunction. Likewise, the ability of the RV to recover after its load is removed, such as occurs following lung transplant in pulmonary hypertension, even though fibrosis is thought to be irreversible, raises questions regarding the clinical significance of fibrosis and whether it is a truly irreversible process.

Our findings suggest that in RV pressure loading and in pulmonary hypertension, LV fibrosis occurs predominantly at the septal hinge points, in conjunction with an upregulation of elastin that may act as a protective buffer, protecting the LV from more extensive damage, despite increased LV end-diastolic pressures. However, the significance of these experimental findings and whether pharmacologically increasing elastin production is a viable and effective therapeutic option remains unknown.

Our studies show that the pathophysiology of RV dysfunction in pulmonary hypertension is different from pulmonary stenosis and indeed the clinical course and outcomes of these 2 pressure-loading conditions is very different. The different pulmonary vascular dynamics and the possible presence of reflective waves in pulmonary hypertension which act to increase the load on the RV may explain some of these differences but was not investigated in this thesis. While pulmonary stenosis is thought to produce adaptive hypertrophy and pulmonary hypertension maladaptive failure, our results, especially our experimental results in our animal models, show many similarities between the 2 conditions that questions why this differential response occurs. In both conditions we observed RV remodeling with increased RV end-systolic and end-diastolic dimensions, markedly increased fibrosis, increased end-diastolic pressures and decreased function by echocardiography. However, myocardial strain was lower in pulmonary hypertension versus pulmonary stenosis, across a range of similar RV pressures. This suggests that RV myocardial function is worse in PAH, even if other features of RV 'failure' are present in both. Still, it may be that pulmonary stenosis being a congenital condition allows adaptive function of the RV-from fetal life, whereas in pulmonary hypertension, the load, in most cases, is acquired, rapidly increases and cannot be adequately alleviated. These may explain the differences between the 2 conditions.

Chapter 12

Acknowledgment

Many people deserve thanks. There is not enough scope to mention all, but to point out a few.

Danielle Warner and Bianca Gorski-Feenstra for their tireless work, patience and administrative support in producing this book.

Dr. Norman Silverman who taught me echo and beyond and what it means for a mentor to care for his mentees.

Dr. Andrew Redington for his exceptional insight, for supporting my academic career and for nudging me into laboratory research.

Dr. Luc Mertens and my colleagues in the echo lab at the Hospital for Sick Children for their long-lasting collaboration, collegiality and support.

Dr. Denis Daneman for being a role model as a wise, holistic, academic-physician and for allowing me to blossom at SickKids.

Cameron Slorach and Wei Hui, who have supported me so much over the years in acquiring and analyzing data and for always being willing to help.

Dr. Mei Sun for managing, supporting and maintaining the lab.

Many trainees and students who worked so hard and taught me so much. As evident from the author lists of the various papers, this PhD is as much their work as it is mine.

Many colleagues from around the globe who are friends, community and inspiration.

My supervisors Frits Prinzen, Joost Lumens and Folkert Meijboom. You have been scientific role models for me long before you became my PhD supervisors. I had looked up to you, long before I met you. I am just thrilled that you are my mentors, colleagues and friends. Thank you for making this happen.

My loving and supportive family- My parents Jack and Janice, my spouse, Sharon and my sons, Daniel, Jonathan and Ethan.